

Cross-Linked Poly(vinylphosphonates): From Fundamental Material Synthesis and Characterization to Multifaceted Applications of Three-Dimensional Materials

Anton Stefan Maier

Vollständiger Abdruck der von der TUM School of Natural Sciences der Technischen
Universität München zur Erlangung eines
Doktors der Naturwissenschaften (Dr. rer. nat.)
genehmigten Dissertation.

Vorsitz: Priv.-Doz. Dr. Alexander Pöthig

Prüfende der Dissertation:

1. Prof. Dr. Dr. h. c. Bernhard Rieger
2. Prof. Dr. Tom Nilges
3. Prof. Dr. Karin Stana Kleinschek

Die Dissertation wurde am 13.02.2025 bei der Technischen Universität München eingereicht
und durch die TUM School of Natural Sciences am 10.03.2025 angenommen.

“And I knew exactly what to do. But in a much more real sense, I had no idea what to do.”

- Michael Scott

„Education is the most powerful weapon which you can use to change the world.“

- Nelson Mandela

Für meine Eltern

Danksagung

In erster Linie möchte ich Prof. Dr. Dr. h.c. Bernhard Rieger für die Aufnahme an den Lehrstuhl, das entgegengebrachte Vertrauen in mich und die großzügig gewährten Freiheiten während meiner Doktorarbeit danken. Dies gab mir die Möglichkeiten, mich fachlich und persönlich zu entfalten und mich zu dem Chemiker zu entwickeln, der ich heute bin. Vielen Dank dafür! Further I want to extend my sincere gratitude to my second supervisor Prof. Dr. Job Boekhoven for integrating me into the RISE network and Prof. Dr. Angela Casini for involving me in ARTEMIS.

Einen erheblichen Teil zu meiner großartigen Zeit am WACKER-Lehrstuhl für Makromolekulare Chemie haben Dr. Carsten Troll und Dr. Sergei Vagin beigetragen. Ihr beiden hattet stets ein offenes Ohr für alle fachlichen und organisatorischen Belange, gute Tipps und Hilfestellungen bei der Gerätereparatur und wart immer für einen Spaß in der Kaffeeküche zu haben. Weiterhin möchte ich auf diesem Wege Frau Bauer, der guten Seele des Lehrstuhls, für die Unterstützung mit vertraglichen Angelegenheiten, Dienstreiseanträgen und sonstigem Papierkram danken. Ebenso gilt mein Dank Katia Rodewald, die stets für ein volles Lager und eine aktualisierte Website gesorgt hat. Ich danke euch allen!

Besondere Erwähnung muss auch Prof. Dr. Karin Stana Kleinschek und das gesamte Kollegium von der TU Graz finden. Vielen Dank für die unkomplizierte Aufnahme am Lehrstuhl, die familiäre Atmosphäre, eure Hilfsbereitschaft in jeder Hinsicht und die tolle Zusammenarbeit. Lieber Flo, Tobi und Rupert, gerne denke ich an den ein oder anderen Abend mit euch in einem Bausatzlokal oder der OKS zurück.

Ein besonderes Dankeschön möchte ich auch an meine beiden Masterarbeitsbetreuer Moritz Kränzlein und Christopher Thomas richten. Danke, dass ihr mir nicht nur einen großartigen Einstieg in den Lehrstuhl ermöglicht und viel beigebracht habt, sondern auch dass wir gute Freundschaften über die Uni hinaus entwickelt haben.

Weiterhin möchte ich mich bei den vielen (ehemaligen) Mitgliedern des Lehrstuhls bedanken, die für so eine tolle Atmosphäre gesorgt haben, weshalb ich jeden Tag gerne in die Arbeit gegangen bin. Besonders möchte ich Philipp Weingarten und meiner Laborpartnerin Kerstin Halama für die Gaudi und die guten Gespräche in WG, Labor und Kaffeeküche jeden Tag danken. Dank euch sind die viereinhalb Jahre seit der Masterarbeit im Flug vergangen! Ich möchte außerdem Marina Wittig, mit der ich schon im 2. Semester im Labor stand, für das stets offene Ohr und ihre Späße danken.

Danksagung

Verrückt, dass wir jetzt einfach beide am Ende unserer Promotion sind. Maßgeblich zu dieser coolen Zeit in der Makro haben auch der Rest unserer Puerto Rico Crew – Jonas Futter und Steffi Hörl -, sowie Lucas Stieglitz, Paula Großmann, Jonas Breitsameter und Hannah Venskutonis beigetragen. Ich danke euch allen für die gute Zeit und hoffe, dass wir uns nicht aus den Augen verlieren!

Einen sehr wichtigen Beitrag zum Erfolg dieser Arbeit haben meine Studenten und Kollaborationspartner geliefert. Hier möchte ich vor allem meiner Masterandin Jana Knezevic danken – es war eine Freude dein Betreuer zu sein. Ich wünsche dir das Beste für die Zukunft auf deinem weiteren persönlichen und beruflichen Weg. Außerdem gebührt mein Dank auch dem Rest meiner Studenten: Cara Bommer, Julie Gréus, Sophia Ignée, Leonie Kauling und Felix Wiesmann – danke für euren Fleiß, Eifer und den Spaß im Labor. Thank you Salma Mansi and Beatrice De Chiara for the smooth and successful collaborations.

Außerdem möchte ich mich bei meiner Clique aus dem Studium bedanken. Ihr habt mich den ganzen Weg begleitet, wir sind gemeinsam in Prüfungsphasen verzweifelt und haben aber auch schon Hochzeiten miteinander zelebriert. Mein großer Dank geht an Philipp Weingarten, Maximilian Maidl, Florian Naßl, Sebastian Hallweger, Alper Dönmez, Maximilian Iglhaut, Lukas Deffner und Jonas Futter. Ich hoffe wir verbringen auch in Zukunft den ein oder anderen Hüttenabend und freue mich schon auf zahlreiche anstehende Promotionsfeiern!

Ich bin sehr dankbar für meine Freunde aus dem Chiemgau, die mich seit meiner Kindheit begleitet haben und mit denen ich einfach mal über Sachen außerhalb der Uni reden konnte. Danke an die Mitglieder der „Feldein“ und meinen langjährigen Mitbewohner und engen Freund Maximilian Glück.

Zum Schluss möchte ich mich von ganzem Herzen bei meiner Familie bedanken. Liebe Mama, lieber Papa, lieber Simon und liebe Sophia – danke, dass ihr mich immer bedingungslos unterstützt, motiviert und wenn notwendig, abgelenkt habt. Nicht viele junge Menschen haben das Privileg, eine so harmonische und intakte Familie zu haben! Ich wünsche euch allen nur das Beste für die Zukunft und freue mich jedes Mal, wenn wir uns alle Daheim in Inzell treffen. Zu guter Letzt möchte ich dir, liebe Annika, danken. Ohne dich wäre mir diese Arbeit wesentlich schwerer gefallen. Danke für dein offenes Ohr, deine volle Unterstützung in allen Bereichen und die tollen Wanderungen, die du immer für uns planst!

Table of contents

List of abbreviations.....	XII
List of publications	XV
Abstract	1
Kurzzusammenfassung	2
1 Advanced polymer materials for future challenges	4
2 Development of polymer materials for functional applications	5
2.1 Rare earth metal-mediated group-transfer polymerization	5
2.1.1 General aspects of group-transfer polymerization	5
2.1.2 Mechanistic aspects and catalyst scope.....	12
2.1.3 Monomer scope and copolymerization	18
2.1.4 Polymer functionalization approaches for poly(vinylphosphonates)	21
2.2 Cross-linked polymer materials	26
2.2.1 Classification of cross-linking mechanisms	27
2.2.2 Structure-property relationships in cross-linked materials	33
2.2.3 Application areas of hydrogels	38
3 Aim of the thesis	42
3.1 Development and fundamental characterization of cross-linked materials.....	42
3.2 Synthesis of hydrophilic, pH-responsive hydrogels.....	43
3.3 Application of photochemical cross-linking in additive manufacturing.....	45
3.4 Dynamic covalent networks	46
4 Synthesis and characterization of photochemically cross-linked poly(vinylphosphonates)	47
4.1 Bibliographic data	47
4.2 Table of content graphic.....	47
4.3 Content	48
4.4 Manuscript	49

Table of contents

4.5 Author contributions	62
5 Synthesis and characterization of highly hydrophilic networks	63
5.1 Bibliographic data	63
5.2 Table of content graphic.....	63
5.3 Content	64
5.4 Manuscript	65
5.5 Author contributions	80
6 Additive manufacturing of poly(vinylphosphonate)-based hydrogels	81
6.1 Bibliographic data	81
6.2 Table of content graphic.....	81
6.3 Content	82
6.4 Manuscript	83
6.5 Author contributions	94
7 Dynamic covalent networks	95
7.1 Bibliographic data	95
7.2 Table of content graphic.....	95
7.3 Content	96
7.4 Manuscript	97
7.5 Author contributions	108
8 Summary and Outlook.....	109
9 References	113
10 Appendix.....	147
10.1 List of figures.....	147
10.2 Supporting information	150
10.2.1 Supporting information for chapter 4	150
10.2.2 Supporting information for chapter 5	192
10.2.3 Supporting information for chapter 6	212

Table of contents

10.2.4 Supporting information for chapter 7	234
10.3 Reprint Permissions of Copyrighted Material	260

List of abbreviations

Abbreviation	Description
AFM	Atomic force microscopy
AIBN	Azobis(isobutyronitrile)
Alg	Sodium alginate
ATRP	Atom transfer radical polymerization
<i>b</i>	block
BBL	β -Butyrolactone
CGCs	Constrained geometry catalysts
CL	ϵ -Caprolactone
Cp	Cyclopentadienyl ligand
Cp*	1,2,3,4,5-Pentamethylcyclopentadienyl ligand
CRP	Controlled radical polymerization
DAVP	Dialkyl vinylphosphonate
DAIVP	Diallyl vinylphosphonate
DCN	Dynamic covalent network
DEVp	Diethyl vinylphosphonate
DIW	Direct ink writing
DMAA	N,N-Dimethyl acrylamide
DMPA	2,2-Dimethoxy-2-phenylacetophenone
DMVP	Dimethyl vinylphosphonate
DP _r TMSVP	Di(trimethylsilyl)propargyl vinylphosphonate
DPVP	Dipropyl vinylphosphonate
E. Coli	Escherichia coli
EO	Ethylene oxide
ESI-MS	Electrospray ionization mass spectrometry

List of abbreviations

Abbreviation	Description
FLP	Frustrated Lewis pair
FLP-GTP	Frustrated Lewis pair group-transfer polymerization
FRP	Free radical polymerization
GTP	Group-transfer polymerization
HIP	Highly interacting Lewis pair
iPOx	2-Isoprenyl-2-oxazoline
LCST	Lower critical solution temperature
Ln	Rare earth metal center
MA	Methyl acrylate
MMA	Methyl methacrylate
M _n	Number average molecular weight
M _w	Weight average molecular weight
MWCNT	Multi-walled carbon nanotubes
NFC	Nanofibrillated cellulose
NHC	N-Heterocyclic carbene
NHS	N-Hydroxysuccinimide
NMR	Nuclear magnetic resonance
PAA	Poly(acrylic acid)
PEG	Poly(ethylene glycol)
PNIPAAm	Poly(N-isopropyl acrylamide)
PVA	Poly(vinyl alcohol)
QCM-D	Quartz crystal microbalance with dissipation monitoring
r	Radius
r ₁	Copolymerization parameter
r ₂	Copolymerization parameter
RAFT	Reversible addition-fragmentation chain transfer

List of abbreviations

Abbreviation	Description
r.d.s.	Rate determining step
REM-GTP	Rare earth metal-mediated group-transfer polymerization
ROMP	Ring-opening metathesis polymerization
iROP	Immortal ring-opening polymerization
S. Aureus	Staphylococcus aureus
SKA	Silyl ketene acetal
SKA-GTP	Silyl ketene acetal group-transfer polymerization
<i>stat</i>	statistical
<i>sym-col</i>	2,4,6-Trimethylpyridine
TBDMS	<i>tert</i> -Butyldimethylsilyl
THF	Tetrahydrofuran
TMPy	2,3,5,6-tetramethylpyrazine
TMSBr	Trimethylsilyl bromide
ToF-SIMS	Time-of-flight secondary ion mass spectrometry
UV	Ultraviolet
VBpy	4-Vinyl-4'-methyl-2,2'-bipyridine
VPA	Vinylphosphonic acid
X_n	Degree of polymerization
2-VP	2-Vinylpyridine
4-VP	4-Vinylpyridine
\bar{D}	Polydispersity index
X	Conversion
XPS	X-Ray photoelectron spectroscopy

List of publications

1. Maier, A. S., Mansi, S., Halama, K., Weingarten, P., Mela, P., and Rieger, B., Cytocompatible Hydrogels with Tunable Mechanical Strength and Adjustable Swelling Properties through Photo-Cross-Linking of Poly(vinylphosphonates). *ACS Appl. Mater. Interfaces*, **2024**, 16, 43, 58135-5817.
2. Maier, A. S., Finšgar, M., De Chiara, B., Kargl, R., Wolfrum, B., Stana Kleinschek, K., and Rieger, B., Water Uptake, Thin-Film Characterization, and Gravimetric pH-Sensing of Poly(vinylphosphonate)-Based Hydrogels. *ACS Appl. Mater. Interfaces*, **2025**, 17, 1, 2577-2591.
3. Maier, A. S.*, Lackner, F.*, Fink, J., Steindorfer, T., Hofmann, E., Stana Kleinschek, K., and Rieger, B., High-Fidelity Direct Ink Writing of Poly(vinylphosphonate)-Reinforced Polysaccharide Inks with Tunable Properties. *ACS Appl. Polym. Mater.*, **2025**, 7, 3, 1752-1762.
** These authors contributed equally.*
4. Knezevic, J.*, Maier, A. S.*, Lackner, F., Stana Kleinschek, K., and Rieger, B., Modifications of Poly(vinylphosphonates) Toward Dynamic Covalent Networks. *Macromolecules*, **2025**, 58, 5, 2683-2693.
** These authors contributed equally.*

Publications beyond the scope of this thesis

5. Maier, A. S.*, Thomas, C.*, Kränzlein, M.*, Pehl, T. M., and Rieger, B., Macromolecular Rhenium-Ruthenium Complexes for Photocatalytic CO₂ Conversion: From Catalytic Lewis Pair Polymerization to Well-Defined Poly(vinyl bipyridine)-Metal Complexes. *Macromolecules*, **2022**, 55, 16, 7039-7048.
** These authors contributed equally.*
6. Späth, F., Maier, A. S., Stasi, M., Bergmann, A. M., Halama, K., Wensch, M., Rieger, B., and Boekhoven, J., The Role of Chemically Innocent Polyanions in Active, Chemically Fueled Complex Coacervate Droplets. *Angew. Chem., Int. Ed.*, **2023**, 62, 41, e202309318.
7. Kriebisch, C. M. E., Kriebisch, B. A. K., Langlais, J., Maier, A. S., Rieger, B., Braun, D., and Boekhoven, J., The Multifunctional Role of Templates in Chemically Fueled Dynamic Combinatorial Libraries. *ChemSystemsChem*, **2025**, e202400087, DOI: 10.1002/syst.202400087.

Conference contributions

1. Maier, A. S., Späth, F., Boekhoven, J., and Rieger, B., A step towards membraneless organelles – poly(vinylphosphonates) as functionalizable polyelectrolytes for complex coacervation. *Macromolecular Colloquium Freiburg – MAKRO 2023*, **2023**, Freiburg, Germany, poster presentation.
2. Maier, A. S., Poly(vinylphosphonate)-based hydrogels exhibiting high biocompatibility and tunable material properties. *ACS Spring 2024*, **2024**, New Orleans, United States of America, conference talk.

Abstract

Hydrogels have emerged as a versatile class of polymer materials, addressing critical challenges across various disciplines and driving innovation in material science. Herein, the synthesis, characterization, and application of different hydrogels based on poly(vinylphosphonates) obtained via rare earth metal-mediated group-transfer polymerization is described. First, these innovative materials formed via photochemical cross-linking of polymers applying thiol-ene click chemistry are thoroughly characterized regarding their mechanical properties, water uptake, and biocompatibility, revealing tunable mechanical features and swelling behavior while supporting cell adhesion, allowing endothelialization and displaying antibacterial activities, hence suggesting significant biomedical application potential. Aiming at increased water absorption values, partial polymer-analogous hydrolysis of the poly(vinylphosphonates) introduces vinylphosphonic acid units in the polymers, yielding superabsorbent networks upon cross-linking. Thin films of these hydrogels tethered to the gold surfaces of sensors of a quartz crystal microbalance with dissipation monitoring (QCM-D) display strongly pH-dependent swelling behavior and high film stabilities on the surfaces, as confirmed by in-depth film and surface characterization, allowing gravimetric pH-sensing via QCM-D. Besides this, the photochemical cross-linking of poly(vinylphosphonates) is applied to structurally reinforce natural nanofibrillated cellulose/alginate inks in direct ink writing (DIW), enabling the printing of sophisticated structures with high shape fidelities and excellent resolution through layer-by-layer deposition with intermediate cross-linking. In this context, the synthetic polymers dictate the printed objects' swelling behavior and mechanical properties. Cytotoxicity testing reveals that the pristine inks display only slight cytotoxicities toward different cell types, therefore serving as a sound foundation for further research on tissue engineering applications. Finally, targeting more dynamic hydrogel systems applicable in direct ink writing is achieved by introducing dynamic covalent chemistry into poly(vinylphosphonates). The corresponding materials are obtained by functionalizing the polymers with diols, followed by complexation with boronic acid derivatives. This yields DIW inks with tunable viscoelastic properties and shear-thinning behavior, allowing self-healing and displaying pH-responsiveness.

Kurzzusammenfassung

Hydrogele haben sich als eine vielseitige Klasse von Polymermaterialien etabliert, die wesentliche Problemstellungen in verschiedenen Fachrichtungen adressieren und zu Innovationen in der Materialwissenschaft beitragen. In dieser Arbeit werden die Synthese, Charakterisierung und Anwendung verschiedener Hydrogele auf Basis von Poly(vinylphosphonaten), die durch Seltenerdmetall-mediierte Gruppentransferpolymerisation hergestellt werden, beschrieben. Zunächst werden diese neuartigen Materialien, die durch photochemische Vernetzung der Polymere mittels Thiol-En Klickreaktionen gebildet werden, hinsichtlich ihrer mechanischen Eigenschaften, Wasseraufnahme und Biokompatibilität charakterisiert. Dabei zeigen sich anpassbare mechanische Merkmale und Quellverhalten, während sie gleichzeitig die Zelladhäsion unterstützen, Endothelisierung ermöglichen und antibakterielle Aktivitäten zeigen. Dies lässt auf ein erhebliches biomedizinisches Anwendungspotenzial schließen. Um die Wasserabsorption zu erhöhen, werden durch eine partielle polymeranaloge Hydrolyse der Poly(vinylphosphonate) Vinylphosphonsäure-Einheiten in die Polymere eingeführt, wodurch bei der Vernetzung superabsorbierende Netzwerke entstehen. Dünne Filme dieser Hydrogele, die auf die Goldoberflächen von Sensoren einer Quarzkristall-Mikrowaage mit Dissipationsmessung (QCM-D) aufgebracht sind, zeigen ein stark pH-abhängiges Quellverhalten und eine hohe Filmstabilität auf diesen Oberflächen, wie durch eine vielseitige Film- und Oberflächencharakterisierung bestätigt wurde, sodass eine gravimetrische pH-Messung mittels QCM-D möglich ist. Darüber hinaus wird die photochemische Vernetzung von Poly(vinylphosphonaten) eingesetzt, um natürliche, nanofibrillierte Cellulose/Alginate-Tinten beim Direct-Ink-Writing (DIW) strukturell zu verstärken, was den Druck anspruchsvoller Strukturen mit hoher Formstabilität und hervorragender Auflösung durch schichtweises Drucken mit intermediärer Vernetzung ermöglicht. In diesem Zusammenhang bestimmen die synthetischen Polymere das Quellverhalten und die mechanischen Eigenschaften der gedruckten Objekte. Zytotoxizitätstests zeigen, dass die unbehandelten Tinten gegenüber verschiedenen Zelltypen nur geringe Zytotoxizitäten aufweisen und weshalb diese eine solide Grundlage für weitere Forschungen hinsichtlich des künstlichen Anzüchtens von Geweben darstellen. Schließlich wird durch die

Einführung dynamischer kovalenter Chemie in Poly(vinylphosphonate) die Entwicklung dynamischer Hydrogelsysteme für das Direct Ink Writing erreicht. Die entsprechenden Materialien werden durch Funktionalisierung der Polymere mit Diolen und anschließende Komplexierung mit Boronsäurederivaten erhalten. Dadurch entstehen DIW-Tinten mit einstellbaren viskoelastischen Eigenschaften und scherverdünnendem Verhalten, welche Selbstheilung ermöglichen und pH-responsiv sind.

1 Advanced polymer materials for future challenges

Research into innovative materials capable of addressing modern and future scientific and societal issues has long moved beyond investigating commodity polymers such as polyolefins or polyesters. Instead, there is an increasing demand for advanced polymeric materials with tailored properties and multifunctionality to address critical challenges in the fields of healthcare, agriculture, biomedicine, construction, and energy conversion, to name only some examples.¹ Among these emerging materials, hydrogels obtained a prominent role due to their unique ability to combine high water content with a three-dimensional polymeric network, mimicking biological systems, responding to external stimuli (pH, light, temperature, electric fields), and exhibiting widely tunable material properties through sophisticated structural design.²⁻⁴ In the fabrication of hydrogels, precision polymer synthesis is a key factor in developing innovative systems, as it enables the modulation of the molecular architecture and microstructure of polymers, precisely tuning their macroscopic properties.⁵ In this context, rare earth metal-mediated group-transfer polymerization (REM-GTP) provides an advanced synthetic method toward well-defined, high-performance polymers, offering excellent control over polymer molecular weights, copolymer compositions, and functionality while maintaining narrow dispersities.⁶⁻⁸ Leveraging REM-GTP for hydrogel synthesis holds the promise of precisely adjusting network properties through tailored polymer synthesis, introducing functionality and stimuli-responsiveness into the materials, and, ultimately, generating a new generation of 'smart' materials with considerable application potential across various fields. After more than 10 years of research focusing on understanding the catalysis, expanding monomer and catalyst scope, and seeking applications for (co)polymers obtained via REM-GTP, this thesis explores the potential of cross-linked poly(vinylphosphonates) by applying these previous findings. It represents a holistic approach to material development, starting with the fundamental synthesis and characterization of a material, putting the material properties into perspective, and understanding the substantial structure-property relationships before transferring them to applications.

2 Development of polymer materials for functional applications

2.1 Rare earth metal-mediated group-transfer polymerization

2.1.1 General aspects of group-transfer polymerization

Living-type polymerization

The term 'living' polymerization was first mentioned by Michael Szwarc, who described the controlled anionic copolymerization of styrene and isoprene initiated by sodium naphthalenide.⁹ The authors of these early studies assigned characteristics of biological life, such as birth, growth by the metabolism of monomers, and death, to chemical reactions and concluded that polymerizations should be immortal if termination reactions are nonexistent.¹⁰ In the polymerization experiments, sodium naphthalenide, an efficient electron-transfer agent, initiated the polymerization by reducing the styrene monomer, which subsequently could undergo dimerization, generating a dianionic species.^{11,12} By choice of tetrahydrofuran (THF) as a polar, aprotic solvent, termination reactions by the abstraction of protons by the growing anionic chains were suppressed, yielding anionic, dormant species as shown in Figure 1.⁹⁻¹¹

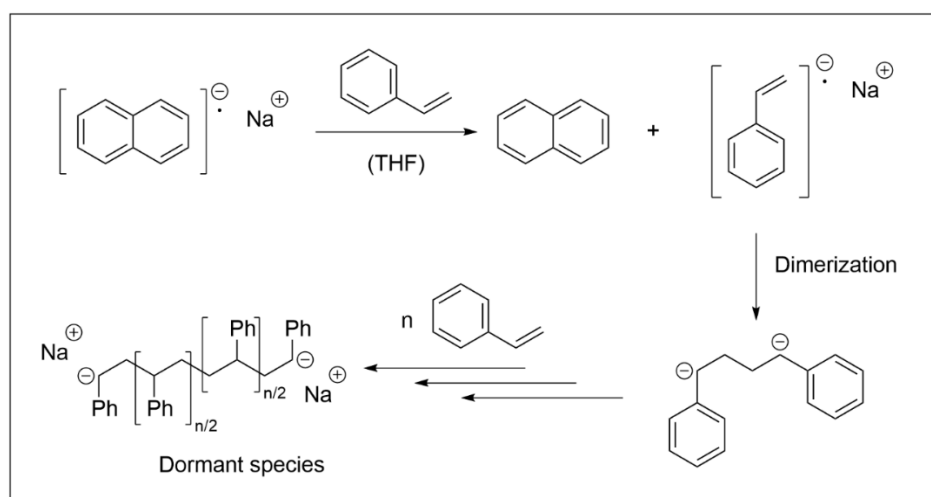


Figure 1: Sodium naphthalenide-initiated anionic 'living' polymerization of styrene.^{9,10}

The authors demonstrated that the dormant species, which they termed 'living polymer', could polymerize either a second batch of styrene or a block of isoprene

when thoroughly excluding terminating agents such as oxygen, moisture, and carbon dioxide.^{9,10,13} The virtual absence of a termination reaction in this polymerization process allows control over the degree of polymerization (X_n) by the monomer-to-initiator ratio, simultaneously resulting in narrow polydispersities.¹⁴ This aligned with previous studies of Flory, who investigated the living polymerization of ethylene oxide (EO) and proposed that the concurrent growth of all chains with the same rate enables control of X_n and leads to Poisson molecular weight distributions.^{15,16} In general, ideal living polymerizations are characterized by a linear growth of the polymer molecular weight with conversion. In contrast, in other polymerization types, high molecular weight polymer is formed towards the end of polymerization (step-growth polymerization) or already at low monomer conversions (free radical polymerization), as shown in Figure 2.¹⁷

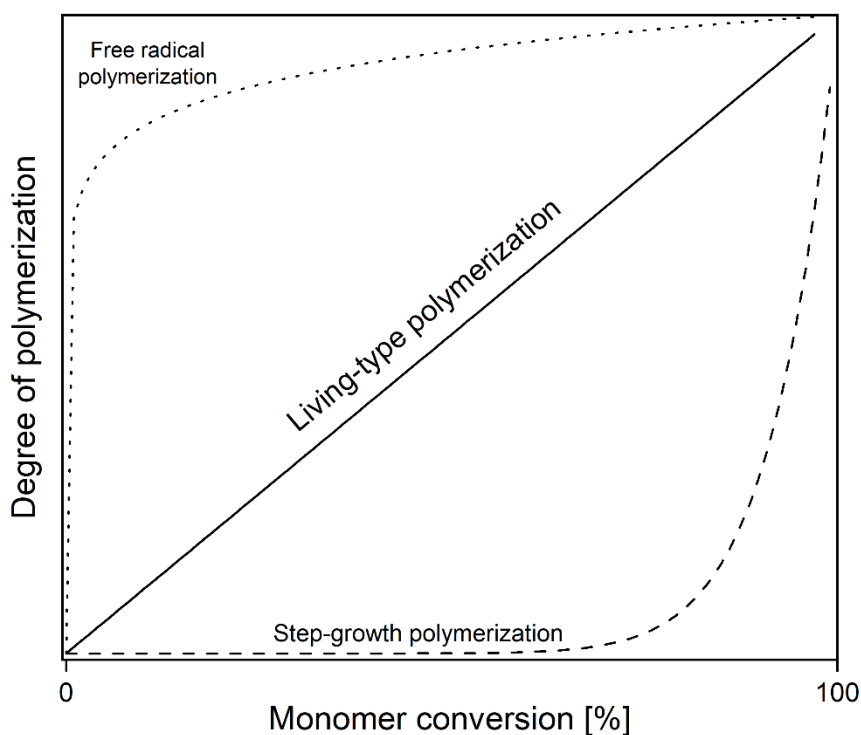


Figure 2: Degree of polymerization with monomer conversion for different polymerization types. Free radical polymerization (dotted line), living-type polymerization (solid line), and step-growth polymerization (dashed line).

At this point, it must be noted that the term 'living' polymerization represents an idealized image in different polymerization approaches, assuming the total absence of side reactions, such as chain transfer, chain breaking, or termination. In real systems, however, these processes can play significant roles. In this context, achieving high relative ratios of propagation rate to any side reaction is important to maintain

maximum control over the polymerization. Processes in which the propagation step prevails over termination or chain transfer are often termed 'controlled' polymerization rather than 'living polymerization'.¹⁸⁻²¹ In the further course of this thesis, systems meeting these requirements will be designated as 'living-type' or 'controlled' polymerizations. The presence of dormant species as resting states in living-type polymerizations is a powerful tool for developing tailored, functional polymers. In this context, sequential monomer addition gives access to block copolymers, and quenching of the active chain ends with appropriate, functional substrates enables end-capping of polymer chains. The discovery of living polymerization, thus, laid the foundation for the precise design of macromolecular structures with well-defined morphologies and specific topologies.^{11,17,18,22,23} Such mechanisms have been realized in various polymerization types, each differing from the others in terms of initiation, propagation, and potential terminating steps. Anionic living-type polymerizations like the abovementioned example involve monomers like styrene, butadiene, methacrylates, or ethylene oxide. In these cases, metalorganic compounds often initiate the polymerization, and the corresponding metal ions stabilize the active chain ends.^{24,25} In contrast, electron-rich vinyl monomers, such as vinyl ethers, isobutene, and (substituted) styrenes, can be polymerized in a highly controlled cationic fashion by applying more sophisticated initiating systems, mostly involving Lewis acids.^{26,27} Another big class of living-type polymerization methods is presented by controlled radical polymerizations (CRPs). Unlike free radical polymerization (FRP), the precise synthesis of polymers via CRP proceeds via a fast initiation process and the suppression of termination reactions by maintaining low concentrations of radicals. This is commonly achieved by establishing a dynamic equilibrium between an active propagating radical species and a dormant species, termed reversible-deactivation radical polymerization.¹⁸ A famous example of CRP includes atom transfer radical polymerization (ATRP), which involves a transition metal catalyst capable of oxidation/reduction, thereby reversibly cleaving an alkyl halide bond by abstraction of the halide ligand and, thus, generating a radical species.^{28,29} Another well-studied example of CRP is given through reversible addition-fragmentation chain transfer (RAFT) polymerization, which affords controlled polymerization in terms of molecular weight and polydispersity by employing thiocarbonylthio compounds as chain transfer

agents leading to low radical concentrations.^{30,31} The monomer scope of CRP methods is wide, ranging from 'classical' monomers like styrene derivatives to N-vinyl monomers and functional building blocks like substituted (meth)acrylates and acrylamides.^{32–34} The final approach that will be considered in this general overview of living-type polymerizations is coordinative polymerization. Similarly to anionic polymerizations, metal-catalyzed, coordinative approaches proceed in a living fashion with a stabilization of the active chain ends by coordination to a metal center. One famous example of this type of polymerization includes the 'immortal' ring-opening polymerizations (iROP) of lactones like β -butyrolactone (BBL) or ϵ -caprolactone (CL) utilizing aluminum, zinc, or rare earth metal catalysts.^{17,35,36} Another living-type polymerization involving transition metal catalysts based on, e.g., titanium, tungsten, or ruthenium, is ring-opening metathesis polymerization (ROMP), which is applicable to a broad range of cyclic olefins such as (substituted) norbornene or cyclooctatetraene.^{37–39} Linear α -olefins, in turn, are polymerizable via a coordination-insertion mechanism using homogenous metallocene catalysts of group 4 metals ($M = \text{Ti, Zr, Hf}$) or heterogeneous systems combined with appropriate cocatalysts.^{40–42} A significant contribution to the precision polymerization of polar monomers was made by the discovery of group-transfer polymerization (GTP) by Owen W. Webster at DuPont in 1983.⁴³ In the following sections, different types of GTP, which have been developed over the last 40 years will be presented.

Silyl ketene acetal group-transfer polymerization

The first report of group-transfer polymerization dates back to 1983. This year, Owen W. Webster and colleagues from DuPont reported a fundamentally new polymerization method for acrylic monomers using silyl ketene acetals (SKA) as initiators combined with nucleophilic catalysts. In their initial study, the authors described methyl methacrylate (MMA) polymerization with dimethylketene methyl trimethylsilyl acetal as initiator and a nucleophilic catalyst (HF_2^-) at 80 °C, allowing unprecedented control of the polymerization process as evidenced by narrow polydispersities and molecular weights up to 20 kg/mol.⁴³ Besides this initial system for SKA-GTP, other silyl ketene acetals were employed with several nucleophilic catalysts (e.g. HF_2^- , CN^- , N_3^- , bibenzoates) to polymerize a broad range of methacrylate monomers in a living-type fashion, in which the molecular weight was controlled by the ratio of monomer to

initiator while maintaining narrow polydispersities.^{43–45} Regarding the mechanism of SKA-GTP, two mechanistic models were proposed. In the associative pathway, the SKA group reacts with the nucleophile, forming a complex, which can subsequently transfer a silyl group to an incoming monomer. The silyl group remains on the same polymer chain throughout the polymerization until it reversibly undergoes silyl end group exchange to liberate the catalyst nucleophile. In the dissociative mechanism, the first step also involves catalyst complexation. However, the formed complex of SKA and nucleophile can reversibly decompose, generating an enolate end for repeated conjugate 1,4-addition of MMA until the poly(methyl methacrylate) (PMMA) chains are capped by the silicon species, regenerating the SKA end group.⁴⁴ Both mechanistic pathways for the polymerization of MMA via SKA-GTP are shown in Figure 3.

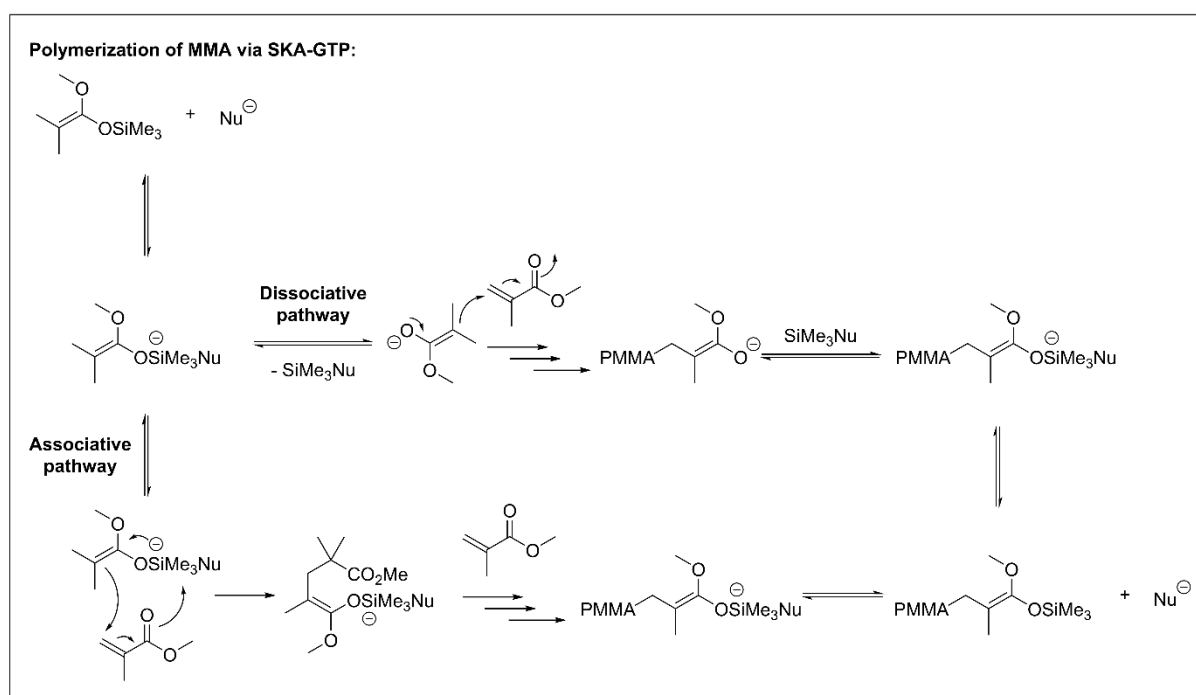


Figure 3: Mechanistic pathways of the SKA-GTP of MMA.⁴⁴

After vigorous discussions about the mechanism of SKA-GTP, numerous studies suggested that a dissociative mechanism is likely to occur based on the observed retardation of the polymerization upon increasing the amount of SKA agent (indicating that the complex itself is not adding MMA), the long induction periods (required for dissociation and addition to the MMA double bond), and the decrease in the activity in the presence of excess catalyst (causing too high amounts of unstable bare enolate).^{46–50} Despite the absence of an actual group transfer, the notion of SKA-GTP

persists until today, and SKA compounds are often applied in the precise synthesis of complex polymeric architectures (co- and terpolymers, star-shaped structures) from different alkyl (meth)acrylates and acrylamides.^{51–55}

Frustrated Lewis pair group-transfer polymerization

Another catalytic approach allows the highly controlled polymerization of α,β -unsaturated monomers (1,4-Michael acceptors) by using frustrated Lewis pairs (FLPs) in group-transfer polymerization. The term ‘frustrated Lewis pair’ was originally introduced by Stephan et al. to describe combinations of sterically hindered Lewis acids and equally bulky Lewis bases.⁵⁶ The first report on living-type polymerization utilizing FLPs described the polymerization of MMA and two methylene butyrolactones applying the strong Lewis acid $\text{Al}(\text{C}_6\text{F}_5)_3$ combined with phosphine and N-heterocyclic carbene (NHC) Lewis bases.⁵⁷ The polymerization of polar, Michael-type monomers with FLPs proceeds via repeated 1,4-conjugate addition in which the Lewis base initiates the polymerization and the Lewis acid stabilizes the negative charge at the acceptor-heteroatom of the monomer. Mechanistic experiments combined with computational studies suggested that the propagation involves a bimetallic step in which the aluminum-stabilized active species adds a Lewis-acid activated monomer, as shown in Figure 4.⁵⁸ The monomers for FLP-GTP contain the structural motif of a double bond in conjugation to a heteroatom. Aside from MMA and a series of lactones, this polymerization method also enabled the synthesis of polymers from the polar vinyl-monomers 2-isoprenyl-2-oxazoline (iPOx) and 2-vinylpyridine (2-VP).⁵⁹ The monomer scope was significantly broadened by Rieger et al. in 2016, reporting the polymerization of different methacrylate monomers, diethyl vinylphosphonate (DEVP), N,N-dimethyl acrylamide (DMAA), and the 1,6-Michael system 4-vinylpyridine (4-VP) utilizing different combinations of highly interacting Lewis pairs (HIPs) with fewer sterical demand than FLPs.⁶⁰ Transferring this concept to another extended Michael system allowed the controlled polymerization of 4-vinyl-4'-methyl-2,2'-bipyridine (VBpy) with HIPs, which gave access to macromolecular catalysts with high activities in the photocatalytic reduction of CO_2 to CO .⁶¹ A general overview of the Lewis acids and bases, the propagation step, and the monomer scope of the controlled polymerization of α,β -unsaturated monomers with FLPs or HIPs is given in Figure 4.

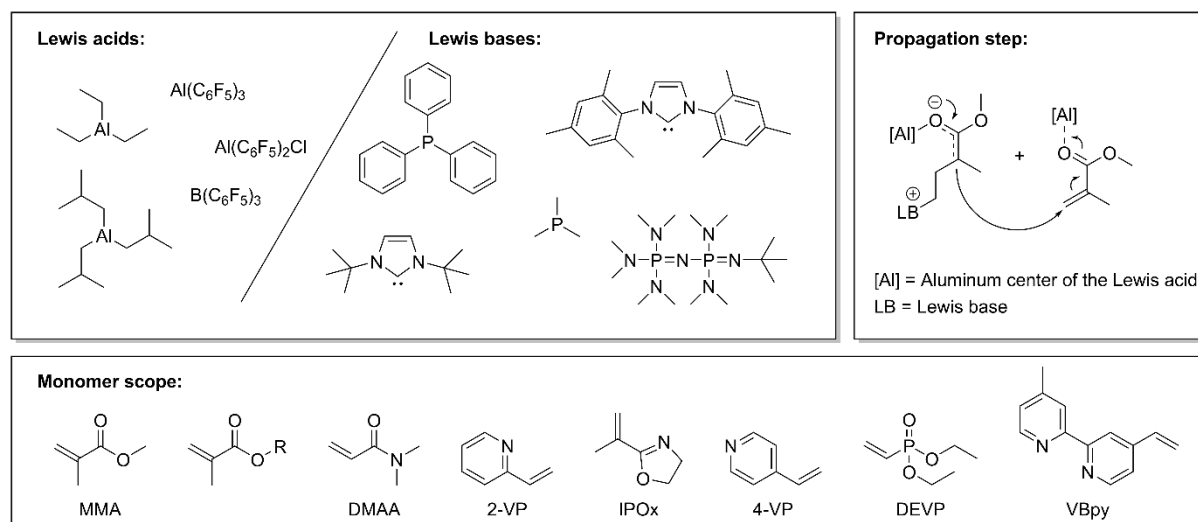


Figure 4: Overview of exemplary Lewis acids, Lewis bases, propagation step, and monomers of group-transfer polymerization with frustrated and highly interacting Lewis pairs.^{57,59–61}

Rare earth metal-mediated group-transfer polymerization

Following the discovery of SKA-GTP, two independent research groups reported the living-type polymerization of MMA by group-transfer polymerization. In 1992, Collins and Ward applied cationic zirconocenes $[\text{Cp}_2\text{ZrMe}_2]/[\text{Cp}_2\text{ZrMe}(\text{THF})]^+[\text{BPh}_4]^-$ ($\text{Cp} = \text{C}_5\text{H}_5^-$) to polymerize MMA by a bimetallic GTP mechanism, yielding syndiotactically-enriched PMMA with polydispersities (\mathcal{D}) below 1.40 and molecular weights up to 160 kg/mol.⁶² In contrast, Yasuda and coworkers utilized organolanthanide complexes to obtain high molecular weight PMMA ($M_n > 550$ kg/mol) with exceptionally low polydispersities ($\mathcal{D} < 1.05$). With their seminal work on MMA polymerization with binuclear samarocene complexes of the type $[\text{Cp}^*_2\text{SmH}]_2$ ($\text{Cp}^* = \text{C}_5\text{Me}_5^-$), Yasuda et al. laid the foundation for all further developments of REM-GTP. Based on polymerization experiments and X-ray structural data, an eight-membered transition state of the polymerization was postulated, involving the coordination of one MMA unit in the enolate form, whereas a second monomer binds to the Sm center via the carbonyl functionality. Initiation was proposed to proceed via a hydride transfer of the catalyst to a monomer. The initiation of MMA GTP with $[\text{Cp}^*_2\text{SmH}]_2$ and the transition state of the polymerization are shown in Figure 5.⁶³ More insights into the polymerization mechanism, catalysts, and monomers, as well as the application of REM-GTP for synthesizing functional polymer materials, will be discussed in the following chapters.

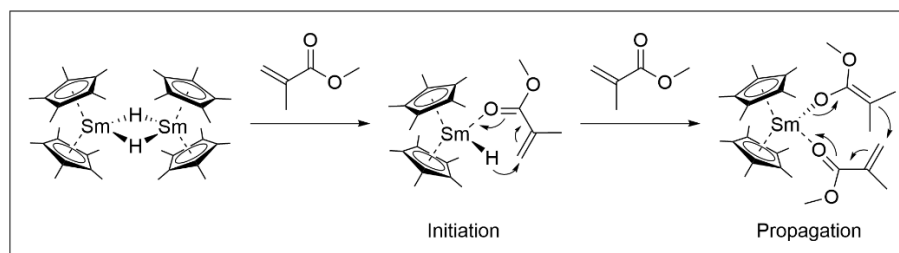


Figure 5: Mechanism of initiation and propagation of the polymerization of MMA via REM-GTP with $[\text{Cp}^*_2\text{SmH}]_2$.⁶³

2.1.2 Mechanistic aspects and catalyst scope

The first step of polymerizing polar monomers like vinyl phosphonates via REM-GTP involves initiating the chain growth of monomers by forming an active chain end. In controlled polymerizations, this occurs by a transfer of an initiating ligand of the catalyst onto the first monomer unit, as shown for the hydride ligand in Figure 5. In the first study on living-type DEVP polymerization, reporting the synthesis of high molecular weight poly(vinylphosphonates) (M_w up to 10^3 kg/mol), σ -donor chloro and methyl ligands were applied in Cp_2YbX complexes (X = initiating ligand).⁶⁴ However, several other initiation pathways besides a ligand transfer have been identified in REM-GTP of trivalent lanthanocenes, depending on the nature of the initiating ligand.⁶⁵ The initiation mechanism of REM-GTP with non-metallocene catalysts proceeds similarly.^{6,7,66–69} Since the potential initiation pathways of REM-GTP are best studied for metallocenes of the type Cp_2LnX (Ln = rare earth metal center), the focus will be on these in the following. Depending on the precursor catalyst, the first step of the initiation reaction either involves the dissociation of a bimetallic metal complex by coordination of a monomer or a displacement of a weakly bound ligand such as THF by an incoming monomer, as illustrated in Figure 6, which displays an overview of initiation pathways for REM-GTP of dialkyl vinylphosphonates (DAVP) with $\text{Cp}_2\text{LnX}(\text{THF})$ and binuclear $[\text{Cp}_2\text{LnX}]_2$.⁶⁵ Notably, the coordination strength of binuclear catalysts must be low enough to allow fast intercalation of monomers. If this is not the case and the dimeric structure is opened only slowly, the consequent initiation delay causes a broadening of the dispersity and a loss of control over the polymerization.⁶ Both cases for initial monomer coordination yield a catalyst species with a monomer and X bound to the metal center. Starting from this, three different pathways have been identified, presented in Figure 6.

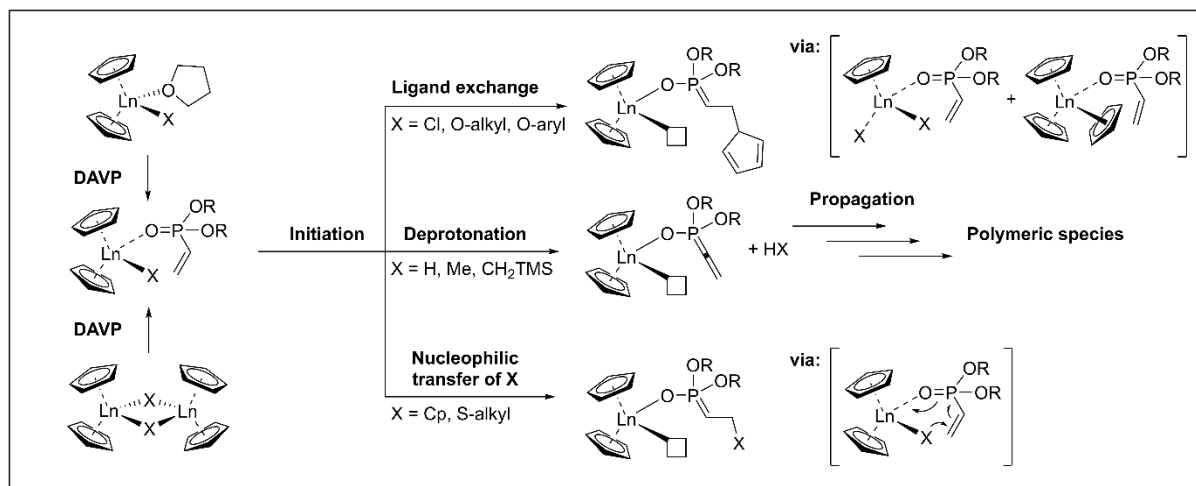


Figure 6: Possible initiation pathways of DAVP polymerization with $\text{Cp}_2\text{LnX}(\text{THF})$ or $[\text{Cp}_2\text{LnX}]_2$ catalysts via REM-GTP.⁶⁵

The first initiation pathway occurs by a ligand exchange reaction and was confirmed via ^1H - and ^{31}P nuclear magnetic resonance (NMR) spectroscopic experiments with the non-polymerizable, DEVP-related substrate diethyl ethylphosphonate (DEEP). Treating $\text{Cp}_2\text{LnX}(\text{THF})$ complexes with DEEP resulted in the formation of $\text{Cp}_3\text{Ln}(\text{DEEP})$ and $\text{CpLnX}_2(\text{DEEP})$ in equilibrium, which was confirmed by single-crystal X-ray crystallography. This exchange reaction is induced by donor ligands like alkoxides and chloro ligands in $\text{Cp}_2\text{LnX}(\text{THF})$.⁶⁵ The trivalent cyclopentadienyl lanthanide complex formed upon ligand exchange is a well-known catalyst for vinylphosphonate polymerization, initiating the polymerization by transferring a Cp ligand onto the first DAVP monomer.⁷⁰ Secondly, strongly basic initiators such as methyl, hydride, and CH_2TMS ligands, commonly applied for the polymerization of MMA, were found to initiate the polymerization of DAVP by deprotonation.^{62–65,71,72} Electrospray ionization mass spectrometry (ESI-MS) confirmed the initiation of the DEVP polymerization with CH_2TMS initiators by the slow deprotonation of the acidic α -CH of the monomer, yielding the allenyl phosphonate intermediate shown in Figure 6.^{6,65} The final initiation pathway of REM-GTP with rare earth metallocenes involves the nucleophilic transfer of X ($\text{X} = \text{Cp}$, thiolates) by the 6-electron mechanism already proposed for MMA GTP (Figure 5), which is presented at the bottom of Figure 6.^{6,63,70} Besides the three initiation pathways presented above, other studies on REM-GTP with metallocene catalysts reported an initiation by redox reactions, which will not be addressed in this chapter.^{73,74} The presence of different initiation mechanisms in REM-

GTP of vinylphosphonates and their extent and rates depending on the nature of the initiating ligand X causes broad dispersities and a loss of control over the polymerization.^{6,65} An efficient initiation of DAVP polymerization was possible by thiolato complexes. However, the resulting end group was prone to elimination, and these complexes were unsuitable for other monomers like iPOx and 2-VP.^{65,75} To ensure fast and efficient initiation without side reactions, initiators simulating the active propagating species by an 8-electron initiation pathway were developed. In this context, rare earth metal alkyl complexes can be functionalized with pyridines and other substrates via σ -bond metathesis.^{76,77} The σ -bond metathesis mechanistically proceeds as a concerted [2+2]-cycloaddition reaction with a kitelike transition state, leading to an exchange of a metal-ligand σ -bond with one of an incoming substrate.^{78,79} Applying the CH-bond activation of CH-acidic substrates by yttrium complexes to REM-GTP allows the introduction of distinct end groups into the polymers.^{80,81} CH-bond activation of 2,4,6-trimethylpyridine (*sym*-collidine = *sym*-col) with $\text{Cp}_2\text{YCH}_2\text{TMS}(\text{THF})$ led to the in situ formation of $\text{Cp}_2\text{Y}(\textit{sym}\text{-col})$, as shown in Figure 7.

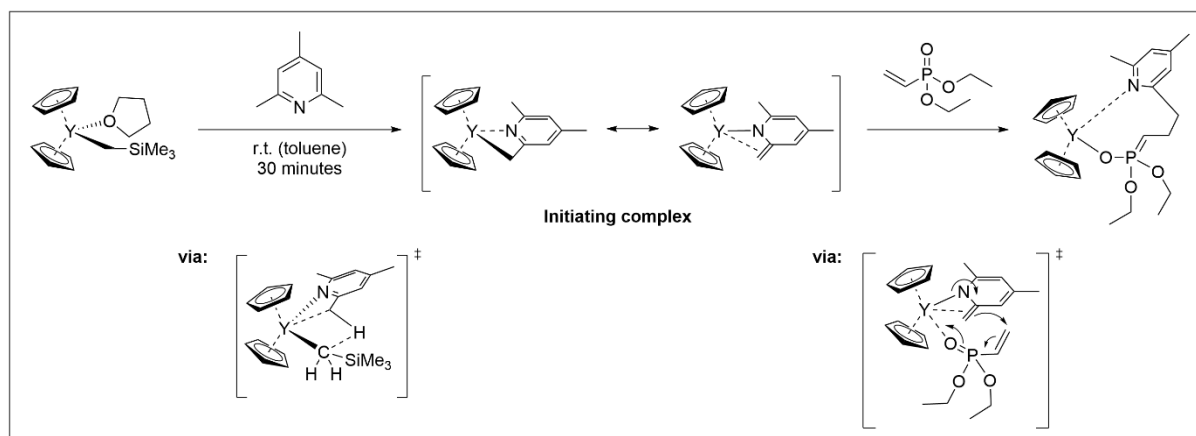


Figure 7: CH-bond activation of 2,4,6-trimethylpyridine with $\text{Cp}_2\text{YCH}_2\text{TMS}(\text{THF})$ generating $\text{Cp}_2\text{Y}(\textit{sym}\text{-col})$ in situ and transition state of the σ -bond metathesis reaction. Subsequent addition of DEVP initiates polymerization via the indicated transition state.

The structure of this complex was also isolated and confirmed by crystallographic data. When applying it to REM-GTP of DEVP, the complex exhibited high activities and led to a living-type polymerization, resulting in high molecular weight polymers with narrow polydispersities. ESI-MS measurements of oligomers revealed exclusive incorporation of *sym*-col as chain ends and, thus, nucleophilic transfer as the dominant initiation pathway, which also explained the high initiator efficiencies and can be attributed to the lower basicity of *sym*-col compared to CH_2TMS or other alkyl initiating groups.⁸²

Similarly, CH-bond activation of 2,3,5,6-tetramethylpyrazine (TMPy) can be applied to yield bimetallic catalysts, as shown in studies of Rieger et al. and Mashima et al.^{81,83} Incorporating *sym*-col as a distinct end group into the growing polymer chain is a beneficial feature of this approach, allowing for the precise introduction of functional motifs into polymers obtained via REM-GTP, which will be addressed later in this work. After initiation of DAVP polymerization by transferring a ligand from the catalyst onto the first monomer unit, the monomer is bound to the catalyst in its enolate form, and another incoming DAVP molecule can coordinate to the rare earth metal center via the keto form. Following that, the monomer coordinated via the enolate form attacks the keto-coordinated monomer in an eight-membered transition state according to the monometallic Yasuda-type propagation mechanism presented for MMA polymerization in Figure 5. This 1,4-conjugate addition results in the eight-membered resting state of the polymerization, with the last two monomers added to the chain coordinated to the catalyst shown in Figure 8.

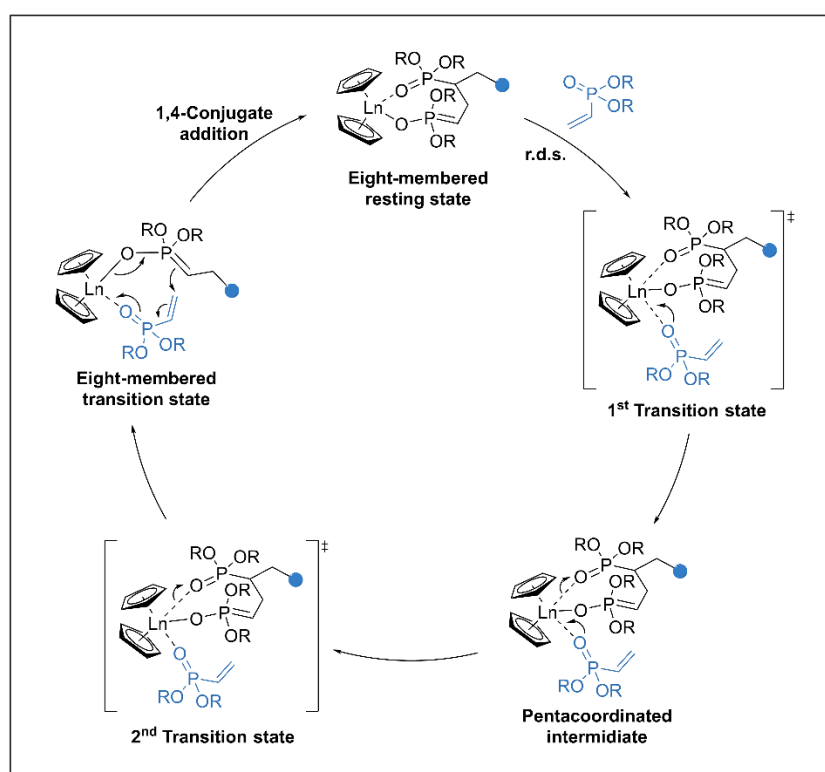


Figure 8: Yasuda-type, monometallic propagation mechanism of REM-GTP of vinylphosphonate monomers with key intermediates and transition states.⁶⁵

For subsequent monomer insertions, this intermediate must be opened by an S_N2 -type associative displacement of the polymer chain before the new monomer can

coordinate via the electronegative acceptor atom. Mechanistically, this intercalation presents the rate-determining step (r.d.s.) for the polymerization reaction and presumably occurs via a pentacoordinated intermediate, as shown above.⁶⁵ Overall, the propagation of vinylphosphonate polymerization by REM-GTP proceeds by repeated 1,4-conjugate addition of the monomers, maintaining coordination to the catalytically active metal center. This ensures the narrow polydispersities and living-type behavior observed in many studies.^{8,63,67,68,72} Upon consumption of the monomer, the polymerization remains in the eight-membered resting state presented in Figure 8 until a subsequent monomer is added or the workup with a protic solvent leads to termination of the polymerization.⁶⁵

The abovementioned propagation mechanism is generally applicable to different Michael-type monomers. However, the polymerization activity significantly depends on the catalyst applied for REM-GTP. In REM-GTP, three major catalyst classes can be identified. Besides the large group of metallocene complexes of the type Cp_2LnX , originally introduced by Yasuda et al. in their report on MMA polymerization with $[Cp^*_2SmH]_2$, numerous other examples of efficient rare earth metal-based catalyst systems have been reported.^{6,67,70,72,82} In addition to metallocenes, half-metallocene complexes have been investigated for REM-GTP of vinylphosphonate and acrylate monomers. In these compounds, only one Cp ligand is bound to the metal center, while the second ligand is a different donor, e.g., a chelating amidinate ligand.^{84,85} Among the half-metallocenes for REM-GTP, a subclass is presented by constrained geometry catalysts (CGCs) in which a bridge to another ligand (e.g. amido ligand) is introduced into a cyclopentadienyl-derived ligand. While the constrained geometry limits the flexibility of the Cp-analogous ligand, the resulting complexes exhibit higher steric accessibility due to the smaller second ligands and differ in their electronic configuration compared to their metallocene counterparts. These features of half-metallocene complexes bear great potential in the stereospecific polymerization of polar monomers.⁸⁶ A final class of REM-GTP catalysts are the non-metallocene catalysts. In these systems, there is a large scope of chelating ligands, like bis(phenolate) ethers, bis(phosphinimino)methanide and bis(pyrrolylaldiminato) ligands, ene-diamido motifs and numerous other structures coordinated to the metal centers and exhibiting polymerization activity for different Michael-type monomers.⁶⁶⁻

69,81,83,87–90 An overview of exemplary catalysts from each class presented above is given in Figure 9.

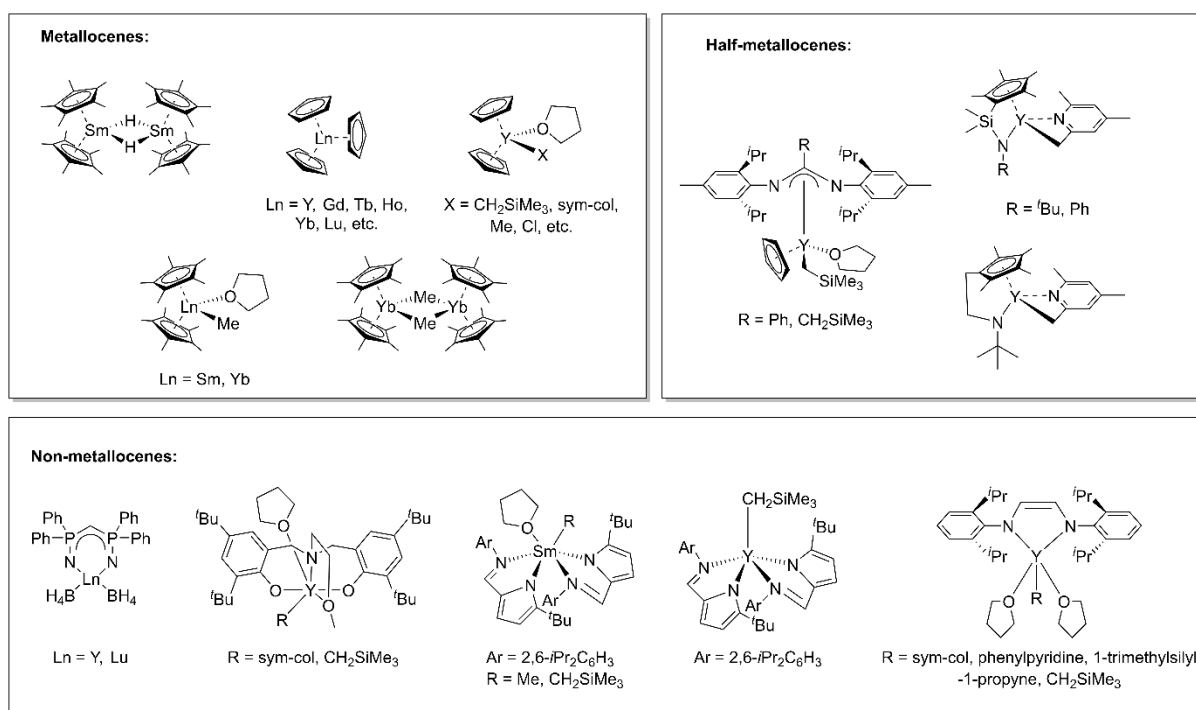


Figure 9: Overview of different catalyst classes for REM-GTP with exemplary structures for each group: Metallocenes, half-metallocenes, and non-metallocene catalysts.^{65,66,68–71,77,81,84–90}

For the widely applied class of metallocene catalysts, the catalyst activity in REM-GTP significantly depends on several parameters. Firstly, the radii of the rare earth metal centers tremendously impact catalyst performance. In contrast to previous studies on MMA polymerization by Yasuda et al.,^{91,92} the activity of two structurally identical catalysts increases with decreasing ionic radius of the metal center for the polymerization of vinylphosphonates. Studies of the Rieger group on the polymerization of DEVP with rare earth metal complexes revealed an activity increase with decreasing ionic radii ($r(\text{Sm}) > r(\text{Y}) > r(\text{Yb}) > r(\text{Lu})$). In-depth thermodynamic considerations attributed this effect to entropic reasons rather than enthalpy changes.⁶⁵ Further, the propagation rate for vinylphosphonate REM-GTP mainly depends on the steric demand of the growing polymer chain rather than that of the incoming monomer.^{93,94} Another kinetic aspect of REM-GTP affected by the metallocene structure is the effect of the ligand sphere on the catalyst activity. Different studies demonstrated that introducing sterically more demanding ligands accelerates polymerization.^{72,95} In this context, the incorporation of TMS and methyl groups into Cp

ligands of structurally identical complexes with the same central metal significantly decreased the polymerization time for DEVP polymerization and rendered even early lanthanocenes active.⁹⁵ One drawback of the metallocene catalysts is their relatively poor activity toward the N-containing monomers such as iPOx and 2-VP, hampering the synthesis of high molecular weight polymers and (block) copolymers.⁷⁵ This was solved by applying the abovementioned non-metallocene catalysts for their polymerization, giving access to high catalyst activities and enabling copolymerization with vinylphosphonates.^{68,75,81} A more detailed overview of the monomer scope for REM-GTP and the copolymerization of Michael-type monomers will be given in the next chapter.

2.1.3 Monomer scope and copolymerization

The general monomer structure for GTP is a Michael acceptor motif (α,β -unsaturated monomers), with a double bond in conjugation to a heteroatom for catalyst coordination, thus allowing for repetitive 1,4-conjugate addition as shown in the general polymerization scheme in Figure 10. Electronically, the monomers applied in REM-GTP require the overlap of p-orbitals in the α - and β -position of the heteroatoms to ensure an efficient conjugation of both double bonds. Therefore, the steric demand of substituents bound to the Michael-acceptor motif determines whether a monomer is polymerizable according to a GTP mechanism. Consequently, monomers like methyl acrylate (MA), MMA, and DMAA are accessible via (REM-)GTP (MA cannot be polymerized by REM-GTP, but is accessible with SKA-GTP). In turn, the distortion of the C-C bond of dimethyl methacrylamide (DMMA) due to a steric repulsion of the methyl substituents of the amide and in the α -position causes an insufficient overlap of said orbitals, hindering GTP (Figure 10).⁶⁷ The versatility of REM-GTP is, among others, founded on its broad monomer scope. Generally, the monomers are divided into N-coordinating and O-coordinating monomers. Structures that can be polymerized with rare earth metallocenes include a variety of (meth)acrylates, different N-containing vinylpyridine monomers, vinylphosphonates, acrylamides, and oxazolines as presented in the overview given in Figure 10.^{7,8,66–69,96,97} Despite applying a different catalyst system, Rieger et al. showed that also ‘extended’ Michael-type monomers could be polymerized via 1,6-conjugate addition following a GTP pathway.^{60,61}

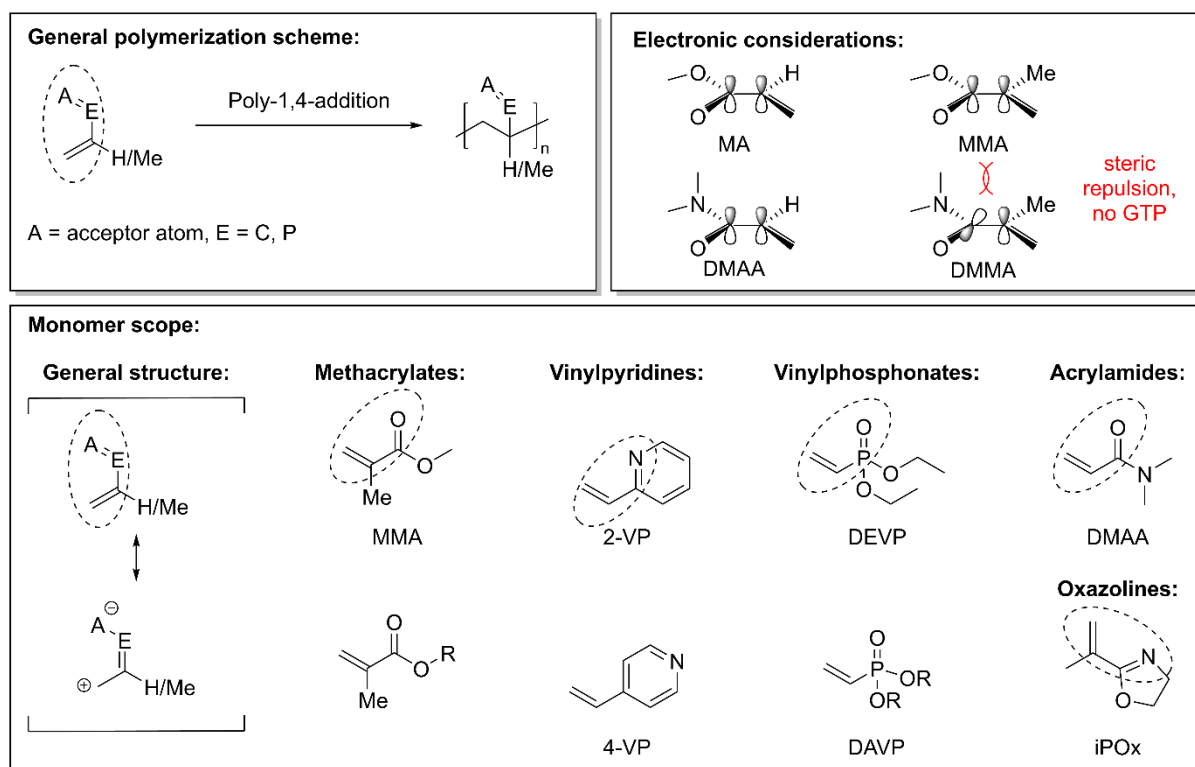


Figure 10: General reaction scheme of GTP and steric configurations of different Michael-type monomers (top). General resonance structure of α,β -unsaturated monomers for REM-GTP and examples of different Michael acceptor monomers (bottom).

A notable feature of poly(vinylphosphonates) is their thermoresponsive behavior. Aqueous solutions of DEVP homopolymers exhibit a lower critical solution temperature (LCST) and undergo reversible coil-globule transition within the physiological temperature range.^{64,70} A precise adjustment of the LCST in the range between 5 and 92 °C is possible upon copolymerizing different types of DAVPs and varying the ionic strength by adding NaCl. The statistical copolymerization of different alkyl-substituted vinylphosphonate monomers was confirmed via analysis of the copolymerization parameters ($r_1, r_2 \approx 1$), enabling a modification of the cloud points of DEVP upon copolymerizing varying amounts of either dimethyl vinylphosphonate (DMVP) or the propyl-substituted analog (DPVP).⁹³ Besides LCST behavior, poly(vinylphosphonates) were found to be promising candidates for flame retardants due to their excellent thermal stability.⁹⁸ Other appealing application areas of poly(vinylphosphonates) and Michael-type monomers, in general, become accessible upon copolymerization of different monomer classes. As REM-GTP remains in the eight-membered resting state presented in Figure 8 upon complete conversion of a monomer, block copolymerization with a second monomer is feasible by sequentially adding monomers to the catalyst.

Here, the coordination strength of the monomer to the catalyst metal center plays a crucial role. The sequential polymerization of monomers to yield block structures is only possible if the order of monomer addition corresponds to the coordination strength since weaker coordinating monomers cannot displace stronger coordinating monomers. Consequently, if the coordination strength of the first added monomer exceeds the coordination strength of the second monomer, only homopolymerization occurs. Detailed studies on block copolymerization of different Michael-type monomers via REM-GTP found the order presented in Figure 11.^{6,64,93,99}

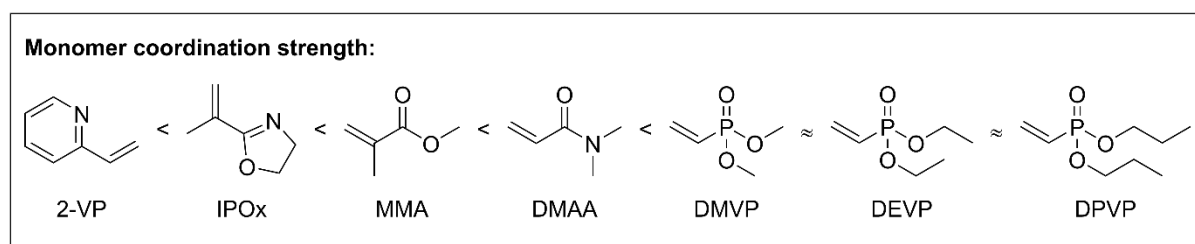


Figure 11: Coordination strength of different Michael-type monomers to the catalyst metal center.

A well-studied example of copolymerization involves combining 2-VP and DEVP, yielding amphiphilic AB-type P(2-VP-*b*-DEVP) block copolymers with both thermoresponsive and pH-responsive properties.¹⁰⁰ These copolymers involve hydrophobic, pH-responsive P(2-VP) blocks together with hydrophilic, thermoresponsive P(DEVP) blocks and, thus, can form micelles that respond to different stimuli, which makes them attractive polymers for diverse biomedical applications.^{7,83,100} By copolymerizing 2-VP as a first block, DEVP as a second block, diallyl vinylphosphonate (DAIVP) as the third monomer, and applying bifunctional pyrazine initiators yielding B'BABB'-type polymers, Rieger et al. realized the synthesis of dual-responsive nanoparticles with a cross-linkable shell bearing great potential for nanomedicine.¹⁰¹ In this context, similar studies utilized copolymers of 2-VP and vinylphosphonates as efficient nanocarriers for the anti-cancer drug doxorubicin or the delivery of small interfering RNA (siRNA).^{102,103} Considering a biomedical application area, these unique features of P(2-VP-*b*-DEVP) block copolymers are complemented by the high cytocompatibility of poly(vinylphosphonates), which has been subject to numerous studies.^{104,105} A final example of utilizing the amphiphilic character of this class of copolymers is the application to form photocatalytically active micelles for the reduction of CO₂. By introducing ortho-methylated bipyridines as initiators into a 2-

methoxyethylamino-bis(phenolate) yttrium catalyst via CH-bond activation and sequential monomer addition, the authors obtained multi-stimuli-responsive micelles with binding sites for a rhenium catalyst, which, in turn, could convert CO₂ to CO with moderate turnover frequencies.¹⁰⁶ In another study, the same synthetic approach could also be applied to the synthesis of responsive, ruthenium-containing micelles capable of reducing biomass-derived aldehydes.¹⁰⁷ Besides their stimuli-responsiveness, different synthetic polymer functionalization approaches exist to incorporate functionality into poly(vinylphosphonates), which will be discussed in the next chapter.

2.1.4 Polymer functionalization approaches for poly(vinylphosphonates)

End-group functionalization

CH-bond activation of 2,6-dimethyl pyridine motifs, as shown in Figure 7, emerged as an efficient tool to selectively incorporate distinct end-groups into polymers obtained via REM-GTP. In this context, a series of initiators that can be used in their native form and are preserved in the final polymer structure were introduced by Rieger et al. Besides classic *sym*-col applied in initial studies on the CH-bond activation of 2,6-dimethyl pyridines with rare earth metal catalysts, TMPy is a simple derivative that yields bimetallic catalysts. These binuclear species are of great interest as they enable the synthesis of BAB-type block copolymers from 2-VP and DEVP, successfully applied as multi-stimuli-responsive nanocarriers for the targeted delivery of doxorubicin to cancer cells.⁸³ Similarly, the application of 2-methyl bipyridine structures enabled copolymerization toward P(2-VP-*b*-DEVP), incorporating rhenium or ruthenium anchoring sites as end-groups in the polymers and thus giving access to catalytically active micelles.^{106,107} Next to these initiators, two ready-to-use *sym*-col derivatives susceptible to post-polymerization functionalization via click chemistry were presented. On the one hand, an azide-containing moiety enabled the polymerization of DEVP, which could be attached to multi-walled carbon nanotubes (MWCNT) via nitrene [2+1] cycloaddition in a graft-to approach, successfully stabilizing aqueous suspensions of MWCNT against coagulation.¹⁰⁸ On the other hand, a vinyl group-containing *sym*-col derivative was successfully attached to PDEVP following the general in situ catalyst generation and polymerization pathway. The corresponding polymer allowed the site-selective introduction of biologically active substrates such as thiocholesterol via thiol-

ene click chemistry.¹⁰⁹ Finally, a macroinitiator prepared via hydrosilylation enabled the polymerization of various monomers by either REM-GTP or ROP, yielding hybrid materials with an intermediate poly(dimethylsiloxane) block, demonstrating the high versatility of CH bond activation.¹¹⁰ Since REM-GTP does not tolerate acidic protons, initiators designed to introduce hydroxyl, amine, and thiol groups must be protected to facilitate polymerization via REM-GTP. These functionalities could be successfully introduced into poly(vinylphosphonates) by applying appropriate protecting groups, as shown in Figure 12. Subsequent deprotection under suitable conditions for each protecting group liberates the free functional end-groups of the polymers, making them accessible for further polymer-analogous transformations.^{111,112} Analogously, DEVP could successfully be polymerized with yttrium catalysts bearing a TMS-protected alkyne group, which was deprotected with K_2CO_3 to generate a motif for azide-alkyne click chemistry to decorate gold nanoparticles with PDEVP chains.¹¹³ Since only one motif of the initiator is present per chain, the *tert*-butyldimethylsilyl (TBDMS)-protected hydroxyl derivative could potentially be applied to estimate copolymer compositions via 1H NMR spectroscopy due to the distinct TBDMS-signals in the proton spectrum. Overall, the distinct position of the 2,6-dimethyl pyridine derivatives in the isolated polymers is an ideal site for end-group functionalization to introduce functionality into REM-GTP-originated polymers or to tether them to existing materials to modify their properties. An overview of different 2,6-dimethyl pyridine derivatives that were applied in REM-GTP of poly(vinylphosphonates) is given in Figure 12.

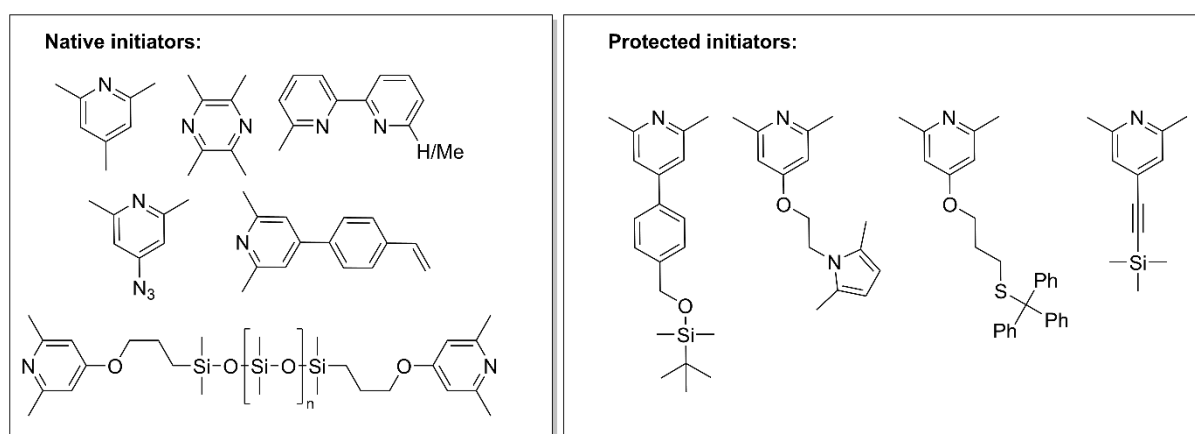


Figure 12: Overview of different 2,6-dimethyl pyridine derivatives introduced as initiators into rare earth metal complexes via CH-bond activation: Native initiators without the necessity for post-polymerization modification and protected initiators requiring end-group deprotection under appropriate conditions.^{83,106–112}

Next to end-group functionalization, various synthetic approaches for developing innovative polymer materials for functional applications exist to specifically target the side chains of poly(vinylphosphonates). An overview of these methods will be provided in the next section.

Side chain functionalization

Living-type polymerization techniques such as REM-GTP allow the precise control of molecular weights, compositions, and architectures while maintaining narrow polydispersities. Nevertheless, many controlled polymerization techniques are severely limited in their scope of functional monomers as functional groups often interfere with the living-type character or cause side reactions, leading to a loss of reaction control.¹¹⁴ In REM-GTP, the catalysts' sensitivity to any protic motifs excludes numerous functional groups, wherefore suitable protecting group strategies were developed.¹¹¹ An elegant approach to circumvent these limitations is introducing functionality via post-polymerization functionalization of monomers with inert side chains that allow living-type polymerization.¹¹⁴ For poly(vinylphosphonates), the groundwork for this was laid by the introduction of diallyl vinylphosphonate (DAIVP) as a 'disguised' functional monomer, which can be statistically or block copolymerized with DEVP and is susceptible to polymer-analogous transformations via thiol-ene click chemistry.^{96,101,102} Other functionalization approaches of the DAIVP side chains explored the bromination and epoxidation of the double bonds. While this partially succeeded, these procedures were discarded due to low functionalization degrees and solubility issues of the functionalized polymers.⁹⁶ For allyl group-containing poly(vinylphosphonates), the thiol-ene click reaction is the method of choice since it is highly efficient and reliable, outperforming other approaches. Thiol-ene click reactions proceed with high rate, selectivity, and conversion under mild conditions, yielding little to no side products. Furthermore, the reaction tolerates a broad range of functional groups among the substrate scope of thiols and is relatively robust toward moisture and oxygen. Additionally, it can be photoinitiated, allowing a high spatiotemporal control over the initiation. Finally, thiol-ene click reactions are orthogonal to other common organic reaction types, making it a highly suitable and efficient tool for incorporating functional motifs into vinyl group-containing polymers.^{115–119} Mechanistically, the thiol-ene reaction involves a thiol and an 'ene', referring to a

double bond, to form a thioether. Depending on the alkene substrate, the reaction proceeds base or nucleophile-initiated as a thiol-Michael addition for electron-deficient, acceptor-substituted alkenes (A = ester, amide, nitrile, Figure 13) or according to a radical mechanism for all other alkenes. For the more common radical processes, the mechanism includes initiation, propagation, chain transfer, and different termination reactions. Initiation is achieved thermally or photochemically by applying appropriate initiators, e.g., azobis(isobutyronitrile) (AIBN) or 2,2-dimethoxy-2-phenylacetophenone (DMPA) and leading to the formation of thiyl radicals by hydrogen abstraction. These react with the double bonds to yield the C-S bond and a carbon radical in the propagation step, resulting in the anti-Markovnikov product. The catalytic cycle is completed by a chain transfer presenting the rate-determining step in most cases, in which the carbon-centered radical abstracts a proton of another thiol substrate and sustains the reaction. As for most radical processes, different termination reactions by the combination of two radicals can take place, as shown in Figure 13.^{116,119–121}

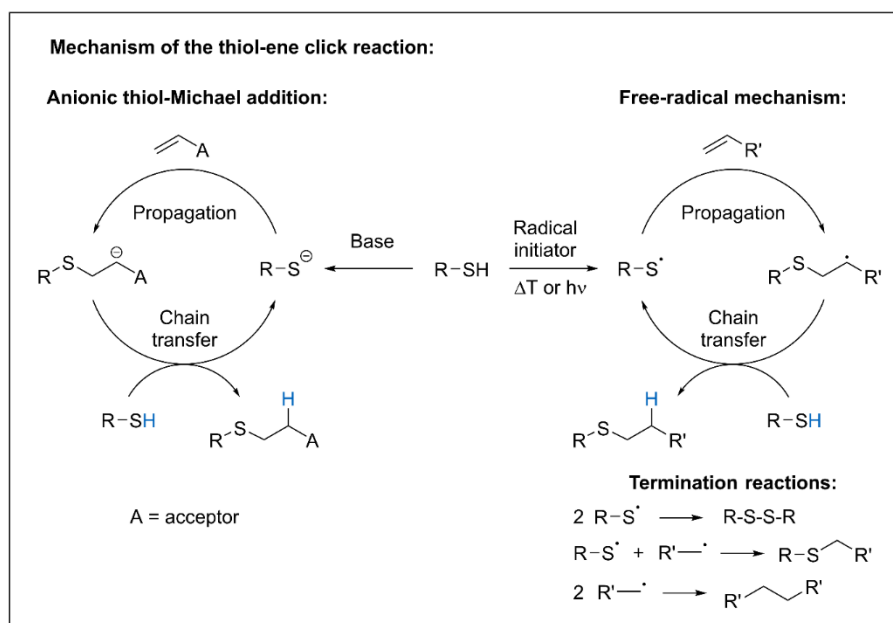


Figure 13: Mechanisms of the thiol-ene click reaction: Anionic thiol-Michael addition, free-radical mechanism and termination reactions.

For poly(vinylphosphonates), thiol-ene click chemistry was widely applied to transform vinyl group-containing end groups introduced via the initiator or side chains of DAIVP-containing co- and terpolymers. In this context, different biologically active substrates like thiocholesterol (targeting the cell walls) or folic acid (growth factor) in a two-step approach involving a click reaction with cysteamine and subsequent amide formation

were attached to the end or side groups of allyl group-containing poly(vinylphosphonates).¹⁰⁹ Elaborate studies focused on incorporating these motifs into the same polymer in a modular, highly precise fashion. This was possible by integrating di(trimethylsilyl)propargyl vinylphosphonate (DPrTMSVP) as a third block into P(DEVP-*b*-DAIVP) block copolymers, allowing the incorporation of thiocholesterol by thiol-ene click chemistry preserving the propargyl groups for a following azide-alkyne cycloaddition to introduce the folic acid structure. Ultimately, this resulted in the synthesis of functional polymer materials with biomedical application potential due to cytocompatibility.¹⁰⁴ Other innovative approaches for applying poly(vinylphosphonates) in biological settings involved synthesizing dual-responsive ABB' triblock terpolymers P(2-VP-*b*-DEVP-*b*-DAIVP) to form micelles with a cross-linkable shell. These cross-linked nanoparticles showed attractive material properties exhibiting pH-responsiveness inherent to the 2-VP units and LCST behavior caused by the poly(vinylphosphonates).¹⁰¹ Similar uncross-linked systems allowed the efficient delivery of the anti-cancer drug doxorubicin to cancer cells with these carefully designed, non-cytotoxic nanocarriers, revealing the large potential of such high-precision nanoobjects.⁸³ Based on these studies and the possibility of statistical DEVP and DAIVP copolymerization to P(DEVP-*stat*-DAIVP), the thiol-ene click reaction is an elegant approach to cross-link poly(vinylphosphonates) covalently with appropriate dithiols. Such cross-linked polymer materials exhibit vast application potential, which will be discussed in later chapters.

An alternative method for the post-polymerization modification of side chains already reported in fundamental studies on vinylphosphonate REM-GTP was the polymer-analogous hydrolysis of poly(vinylphosphonates) toward poly(vinylphosphonic acid) (PVPA).⁷⁰ This well-established procedure involves the reaction of polymers with trimethylsilyl bromide (TMSBr) under elevated temperature, leading to a side chain dealkylation of the phosphonates, as shown in Figure 14.¹²²

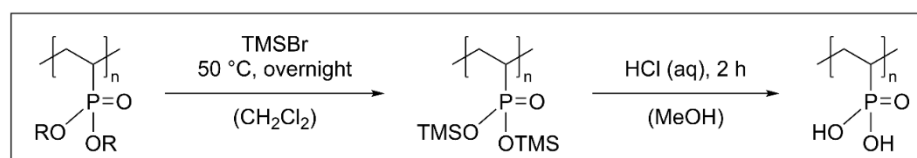


Figure 14: Polymer-analogous hydrolysis of poly(vinylphosphonates) to poly(vinylphosphonic acid).^{70,122}

One application of this synthetic approach is the quantitative hydrolysis of PDEVP toward PVPA, yielding a polyelectrolyte for complex coacervation, a field of research particularly interesting for understanding fundamental processes related to the origin of life. In this context, mixtures of oppositely charged polyelectrolytes undergo liquid-liquid phase separation, forming a polyelectrolyte-rich phase (coacervate) and a polyelectrolyte-dilute phase (supernatant). Thus, combining PVPA with polycationic peptides, which could be activated and deactivated by an esterification/hydrolysis cycle with chemical fuel, reversibly removing and adding charges, led to the formation of highly dynamic coacervate droplets.^{123–125}

2.2 Cross-linked polymer materials

Cross-linked polymer materials comprise a large class of materials, ranging from stiff and robust materials like epoxy resins or cross-linked polyurethanes to flexible materials like silicone rubbers to soft, tissue-like materials like hydrogels, to name only some examples.^{3,126–128} They can, among others, be classified according to their cross-linking mechanism (chemically cross-linked, physically cross-linked, dynamic covalent bonds), structural characteristics (thermosets, elastomers, hydrogels), chemical composition (natural polymers, synthetic polymers) or according to their application area.^{129–138} Hydrogels are a subclass of cross-linked materials that can retain significant amounts of water within their three-dimensional, cross-linked structures without dissolving.¹³⁹ Hydrogels exhibit a broad range of attractive material properties, including high water absorption, mechanical stability, biocompatibility, stimuli-responsiveness, and degradability, making them appealing candidates for a large spectrum of applications.^{140–145} The polymers commonly utilized for hydrogel formation are divided into natural and synthetic polymers depending on their origin. Famous examples of natural polymers include alginate,¹⁴⁶ chitosan,¹⁴⁷ agarose,¹⁴⁸ hyaluronic acid,¹⁴⁹ or cellulose derivatives.¹⁵⁰ In contrast, synthetic networks are often formed from hydrophilic polymers like poly(ethylene glycol) (PEG),^{151,152} poly(vinyl alcohol) (PVA),^{153,154} poly(acrylic acid) (PAA),^{155,156} or poly(N-isopropyl acrylamide) (PNIPAAm),^{157,158} among many more. An overview of these examples is given in Figure 15.

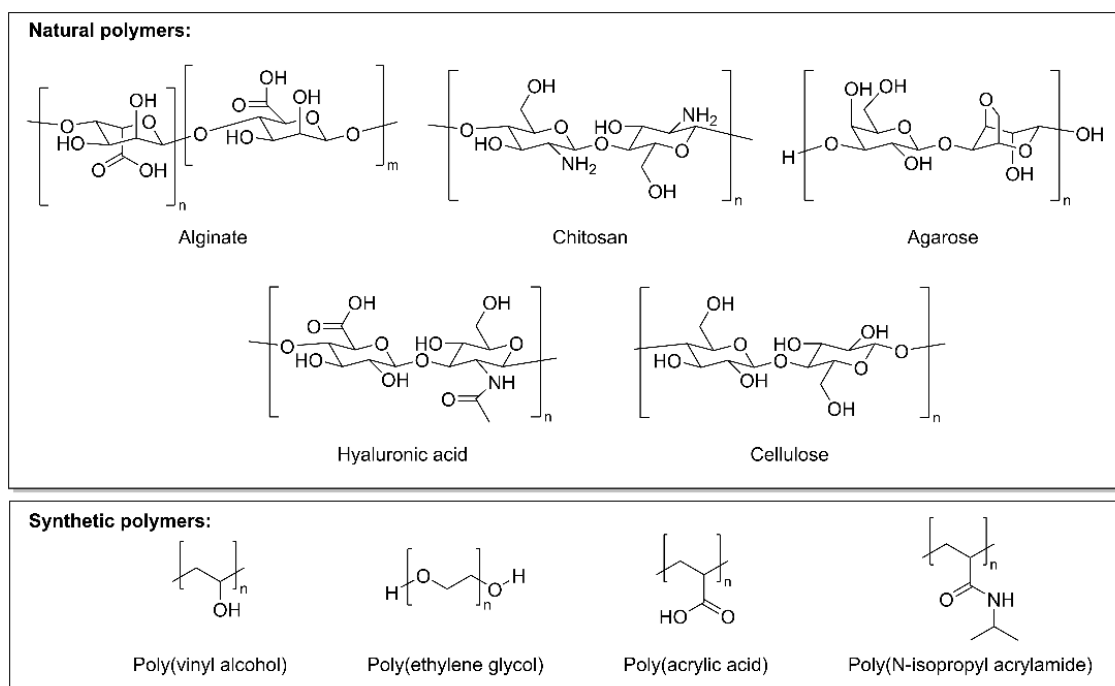


Figure 15: Overview of selected examples of natural and synthetic polymers for hydrogel synthesis.

2.2.1 Classification of cross-linking mechanisms

Several cross-linking mechanisms exist to form hydrogels from precursor polymers. Different cross-linking types have been defined depending on the nature of the cross-links to induce network formation. The following overview introduces various cross-linking mechanisms and highlights their advantages and drawbacks.

Chemical cross-linking

Chemically cross-linked hydrogels are classified as three-dimensional networks held together by covalent linkages between the polymer chains. For such covalently cross-linked hydrogels, numerous cross-linking chemistries have been reported with specific advantages inherent to the reaction conditions of each cross-linking reaction. In general, since its introduction by Sharpless and co-workers in 2001, click chemistry emerged as an efficient tool for such cross-linking processes since it ensures high yields and selectivities, non-toxic side-products, and mild reaction conditions.¹⁵⁹ A significant advantage of these reactions, which simply ‘click’ (high reaction rates, yields, and selectivities) and do not require elaborate reaction protocols, is that they open up the field of hydrogels for many applications since this chemistry is implementable by researchers across diverse fields who are not chemical experts.¹⁶⁰

Examples of such click chemistries for hydrogel formation involve thiol-ene click reactions^{161–163} or copper-catalyzed azide-alkyne cycloaddition.^{164,165} Besides this, traditional radical polymerization methods with polar monomers yield hydrophilic, cross-linked materials by copolymerization with multifunctional monomers, resulting in chain growth in different dimensions and the one-pot synthesis of cross-linked networks. In this context, synthetic hydrogels are often obtained from various (meth)acrylate or acrylamide derivatives as well as different PEG-based monomers.^{166–169} Chemical cross-linking often involves auxiliary reagents capable of undergoing irreversible reactions with pendant polymer side chains. These cross-linking reagents incorporate reactive groups like aldehydes, halides, or epoxides, which readily react when combined with polymers with nucleophilic groups like alcohols or amines. Well-researched representatives of such cross-linking reagents are epichlorohydrin and glutaraldehyde, widely used to form poly(saccharide)- or PVA-derived hydrogels^{170–173} In case the cross-linkers cannot react with the polymers directly, either of the compounds may be activated by appropriate chemical transformations such as conversion into active esters using N-hydroxysuccinimide (NHS).^{174,175} A final approach toward covalent cross-linking of (bio)macromolecules utilizes enzymes such as transglutaminase, peroxidases, lactamases, or phosphatases to cross-link appropriate substrates with high selectivity by either activating the substrates or catalyzing covalent bond formation.^{176–178} Regardless of the synthetic approaches toward covalently cross-linked hydrogels, chemical cross-linking of polymer chains offers several advantages from an application perspective. Covalently cross-linked polymer networks generally offer a relatively high mechanical strength as the covalent bond is the strongest among the intramolecular interactions. Consequently, materials formed upon chemical cross-linking can be very tough and resilient, showing no fatigue and high fracture energies due to efficient energy dissipation caused by the rigidity of covalent bonds. This is crucial for applications with high mechanical stress, such as wearable devices or tissue engineering.^{179,180} The mechanical strength is also linked to exceptional durability, resistance to degradation, and thermal and chemical stability, which must be ensured for several (bio)medical applications to guarantee longevity and reliability.^{181–184} Another advantage is that macromolecular bond engineering to form covalently cross-linked materials can be

applied to form tailored network architectures. In this regard, synthetic, covalently cross-linked polymers often allow a precise adjustment of the cross-linking density, which controls water uptake, mechanical properties, and pore sizes and provides a good reproducibility of hydrogel synthesis.^{185,186} Finally, these tailored architectures enable the incorporation of specific properties into the cross-linked materials by, e.g., functionalizing the cross-linker with cleavable groups and creating specific release profiles by controlling network degradation.^{187–189}

Nevertheless, these permanent, static cross-links suffer from certain drawbacks. As the covalent cross-links are formed irreversibly, damage to the materials can cause a loss of material properties as these materials cannot self-heal. Furthermore, chemical cross-linking often relies on complex synthetic procedures, which cannot only be tedious but might also suffer from the use of toxic chemicals. Such hydrogels can only be employed in biological settings if potentially cytotoxic compounds such as cross-linking agents or initiators are carefully removed upon purification of the materials.¹⁷⁶ Inspired by nature, covalent cross-links are often complemented by physical cross-links to overcome some of these issues. The next section will explain these supramolecular interactions in more detail. The advantages and drawbacks of chemical cross-linking are summarized in Figure 16.

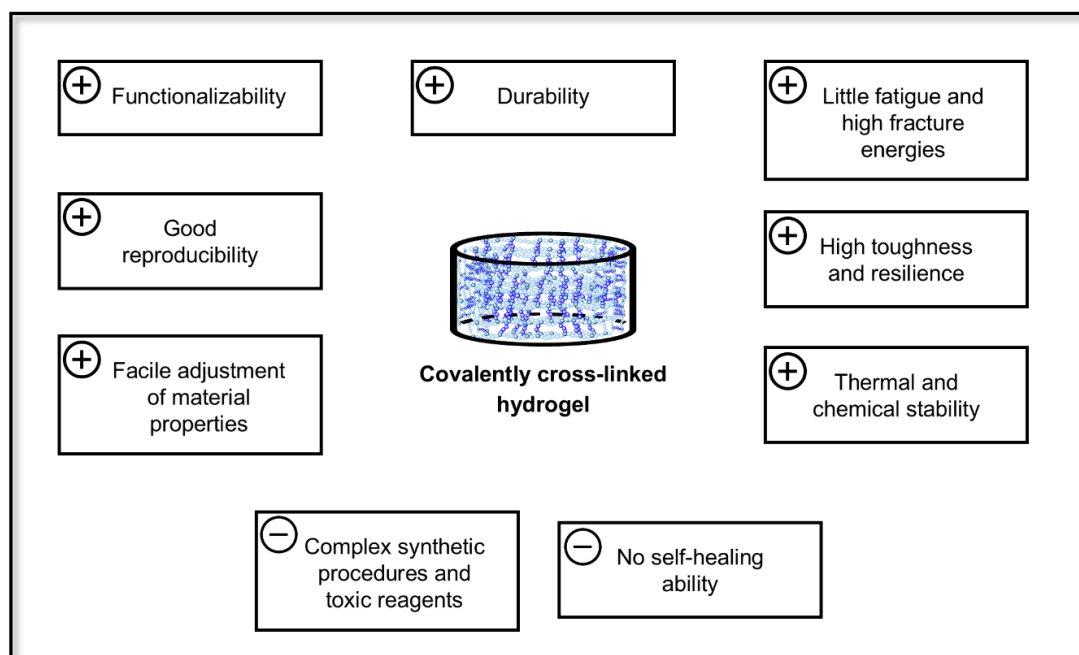


Figure 16: Advantages and drawbacks of chemically cross-linked hydrogels.

Physical cross-linking

Contrasting the chemically cross-linked hydrogels discussed above, physical cross-linking involves supramolecular interactions between the polymer chains in a network rather than covalent chemical bonds. To form hydrogels, numerous physical interactions have been reported. These include hydrogen bonding,^{190,191} ionic interactions,^{192,193} Van der Waals forces,¹⁹⁴ hydrophobic interactions,^{195,196} host-guest chemistry,^{197,198} and physical entanglements,^{199,200} or combinations of multiple supramolecular interactions.^{201,202} Supramolecular networks are often formed on the base of natural polymers, causing intrinsically higher biocompatibilities of these networks compared to their synthetic analogs, which is attractive for applications in a biomedical context.^{203,204} Another notable feature of hydrogels formed upon physical cross-linking is their ability to self-heal due to the high reversibility of non-covalent cross-links. Unlike covalently cross-linked materials, supramolecular networks retain their original properties after structural damage by reforming the physical cross-links.^{205,206} Accompanied by these highly dynamic bonds, physical hydrogels reveal shear-thinning behavior, rendering them applicable as injectable drug delivery platforms. This feature is often complemented by the stimuli-responsiveness of the polymers applied in supramolecular hydrogels, leading to a vast potential for application in targeted drug delivery.^{207,208} In the context of drug delivery, physical cross-linking allows precisely tuning the hydrogel degradation kinetics, ensuring a site-specific release of encapsulated drugs with the desired release profile.^{209,210} This is facilitated by the high water contents in physically cross-linked networks through extensive swelling, mimicking the extracellular matrix, and reducing the toxicity of potentially harmful substances.^{211,212} A final advantage of physical hydrogels worth mentioning is their excellent recyclability, as the high reversibility of supramolecular interactions allows the reuse and reprocessing of the materials.^{213,214} These advantages are summarized in Figure 17 and compared to chemically cross-linked hydrogels.

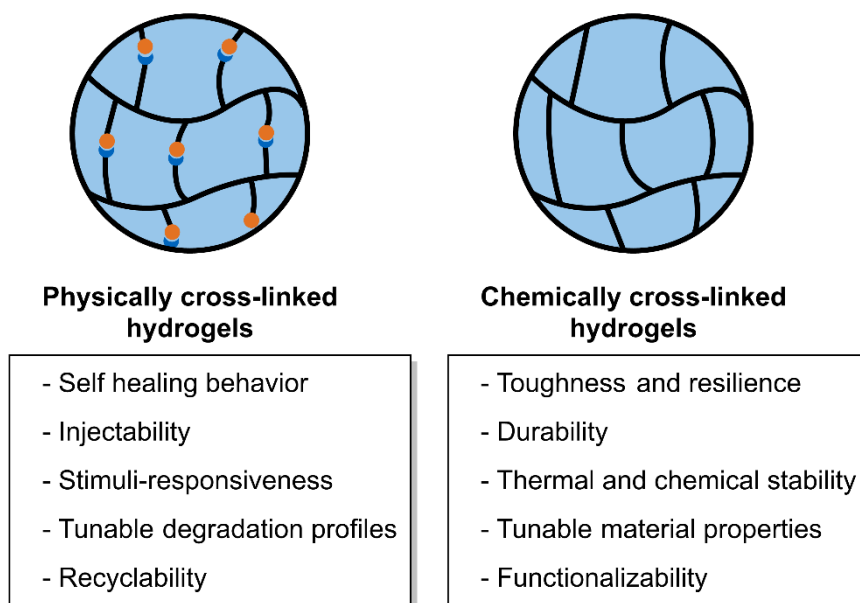


Figure 17: Advantages of physically cross-linked hydrogels compared to the advantages of chemically cross-linked hydrogels.

Nevertheless, physically cross-linked systems also suffer from certain drawbacks that, in some cases, restrict an even broader application potential. In this context, their low mechanical stability, load-bearing capacity, and limited long-term stability sometimes make them unsuitable for, e.g., cartilage replacements or bone repair.^{215,216} Furthermore, as many systems are based on natural polymers, functionality is harder to introduce than in synthetic, covalently cross-linked analogs.²¹⁷ Additionally, extensive swelling can lead to a loss of the structural integrity of the hydrogels, which is required for some purposes and might also lead to the undesired leaching of substances from the networks.²¹⁸ To overcome these drawbacks while maintaining the beneficial properties of physically cross-linked hydrogels, materials based on dynamic covalent interactions were developed, which will be presented in the next section.

Dynamic covalent chemistry

Dynamic covalent chemistry emerged as a promising synthetic platform for developing materials that combine the beneficial properties of chemically and physically cross-linked networks. Dynamic covalent cross-links blend the strength of covalent bonds with the reversibility of supramolecular interactions, thereby creating remarkable properties of the resulting materials.²¹⁹ The corresponding materials, often referred to as dynamic covalent networks (DCNs), exhibit shear-thinning behavior, enabling extrusion and facilitating injectability, and allow self-healing through reversible covalent

bond formation, which, in addition, enables processing via molding.^{220–223} Similarly to the supramolecular hydrogels in the section above, these systems are widely applied in targeted drug delivery. Here, DCNs are highly relevant candidates as they can serve as injectable drug carriers, and the reversibility of the dynamic covalent bonds causes hydrogel formation and dissociation in response to triggers such as temperature, pH value, or the presence of specific chemical motifs.^{224–227} Additionally, materials formed through dynamic covalent chemistries are highly adaptable and reconfigurable, resulting in excellent recyclability due to the highly dynamic bond character while at the same time enabling a facile adjustment of the mechanical properties by varying the cross-linking density.^{228,229} As these hydrogels combine the properties of chemically and physically cross-linked networks, their durability is increased compared to the supramolecular compounds.²³⁰ Combining all of the properties mentioned above allows applications of DCNs in advanced research fields such as drug delivery, smart coatings, optics, and electronics.^{225–227,230–232} Despite the numerous advantages of DCNs facilitated by the high network dynamics, it must be noted that the development of innovative materials based on dynamic covalent bonds requires careful consideration of the trade-off between the mechanical strength and the dynamics (responsible for self-healing, reconfiguration, etc.).²²⁹

Various dynamic covalent chemistries have been reported, including Diels-Alder reactions,^{233,234} Schiff base equilibria,²³⁵ transesterifications,²³⁶ disulfide bond formation,^{237,238} and dynamic boronic ester complexation.^{221,222,225} An overview of different dynamic covalent interactions is presented in Figure 18. One example of interest for this thesis are DCNs formed upon boronic ester complexation. In this context, boronic acids tend to undergo cyclization reactions with 1,2- and 1,3-diols, forming stable five- or six-membered rings (Figure 18, bottom).²³⁹ The condensation reaction occurs at high rates without a catalyst, with reaction rates influenced by the specific boronic acid and diol substrates, resulting in product formation governed by thermodynamic control.^{135,222,240,241} This binding specificity renders DCNs based on boronic ester complexation applicable as probes for, e.g., sugar sensing, and the highly dynamic bond character gives access to biocompatible, injectable hydrogels appropriate for drug delivery.^{221,225,242,243}

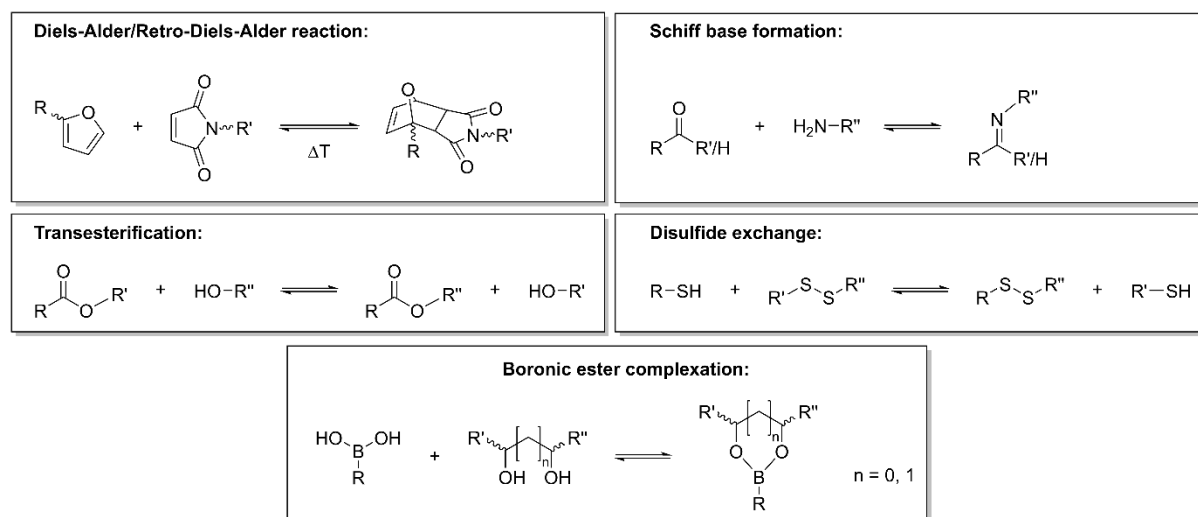


Figure 18: Overview of different dynamic covalent chemistries.

Generally, tailoring the material properties toward the requirements of a particular application demands an in-depth analysis of newly developed materials to obtain a profound understanding of the structure-property relationships governing their macroscopic properties. The next chapter will elucidate such structure-property relationships and aims to generalize some structural features and their corresponding effects on the hydrogel properties to introduce some design principles for developing materials for functional applications.

2.2.2 Structure-property relationships in cross-linked materials

Mechanical properties

The mechanical properties of hydrogels strongly depend on various factors. First and foremost, as discussed in the previous chapter, the hydrogels' mechanical strength and toughness are strongly affected by the type of interactions forming the cross-links. Whereas covalent bonds tend to form more robust hydrogels, physical interactions result in softer materials due to the intrinsic bond strength of the respective interaction. Nevertheless, numerous structural parameters are available to precisely tune the mechanical properties to the targeted application. Cross-linking density plays a crucial role in modulating hydrogels' mechanical features, with highly cross-linked gels often exhibiting higher stiffness and strength at the cost of reduced elasticity and swelling capacity.^{244,245} Similarly, the cross-linker contributes to the overall mechanical performance by controlling the material properties depending on its concentration,

rigidity, and architecture.^{245,246} Another essential criterion of hydrogel structures impacting the resilience of cross-linked materials is network homogeneity, which must be ensured to guarantee a uniform load-bearing capacity.^{247,248} The mechanical properties can also be steered by applying synthetic polymer chemistry to control the hydrophilicity and structures of monomers, which can, e.g., induce secondary supramolecular interactions in the hydrogel structures, inducing additional mechanical strength.²⁴⁹ In this context, combinations of different cross-linking approaches in double networks can yield strong and stiff structures with primary structures formed upon covalent cross-linking and supramolecular secondary structures, combining the advantages of different hydrogels.²⁵⁰ Similar synergistic effects were also achieved by combining only physical cross-linking methods, whereas this additionally provided advantages like shape memory or self-healing.^{201,202} Lastly, controlling the mechanical features of hydrogels is possible through composite or hybrid structures. In this context, nanofillers such as nanofibers or nanoparticles are embedded as additives in the hydrogels, modulating the mechanical properties of the materials.^{251,252}

Water uptake

In analogy to the mechanical properties, the water uptake of hydrogels is intricately linked to their molecular structure, chemical composition, and interactions with the environment. The water absorption capacity inversely correlates with the cross-linking density as it is strongly associated with the chain mobility of the polymers required for hydration.²⁵³ As with the mechanical features, the homogeneity of the networks enables uniform and even swelling, which is desired in most cases.²⁵⁴ Another structural feature attributed to the water uptake is the pore size and pore size distribution in the hydrogels. In this context, hydrogels with larger pores reveal faster swelling kinetics as they accommodate more water within their structures.²⁵⁵ Beyond structural considerations, the hydrogels' chemical composition is crucial concerning water uptake. Hydrophilic polymers containing hydroxyl, amine, or carboxylic acid groups, often found in naturally occurring biopolymers, lead to high water uptakes.^{143,146,149,150} Additionally, introducing ionic or charged groups such as sulfonates or carboxylates tremendously increases the water uptake by electrostatic interactions (solvation of ionic species) and through osmotic effects, causing water diffusion into the networks. This effect is the base of superabsorbent hydrogels used

in diapers and other fields.^{256,257} Synthetic polymer chemistry allows the selective introduction of ionic species like sulfonates into the networks, significantly increasing the water absorption values.²⁵⁸ An indirect factor in this respect concerns acid- or base-responsive moieties in the polymers. Hydrogels incorporating carboxylic acid units, such as carboxymethylcellulose-derived hydrogels or amines like chitosan-based hydrogels, exhibit pH-responsive swelling. Consequently, such functional groups in the hydrogel microstructure affect their water absorption behavior.^{259,260} Overall, this section demonstrates the delicate interplay between polymer structural features, cross-linking density, and other factors governing the water uptake, which must be considered when tailoring the water uptakes of certain materials to specific applications.

Biocompatibility

A crucial feature of hydrogels for applications in a biomedical context is their biocompatibility, which is governed by different factors, some of which should be discussed in the following. These include the presence of specific functional groups and bioactive domains, the application of natural polymers, and different structural features such as porosity and surface roughness. Firstly, hydrophilic functional groups like hydroxyl, amine, sulfonate, or carboxylic acid moieties positively impact biocompatibility since these groups tend to enhance the water affinity, thereby minimizing unspecific protein adsorption and decreasing inflammatory response. Furthermore, these hydrophilic motifs can improve the immobilization of cells. The high water contents of such hydrophilic polymer networks mimic the extracellular environment and allow cell proliferation.^{261–264} Biocompatibility can be further enhanced by incorporating biologically active domains, such as RGD (arginine-glycine-aspartate) motifs, or adding anti-oxidant motifs to reduce the oxidative stress, thereby increasing the resemblance of the hydrogels to the extracellular matrix.^{265,266} When targeting biomedical applications, natural polymers like alginate or hyaluronic acid are often preferred over synthetic polymers since biopolymers show high biocompatibility.^{146,149} Nevertheless, numerous examples of synthetic, biocompatible hydrogel materials originate from PEG, PVA, or other polymers.^{151,267,268} Two final aspects that should be considered regarding biocompatibility are the morphology and the surface topography of hydrogels for biomedical applications. For designing

biocompatible materials, porous structures could aid in embedding cells, facilitating nutrient and oxygen transport, thus supporting cell viability and proliferation.²⁶⁹ Considering the correlation between hydrogel topography and cell behavior, the effect highly depends on the cell type and cross-linked material. Although there is no clear correlation between surface topography/roughness and biocompatibility, it is essential to remember that this factor can strongly affect the cell adhesion to hydrogel surfaces.²⁷⁰ Many other aspects affect biocompatibility; however, this overview demonstrates the complexity of designing new materials for biomedical applications and provides some design considerations for biocompatible hydrogels.

Functionality

Hydrogel structures can be specifically tailored to inherit a particular function. Firstly, functional, stimuli-responsive, cross-linked materials are highly relevant as there is a high demand for materials that can react to a specific trigger, e.g., temperature or pH value, as the next chapter on applications will demonstrate. To introduce thermo-responsiveness, polymers with LCST behavior are applied for hydrogel synthesis. The most prominent representatives of these materials are hydrogels based on cross-linked PNIPAAm, allowing a precise adjustment of the LCST, resulting in the collapse of the network above that temperature.²⁷¹ For pH-responsive hydrogels, incorporating polymers owing acidic or basic units results in pH-dependent swelling or deswelling of the gels. Famous examples of polymers exhibiting these properties are the biopolymers chitosan or carboxymethylcellulose.^{259,260} Furthermore, the functionality of hydrogels in a biological setting may be increased by introducing cross-linkers with specific degradation profiles, enabling the sustained release of a drug.²⁷² Hydrogel degradation can also be achieved by incorporating light-responsive moieties into the networks, allowing selective photocleavage upon irradiation. Similarly, light-responsive precursors enable the light-induced assembly toward supramolecular hydrogels, and photo-cross-linkable mixtures of monomers with appropriate cross-linkers and initiators facilitate photochemical cross-linking with high spatiotemporal control.^{152,163,273,274} Additionally, numerous studies focus on catalytically active hydrogels formed upon peptide assembly and capable of selectively catalyzing reactions of organic substrates such as ester hydrolysis.²⁷⁵ In a similar approach, catalytic activity could be introduced in peptide-containing hydrogels by incorporating

Cu(I) metal complexes, enabling copper-catalyzed azide-alkyne click reactions of various substrates within the materials.²⁷⁶ Finally, for electrochemical applications, the addition of conductive fillers, polymerization of conductive monomers within an existing hydrogel matrix or the cross-linking of conductive polymers by dopant molecules might be of interest to obtain electrically conductive hydrogels which exhibit significant potential for responsive systems, artificial skins, batteries, solar cells or supercapacitors.²⁷⁷ These selected examples show the widespread application potential of hydrogel materials and underline the facile introduction of functionality into such materials. The key findings of this chapter on structure-property relationships in hydrogels are summarized in Figure 19.




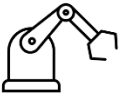
Factors affecting the macroscopic properties of hydrogels			
 Mechanical properties	 Water uptake	 Biocompatibility	 Functionality
<ul style="list-style-type: none"> ▪ Type of cross-links ▪ Cross-linking density ▪ Cross-linker concentration, rigidity, and architecture ▪ Network homogeneity ▪ Synthetic polymer design ▪ Secondary interactions ▪ Nanofillers (e.g. fibers) 	<ul style="list-style-type: none"> ▪ Type of cross-links ▪ Cross-linking density ▪ Pore size ▪ Chemical composition ▪ Hydrophilicity ▪ Presence of ionic or charged groups 	<ul style="list-style-type: none"> ▪ Presence of hydrophilic groups (OH, NH₂, COOH, etc.) ▪ High water contents ▪ Biologically active motifs ▪ Application of biopolymers ▪ Porosity ▪ Consideration of hydrogel topography 	<ul style="list-style-type: none"> ▪ Stimuli-responsive polymers ▪ Light-responsive (dis)assembly ▪ Catalytically active hydrogels ▪ Introduction of metal complexes ▪ Addition of conductive polymers or fillers

Figure 19: Summary of structure-property relationships in hydrogels providing design considerations for developing innovative materials.

2.2.3 Application areas of hydrogels

Stimuli-responsive materials

The importance of stimuli-responsiveness has been highlighted numerous times throughout this theoretical overview of hydrogels. This section will introduce different, highly elaborate applications of cross-linked materials reacting to a specific external stimulus (pH, temperature, light, etc.). Firstly, such hydrogels are highly important candidates for sensing applications. In this context, pH-responsive materials exhibit highly pH-dependent swelling and collapse, allowing monitoring of the pH value by investigating the swelling state. An appropriate analytical technique to obtain insights into the swelling dynamics of hydrogels is a quartz crystal microbalance with dissipation monitoring (QCM-D), widely applied to study the swelling behavior and viscoelastic properties of thin hydrogel films. QCM-D correlates the frequency decrease of resonating quartz electrodes upon mass deposition to the mass on the sensors, simultaneously determining the energy dissipation as a measure of the viscoelastic properties of the film.²⁵⁹ The schematic operating principle of QCM-D is presented in Figure 20.

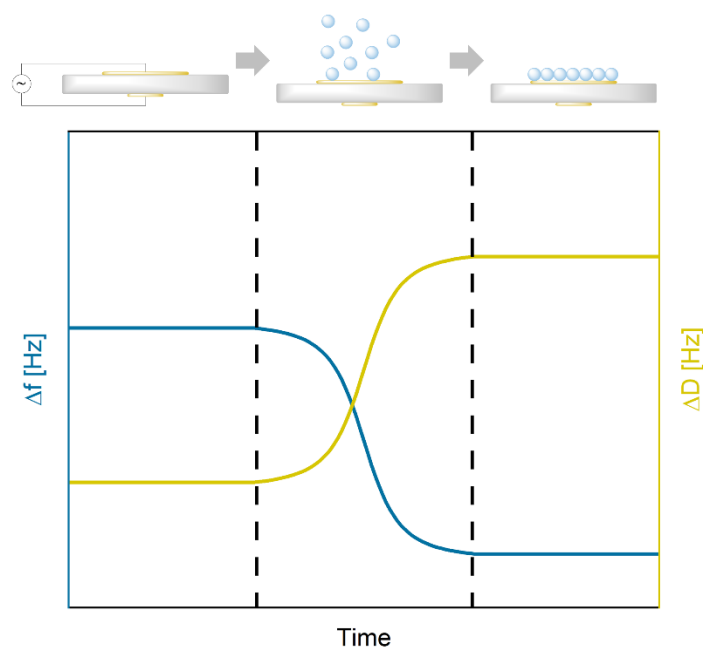


Figure 20: Operating principle of QCM-D.

Applying QCM-D with appropriate, pH-responsive hydrogels allows for the utilization of this analytical technique to obtain gravimetric pH-sensors.^{259,278,279} Another class of

hydrogels for sensing applications involves DCNs formed upon boronic ester complexation. In this context, the binding affinity of different diols to boronic acid derivatives enables diol-sensing and the creation of glucose-responsive hydrogels, which are highly relevant for treating chronic diseases like diabetes.^{226,227,243,280} Furthermore, the group of light-responsive hydrogels incorporating photo-sensitive motifs in their networks is highly interesting for controlled drug delivery by selective network degradation.^{273,274} Besides this, irradiation of hydrogels with photo-isomerizable azobenzene cross-linkers allows the ultraviolet (UV) light-mediated modulation of the hydrogels' mechanical properties. This, in turn, is crucial to studying the behavior of cells on surfaces in response to surface-stiffening, providing a profound understanding of mechanosignaling in cells.^{281,282} Applying photo-cross-linkable mixtures capable of forming hydrogels on surfaces further enables photolithographic micropatterning, which is interesting for cell culture in tissue engineering and microelectronics.^{283–285} An emerging field of research involving stimuli-responsive materials is actuators and soft robotics. In this field, highly elaborate hydrogel hybrid materials are developed. Actuation with hydrogels describes inducing a mechanical motion of a material upon application of an external stimulus. These stimuli, e.g., temperature, pH value, light, or electrical fields, trigger changes in the network structure, leading to swelling, shrinking, or bending. Motion is induced in the hydrogel materials by carefully designing systems with inhomogeneous swelling properties following the external stimulus.⁴ In this context, homogeneous materials undergo deformation by applying inhomogeneous triggers such as a gradient electrical field.²⁸⁶ In contrast, combining different hydrogels toward inhomogeneous hybrid materials like bi-layered hydrogels allows directed motion by applying a homogeneous stimulus like a temperature change.^{287,288} Following these design guidelines for actuators, various actuators and soft robots for different applications were developed based on pH-,^{289,290} light-,^{291,292} and thermo-responsiveness.^{287,293–295}

Biomedical applications

Hydrogels are commonly applied in biological settings, as they can be derived from biocompatible, non-cytotoxic natural or synthetic polymers, and their soft, water-swollen structures resemble biological tissues and the extracellular matrix. Further, as discussed in the previous chapter, hydrogel structures can be tailored to meet the specific application requirements by modification of the pore size, degradation profiles, and stimuli-responsiveness.^{261–263,269} Therefore, hydrogels represent a broad platform for drug delivery, allowing the controlled release of active pharmaceutical ingredients and targeted therapies for chronic diseases.^{203,210,225,296} Next to this, hydrogels are often applied in regenerative medicine and tissue engineering, serving as scaffolds for the regeneration of skin, cartilage, and bone.^{148,180,297–299} Furthermore, they support wound healing by serving as moisture-retaining components in wound dressings with the ability to deliver growth factors and antimicrobial agents.^{300,301} Hydrogels with antibacterial properties are appealing candidates for functional coatings of materials applied in biomedical contexts, e.g., biosensors or other implantable devices.^{268,302} Finally, hydrogels are implemented in medical products such as soft contact lenses, enabling oxygen permeability and extended wear.^{303,304} In biomedical contexts, additive manufacturing emerged as an efficient processing method for fabricating tailored hydrogel structures in a highly precise manner, which is inevitable for these sensitive applications and will, therefore, be discussed in more detail in the next section.

Additive manufacturing

Tissue engineering emerged as a highly interdisciplinary field in medicine, enabling the regeneration of lost tissue and organs after disease.^{297,305} In addition, in vitro and in vivo modeling of disease-related processes contribute to a better understanding of pathological conditions and aid in simulating the complex pathways related to the biological development of malignant tissue.³⁰⁶ Direct ink writing (DIW) is a key 3D printing technique enabling the creation of intricate models from materials with suitable flow properties, allowing ink extrusion through nozzles and layer-by-layer deposition.^{307,308} A highly abundant natural polymer meeting the requirements of DIW is nanofibrillated cellulose (NFC), exhibiting good mechanical strength and stiffness due to a high aspect (length/diameter) ratio.^{309–311} NFC is either produced by bacteria

or obtained in a less defined form by mechanical and chemical treatment of cellulose fibers.^{312–314} The shear-force alignment of NFC upon extrusion is responsible for the shear-thinning behavior, facilitating DIW.^{315–317} Additional modification of the ink rheology by adding the biopolymer sodium alginate (Alg), obtained from brown algae, as a thickener further improved the mechanical ink properties by increasing the viscosity and allowing for ionic cross-linking of printed objects with Ca^{2+} ions.^{318–320} With these NFC/Alg inks, the printing of highly sophisticated, cytocompatible structures with gradual mechanical properties and even materials with anisotropic mechanical features (imitating the biophysical properties of blood vessels) was possible, showcasing the great potential of DIW of biopolymers for tissue engineering.^{321–323}

Other applications

Hydrogels are versatile materials with numerous additional applications to the ones presented in previous sections. In wastewater purification, hydrogels are, for example, applied to remove pollutants such as heavy metal ions or dyes due to their excellent absorption properties.^{324,325} In agriculture, superabsorbent hydrogels are implemented to improve soil water retention and supply nutrients loaded into the networks to the plants.²⁵⁶ Furthermore, their superabsorbent properties are implemented in hygiene products such as baby diapers and band-aids, providing good water absorption.^{257,326} In the food industry, hydrogels serve as thickening agents, stabilizers, and encapsulation systems for flavors, nutrients, or probiotics, ensuring controlled release and improved shelf life, or can play a role in smart packaging applications.^{327–329} Finally, hydrogels are even integral parts of lab-on-a-chip applications, where they can serve as thermo- and pH-responsive valves.³³⁰ The broad application scope of hydrogels presented in this chapter demonstrates the high versatility of this class of materials and emphasizes the necessity to research new materials to expand the range of functional hydrogels.

3 Aim of the thesis

3.1 Development and fundamental characterization of cross-linked materials

For more than 10 years, the group of Rieger et al. focused on understanding the catalysis of vinylphosphonate REM-GTP, expanding the monomer and catalyst scope, and searching for applications of (co)polymers obtained by this catalytic polymerization.⁶⁻⁸ However, no efforts have been made to investigate cross-linked materials from this polymer class, even though it is well-known that different DAVPs are statistically copolymerizable and that functionalization of allyl group-containing polymers via thiol-ene click chemistry with appropriate (di)thiols is possible.^{93,96,104}

Hence, the first goal of this thesis is to develop and characterize three-dimensional hydrogel materials based on the photochemical cross-linking of poly(vinylphosphonates) applying thiol-ene click chemistry with a PEG-based model cross-linker. By employing the excellent control over polymer microstructure and dispersity offered by REM-GTP, synthesizing different statistical copolymers containing DEVP and DAIVP allows studies on the best conditions for cross-linking and yields polymers with different amounts of cross-linkable DAIVP units. Further, another objective is to explore how the highly precise polymer synthesis can be applied to steer the material properties relevant to the application of hydrogels. This mainly includes studying correlations between the copolymer composition, mechanical properties, and swelling behavior of the corresponding hydrogels. Finally, understanding the biocompatibility and antibacterial properties is desirable for a fundamental study of hydrogels since they are often applied in biomedical contexts. Therefore, biological tests are intended in the first phase of this project to investigate the leakage of cytotoxic compounds from the materials and to examine cell growth and proliferation. For in vivo applications, further aspects worth considering include testing the immune response toward these materials and inspecting bacterial growth on the surfaces. After fundamentally exploring all the material properties of poly(vinylphosphonate)-based hydrogels mentioned above, the insights gained from these studies will guide the

direction of subsequent research and shape the project's next steps. An overview of the workflow of the first project within this thesis is presented in Figure 21.

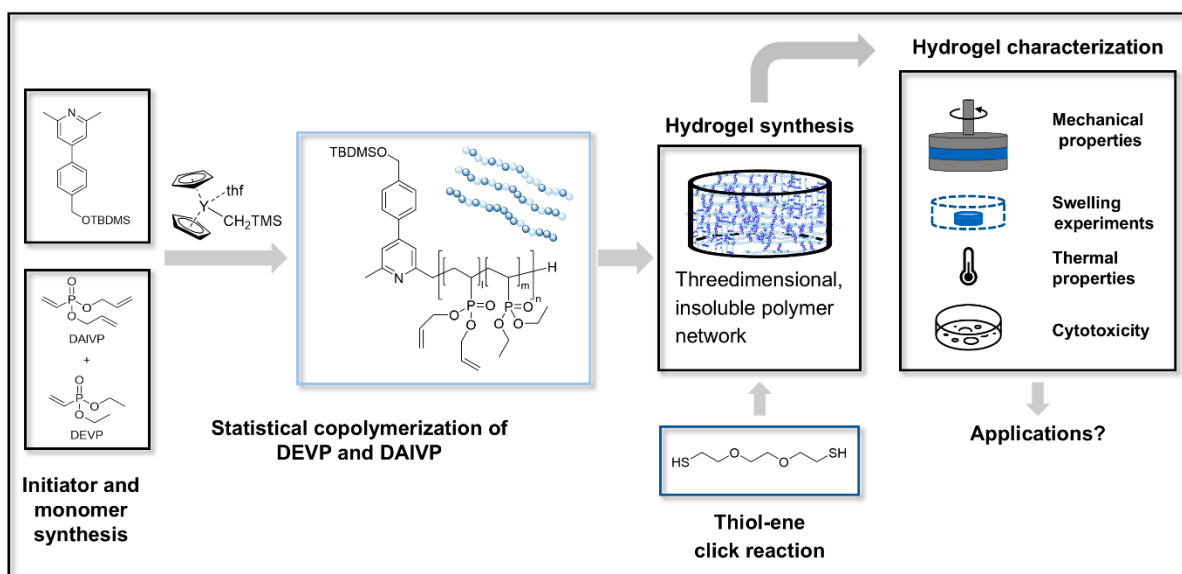


Figure 21: Workflow for the synthesis and characterization of hydrogel materials obtained by photochemical cross-linking of poly(vinylphosphonates) applying thiol-ene click chemistry.

3.2 Synthesis of hydrophilic, pH-responsive hydrogels

A well-established post-polymerization modification of poly(vinylphosphonates) is the polymer-analogous hydrolysis toward poly(vinylphosphonic acid).^{70,123} Combining this synthetic step with the photochemical cross-linking of poly(vinylphosphonates) explored in the first work package of this thesis holds the potential of leading to networks with significantly increased hydrophilicity, resembling the polyelectrolyte structures commonly applied in superabsorbers.^{256,258,326,328} Additionally, introducing VPA units aims to introduce stimuli-responsiveness into the cross-linked polymer materials, as the VPA assumes different extents of deprotonation depending on the pH value of the swelling medium. This, in turn, is a prerequisite for numerous hydrogel applications in biosensors, actuators, and soft robotics.^{4,279,289,290} Therefore, one main objective of this part of the thesis is to achieve the synthesis of such materials, with the subsequent goal of establishing an effective method for characterizing the pH-responsiveness as this provides key insights into the behavior of this functional material in different environments, which is the foundation for potential applications. One possibility to obtain insights into hydrogels' pH-responsiveness and swelling

dynamics involves a quartz crystal microbalance with dissipation monitoring (QCM-D), widely applied to study the pH-dependent swelling and viscoelastic properties of thin hydrogel films. Consequently, this part of the thesis focuses on the processing of cross-linkable mixtures containing poly(vinylphosphonates) into homogenous, thin films, which is usually monitored and confirmed by numerous analytical techniques such as atomic force microscopy (AFM), profilometry, light microscopy, X-ray photoelectron spectroscopy (XPS), and time-of-flight secondary ion mass spectrometry (ToF-SIMS). The comprehensive characterization of thin films is equally critical for accurately interpreting QCM measurements and translating the resulting insights into advanced applications, such as piezoelectric sensors and actuators. An overview of the two-step synthetic approach for developing highly hydrophilic cross-linked materials and the necessity of understanding thin-film behavior and macroscopic swelling is summarized in Figure 22.

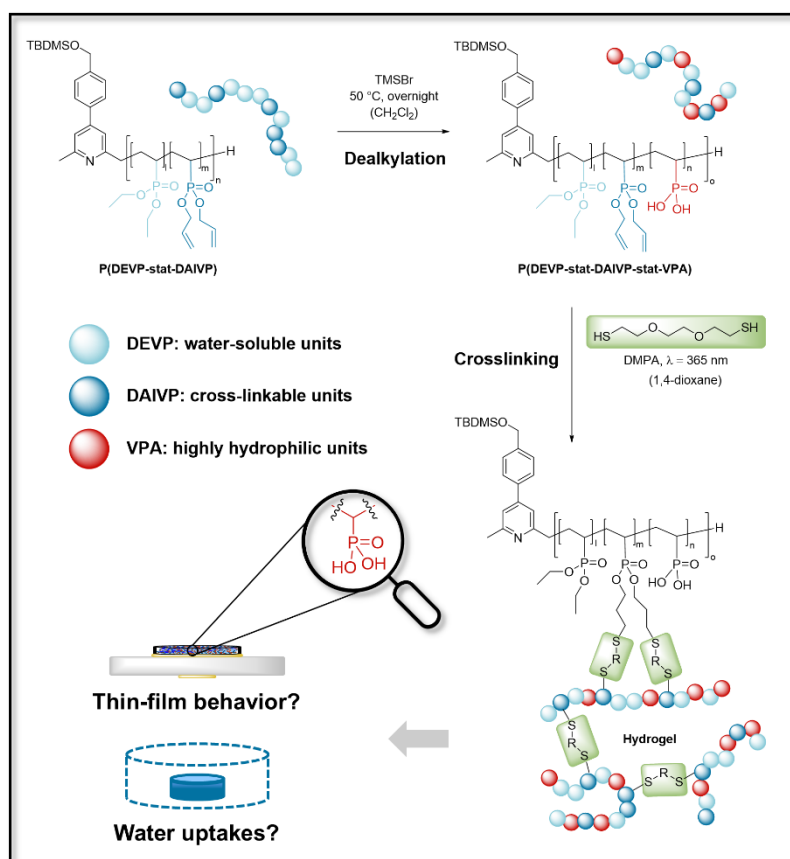


Figure 22: Two-step synthetic procedure toward highly hydrophilic, VPA-containing hydrogels with application potential as stimuli-responsive materials and superabsorbers.

3.3 Application of photochemical cross-linking in additive manufacturing

Additive manufacturing plays a crucial role in processing polymeric materials for tailored applications. Among the various techniques, direct ink writing (DIW) of natural polymers emerged as a promising approach, particularly for biomedical applications like tissue engineering. In this context, nanofibrillated cellulose (NFC) introduces significant strength and stiffness into the objects due to a high aspect (length/diameter) ratio, simultaneously enabling extrusion-based printing through shear-force alignment of the fibers. To modify the rheology and incorporate sites for cationic cross-linking, sodium alginate (Alg) is a common natural additive obtained from brown algae.^{315–318,322,323} Nevertheless, NFC/Alg inks face some challenges, such as poor dimensional stability due to uncontrolled swelling upon cross-linking in Ca^{2+} ion-containing solutions. Reversely, the leaching of ions upon long-time storage of the objects is problematic, causing a collapse of the printed structures.^{331,332} One way of overcoming these drawbacks is the covalent reinforcement of supramolecular hydrogels.^{333,334} Similarly, this chapter of the thesis aims to apply photochemical cross-linking of poly(vinylphosphonates) to solve these problems. An overview of the workflow for this project is given in Figure 23.

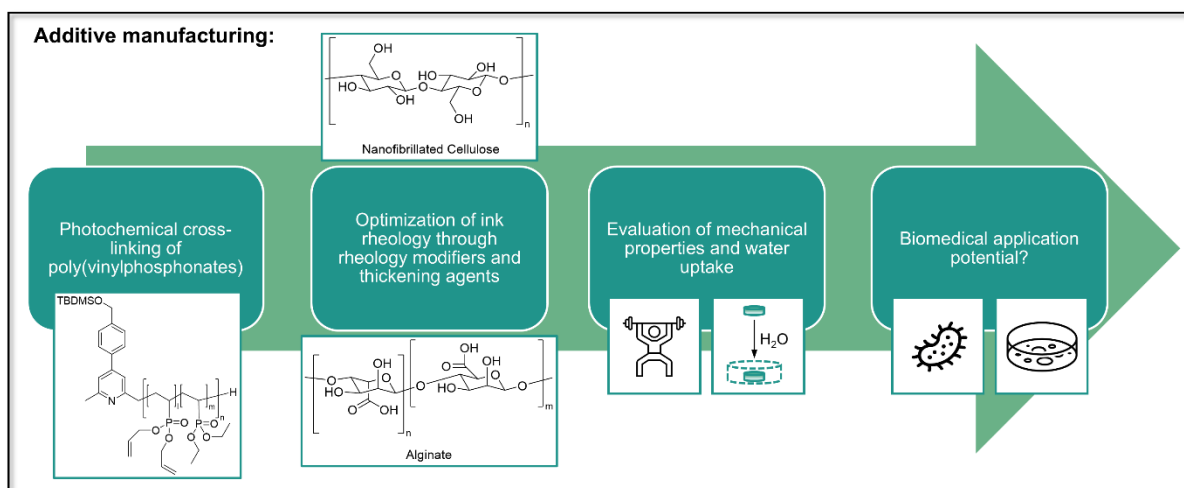


Figure 23: Combination of photochemical cross-linking of poly(vinylphosphonates) with DIW of NFC/Alg inks to access printed objects with high dimensional stability upon swelling.

3.4 Dynamic covalent networks

DCNs are appealing candidates for different (biomedical) applications as they combine the mechanical strength of covalently cross-linked materials with the high dynamics and, consequently, beneficial features of supramolecular networks. The corresponding materials exhibit shear-thinning behavior, enabling extrusion and rendering them injectable. Further, DCNs allow self-healing facilitated by the high reversibility of these dynamic bonds. This additionally enables the processing of the networks via molding and often yields recyclable materials.^{219–223} Considering the attractive material properties of DCNs, combining them with the beneficial properties of poly(vinylphosphonates) obtained by high-precision polymerization via REM-GTP like excellent control over molecular weight and polymer microstructure, narrow dispersities, cytocompatibility, promises great potential in creating innovative, functional hydrogel materials. One way of incorporating dynamic covalent interactions worth exploring is the introduction of the dynamic boronic ester chemistry shown in Figure 24 into poly(vinylphosphonates) since it proceeds under mild conditions and at high rates without catalysts.^{222,240,241} A facile approach toward achieving this goal investigated in this chapter of the thesis intends to utilize poly(vinylphosphonate) functionalizations via thiol-ene click chemistry to establish DCNs formed by boronic ester complexation. Upon successful synthesis, the versatile properties of these networks, like the self-healing illustrated in Figure 24, will provide valuable insights into their application potential.

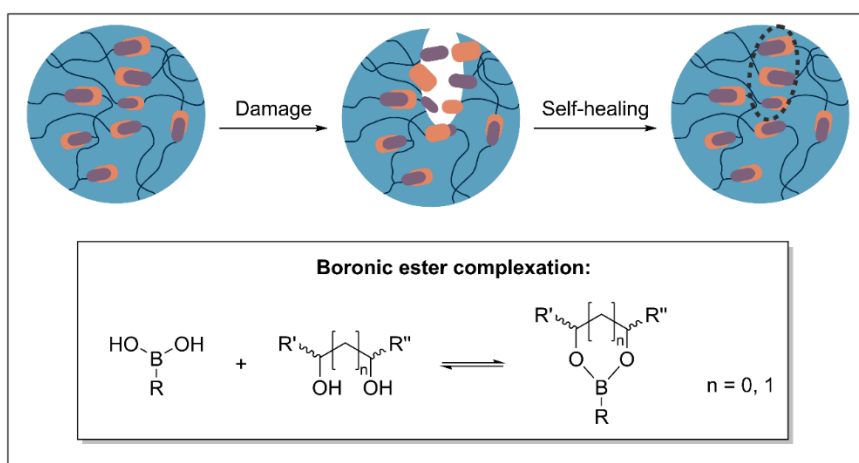


Figure 24: Self-healing of hydrogel materials facilitated by dynamic boronic ester complexation.

4 Synthesis and characterization of photochemically cross-linked poly(vinylphosphonates)

4.1 Bibliographic data

Title: “Cytocompatible Hydrogels with Tunable Mechanical Strength and Adjustable Swelling Properties through Photo-Cross-Linking of Poly(vinylphosphonates)”

Status: Paper, Publication date: 15.10.2024

Journal: ACS Applied Materials & Interfaces

Publisher: American Chemical Society (ACS)

DOI: 10.1021/acsami.4c07860

Authors: Anton S. Maier, Salma Mansi, Kerstin Halama, Philipp Weingarten, Petra Mela, and Bernhard Rieger

4.2 Table of content graphic

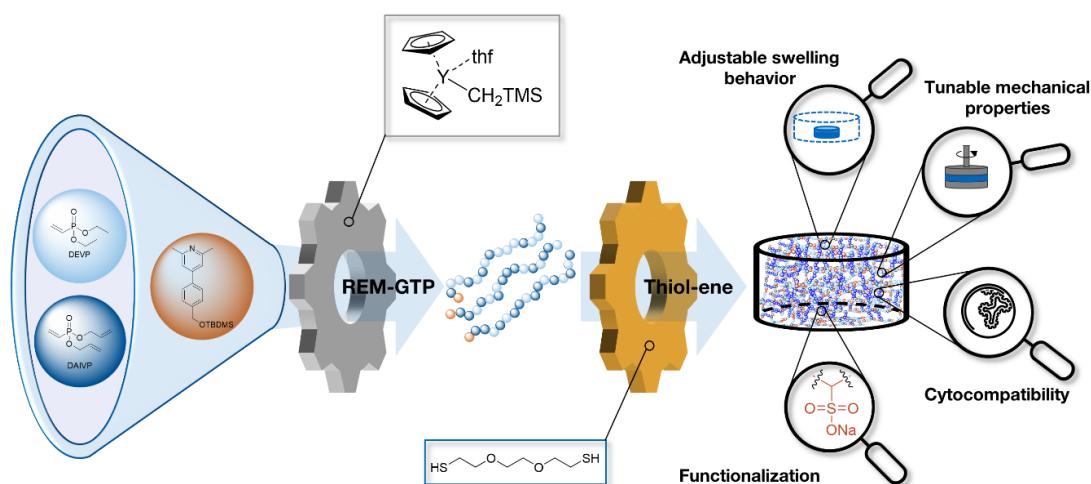


Figure 25: Table of content graphic for the manuscript entitled “Cytocompatible Hydrogels with Tunable Mechanical Strength and Adjustable Swelling Properties through Photo-Cross-Linking of Poly(vinylphosphonates)”.

4.3 Content

This study introduces hydrogel materials based on the photochemical cross-linking of poly(vinylphosphonates) applying thiol-ene click chemistry. First, different statistical copolymers composed of DEVP and DAIVP are synthesized by applying the yttrium catalyst $\text{Cp}_2\text{YCH}_2\text{TMS}(\text{THF})$, demonstrating a precise control over polymer chain length and copolymer composition along with narrow dispersities ($\text{Đ} \leq 1.34$). After elaborating on the best conditions, the P(DEVP-*stat*-DAIVP) polymers are cross-linked under photochemical reaction conditions with 3,6-dioxa-1,8-octanedithiol as a cross-linker and DMPA as the photoinitiator. Oscillatory rheology reveals high reaction rates ($t < 3$ s), further enabling online monitoring of the cross-linking reaction based on the storage and loss moduli. Furthermore, comparing the equilibrium storage moduli of different systems demonstrates increasing elastic portions upon increasing the cross-linking density by incorporating higher amounts of DAIVP into the polymers and applying more rigid cross-linkers. These findings are complemented by nanoindentation experiments, showcasing an increase in the (surface) mechanical properties of the hydrogels with increasing cross-linking density and a drastic decrease in the hardness upon swelling in water. Similarly to the mechanical properties, the water uptake is governed by the cross-linking density, thus decreasing with increasing DAIVP contents. To increase the hydrophilicity of P(DEVP-*stat*-DAIVP) copolymers, a functionalization-cross-linking approach is presented, in which the copolymers are first partially functionalized with 3-mercaptopropane-1-sulfonate, followed by cross-linking under thiol-ene conditions. This remarkably increases the water uptakes up to 54 ± 1 g (H₂O)/g (hydrogel). Finally, the materials introduced in this study are purified via Soxhlet extraction, resulting in the leakage of significant amounts of excess cross-linker and photoinitiator species. The purified hydrogels are subjected to thorough biological characterization. Here, the cross-linked poly(vinylphosphonate) networks enable the growth and proliferation of human umbilical artery smooth muscle cells and the formation of an endothelial layer, both crucial prerequisites for tissue engineering applications. Beyond this, the hydrogels do not trigger a pro-inflammatory immune response as evaluated by cytokine expression, which is crucial for in vivo applications and exhibit antibacterial properties against E. Coli and S. Aureus.

4.4 Manuscript

ACS APPLIED MATERIALS
& INTERFACES

Open Access

This article is licensed under [CC-BY 4.0](https://creativecommons.org/licenses/by/4.0/)www.acsami.org

Research Article

Cytocompatible Hydrogels with Tunable Mechanical Strength and Adjustable Swelling Properties through Photo-Cross-Linking of Poly(vinylphosphonates)

Anton S. Maier, Salma Mansi, Kerstin Halama, Philipp Weingarten, Petra Mela, and Bernhard Rieger*

Cite This: *ACS Appl. Mater. Interfaces* 2024, 16, 58135–58147

Read Online

ACCESS |

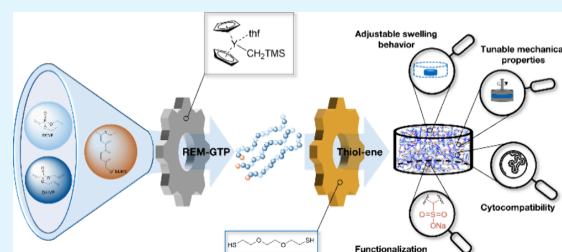
Metrics & More

Article Recommendations

Supporting Information

ABSTRACT: Herein, the synthesis, characterization, and application of a novel synthetic hydrogel based on the photoinitiated cross-linking of poly(vinylphosphonates) is presented. First, statistical copolymers with adjustable ratios of the monomers diallyl vinylphosphonate (DAIVP) and diethyl vinylphosphonate (DEVP), as well as different molecular weights, were obtained via rare earth metal-mediated group-transfer polymerization (REM-GTP) while maintaining narrow polydispersities. The copolymers were cross-linked by applying photoinitiated thiol–ene click chemistry ($\lambda = 365$ nm). The network formation was monitored via oscillatory rheology coupled with UV-irradiation, revealing the high spatiotemporal control of the reaction. Moreover, the equilibrium storage moduli of poly(vinylphosphonate)-based hydrogels increased with a growing number of DAIVP units and upon application of a different cross-linker, which was additionally confirmed by nanoindentation experiments. In contrast, the water uptake of hydrogels decreased with higher DAIVP amounts in the corresponding hydrogels due to lower chain mobility and an overall increase in the hydrophobicity of the samples. Upon successful functionalization of P(DEVP-*stat*-DAIVP) copolymers with sodium 3-mercaptopropane-1-sulfonate, as indicated via ^1H DOSY NMR, the respective cross-linked materials displayed a remarkable increase in the water uptake; thus, presenting highly hydrophilic gels with an apparent interplay between water uptake, cross-linking density, and functionalization degree. Finally, the purified hydrogels showed cytocompatibility and enabled cell adhesion of human umbilical artery smooth muscle cells (HUASMCs) after direct seeding. The materials further allowed the adhesion and growth of an endothelial layer, triggered no pro-inflammatory response as evidenced by cytokine release of M0 macrophages, and exhibited antibacterial properties toward *S. aureus* and *E. coli*.

KEYWORDS: catalytic polymerization, thiol–ene click reaction, hydrogel, oscillatory rheology, cytocompatibility



INTRODUCTION

Hydrogels are a class of materials based on natural or synthetic polymers with the ability to retain significant amounts of water within their cross-linked, three-dimensional network without dissolution.¹ Depending on the mechanism of network formation, these materials are typically classified as supramolecular hydrogels or chemically cross-linked hydrogels. In supramolecular materials, cross-linking occurs through non-covalent interactions, e.g., ionic or van der Waals interactions, host–guest chemistry, or hydrogen bonding. In contrast, hydrogels are categorized as chemically cross-linked if covalent bonds connect the polymer chains.^{2–5} The outstanding physicochemical properties of hydrogels, such as high water absorption, mechanical stability, biocompatibility, and biodegradability, render them appealing candidates for various biomedical applications.^{6–10} In this context, cross-linked polymer materials are highly relevant in drug delivery,^{11–13} tissue engineering,^{14,15} wound healing,^{16,17} and as antimicrobial coatings.^{8,18,19} Beyond biomedicine, hydrogels have gained significant importance in various other fields, inter alia, in

wastewater purification^{20,21} or smart devices like actuators and sensors employing the stimuli-responsiveness (pH, temperature, light) of certain materials.^{22–28} The tunability of the stimuli-responsive properties of hydrogels is one reason why synthetic polymers have emerged as promising candidates for tailored hydrogel applications. Additionally, synthetic polymers allow a facile adjustment of mechanical properties, and swelling behavior and guarantee the reproducibility of hydrogel synthesis. Commonly applied polymers for non-natural hydrogels comprise water-soluble and biocompatible macromolecular compounds, such as poly(ethylene glycol),^{29,30} poly(vinyl alcohol),^{31,32} and poly(acrylate)/poly(acrylamide)

Received: May 13, 2024
 Revised: October 3, 2024
 Accepted: October 7, 2024
 Published: October 15, 2024

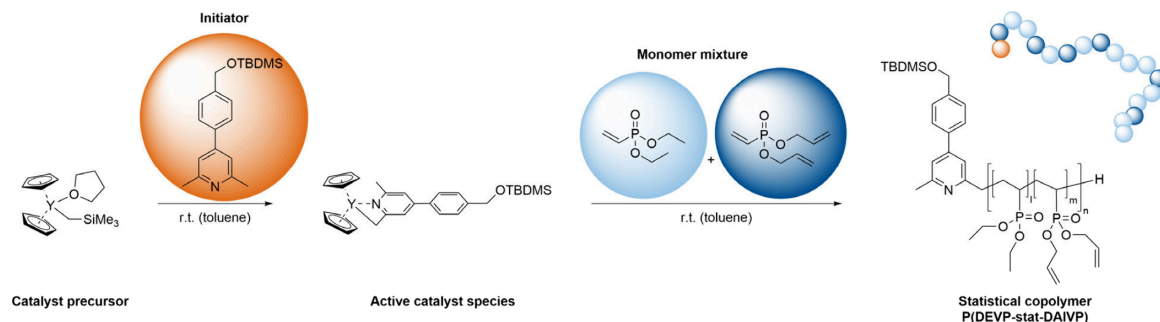


ACS Publications

© 2024 The Authors. Published by
American Chemical Society

58135

<https://doi.org/10.1021/acsami.4c07860>
ACS Appl. Mater. Interfaces 2024, 16, 58135–58147

Scheme 1. Statistical Copolymerization of DEVP and DAIVP with the CH-Bond Activated Species of $\text{Cp}_2\text{YCH}_2\text{TMS}(\text{thf})$

 Table 1. Results of the Copolymerization of DEVP and DAIVP with the CH-Bond Activated Species of $\text{Cp}_2\text{YCH}_2\text{TMS}(\text{thf})$

entry	DEVP/DAIVP/Cat. ^a	targeted DAIVP content [%]	X [%] ^b	DAIVP content [%] ^c	$M_{n,\text{NMR}}^d$	IE ^e	\bar{D}^f
1	180/20/1	10	>99	9.0	39	86	1.08
2	270/30/1	10	>99	9.0	82	61	1.09
3	360/40/1	10	>99	8.8	107	56	1.09
4	450/50/1	10	>99	12.3	173	45	1.24
5	300/100/1	25	>99	23.9	162	37	1.34
6	320/80/1	20	>99	19.7	148	41	1.06
7	340/60/1	15	>99	13.9	200	29	1.06
8	380/20/1	5	>99	5.8	213	29	1.06

^aReactant ratio desired. ^bConversion determined via ^{31}P NMR spectroscopy in MeOD. ^cDetermined via ^1H NMR spectroscopy by comparison of the CH_2 signals of DEVP (4.18 ppm, $m = 1/4$) and DAIVP (4.63 ppm, $n = 1/4$). ^dCalculated via ^1H NMR spectroscopy by comparison of the $-\text{OTBDMS}$ signals of the initiator at 0.14 ppm ($I = 6\text{H}$) and the CH_2 signals of DEVP (4.18 ppm, $m = 1/4$) and DAIVP (4.63 ppm, $n = 1/4$). ^e $\text{IE} = M_{n,\text{calc}}/M_{n,\text{NMR}}$ with $M_{n,\text{calc}} = 327.54 \text{ g/mol} + m \times 164.14 \text{ g/mol} + n \times 188.16 \text{ g/mol}$. ^fPolydispersity determined via size-exclusion chromatography multiangle light scattering (SEC-MALS) in THF:H₂O (1:1) with 340 mg/L 2,6-di-*tert*-butyl-4-methylphenol (BHT) and 9 g/L tetra-*n*-butylammonium bromide (TBAB).

derivatives.^{33,34} Another class of synthetic polymers exhibiting good water solubility, high biocompatibility, as well as a lower critical solution temperature (LCST) are poly(vinylphosphonates) obtained via rare earth metal-mediated group-transfer polymerization (REM-GTP).^{35–37} Polymer synthesis through REM-GTP, enabling the polymerization of Michael-type monomers through repeated 1,4-conjugate addition, is particularly interesting for biomedical applications. The reason for this is the precise control over the polymer microstructure while maintaining narrow polydispersities, resulting in highly defined polymeric structures.^{38,39} This is due to the continuous coordination of the growing polymer chain to the catalyst center, leading to the simultaneous growth of polymer chains at the active catalyst molecules. Furthermore, this propagation mechanism enables the synthesis of block copolymers from various types of α,β -unsaturated monomers in accordance with their coordination strength to the catalyst.^{40,41} In contrast, the synthesis of statistical copolymers from various structurally related dialkyl vinylphosphonates is mainly dependent on the steric demand of the growing chain rather than the coordination strength to the catalyst center.³⁷ In this respect, the copolymerization of a mixture of diallyl vinylphosphonate (DAIVP) and diethyl vinylphosphonate (DEVP) to statistical copolymers is possible and yields water-soluble polymers susceptible to postpolymerization functionalization of the allyl side groups with a variety of synthetic methods.^{42,43} One common approach for functionalizing allylic and vinylic motifs in polymers with, e.g., biologically active substrates involves the application of thiol–ene click chemistry.^{44–46} The thiol–ene reaction is

known for its high reaction rates under mild reaction conditions, high yields, and low to no side products. Moreover, thiol–ene click reactions are very robust, tolerating moisture and oxygen, and are often photoinitiated, allowing high temporal and spatial control over the photochemical initiation.⁴⁷ Finally, thiol–ene click chemistry exhibits high compatibility with a variety of functional groups as well as orthogonality with other common organic reaction types, making it a very versatile tool for introducing functional motifs into vinyl group-containing polymers.^{47–50} Since the beginning of the century, thiol–ene click chemistry has been widely explored in hydrogel synthesis, as it allows the in situ and in vivo formation of soft, tissue-like materials under physiological conditions upon UV-light irradiation. In this context, often biocompatible, PEG- or poly(acrylate)-based polymers with pending vinyl groups are employed in combination with di- or multifunctional thiols for the formation of biodegradable, cross-linked networks with a considerable potential for applications in tissue engineering and drug delivery with specific requirements to the release profile.^{19,30,51–55} In the present study, this concept is transferred to statistical copolymers obtained from DEVP and DAIVP obtained via rare earth metal-mediated group-transfer polymerization (REM-GTP), enabling the synthesis of noncytotoxic hydrogels with tunable mechanical strength. Further, we demonstrate an adjustment of the swelling ratio by control of the cross-linking density and through functionalization of P(DEVP-*stat*-DAIVP) copolymers with sodium 3-mercaptopropane-1-sulfonate via click chemistry prior to cross-linking.

RESULTS AND DISCUSSION

Copolymerization of Diethyl Vinylphosphonate (DEVP) and Diallyl Vinylphosphonate (DAIVP). Prior to the copolymerization of DEVP and DAIVP, in situ CH-bond activation via σ -bond metathesis with equimolar amounts of 4-(4-(((*tert*-butyldimethylsilyloxy)methyl)phenyl)-2,6-dimethylpyridine and the catalyst precursor $\text{Cp}_2\text{YCH}_2\text{TMS}(\text{thf})$ is conducted to form the initiating complex for subsequent polymerization (Scheme 1).^{56–58} The introduction of the 2,4,6-trimethylpyridine-derivative yields an initiating ligand with lower basicity, thus suppressing undesired deprotonation reactions of the monomers, and further incorporates an end-group into the copolymers, exhibiting distinct OTBDMS-signals in the ^1H NMR spectrum. This enables the facile estimation of the molecular weight of the respective copolymers via ^1H NMR spectroscopy, since the determination of the absolute molecular weights of the copolymers using size-exclusion chromatography multiangle light scattering (SEC-MALS) requires the determination of the refractive index increment for each copolymer composition. After quantitative CH-bond activation via ^1H NMR spectroscopy in C_6D_6 is confirmed by the absence of the CH_2 -group signal (doublet, $\delta = -0.66$ ppm) of $\text{Cp}_2\text{YCH}_2\text{TMS}(\text{thf})$ (Figure S1), a mixture of the monomers DEVP and DAIVP is added quickly to ensure simultaneous initiation of the copolymerization at all catalyst centers. Conversion of the monomers is monitored via ^{31}P NMR spectroscopy in MeOD. Upon quantitative conversion, the polymerization is stopped by the addition of 0.5 mL of undried methanol, and the copolymers are purified (for experimental details, see the Supporting Information).

Polymerization experiments yielded copolymers with a tunable composition by adjusting the monomer feed ratio while maintaining narrow polydispersities (Table 1 and Figures S5–S12). The results in Table 1 demonstrate excellent control over polymer microstructure and chain length.

Entries 1–4 (Table 1) display a variation of the polymer chain length while targeting the same proportion of cross-linkable DAIVP units in the copolymers. In all cases, the targeted percentage of DAIVP in the copolymers is met with relatively high precision compared with the values derived from the ^1H NMR spectra. Further, switching toward higher monomer/catalyst ratios, an increase in the molecular weight of the polymers as determined via ^1H NMR spectroscopy is observed, with only a slight decrease in the initiator efficiency and a minor increase in the polydispersity. However, note that the initiator efficiencies given in Table 1 do not rely on absolute molecular weight determinations. Therefore, the significance of those values is rather low, as molecular weight determination via ^1H NMR spectroscopy (Figure S2) is prone to errors. Overall, these results demonstrate a straightforward adjustment of the molecular weight of the P(DEVP-*stat*-DAIVP) copolymers by a variation of the monomer/catalyst ratio. Comparing entry 3 to entries 5–8, the results in Table 1 illustrate a tunable copolymer composition by alteration of the monomer feed ratio. This gives access to different polymer microstructures with varying amounts of cross-linking sites. In all cases, successful copolymer formation was confirmed via ^{31}P NMR and ^1H DOSY NMR spectroscopy (Figures S3 and S4). To reduce catalyst depletion and facilitate handling of the polymers (short-chain polymers exhibit higher tack), we decided to proceed with higher molecular weight polymers (Table 1, entries 3 and 5–8) for the hydrogel synthesis. In

addition to these results, the thermal properties of these novel copolymers were thoroughly investigated to obtain a more detailed understanding of this type of poly(vinylphosphonates). In accordance with previous reports, the copolymers synthesized in this study exhibit fully reversible lower critical solution temperature (LCST) behavior within the physiological temperature range. In this context, an aqueous solution of polymer 1 undergoes coil–globule transition at 36 °C, which was detected by measuring the transmittance of the solution as shown in Figure S13.³⁷ Further, thermogravimetric analysis of entry 3 yielded a thermal decomposition onset of 313 °C (Figure S14), matching the values found in studies on the thermal behavior of poly(vinylphosphonates) very well.⁵⁹ Finally, the differential scanning calorimetry (DSC) results presented in Figure S15 revealed the absence of a melting point in P(DEVP-*stat*-DAIVP), confirming that the statistical copolymerization of DEVP and DAIVP with $\text{Cp}_2\text{YCH}_2\text{TMS}(\text{thf})$ proceeds in a stereoirregular fashion, yielding atactic, amorphous polymers.⁶⁰

Hydrogel Formation and Rheological Characterization. To explore hydrogel formation originating from P(DEVP-*stat*-DAIVP) copolymers upon application of the thiol–ene click reaction, commercially available, PEG-based 3,6-dioxo-1,8-octanedithiol was selected as a model cross-linker for initial experiments. Those experiments involved testing different solvents, reaction conditions, polymer concentrations, and a variation of the curing procedure (Table S1). Concerning the solvent, a mixture of tetrahydrofuran and methanol was selected for the first experiments following reports from Rieger et al.⁴² Additionally, water and 1,4-dioxane were tested in the cross-linking reaction, leading to successful hydrogel formation under photochemical reaction conditions with 2,2-dimethoxy-2-phenylacetophenone (DMPA) as an initiator even in the presence of oxygen. This demonstrates the broad applicability and robustness of the thiol–ene click reaction, as already discussed in the introduction.^{47–50} Considering the choice of solvent for the hydrogel syntheses presented in Table S1, water was not selected due to the surface-active properties of the P(DEVP-*stat*-DAIVP) polymers, causing foaming upon polymer dissolution and leading to inclusions of air bubbles in the cross-linked materials. As this caused poor reproducibility of the synthesis and decreased structural integrity, more focus was placed on the THF/MeOH-mixture and 1,4-dioxane. Both dissolved the polymers equally well, leading to homogeneous solutions and, accordingly, smooth hydrogels. To facilitate experimentation and avoid toxic MeOH, 1,4-dioxane was selected as a solvent instead of the mixture. Further, different polymer concentrations were tested for the cross-linking reaction. Despite successful hydrogel synthesis among all tested concentrations, high polymer concentrations were selected for the standardized synthesis procedure, as this should ideally favor the desired intermolecular cross-linking reaction over intramolecular thiol–ene click reactions of the allyl group-containing poly(vinylphosphonates). Finally, a thermally initiated thiol–ene click reaction with azobis(isobutyronitrile) (AIBN) was compared to the photochemical process applying DMPA. While both reactions resulted in hydrogel formation, the photochemical reaction was preferred because it allows a more detailed study of the sol–gel transition (gelation process) via oscillatory rheology, enabling a high spatial and temporal control over the click reaction by selectively switching on UV-light irradiation (Scheme 2 and Figure 1).⁴⁷

Scheme 2. (A) Schematic Representation of the Cross-Linking of P(DEVP-*stat*-DAIVP) Copolymers via Photoinitiated Thiol–ene Click Reaction, Applying 2,2-Dimethoxy-2-phenylacetophenone (DMPA) as the Photoinitiator and 3,6-Dioxa-1,8-octanedithiol (blue) as Cross-Linker; (B) Underlying Reaction Mechanism of the Thiol–ene Click Reaction

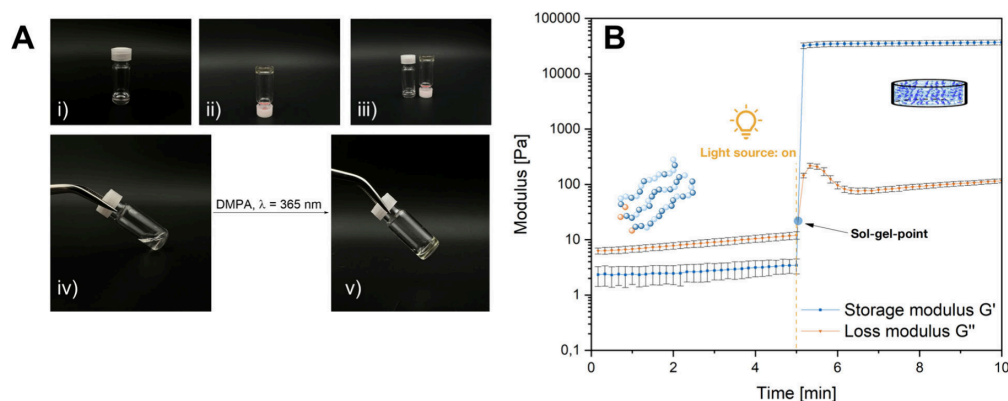
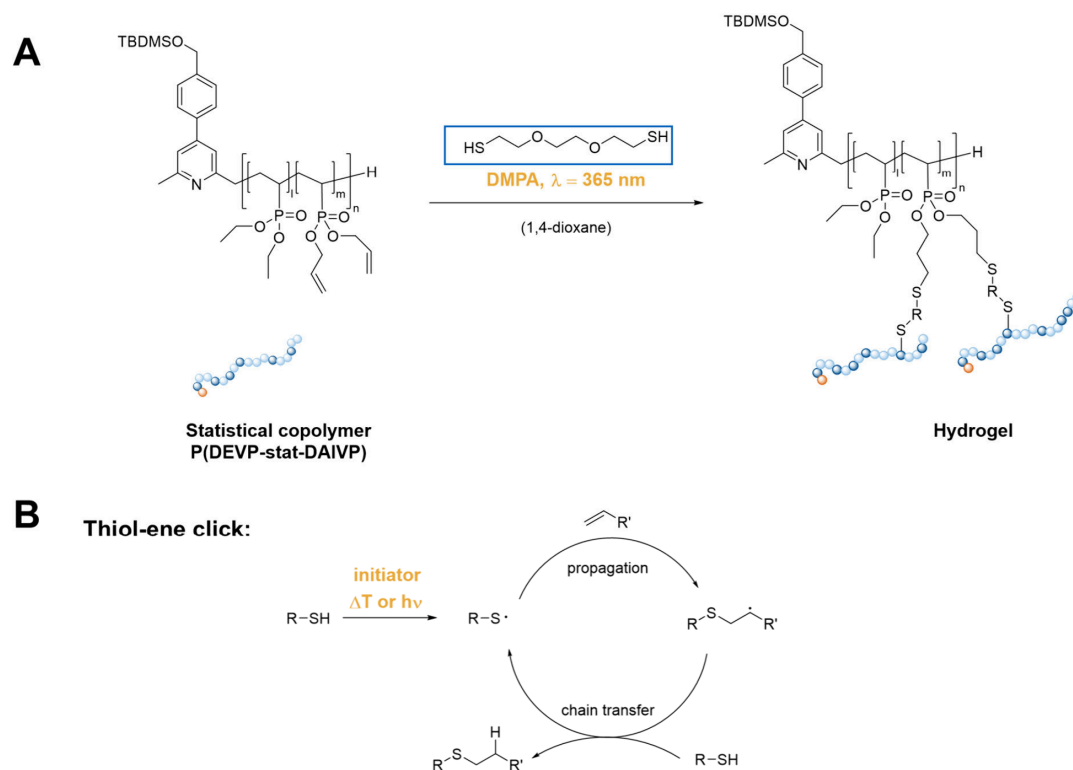


Figure 1. (A) Cross-linking reaction of P(DEVP-*stat*-DAIVP) with 3,6-dioxa-1,8-octanedithiol using UV-light ($\lambda = 365$ nm) initiated thiol–ene click chemistry and 2,2-dimethoxy-2-phenylacetophenone (DMPA) as the photoinitiator. (i) and (iv): Samples in liquid state; (ii) and (v): Cross-linked samples; and (iii): Comparison of solution and gel. (B) Rheological investigation of gelation process: time sweep with the experimentally determined values for the deformation and frequency ($\gamma = 1\%$, $f = 5$ Hz), demonstrating the kinetics of the thiol–ene-mediated cross-linking reaction of P(DEVP-*stat*-DAIVP).

To obtain a profound understanding of the gelation process, the limits of the linear viscoelastic region (LVR), in which nondestructive rheological testing due to proportionality of the shear strain and the shear stress is guaranteed, are determined by a series of rheological experiments. Further, the application of oscillatory rheology within the LVR ensures comparability

of the results obtained for different samples by applying the same measurement frequency and amplitude. The preliminary experiments for evaluating the limits of the LVR consist of four steps:⁵¹ (1) a time sweep with arbitrary frequency and amplitude to determine the rate of gel formation, (2) a deformation sweep on a fully gelled sample with arbitrary

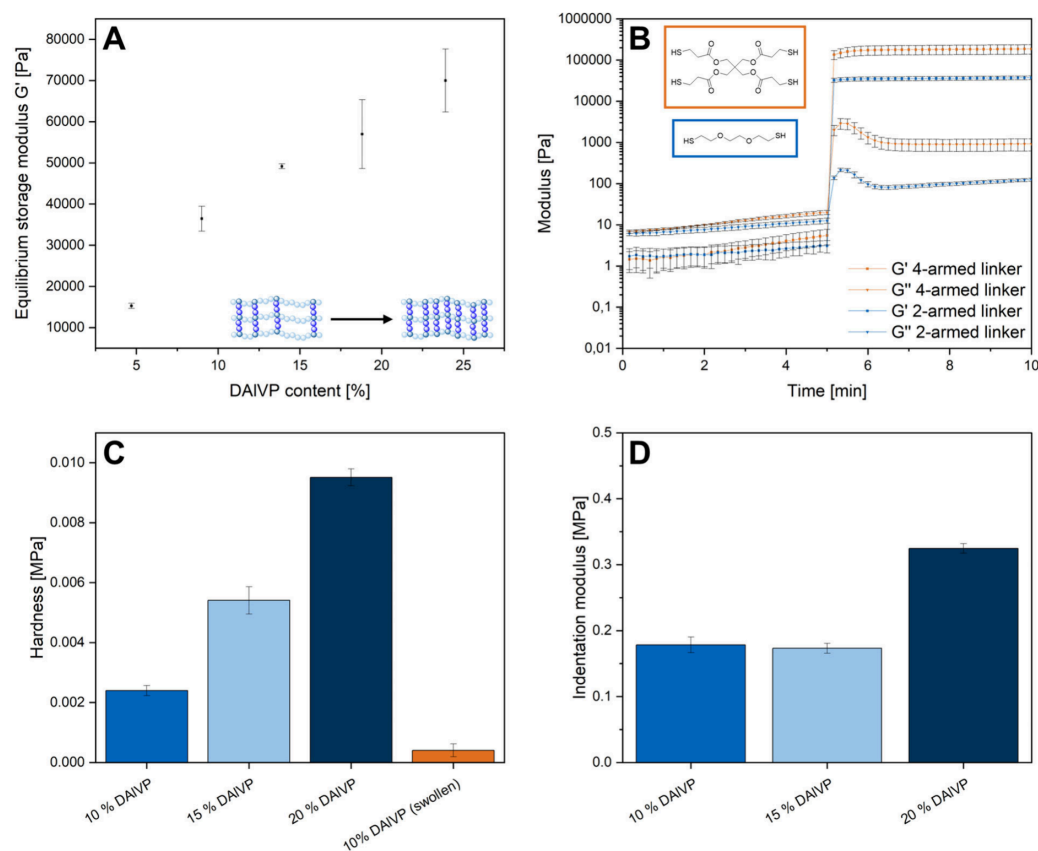


Figure 2. Rheological investigation of the mechanical properties of corresponding hydrogels for different copolymer compositions (Table 1, entries 3 and 5–8) (A) and different cross-linkers (B) at standardized measurement conditions of 5 Hz frequency and 1% deformation. Mechanical properties were obtained through nanoindentation of various samples: Hardness of dried samples compared to a swollen hydrogel sample (C) and indentation moduli of different dry samples (D) with respect to the amount of cross-linkable DAIVP units in the corresponding polymers (Table 1, entries 3, 7, and 6).

frequency to determine the LVR region with regard to the strain, (3) a frequency sweep with the determined amplitude from (2) on a cross-linked sample to evaluate the linear equilibrium modulus plateau of the hydrogel, and (4) a time sweep to obtain the gelation kinetics and the equilibrium moduli with the previously obtained values for amplitude and frequency (Figure 1B). Step (1), however, was not carried out as a rheological experiment, as the initial experiments on hydrogel formation already indicated immediate hydrogel formation upon irradiation. Consequently, the deformation sweep (Figure S18) and subsequent frequency sweep (Figure S19), both performed on fully cross-linked samples, were conducted after irradiation of the polymer solution for 5 min.

For rheological experiments, the hydrogels were formed between the rheometer plates in situ. Therefore, a polymer solution containing photoinitiator and cross-linker was applied onto a glass plate at the rheometer, and the upper plate was lowered, leading to a quantitative filling of the gap. Subsequently, gelation was initiated at the desired time by irradiating the sample through the transparent glass plate at 365 nm from below (for experimental details, see the Supporting Information). The deformation sweep illustrated in Figure S18 indicated linear behavior of the storage modulus

G' and the loss modulus G'' for deformations between 0.1% and 1%. Thus, an amplitude of 1% was selected for the subsequent frequency sweep (Figure S19), in which a low-frequency plateau of the values for G' and G'' appeared between 0.1 and 10 Hz. For conducting time-resolved small-amplitude oscillatory shear experiments, the testing frequency must be within this window.⁶¹ Therefore, a frequency of 5 Hz along with the deformation of 1% was applied in a time-resolved rheological experiment, in which gelation was initiated by irradiation after five min (Figure 1B). As evidenced by the results, the samples exhibited liquid-like behavior before irradiation ($G' < G''$), whereas immediate cross-linking ($t < 3$ s) was observed ($G' > G''$) after activating the light source with an intensity of 150 mW cm⁻² (Figures 1B and S20). This demonstrates the excellent control over the thiol–ene click reaction and its high reaction rates as previously reported.^{47–50} Studying the kinetics of the thiol–ene reaction by monitoring the storage moduli revealed a correlation between the gelation rate and light power intensity (Figure S20). However, we believe the short gelation times obtained in this study are mainly attributed to the high polymer concentrations (333 mg mL⁻¹) and the excess cross-linker used. Considering the behavior of the moduli in Figure 1B upon UV-irradiation, G'

undergoes a stepwise transition, whereas G'' exhibits a maximum, suggesting a rapid transition of the viscous liquid into a glassy state. This behavior is described as vitrification (transition into a glassy state) and is accompanied by a simultaneous peak in the loss factor $\tan \delta$ (ratio between G'' and G') illustrated in Figure S21.^{62,63} As the measurement proceeded, G'' and $\tan \delta$ decreased toward nearly constant plateau values, indicating a decrease in the viscous portion of the complex modulus G^* . Regarding the radical reaction mechanism presented in Scheme 2B, this behavior is likely attributed to the ongoing radical reaction causing a postcuring after initiation until a constant, quantitative cross-linking degree is reached, indicated by the stable G'' and $\tan \delta$ values. Control experiments without irradiation and without the addition of an initiator revealed no gel formation (Figures S23 and S24), whereas the cross-linking process in the absence of a cross-linker led to the slow formation of a weak gel (Figure S25). Therefore, only a minor contribution of the formation of C–C bonds via olefin coupling is proposed, as the kinetic curve presented in Figure 1B in the presence of cross-linker not only exhibits significantly higher reaction rates of the C–S coupling but also results in the formation of a stronger gel as indicated by the values of G' . Figure 1B also demonstrates excellent reproducibility of the experiments, as indicated by the small error bars, justifying the previously determined frequency and amplitude. Furthermore, the experiments shown by the rheological results in Figure 1B serve as proof of concept for hydrogel synthesis via cross-linking of P(DEVP-*stat*-DAIVP) with 3,6-dioxa-1,8-octanedithiol. In addition to the findings presented in Figure 1, a comparison of the infrared spectra of the cross-linker, a polymer (Table 1, Entry 1), and the corresponding hydrogel indicated a successful photochemical cross-linking of poly(vinylphosphonates) with dithiols. This was confirmed in the hydrogel spectrum by the absence of characteristic thiol stretching bands (2550 cm^{-1}) and the appearance of $\text{CH}_2\text{--O--CH}_2$ asymmetric stretching bands ($1180\text{--}1060\text{ cm}^{-1}$) inherent to the PEG-chain of the cross-linker (Figure S16).⁶⁴ Thermogravimetric analysis of water-swollen hydrogels displayed dehydration, as shown in Figure S17, followed by the transitions already observed for the polymers (Figure S14).

Tuning of Mechanical Strength. After the successful application of oscillatory rheology to characterize the gelation kinetics, it was further selected as a tool for evaluating the mechanical strength of hydrogels. The mechanical properties of hydrogels are mainly affected by the cross-linking density, which in turn can be influenced by various factors, such as type of cross-linker or ion concentrations.^{65,66} We selected two approaches for the variation of viscoelastic properties, both aiming at an alteration of the cross-linking density or the mesh size, respectively. First, the effect of the copolymer composition on the rheological results of the corresponding hydrogels was investigated. In this context, copolymers with similar molecular weights but different amounts of cross-linkable DAIVP units (see Table 1, entries 3 and 5–8) were compared when cross-linked with the model cross-linker 3,6-dioxa-1,8-octanedithiol. Oscillatory rheology was conducted under the previously determined, standardized measurement conditions with a frequency of 5 Hz and a deformation of 1% (Figures 1B, S18, and S19). Further, identical ratios of cross-linker and photoinitiator with respect to the number of cross-linkable units in the copolymers were applied to ensure comparability of the results. Measurements were performed at

least in triplicate, and the plateau values of the storage modulus for each kinetic curve were used as a measure of the mechanical strength (for the kinetic curves of each copolymer composition, see the Supporting Information, Figure S22). Figure 2A displays an increase in the mechanical strength of the hydrogels with an increasing number of DAIVP units in the copolymers. This reflects the expected trend, as only DAIVP can undergo a thiol–ene click reaction with the cross-linker. Switching to higher amounts of cross-linkable units (Table 1, entry 5), premature gelation was observed with high reproducibility (Figure S22). This was attributed to the initiation of the cross-linking process by incident light or oxygen diradicals, which is more pronounced if a higher number of cross-linking sites is available and, therefore, is reflected in the increase of moduli during rheological measurements despite light exclusion. However, these results demonstrate tunability of the mechanical properties of the corresponding hydrogels upon adjustment of the monomer feed ratio during polymerization, only limited by premature gelation and decreasing copolymer solubility in polar solvents with increasing DAIVP contents. As a second approach for adjusting the mechanical properties of these novel materials, the cross-linker applied during hydrogel synthesis is easily exchangeable with an impact on the resulting material characteristics. This was demonstrated by performing time-resolved rheological measurements with the same polymer (Table 1, entry 3) but testing different cross-linkers. Figure 2B shows a comparison of the rheological data obtained for the model cross-linker 3,6-dioxa-1,8-octanedithiol (blue curve) and pentaerythritol-tetrakis(3-mercaptopropionate) (orange curve) upon application of equimolar amounts of SH-groups. In other words, only half of the concentration of the 4-armed linker was applied compared to the dithiol to assess the effect of the linker structure exclusively. These measurement results reveal that besides the number of cross-linking sites in the polymer, also the functionality of the linker plays a crucial role with respect to the resulting mechanical properties of the gels. Whereas the model cross-linker is only bifunctional (two thiol groups), the four-armed linker allows for the formation of a more densely cross-linked network, which is reflected in higher values of G' and G'' and corresponds to a higher mechanical strength. Thus, the choice of cross-linker allows for an adjustment of the mechanical properties of materials cross-linked via thiol–ene click reactions. In addition to the rheological characterization of hydrogels, nanoindentation was applied to determine the (surface) mechanical properties of the cross-linked materials. In this context, different dried samples originating from polymers with a rising number of DAIVP units (Table 1, entries 3, 7, and 6) and an increasing cross-linking density were investigated. Regarding the hardness of each sample, higher numbers of DAIVP units in the copolymers resulted in an increased hardness of the cross-linked materials (Figure 2C). Additionally, we observed similar trends regarding the indentation modulus of the samples. Whereas the covalent networks of polymers with 10% and 15% DAIVP units exhibited similar indentation moduli, the sample with the highest cross-linking degree (20% DAIVP) revealed a significantly higher stiffness (Figure 2D). Comparing the water-swollen state of the hydrogels to their dry state, nanoindentation of an exemplary hydrogel revealed a drastically decreased sample hardness after swelling in water. Considering the apparent structure–property relationships between the copolymer structure and the hydrogel properties

found for the swelling behavior (discussed in the next section), the mechanical properties determined via rheology (Figure 2A), and the dry sample hardness (Figure 2C), the trend in the mechanical properties is likely to persist in the swollen hydrogels.

Water Uptake. The water uptake of poly(vinylphosphonate)-based hydrogels was investigated by comparing the weight of hydrogels after drying in vacuo overnight with the weight after immersing the samples in water for 6 h, ensuring equal equilibrium swelling states of all hydrogels as demonstrated by the kinetic curves presented in Figure S26. The ability of hydrogels to absorb water is usually described by the swelling ratio Q , which is given by eq 1 and defines the weight percentage of water in each sample.^{67,68} In this context, M_s denotes the weight of the fully swollen sample, whereas M_d expresses the weight of the dry state.

$$Q = \frac{M_s - M_d}{M_d} \quad (1)$$

As with the mechanical properties of poly(vinylphosphonate)-based hydrogels, a correlation was found between initial copolymer composition and water uptake of the cross-linked material (Figure 3).

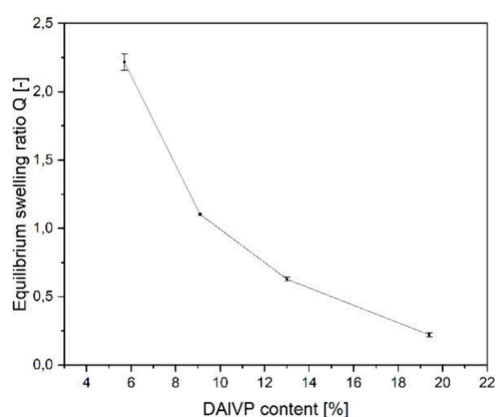


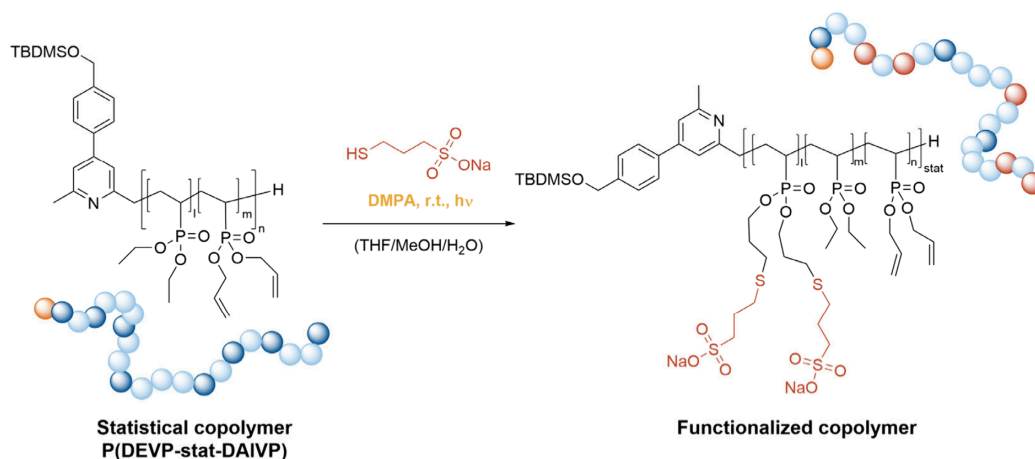
Figure 3. Equilibrium swelling ratio of different hydrogels with respect to the corresponding amounts of DAIVP in the P(DEVP-*stat*-DAIVP) copolymers (Table 1, entries 3 and entries 6–8).

Unlike the mechanical properties, the swelling ratio decreases with an increasing number of DAIVP units and, therefore, cross-links in the material. This can be attributed to reduced chain mobility in more cross-linked networks hindering the solvation of the chains as well as the higher hydrophobicity of the DAIVP compared to the more hydrophilic DEVP monomer. The highest water absorption of 2.22 g of water per gram of dry hydrogel was achieved for a DAIVP content of 5.7%. Further, studying the hydrolytic stability of these novel materials under physiological conditions in phosphate-buffered saline solution (pH = 7.4) at 37 °C revealed no significant degradation over 8 days (Figure S27). To increase the water uptake, the copolymers (Table 1, entry 3 and entries 6–8) were functionalized by performing a click reaction with sodium 3-mercaptopropene-1-sulfonate prior to cross-linking as illustrated in Scheme 3.

The modified polymers were purified via dialysis against water (MWCO = 8 kDa), and successful functionalization was

confirmed via ¹H DOSY NMR spectroscopy (Figure S28). Unfortunately, a comparison of the ¹H NMR spectra of each copolymer before and after functionalization with the sulfonate could not afford the degree of functionalization due to the lack of a reference signal in both spectra (Figure S29). However, ¹H NMR spectroscopy gave access to the composition of unfunctionalized polymers, whereas elemental analysis of the functionalized polymers (Table S2) led to the compositions displayed in Table 2. Subsequently, the purified samples were successfully subjected to hydrogel formation applying thiol–ene click chemistry (for experimental details, see the Supporting Information). The resulting hydrogels were dried in vacuo, and their water uptake was investigated in the same manner as that described above. In this context, each hydrogel synthesis and water absorption experiment was performed in triplicate. The water uptake regarding the polymer composition and a description of the mechanical properties of the swollen hydrogels are provided in Table 2.

As reflected by the compositions in Table 2, starting with P(DEVP-*stat*-DAIVP) copolymers with an increasing number of DAIVP units (Table 1, entries 3 and 6–8) results in different degrees of functionalization upon application of the thiol–ene reaction with sulfonate. In general, the values for the water uptake presented in Table 2 reveal an extraordinary increase in the water uptake of these novel materials. More specifically, hydrogels originating from the functionalized polymers exhibited a roughly 25-fold increase in water uptake up to more than 50 g of water per gram of material (Table 2) compared to the initially applied polymers (Figure 3). This renders these materials applicable as superabsorbers and can be attributed to a significant increase in the hydrophilicity of the polymers used in hydrogel synthesis. Upon introduction of the sulfonate side chains, ionic moieties are introduced into the hydrogel networks. Similarly to acrylic acid–based superabsorbers, introducing sodium salts of deprotonated acids causes a significant increase in water absorption due to the solvation of both anions and cations.⁶⁹ When correlating the polymer composition to the water uptake, a significant increase in the water uptake at lower DAIVP contents is obtained, which, as explained above, is due to a lower cross-linking density. Notably, the amount of functionalized monomer units increased along with the DAIVP content from entries 9 to 12. Therefore, the hydrophilicity-enhancing effect of sulfonate side chains appears to be compensated by a higher number of cross-links in entry 12, for example. This is evidenced by analyzing entries 11 and 12, which exhibited similar amounts of sulfonate-functionalized monomers. Neglecting the differences in the DEVP amounts, the significantly reduced water uptake of hydrogels synthesized from polymer 12 can be attributed to the higher DAIVP ratio. Comparing entries 9 and 10, hydrogels corresponding to the presented terpolymer compositions revealed almost identical swelling ratios. This could potentially demonstrate the interplay between a decreasing number of cross-links (entry 9) and an increasing number of hydrophilic side groups (entry 10). The mechanical properties of the swollen hydrogels were dominated by the amount of DAIVP units available for cross-linking, as denoted in Table 2, which can also be seen in the images of the corresponding swollen networks presented in Figure S30. The correlation between the polymer composition and the mechanical properties of the respective hydrogel is in good accordance with the findings presented earlier in this work. The findings were further complemented by oscillatory frequency sweeps, revealing

Scheme 3. Functionalization of P(DEVP-*stat*-DAIVP) with Sodium 3-Mercaptopropane-1-sulfonate Prior to Hydrogel Synthesis through Photoinitiated Thiol-ene Click Chemistry

Table 2. Calculated Compositions of P(DEVP-*stat*-DAIVP) Copolymers Functionalized with Sodium 3-Mercaptopropane-1-sulfonate, Water Uptake of the Corresponding Hydrogels, and Description of the Mechanical Properties of the Water-Swollen Hydrogel Samples

entry	DEVP [%] ^a	DAIVP [%] ^a	functionalized [%] ^a	water uptake Q [g(H ₂ O)/g(sample)] ^b	description of mechanical properties
9	96.2	3.11	0.69	50 ± 5	no structural integrity
10	90.1	7.82	2.08	54 ± 1	no structural integrity
11	84.7	11.4	3.90	39 ± 3	soft and brittle
12	79.4	16.5	4.10	15 ± 0	soft and brittle

^aPolymer composition of functionalized samples after purification, as determined from ¹H NMR spectroscopy and elemental analysis. ^bWater uptake of corresponding hydrogels with standard deviation. $Q = (M_s - M_d)/M_d$.

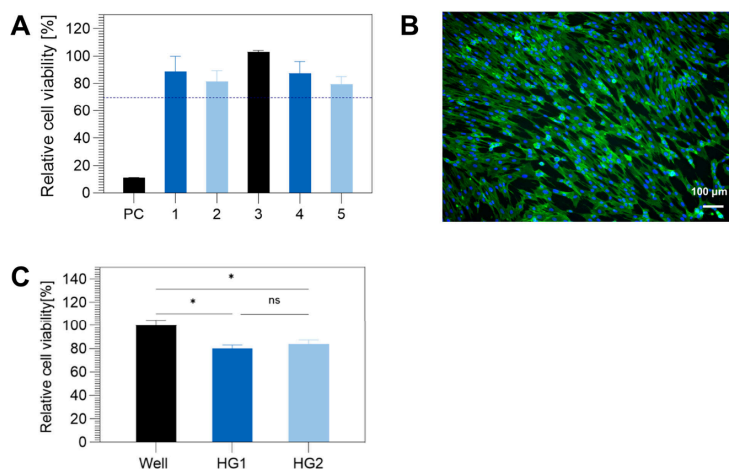


Figure 4. (A) Cytotoxicity test of human umbilical artery smooth muscle cells (HUASMCs) based on the extract test, according to ISO 10993. The cell viability is shown relative to the negative control (NC: untreated medium) upon incubation of the cells with the eluates of Hydrogels 1–5 (Table S3) at 37 °C for 72 h. The eluate of a latex glove served as a positive cytotoxic control (PC). Samples demonstrating cell viability higher than the threshold of 70% are considered noncytotoxic according to ISO 10993. (B) Cell adhesion of human umbilical artery smooth muscle cells (HUASMCs) on poly(vinylphosphonate)-based hydrogels after incubation for 3 days. Scale bar = 100 μm, nuclei are stained in blue and actin in green. (C) Cell viability of smooth muscle cells 3 days after seeding directly on two poly(vinylphosphonate)-based hydrogel samples (HG1 and HG2) relative to the viability on the well plate surface as a control.

increasing storage moduli of dilute, fully cross-linked solutions of entries 9 to 12, aligning well with the increasing DAIVP content in these samples (Figure S31). To conclude, the

combination of functionalizing P(DEVP-*stat*-DAIVP) via thiol-ene click chemistry, followed by cross-linking to hydrogels, demonstrated by this example, could be expanded

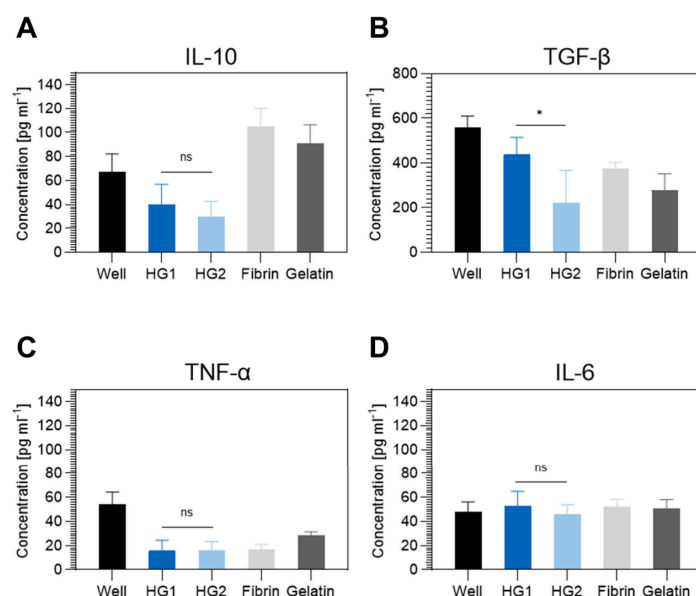


Figure 5. Cytokine expression of THP-1 monocyte-derived M0 macrophages after cultivation on the hydrogel samples (HG1, HG2), tissue culture polystyrene (Well), fibrin gel, and gelatin gel. Concentrations of anti-inflammatory cytokines interleukin-10 (IL-10) (A) and transforming growth factor-beta (TGF- β) (B) and pro-inflammatory cytokines tumor necrosis factor-alpha (TNF- α) (C) and interleukin-6 (IL-6) (D) after a 72 h incubation. Values represent mean \pm standard deviation obtained from 5 independent samples. An unpaired *t* test was conducted to compare the two sample groups.

toward introducing other functionalities into the final materials such as catalytic motifs or biologically active substrates.

Hydrogel Purification and Biocompatibility Studies.

Finally, cytotoxicity investigations were conducted to explore these novel materials' potential in biomedical applications. Initial cytotoxicity tests based on the extract test performed according to ISO 10993 with the unpurified, dried samples revealed relatively low cell viabilities (40–60%) relative to the control (untreated medium) upon incubation of human umbilical artery smooth muscle cells (HUASMCs) with the eluates of the hydrogels at 37 °C for 72 h. Therefore, an additional purification step was introduced after the hydrogel synthesis. In this context, different hydrogel samples were subjected to Soxhlet extraction with either ethanol followed by water or water exclusively. In all cases, this resulted in a significant weight loss of the samples and hinted toward the leakage of potentially cytotoxic compounds as indicated by the ratios of extractable compounds and gel calculated for different hydrogels (Table S3). Further, a ¹H NMR spectrum of the extractable fraction after solvent removal gave evidence of cross-linker, initiator, and its' decomposition products, which were removed from the sample upon Soxhlet extraction (Figure S32). With the purified hydrogels, the cytotoxicity test based on the extract test described above was repeated. The purified hydrogel samples, in which we screened different copolymers, cross-linkers, and purification methods (Table S3) exhibited cell viabilities relative to the control above the 70% threshold defined by the ISO 10993, and were therefore declared noncytotoxic (Figures 4A and S33). Finally, the purified hydrogels were tested for cell adhesion to be evaluated as potential scaffold materials for tissue engineering. Figure 4B shows the cell adhesion to and distribution on the hydrogel surface after incubation with smooth muscle cells for 3 days.

Further, an alignment of smooth muscle cells could be detected, which could not be explained through any aspects of sample preparation and is part of ongoing research. Figure 4C shows the results of the cell adhesion test and demonstrates the cell viability of smooth muscle cells 3 days after seeding directly on the poly(vinylphosphonate)-based hydrogels relative to that on the noncytotoxic surface of the well plate (control surface). Considering this data, it becomes evident that these novel, cytocompatible materials can already be applied as scaffold materials for HUASMCs and be further investigated based on their biological and mechanical properties for their potential in biomedical applications such as tissue engineering. An investigation of the endothelialization of the hydrogels was conducted with human umbilical vein endothelial cells seeded on the surfaces of hydrogels HG1 and HG2. After a 24 h incubation step, the cells were stained, and the layer formation was examined. Images show that both hydrogels supported the adhesion, growth and layer formation of endothelial cells, as shown by CD31 expression in Figure S34. These results show the broad potential of the hydrogels as they could support the endothelialization of tissue-engineered cardiovascular constructs and thereby reduce the risk of thrombosis and inflammation.

Additionally, the host immune response toward these novel materials was tested and compared to the benchmark systems fibrin and gelatin to further elucidate the potential of applying these scaffolds in tissue engineering. In this context, inflammation studies with purified P(DEVP-*stat*-DAIVP)-based hydrogels were conducted in vitro by measuring the cytokine release of THP-1 monocyte-derived M0 macrophages seeded onto the hydrogels. The hydrogels denoted as HG1 and HG2 consisted of cross-linked polymers with 15% and 20% DAIVP units, respectively. To quantify the immune response,

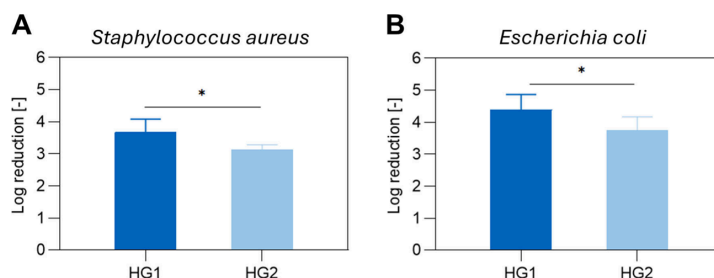


Figure 6. *S. aureus* (A) and *E. coli* (B) adhesion to P(DEVP-*stat*-DAIVP)-based hydrogels. The reduction values represent mean \pm standard deviation obtained from 5 independent samples. An unpaired *t* test was conducted to compare the two sample groups.

the release of the anti-inflammatory cytokines interleukin-10 (IL-10) and transforming growth factor-beta (TGF- β) and the pro-inflammatory cytokines tumor necrosis factor-alpha (TNF- α) and interleukin-6 (IL-6) were quantified. As shown in Figure 5, the released cytokine concentrations of IL-6, TNF- α , and the anti-inflammatory cytokine IL-10 show no significant difference for the two hydrogel samples. Regarding the release of TGF- β , HG1 exhibits higher values than HG2, potentially attributed to differences in the composition (monomer ratios, different amounts of incorporated PEG-based cross-linker, etc.). In general, however, the results of these experiments indicate that the novel poly(vinylphosphonate)-based hydrogels perform similarly to hydrogels commonly applied in tissue engineering applications, underlining their great potential for biomedical applications.

Lastly, the antibacterial properties of HG1 and HG2 were explored by performing bacterial adhesion tests with *Staphylococcus aureus* and *Escherichia coli* after seeding directly onto the hydrogel surfaces and incubation at 37 °C for three hours. Quantification of the adherent bacteria on the samples yielded log reduction values between 3 and 4 for both bacterial strains, corresponding to a 99.9–99.99% reduction of bacteria (Figure 6), which indicates the antibacterial properties of these hydrogels.

CONCLUSION

To summarize, this study successfully demonstrated the synthesis of hydrogels from statistical P(DEVP-*stat*-DAIVP) copolymers upon application of photoinitiated thiol–ene click chemistry. The copolymerization allows a facile adjustment of chain length and copolymer composition through variation of the monomer feed and monomer/catalyst ratio, while maintaining narrow polydispersities. After a series of preliminary experiments, the cross-linking process could be visualized by time-resolved rheological experiments with coupling to a UV lamp. Subsequently, oscillatory rheology was applied to characterize the mechanical properties of the various hydrogels. In this context, the mechanical strength of cross-linked samples increased with higher amounts of allyl group-containing DAIVP units in the copolymer as well as upon application of linkers containing more than two thiol functionalities. Mechanical characterization of different cross-linked samples by nanoindentation revealed increasing sample hardness and stiffness with higher cross-linking degrees and a significantly reduced hardness in the water-swollen state of the gels. Regarding the water uptake, more cross-linked hydrogels exhibited lower water absorption, attributed to decreased chain mobility and overall increased hydrophobicity of the samples.

However, a significant increase in the swelling ratio was observed with the utilization of sulfonate-functionalized polymers for hydrogel synthesis. Despite showing a 25-fold increase in the water absorption capacity, which was assigned to the increased hydrophilicity, the water uptake was seemingly still governed by the cross-linking density. Finally, the hydrogels exhibited cytocompatibility after a successful purification via Soxhlet extraction. Further, smooth muscle cells readily proliferated and adhered on the surfaces of purified poly(vinylphosphonate)-based hydrogels 3 days after direct seeding. Additional biocompatibility investigations revealed the ability to support endothelialization, no pro-inflammatory response toward these novel hydrogels, and antibacterial properties based on a reduction of the adhesion of *S. aureus* and *E. coli* on the sample surfaces. Overall, these widely tunable material properties in terms of mechanical performance and swelling behavior, in combination with low cytotoxicity, render these hydrogels appealing candidates for potential biomedical applications such as tissue engineering. Additionally, the fundamental structure–property relationships of polymer to hydrogel presented in this study offer a platform for further research ambitions. In this context, a profound understanding of the material properties of poly(vinylphosphonate)-based hydrogels can contribute to ongoing studies on the application of this photochemical cross-linking process in, e.g., additive manufacturing of these novel materials.

ASSOCIATED CONTENT

Supporting Information

The Supporting Information is available free of charge at <https://pubs.acs.org/doi/10.1021/acsami.4c07860>.

Materials and methods; Polymer characterization; Experimental procedures; Hydrogel synthesis and characterization; Rheological control experiments; Swelling kinetics; Elemental analysis of functionalized copolymers; Hydrogel purification; Cytotoxicity testing; Additional data for biological tests (PDF)

AUTHOR INFORMATION

Corresponding Author

Bernhard Rieger – Technical University of Munich, Germany, TUM School of Natural Sciences, Department of Chemistry, WACKER-Chair of Macromolecular Chemistry, 85748 Garching, Germany; orcid.org/0000-0002-0023-884X; Email: rieger@tum.de

Authors

Anton S. Maier – Technical University of Munich, Germany, TUM School of Natural Sciences, Department of Chemistry, WACKER-Chair of Macromolecular Chemistry, 85748 Garching, Germany

Salma Mansi – Technical University of Munich, Germany, TUM School of Engineering and Design, Department of Mechanical Engineering, Chair of Medical Materials and Implants, Munich Institute of Biomedical Engineering, Munich Institute of Integrated Materials, Energy and Process Engineering, 85748 Garching, Germany; orcid.org/0000-0001-5052-9840

Kerstin Halama – Technical University of Munich, Germany, TUM School of Natural Sciences, Department of Chemistry, WACKER-Chair of Macromolecular Chemistry, 85748 Garching, Germany

Philipp Weingarten – Technical University of Munich, Germany, TUM School of Natural Sciences, Department of Chemistry, WACKER-Chair of Macromolecular Chemistry, 85748 Garching, Germany

Petra Mela – Technical University of Munich, Germany, TUM School of Engineering and Design, Department of Mechanical Engineering, Chair of Medical Materials and Implants, Munich Institute of Biomedical Engineering, Munich Institute of Integrated Materials, Energy and Process Engineering, 85748 Garching, Germany; orcid.org/0000-0001-6503-076X

Complete contact information is available at: <https://pubs.acs.org/10.1021/acsami.4c07860>

Author Contributions

The manuscript was written through contributions of all authors. All authors have given approval to the final version of the manuscript.

Funding

A.S.M. is grateful for the generous funding within a Kekulé fellowship from the Fonds der Chemischen Industrie. P.W. and S.M. acknowledge support from the TUM Innovation Network “Artificial Intelligence Powered Multifunctional Material Design” (ARTEMIS).

Notes

The authors declare no competing financial interest.

ACKNOWLEDGMENTS

The authors would like to acknowledge the help of Dr. Florian Lackner, Tobias Steindorfer, and Dr. Tamilselvan Mohan with the nanoindentation experiments at the Technical University of Graz. In this context, the use of the Somapp Lab, a core facility supported by the Austrian Federal Ministry of Education, Science and Research, the Graz University of Technology, the University of Graz, and Anton Paar GmbH, is appreciated. Support from the TUM Innovation Network project ARTEMIS is acknowledged. The authors are grateful for Moritz Kränzlein’s and Andreas Schaffer’s initial ideas regarding the conceptualization of this project. The authors further want to thank Paula Großmann and Matthias Nobis for help with the first rheological experiments and fruitful discussions about the rheological data. Finally, the authors wish to acknowledge the assistance of Jonas Futter in proofreading this manuscript.

ABBREVIATIONS

DAIVP, diallyl vinylphosphonate; DEVP, diethyl vinylphosphonate; REM-GTP, rare earth metal-mediated group-transfer polymerization; HUASMCs, human umbilical artery smooth muscle cells; P(DEVP-*stat*-DAIVP), statistical copolymers composed of DEVP and DAIVP; LVR, linear viscoelastic region; DMPA, 2,2-dimethoxy-2-phenylacetophenone; AIBN, azobisisobutyronitrile; IE, initiator efficiency; *D*, polydispersity index; PEG, polyethylene glycol.

REFERENCES

- (1) Fu, J.; in *het Panhuis, M. Hydrogel Properties and Applications. J. Mater. Chem. B* **2019**, *7* (10), 1523–1525.
- (2) Loebel, C.; Ayoub, A.; Galarra, J. H.; Kossover, O.; Simaan-Yameen, H.; Seliktar, D.; Burdick, J. A. Tailoring Supramolecular Guest-Host Hydrogel Viscoelasticity With Covalent Fibrinogen Double Networks. *J. Mater. Chem. B* **2019**, *7* (10), 1753–1760.
- (3) Cao, T.; Jia, H.; Dong, Y.; Gui, S.; Liu, D. In Situ Formation of Covalent Second Network in a DNA Supramolecular Hydrogel and Its Application for 3D Cell Imaging. *ACS Appl. Mater. Interfaces* **2020**, *12* (4), 4185–4192.
- (4) Rodell, C. B.; MacArthur, J. W.; Dorsey, S. M.; Wade, R. J.; Wang, L. L.; Woo, Y. J.; Burdick, J. A. Shear-Thinning Supramolecular Hydrogels with Secondary Autonomous Covalent Crosslinking to Modulate Viscoelastic Properties In Vivo. *Adv. Funct. Mater.* **2015**, *25* (4), 636–644.
- (5) Takashima, Y.; Harada, A. Stimuli-Responsive Polymeric Materials Functioning via Host-Guest Interactions. *J. Incl. Phenom. Macrocycl. Chem.* **2017**, *88* (3–4), 85–104.
- (6) Du, H.; Zha, G.; Gao, L.; Wang, H.; Li, X.; Shen, Z.; Zhu, W. Fully Biodegradable Antibacterial Hydrogels via Thiol-Ene “Click” Chemistry. *Polym. Chem.* **2014**, *5* (13), 4002–4008.
- (7) Chen, F.; Lu, S.; Zhu, L.; Tang, Z.; Wang, Q.; Qin, G.; Yang, J.; Sun, G.; Zhang, Q.; Chen, Q. Conductive Regenerated Silk-Fibroin-Based Hydrogels With Integrated High Mechanical Performances. *J. Mater. Chem. B* **2019**, *7* (10), 1708–1715.
- (8) Li, P.; Poon, Y. F.; Li, W.; Zhu, H.-Y.; Yeap, S. H.; Cao, Y.; Qi, X.; Zhou, C.; Lamrani, M.; Beuerman, R. W.; Kang, E.-T.; Mu, Y.; Li, C. M.; Chang, M. W.; Leong, S. S. J.; Chan-Park, M. B. A Polycationic Antimicrobial and Biocompatible Hydrogel With Microbe Membrane Suctioning Ability. *Nat. Mater.* **2011**, *10* (2), 149–156.
- (9) Ibrahim, S. M.; El Salmawi, K. M.; Zahran, A. H. Synthesis of Crosslinked Superabsorbent Carboxymethyl Cellulose/Acrylamide Hydrogels Through Electron-Beam Irradiation. *J. Appl. Polym. Sci.* **2007**, *104* (3), 2003–2008.
- (10) Chang, C.; Duan, B.; Cai, J.; Zhang, L. Superabsorbent Hydrogels Based on Cellulose for Smart Swelling and Controllable Delivery. *Eur. Polym. J.* **2010**, *46* (1), 92–100.
- (11) Wei, L.; Cai, C.; Lin, J.; Chen, T. Dual-Drug Delivery System Based on Hydrogel/Micelle Composites. *Biomaterials* **2009**, *30* (13), 2606–2613.
- (12) Freichel, O. L.; Lippold, B. C. A New Oral Erosion Controlled Drug Delivery System With a Late Burst in the Release Profile. *Eur. J. Pharm. Biopharm.* **2000**, *50* (3), 345–351.
- (13) Zhang, S.; Ermann, J.; Succi, M. D.; Zhou, A.; Hamilton, M. J.; Cao, B.; Korzenik, J. R.; Glickman, J. N.; Vemula, P. K.; Glimcher, L. H.; Traverso, G.; Langer, R.; Karp, J. M. An Inflammation-Targeting Hydrogel for Local Drug Delivery in Inflammatory Bowel Disease. *Sci. Transl. Med.* **2015**, *7* (300), 300ra128–300ra128.
- (14) Zhao, X.; Lang, Q.; Yildirimer, L.; Lin, Z. Y.; Cui, W.; Annabi, N.; Ng, K. W.; Dokmeci, M. R.; Ghaemmaghami, A. M.; Khademhosseini, A. Photocrosslinkable Gelatin Hydrogel for Epidermal Tissue Engineering. *Adv. Healthc. Mater.* **2016**, *5* (1), 108–118.
- (15) Mann, B. K.; Gobin, A. S.; Tsai, A. T.; Schmedlen, R. H.; West, J. L. Smooth Muscle Cell Growth in Photopolymerized Hydrogels With Cell Adhesive and Proteolytically Degradable Domains:

- Synthetic ECM Analogs for Tissue Engineering. *Biomaterials* **2001**, *22* (22), 3045–3051.
- (16) Fan, Z.; Liu, B.; Wang, J.; Zhang, S.; Lin, Q.; Gong, P.; Ma, L.; Yang, S. A Novel Wound Dressing Based on Ag/Graphene Polymer Hydrogel: Effectively Kill Bacteria and Accelerate Wound Healing. *Adv. Funct. Mater.* **2014**, *24* (25), 3933–3943.
- (17) Li, M.; Liang, Y.; He, J.; Zhang, H.; Guo, B. Two-Pronged Strategy of Biomechanically Active and Biochemically Multifunctional Hydrogel Wound Dressing To Accelerate Wound Closure and Wound Healing. *Chem. Mater.* **2020**, *32* (23), 9937–9953.
- (18) Claus, J.; Jastram, A.; Piktel, E.; Bucki, R.; Janmey, P. A.; Kragl, U. Polymerized Ionic Liquids-Based Hydrogels With Intrinsic Antibacterial Activity: Modern Weapons Against Antibiotic-Resistant Infections. *J. Appl. Polym. Sci.* **2021**, *138* (16), 50222.
- (19) Zhou, C.; Truong, V. X.; Qu, Y.; Lithgow, T.; Fu, G.; Forsythe, J. S. Antibacterial Poly(ethylene Glycol) Hydrogels From Combined Epoxy-Amine and Thiol-Ene Click Reaction. *J. Polym. Sci., Part A: Polym. Chem.* **2016**, *54* (5), 656–667.
- (20) Basak, S.; Nandi, N.; Paul, S.; Hamley, I. W.; Banerjee, A. A Tripeptide-Based Self-Shrinking Hydrogel for Waste-Water Treatment: Removal of Toxic Organic Dyes and Lead (Pb²⁺) Ions. *Chem. Commun.* **2017**, *53* (43), 5910–5913.
- (21) Maciel, D. J.; da Silva, M. R.; Ferreira, I. L. M. Preparation of a Superparamagnetic Nanocomposite Hydrogel for Adsorptive Performance in the Wastewater Treatment. *J. Appl. Polym. Sci.* **2019**, *136* (26), 47705.
- (22) Fusi, G.; Del Giudice, D.; Skarsetz, O.; Di Stefano, S.; Walther, A. Autonomous Soft Robots Empowered by Chemical Reaction Networks. *Adv. Mater.* **2023**, *35* (7), No. e2209870.
- (23) Han, Z.; Wang, P.; Mao, G.; Yin, T.; Zhong, D.; Yiming, B.; Hu, X.; Jia, Z.; Nian, G.; Qu, S.; Yang, W. Dual pH-Responsive Hydrogel Actuator for Lipophilic Drug Delivery. *ACS Appl. Mater. Interfaces* **2020**, *12* (10), 12010–12017.
- (24) Li, M.; Wang, X.; Dong, B.; Sitti, M. In-Air Fast Response and High Speed Jumping and Rolling of a Light-Driven Hydrogel Actuator. *Nat. Commun.* **2020**, *11* (1), 3988.
- (25) Li, J.; Ma, Q.; Xu, Y.; Yang, M.; Wu, Q.; Wang, F.; Sun, P. Highly Bidirectional Bendable Actuator Engineered by LCST-UCST Bilayer Hydrogel with Enhanced Interface. *ACS Appl. Mater. Interfaces* **2020**, *12* (49), 55290–55298.
- (26) Jiang, Z.; Tan, M. L.; Taheri, M.; Yan, Q.; Tsuzuki, T.; Gardiner, M. G.; Diggle, B.; Connal, L. A. Strong, Self-Healable, and Recyclable Visible-Light-Responsive Hydrogel Actuators. *Angew. Chem.* **2020**, *132* (18), 7115–7122.
- (27) Lee, B. P.; Konst, S. Novel Hydrogel Actuator Inspired by Reversible Mussel Adhesive Protein Chemistry. *Adv. Mater.* **2014**, *26* (21), 3415–3419.
- (28) Liu, Z.; Calvert, P. Multilayer Hydrogels as Muscle-Like Actuators. *Adv. Mater.* **2000**, *12* (4), 288–291.
- (29) Tan, H.; DeFail, A. J.; Rubin, J. P.; Chu, C. R.; Marra, K. G. Novel Multiarm PEG-Based Hydrogels for Tissue Engineering. *J. Biomed. Mater. Res., Part A* **2010**, *92* (3), 979–987.
- (30) Yang, T.; Malkoch, M.; Hult, A. Sequential Interpenetrating Poly(ethylene Glycol) Hydrogels Prepared by UV-Initiated Thiol-Ene Coupling Chemistry. *J. Polym. Sci. A Polym. Chem.* **2013**, *51* (2), 363–371.
- (31) Millon, L. E.; Mohammadi, H.; Wan, W. K. Anisotropic Polyvinyl Alcohol Hydrogel for Cardiovascular Applications. *J. Biomed. Mater. Res. B* **2006**, *79* (2), 305–311.
- (32) Zhang, H.; Xia, H.; Zhao, Y. Poly(vinyl alcohol) Hydrogel Can Autonomously Self-Heal. *ACS Macro Lett.* **2012**, *1* (11), 1233–1236.
- (33) Zhou, X.; Weng, L.; Chen, Q.; Zhang, J.; Shen, D.; Li, Z.; Shao, M.; Xu, J. Investigation of pH Sensitivity of Poly(acrylic Acid-Co-Acrylamide) Hydrogel. *Polym. Int.* **2003**, *52* (7), 1153–1157.
- (34) Lee, D.; Cho, S.; Park, H. S.; Kwon, I. Ocular Drug Delivery through pHEMA-Hydrogel Contact Lenses Co-Loaded with Lipophilic Vitamins. *Sci. Rep.* **2016**, *6*, 34194.
- (35) Schwarzenböck, C.; Vagin, S. I.; Heinz, W. R.; Nelson, P. J.; Rieger, B. Studies on the Biocompatibility of Poly(diethyl vinylphosphonate) with a New Fluorescent Marker. *Macromol. Rapid Commun.* **2018**, *39* (15), No. e1800259.
- (36) Salzinger, S.; Seemann, U. B.; Plikhta, A.; Rieger, B. Poly(vinylphosphonate)s Synthesized by Trivalent Cyclopentadienyl Lanthanide-Induced Group Transfer Polymerization. *Macromolecules* **2011**, *44* (15), 5920–5927.
- (37) Zhang, N.; Salzinger, S.; Rieger, B. Poly(vinylphosphonate)s with Widely Tunable LCST: A Promising Alternative to Conventional Thermoresponsive Polymers. *Macromolecules* **2012**, *45* (24), 9751–9758.
- (38) Salzinger, S.; Soller, B. S.; Plikhta, A.; Seemann, U. B.; Herdtweck, E.; Rieger, B. Mechanistic Studies on Initiation and Propagation of Rare Earth Metal-Mediated Group Transfer Polymerization of Vinylphosphonates. *J. Am. Chem. Soc.* **2013**, *135* (35), 13030–13040.
- (39) Späth, F.; Maier, A. S.; Stasi, M.; Bergmann, A. M.; Halama, K.; Wenisch, M.; Rieger, B.; Boekhoven, J. The Role of Chemically Innocent Polyaniions in Active, Chemically Fueled Complex Coacervates. *Angew. Chem., Int. Ed.* **2023**, *62*, No. e202309318.
- (40) Adams, F.; Altenbuchner, P. T.; Werz, P. D. L.; Rieger, B. Multiresponsive Micellar Block Copolymers From 2-Vinylpyridine and Dialkylvinylphosphonates With a Tunable Lower Critical Solution Temperature. *RSC Adv.* **2016**, *6* (82), 78750–78754.
- (41) Zhang, N.; Salzinger, S.; Soller, B. S.; Rieger, B. Rare Earth Metal-Mediated Group-Transfer Polymerization: From Defined Polymer Microstructures to High-Precision Nano-Scaled Objects. *J. Am. Chem. Soc.* **2013**, *135* (24), 8810–8813.
- (42) Halama, K.; Schaffer, A.; Rieger, B. Allyl Group-Containing Polyvinylphosphonates as a Flexible Platform for the Selective Introduction of Functional Groups via Polymer-Analogous Transformations. *RSC Adv.* **2021**, *11* (61), 38555–38564.
- (43) Halama, K.; Lin, M. T.-Y.; Schaffer, A.; Foith, M.; Adams, F.; Rieger, B. Cytocompatible Triblock Copolymers with Controlled Microstructure Enabling Orthogonally Functionalized Bio-polymer Conjugates. *Macromolecules* **2024**, *57* (4), 1438–1447.
- (44) Posner, T. Beiträge zur Kenntnis der ungesättigten Verbindungen. II. Ueber die Addition von Mercaptanen an ungesättigte Kohlenwasserstoffe. *Ber. Dtsch. Chem. Ges.* **1905**, *38* (1), 646–657.
- (45) Schwarzenböck, C.; Schaffer, A.; Pahl, P.; Nelson, P. J.; Huss, R.; Rieger, B. Precise Synthesis of Thermoresponsive Polyvinylphosphonate-Biomolecule Conjugates via Thiol-Ene Click Chemistry. *Polym. Chem.* **2018**, *9* (3), 284–290.
- (46) Schwarzenböck, C.; Nelson, P. J.; Huss, R.; Rieger, B. Synthesis of Next Generation Dual-Responsive Cross-Linked Nanoparticles and Their Application to Anti-Cancer Drug Delivery. *Nanoscale* **2018**, *10* (34), 16062–16068.
- (47) Hoyle, C. E.; Bowman, C. N. Thiol-Ene Click Chemistry. *Angew. Chem., Int. Ed.* **2010**, *49* (9), 1540–1573.
- (48) Morgan, C. R.; Magnotta, F.; Ketley, A. D. Thiol/Ene Photocurable Polymers. *J. Polym. Sci. Polym. Chem. Ed.* **1977**, *15* (3), 627–645.
- (49) Kade, M. J.; Burke, D. J.; Hawker, C. J. The Power of Thiol-Ene Chemistry. *J. Polym. Sci. A Polym. Chem.* **2010**, *48* (4), 743–750.
- (50) Hoyle, C. E.; Lee, T. Y.; Roper, T. Thiol-Ene: Chemistry of the Past With Promise for the Future. *J. Polym. Sci. A Polym. Chem.* **2004**, *42* (21), 5301–5338.
- (51) Zhu, L.; Zimudzi, T. J.; Li, N.; Pan, J.; Lin, B.; Hickner, M. A. Crosslinking of Comb-Shaped Polymer Anion Exchange Membranes via Thiol-Ene Click Chemistry. *Polym. Chem.* **2016**, *7* (14), 2464–2475.
- (52) Rydholm, A. E.; Bowman, C. N.; Anseth, K. S. Degradable Thiol-Acrylate Photopolymers: Polymerization and Degradation Behavior of an In Situ Forming Biomaterial. *Biomaterials* **2005**, *26* (22), 4495–4506.
- (53) Reddy, S. K.; Anseth, K. S.; Bowman, C. N. Modeling of Network Degradation in Mixed Step-Chain Growth Polymerizations. *Polymer* **2005**, *46* (12), 4212–4222.

- (54) Elbert, D. L.; Pratt, A. B.; Lutolf, M. P.; Halstenberg, S.; Hubbell, J. A. Protein delivery from materials formed by self-selective conjugate addition reactions. *J. Controlled Release* **2001**, *76* (1–2), 11–25.
- (55) Lutolf, M. P.; Hubbell, J. A. Synthesis and Physicochemical Characterization of End-Linked Poly(ethylene Glycol)-Co-Peptide Hydrogels Formed by Michael-Type Addition. *Biomacromolecules* **2003**, *4* (3), 713–722.
- (56) Schaffer, A.; Kränzlein, M.; Rieger, B. Synthesis and Application of Functional Group-Bearing Pyridyl-Based Initiators in Rare Earth Metal-Mediated Group Transfer Polymerization. *Macromolecules* **2020**, *53* (11), 4345–4354.
- (57) Pehl, T. M.; Kränzlein, M.; Adams, F.; Schaffer, A.; Rieger, B. C-H Bond Activation of Silyl-Substituted Pyridines with Bis-(Phenolate)Yttrium Catalysts as a Facile Tool towards Hydroxyl-Terminated Michael-Type Polymers. *Catalysts* **2020**, *10* (4), 448.
- (58) Soller, B. S.; Salzinger, S.; Jandl, C.; Pöthig, A.; Rieger, B. C-H Bond Activation by σ -Bond Metathesis as a Versatile Route toward Highly Efficient Initiators for the Catalytic Precision Polymerization of Polar Monomers. *Organometallics* **2015**, *34* (11), 2703–2706.
- (59) Lanzinger, D.; Salzinger, S.; Soller, B. S.; Rieger, B. Poly(vinylphosphonate)s as Macromolecular Flame Retardants for Polycarbonate. *Ind. Eng. Chem. Res.* **2015**, *54* (6), 1703–1712.
- (60) Weger, M.; Pahl, P.; Schmidt, F.; Soller, B. S.; Altmann, P. J.; Pöthig, A.; Gemmecker, G.; Eisenreich, W.; Rieger, B. Isospecific Group-Transfer Polymerization of Diethyl Vinylphosphonate and Multidimensional NMR Analysis of the Polymer Microstructure. *Macromolecules* **2019**, *52* (18), 7073–7080.
- (61) Zuidema, J. M.; Rivet, C. J.; Gilbert, R. J.; Morrison, F. A. A Protocol for Rheological Characterization of Hydrogels for Tissue Engineering Strategies. *J. Biomed. Mater. Res. B* **2014**, *102* (5), 1063–1073.
- (62) Štaffová, M.; Ondreáš, F.; Svatík, J.; Zbončák, M.; Jančář, J.; Lepcio, P. 3D Printing and Post-Curing Optimization of Photopolymerized Structures: Basic Concepts and Effective Tools for Improved Thermomechanical Properties. *Polym. Test.* **2022**, *108*, 107499.
- (63) Zhang, X. N.; Du, C.; Du, M.; Zheng, Q.; Wu, Z. L. Kinetic Insights Into Glassy Hydrogels With Hydrogen Bond Complexes As the Cross-Links. *Mater. Today Phys.* **2020**, *15*, 100230.
- (64) Pretsch, E. *Spektroskopische Daten zur Strukturklärung organischer Verbindungen*, 4, vollst. überarb. u. erw. Aufl.; Springer, 2001. DOI: 10.1007/978-3-662-09972-8.
- (65) Kloxin, A. M.; Kloxin, C. J.; Bowman, C. N.; Anseth, K. S. Mechanical Properties of Cellularly Responsive Hydrogels and Their Experimental Determination. *Advanced materials* **2010**, *22* (31), 3484–3494.
- (66) Liling, G.; Di, Z.; Jiachao, X.; Xin, G.; Xiaoting, F.; Qing, Z. Effects of Ionic Crosslinking on Physical and Mechanical Properties of Alginate Mulching Films. *Carbohydr. Polym.* **2016**, *136*, 259–265.
- (67) Park, H.; Guo, X.; Temenoff, J. S.; Tabata, Y.; Caplan, A. I.; Kasper, F. K.; Mikos, A. G. Effect of Swelling Ratio of Injectable Hydrogel Composites on Chondrogenic Differentiation of Encapsulated Rabbit Marrow Mesenchymal Stem Cells In Vitro. *Biomacromolecules* **2009**, *10* (3), 541–546.
- (68) Ganji, F.; Vasheghani-Farahani, S.; Vasheghani-Farahani, E. Theoretical Description of Hydrogel Swelling: A Review. *Iran. Polym. J.* **2010**, *19* (5), 375–398.
- (69) Brelle, L.; Faÿ, F.; Ozturk, T.; Didier, N.; Renard, E.; Langlois, V. Hydrogel Based on Polyhydroxyalkanoate Sulfonate: Control of the Swelling Rate by the Ionic Group Content. *Biomacromolecules* **2023**, *24* (4), 1871–1880.

4.5 Author contributions

Anton Maier synthesized the catalyst and monomers, performed the polymerization experiments, and characterized all polymers (NMR, SEC-MALS, FT-IR, thermal analyses, etc.). A. M. synthesized, characterized, and purified all cross-linked materials. Furthermore, A. M carried out all rheological characterizations and performed all experiments regarding the studies on water uptake. A. M. conceptualized the project and initiated the collaborations with all the coauthors. A. M. analyzed the measurement results and wrote the original draft's polymer- and hydrogel-related parts.

5 Synthesis and characterization of highly hydrophilic networks

5.1 Bibliographic data

Title: “Water Uptake, Thin-Film Characterization, and Gravimetric pH-Sensing of Poly(vinylphosphonate)-Based Hydrogels”

Status: Paper, Publication date: 20.12.2024

Journal: ACS Applied Materials & Interfaces

Publisher: American Chemical Society (ACS)

DOI: 10.1021/acsami.4c17704

Authors: Anton S. Maier, Matjaž Finšgar, Beatrice De Chiara, Rupert Kargl, Bernhard Wolfrum, Karin Stana Kleinschek, and Bernhard Rieger

5.2 Table of content graphic

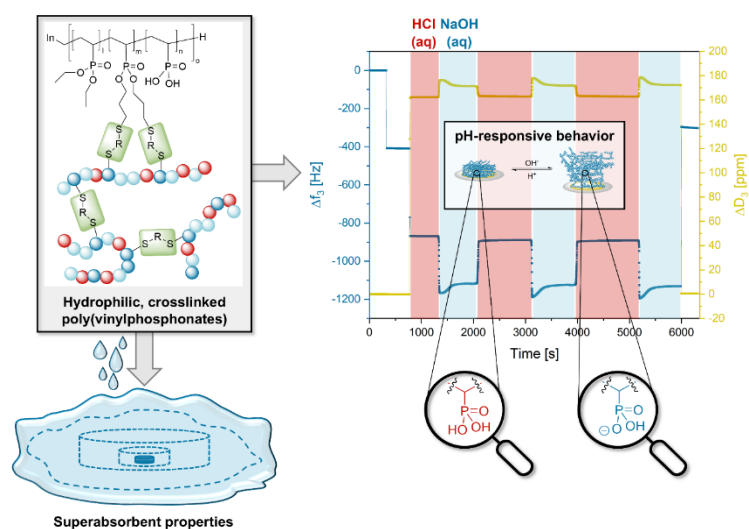


Figure 26: Table of content graphic for the manuscript entitled “Water Uptake, Thin-Film Characterization, and Gravimetric pH-Sensing of Poly(vinylphosphonate)-Based Hydrogels”.

5.3 Content

Intending to increase the water uptake of poly(vinylphosphonate)-based hydrogels, this study introduces a facile two-step synthesis route, combining the polymer-analogous hydrolysis of P(DEVP-*stat*-DAIVP) copolymers – introducing vinylphosphonic acid (VPA) units – with the photochemical cross-linking toward covalent networks. The resulting materials exhibit drastically increased water uptakes up to 150 ± 27 g (H₂O)/g (hydrogel) due to higher hydrophilicity and evident structure-property relationships between polymer composition and hydrogel properties regarding water uptake and mechanical strength. Polymer solutions containing the partially dealkylated poly(vinylphosphonates), a photoinitiator, and the cross-linker are spin-coated onto different substrates, including silicon wafers and the gold surfaces of QCM-D sensors and subsequently cross-linked by UV irradiation ($\lambda = 365$ nm). These thin films are thoroughly characterized by profilometry, light microscopy, AFM, and dry-film QCM-D, revealing a quantitative, homogeneous coverage of the substrates with a film thickness of 39.4 ± 2.33 nm. Subsequently, the hydrogel films are subjected to QCM-D measurements in different aqueous environments, demonstrating strongly pH-dependent swelling behavior in response to the pH values of the environment (1, 6, 10, 13). This is attributed to electrostatic repulsions within the networks caused by deprotonation and protonation of VPA, inducing a fully reversible swelling and deswelling of the hydrogel films. Consequently, spin-coating these hydrogel materials onto QCM-D electrodes creates gravimetric pH-sensors to discriminate between pH values by monitoring the network's swelling states. The hydrogels exhibit excellent stability on the gold surfaces, with little to no erosion despite applying harsh conditions, suggesting an anchoring of the networks on the substrates through the dithiol cross-linker via Au-S-interactions. This hypothesis is verified by an in-depth characterization of the films on the surfaces by a plethora of analytical methods. AFM, XPS, and ToF-SIMS measurements confirm the expected film composition and unveil an increased S-related signal intensity at the polymer network/Au interface, thus supporting the proposed surface anchoring mechanism.

5.4 Manuscript

ACS APPLIED MATERIALS
& INTERFACES

Open Access

This article is licensed under CC-BY 4.0

www.acsami.org

Research Article

Water Uptake, Thin-Film Characterization, and Gravimetric pH-Sensing of Poly(vinylphosphonate)-Based Hydrogels

Anton S. Maier, Matjaž Finšgar, Beatrice De Chiara, Rupert Kargl,* Bernhard Wolfrum, Karin Stana Kleinschek, and Bernhard Rieger*

Cite This: *ACS Appl. Mater. Interfaces* 2025, 17, 2577–2591

Read Online

ACCESS |

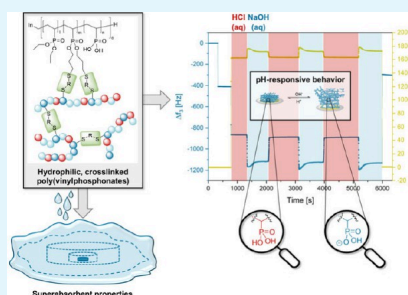
Metrics & More

Article Recommendations

Supporting Information

ABSTRACT: Herein, novel, superabsorbent, and pH-responsive hydrogels obtained by the photochemical cross-linking of hydrophilic poly(vinylphosphonates) are introduced. First, statistical copolymers of diethyl vinylphosphonate (DEVP) and diallyl vinylphosphonate (DAIVP) are synthesized via rare earth metal-mediated group-transfer polymerization (REM-GTP) yielding similar molecular weights ($M_{n,NMR} = 127\text{--}142$ kg/mol) and narrow polydispersities ($D < 1.12$). Subsequently, polymer analogous transformations of P(DEVP-*stat*-DAIVP) introduced vinylphosphonic acid (VPA) units into the polymers. In this context, the partial dealkylation of the polymers revealed a preference for DAIVP hydrolysis, which was observed via ^1H NMR spectroscopy and explained mechanistically. Furthermore, the P(DEVP-*stat*-DAIVP-*stat*-VPA) polymers were cross-linked under photochemical reaction conditions ($\lambda = 365$ nm) via thiol-ene click chemistry, yielding superabsorbent hydrogels with water uptakes up to 150 ± 27 g (H_2O)/g (hydrogel). Regarding water absorption, evident structure–property relationships between cross-linking density, polarity, and swelling behavior were found. Finally, the pH-responsiveness of thin films of these hydrogels was investigated. In this regard, films with a thickness of 39.4 ± 2.33 nm determined via profilometry were spin-coated on sensors of a quartz crystal microbalance with dissipation monitoring (QCM-D) and thoroughly characterized by atomic force microscopy (AFM). QCM-D measurements exposing the hydrogel films to different aqueous media revealed different swelling states of the hydrogels depending on the pH values (1, 6, 10, and 13) of the surrounding environment, as reflected by corresponding frequency and dissipation values. The hydrogels exhibited fully reversible swelling and deswelling upon switching between pH 1 and 13 (three cycles), sustaining the harsh conditions without erosion from the gold surface and thus acting as a gravimetric sensor discriminating between the two pH values. The high stability of the films on the gold surfaces of QCM-D sensors was explained by anchoring of the P(DEVP-*stat*-DAIVP-*stat*-VPA) networks through the dithiol cross-linker as confirmed by detailed X-ray photoelectron spectroscopy (XPS) and time-of-flight secondary ion mass spectrometry (ToF-SIMS) studies.

KEYWORDS: superabsorbent hydrogels, pH-responsiveness, hydrogel thin films, quartz crystal microbalance, pH sensor, reversible swelling, rare earth metal-mediated group-transfer polymerization



INTRODUCTION

In recent years, stimuli-responsive hydrogels have emerged as a promising area of research in biomedical fields such as controlled drug delivery and tissue engineering due to their high biocompatibility and resemblance to biological tissues.^{1–3} In this context, employing these materials enables the release of an active pharmaceutical ingredient, such as a protein or a drug, in a controlled manner through an external trigger or changes in the surrounding conditions.^{4,5} Hydrogels in stimuli-responsive applications often serve as scaffolds reacting to environmental changes, e.g., differences in the pH value,^{6–8} temperature,^{9,10} light,^{11,12} electricity,^{13,14} and the presence of biomolecules.¹⁵ Beyond biomedicine, several other areas employ cross-linked materials with these properties. For instance, in the field of actuators and soft robotics, these components can undergo mechanical motion upon external

stimulation, or in the fabrication of sensors, hydrogels with the ability to respond to variations in an ambient medium are up-and-coming candidates.^{16–20} The swelling behavior and other material characteristics of synthetic and natural hydrogels are often influenced by the pH value of the surrounding medium, affecting the charge of acidic or basic groups in the polymer networks. Notable examples of pH-responsive moieties in hydrogels include acrylic acid-containing networks, along with chitosan and hyaluronic acid derivatives as representatives of

Received: October 14, 2024
 Revised: November 29, 2024
 Accepted: December 10, 2024
 Published: December 20, 2024



ACS Publications

© 2024 The Authors. Published by
American Chemical Society

2577

https://doi.org/10.1021/acsami.4c17704
ACS Appl. Mater. Interfaces 2025, 17, 2577–2591

biopolymers.^{19,21–23} The potential of certain materials reacting to changes in the pH value is highlighted by their widespread implementation in numerous areas of research and everyday life. These include smart and antibacterial coatings,^{22,24–27} smart packaging,²⁸ actuators and sensors,^{16,17,19,20} and lab-on-a-chip applications,²⁹ among others, therefore creating incentives for further research toward the discovery of novel materials with these properties. Before application, the pH-dependent behavior of newly established hydrogels is typically investigated by analyzing the water uptake of different samples across a range of pH values. Additional insights into the response of thin films of cross-linked, pH-sensitive networks can be obtained through a quartz crystal microbalance with dissipation monitoring (QCM-D), providing an online measurement of the swelling state as well as the viscoelastic properties of the sample.^{25,30–32} The water uptake of a hydrogel is usually governed by several factors, including the hydrophilicity of the polymers, the cross-linking density of the network, chain mobility, and external factors like the ionic strength of the medium used for swelling experiments.^{33–35} Further, the water uptake may be increased by introducing sodium salts of deprotonated acids through increased hydrophilicity and solvation of both anions and cations.³⁶ In a recent study, we introduced hydrogels obtained through photochemical cross-linking of statistical copolymers consisting of diethyl vinylphosphonate (DEVP) and diallyl vinylphosphonate (DAIVP) applying thiol–ene click chemistry with dithiols as cross-linkers. The final materials exhibited widely tunable properties in terms of water uptake and mechanical strength, as well as good biocompatibility.³⁷ The corresponding copolymers were obtained with excellent control over the polymer microstructure while maintaining narrow polydispersities by applying yttrium-catalyzed rare earth metal-mediated group-transfer polymerization (REM-GTP).³⁸ This highly precise polymerization technique gives access to well-defined polymeric structures in terms of molecular weight and polydispersity through repeated 1,4-conjugate addition of Michael-type monomers.^{39,40} Further, REM-GTP enables a straightforward introduction of biologically active motifs and other substrates into allyl group-containing poly(vinylphosphonates) under mild conditions through postpolymerization thiol–ene click chemistry.^{41,42} As demonstrated in the study mentioned above, the functionalization of polymers with sodium salts of organic acids prior to photochemical cross-linking toward hydrogels was successfully applied, yielding materials with significantly increased swelling ratios.^{36,37} Another approach for increasing the water uptake worth exploring includes polymer modification rather than functionalization. In this context, the well-established transformation of poly(vinylphosphonates) with trimethylsilyl bromide (TMSBr) results in partial hydrolysis of the polymer side chains toward poly(vinylphosphonic acid) (PVPA). When applied to allyl-group containing poly(vinylphosphonates), this should generate cross-linkable polymers with increased hydrophilicity, potentially inducing pH-responsiveness into the final materials.⁴³ In this study, different P(DEVP-*stat*-DAIVP) copolymers obtained via REM-GTP are subjected to polymer-analogous hydrolysis of the monomers toward statistical P(DEVP-*stat*-DAIVP-*stat*-VPA) terpolymers, which are cross-linked applying photoinitiated thiol–ene click reactions with 3,6-dioxo-1,8-octanedithiol. After being dried, the resulting hydrogels are thoroughly analyzed regarding water uptake. Further, in-depth characterization of thin films of these novel materials and detailed

analyses of the pH-responsiveness through QCM-D measurements contribute to a profound understanding of the high application potential in actuators and sensors.

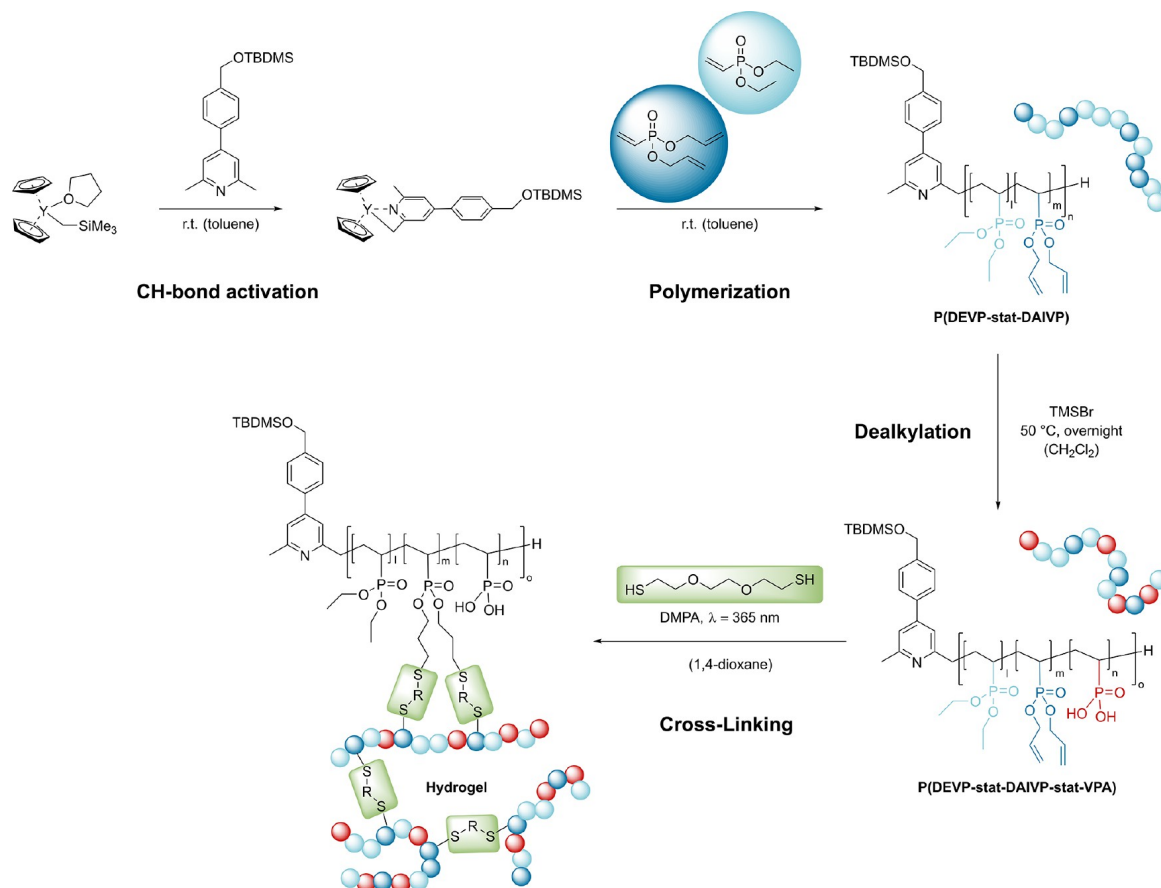
EXPERIMENTAL SECTION

Statistical Copolymerization of Diethyl Vinylphosphonate (DEVP) and Diallyl Vinylphosphonate (DAIVP). The statistical copolymerization of DEVP and DAIVP was performed according to previously reported procedures.^{37,41} In a copolymerization experiment, the calculated amount of catalyst Cp₂YCH₂TMS(thf) (1.00 equiv) was dissolved in dry toluene. The calculated amount of initiator (1.10 equiv) was added to this solution, resulting in a yellow coloration. After 2 h, quantitative conversion of the catalyst toward the initiating species was confirmed via ¹H NMR spectroscopy by withdrawing an aliquot of the reaction mixture (0.1 mL of solution +0.4 mL of C₆D₆), and a mixture of monomers in the desired ratio was added in one motion. The polymerization was stirred at room temperature for 2 h until a second aliquot (0.1 mL of solution +0.4 mL of CD₃OD) confirmed quantitative conversion via ³¹P NMR spectroscopy. Then, polymerization was stopped by adding 0.5 mL of undried MeOH, and the polymers precipitated from hexane. After centrifugation, the residues were taken up in 1,4-dioxane and subjected to lyophilization to yield the purified P(DEVP-*stat*-DAIVP) polymers as white solids.

Partial Hydrolysis of P(DEVP-*stat*-DAIVP) toward Vinylphosphonic Acid (VPA)-Containing Terpolymers. The polymer-analogous hydrolysis of P(DEVP-*stat*-DAIVP) was performed according to a well-established procedure applying trimethylsilyl bromide (TMSBr).⁴³ In an oven-dried Schlenk flask suitable for elevated pressures, P(DEVP-*stat*-DAIVP) was dissolved in dry CH₂Cl₂ (10 mL of solvent per 100 mg of polymer). Further, 0.30 equiv (or 0.15, as specified in the manuscript) of TMSBr was added, and the reaction mixture was refluxed for 16 h. Then, the solvent was removed in vacuo, and the residue was taken up in 20 mL of methanol, and 5 mL of 1 M hydrochloric acid (aq) was added. The resulting reaction mixture was stirred at room temperature for 2 h. Finally, the solvent was removed under reduced pressure, and the crude product was purified via dialysis against deionized water (8 kDa MWCO). Lyophilization yielded the partially hydrolyzed P(DEVP-*stat*-DAIVP-*stat*-VPA) polymers as white solids.

Synthesis of Hydrogels from VPA-Containing Terpolymers. To obtain hydrogels from P(DEVP-*stat*-DAIVP-*stat*-VPA) terpolymers, the reaction conditions reported in an initial study were applied.³⁷ In a typical experiment, 100 mg of polymer were dissolved in 0.3 mL of dioxane. For some polymers, small amounts of water were added to facilitate the solubilization of polymers. To this solution, the calculated amounts of cross-linker 3,6-dioxo-1,8-octanedithiol (2.50 equiv) and 0.40 equiv of the photoinitiator 2,2-dimethoxy-2-phenylacetophenone (DMPA) were added. After homogenization, the reaction mixture was cross-linked through UV irradiation ($\lambda = 365$ nm) for 60 min and dried to weight constancy in vacuo.

Thin-Film Preparation. Stock solutions of P(DEVP-*stat*-DAIVP-*stat*-VPA) for spin-coating silicon wafers and QCM-D sensors were freshly prepared before each experiment. In this context, 25 mg of polymer was dissolved in 3 mL methanol and 0.5 mL distilled water, resulting in a homogeneous, clear solution. Subsequently, the calculated amounts of the cross-linker 3,6-dioxo-1,8-octanedithiol with respect to the allyl groups in the polymer (2.50 equiv per allyl group) and the photoinitiator 2,2-dimethoxy-2-phenylacetophenone (DMPA) (0.40 equiv per allyl group) were added to the solution. To prevent ambient light-induced cross-linking, all samples were prepared and stored in brown glass vials to protect them from surrounding light. The spin-coating of quartz crystals and silicon wafers was performed according to well-established procedures.^{44,45} The P-(DEVP-*stat*-DAIVP-*stat*-VPA)-containing films were deposited on the static substrates by pipetting 50 μ L of an 85 ppm (0.0085 wt %) polymer-containing stock solution in methanol/water (6/1) onto the surfaces of either the QCM-D sensors or the silicon wafers.

Scheme 1. Overview of the Synthetic Pathway toward Highly Water-Absorbing Hydrogels⁴⁴


⁴⁴CH-bond activation of a sym-collidine derivative with $Cp_2YCH_2TMS(thf)$ towards the initiating complex (Step 1); polymerization through addition of the monomers diethyl vinylphosphonate (DEVP) and diallyl vinylphosphonate (DAIVP) (Step 2); polymer-analogous transformation of the copolymer side-chains towards vinylphosphonic acid (VPA) units (Step 3); crosslinking of P(DEVP-stat-DAIVP-stat-VPA) chains via photoinitiated thiol–ene click chemistry to highly hydrophilic hydrogels (Step 4).

Immediately after adding the stock solution, the substrates were rotated at a spinning speed of 4000 rpm with an acceleration of 2500 rpm/s for 60 s. In the final step, the films on the substrates were cross-linked by UV irradiation ($\lambda = 365$ nm) for 60 s.

Workflow of QCM-D Measurements. In a typical QCM-D experiment, the frequencies and dissipation of cleaned and empty QCM-D sensors were monitored in ambient air for 5 min. Subsequently, the substrates were spin-coated with a freshly prepared polymer-, cross-linker-, and photoinitiator-containing solution, as described above.^{44,45} Next, the films on the substrates were cross-linked through UV irradiation ($\lambda = 365$ nm) for 1 min. The frequency change upon spin-coating was evaluated by measuring the sensors in air for another 5 min. Following that, the crystals were subjected to the different aqueous solutions described in the discussion, and the QCM-D response was monitored for the given timeframes, observing different swelling states of the hydrogel films. Finally, the QCM-D crystals were removed from the device, dried thoroughly with nitrogen gas to avoid mechanical removal of the films, and remeasured in air to confirm that no significant sample leaching occurred.

RESULTS AND DISCUSSION

Polymer Synthesis and Modification. As reported in previous studies, statistical copolymers from the water-soluble

monomer diethyl vinylphosphonate (DEVP) and the cross-linkable monomer diallyl vinylphosphonate (DAIVP) were obtained through rare earth metal-mediated group-transfer polymerization (REM-GTP).³⁷ After the quantitative conversion of the $Cp_2YCH_2TMS(thf)$ catalyst toward the initiating species was achieved (Scheme 1, Step 1), as confirmed by 1H NMR spectroscopy in C_6D_6 , a mixture of the monomers was added to initiate the polymerization (Scheme 1, Step 2). Following, once quantitative monomer conversion was confirmed via ^{31}P NMR spectroscopy, the polymers were purified by precipitation and characterized by 1H NMR (Figure S1) and 1H DOSY NMR spectroscopy (Figure S3) as well as size-exclusion chromatography multi-angle light scattering (SEC-MALS). An overview of the polymerization results of different P(DEVP-stat-DAIVP) copolymers is given in Table 1.

As described in previous studies, these results highlight the high precision of REM-GTP in terms of tailoring the copolymer microstructure toward different DEVP/DAIVP ratios by adjusting the amounts of monomers relative to the catalyst while maintaining narrow polydispersities.³⁷ Table 1

Table 1. Selected Polymerization Results of the Polymerization of Diethyl Vinylphosphonate (DEVP) and Diallyl Vinylphosphonate (DAIVP) Applying the Rare Earth Metal-Based Catalyst $Cp_2YCH_2TMS(thf)^{d,e}$

Polymer	DAIVP content [%] ^b	DEVP content [%] ^b	$M_{n,NMR}$ [kg/mol] ^c	IE ^d	\bar{D} ^e
1	10.9	89.1	137	43	1.06
2	19.1	80.9	138	43	1.12
3	24.7	75.3	127	48	1.06
4	24.6	75.4	142	42	1.10

^aAll polymerizations were performed at room temperature in toluene, targeting 400 repetition units and varying the DEVP/DAIVP/Catalyst ratio. Quantitative conversions were determined via ³¹P NMR spectroscopy in CD₃OD. ^bDetermined via ¹H NMR spectroscopy by comparison of the CH₂ signals of DEVP (4.18 ppm, *m* = 1/4) and DAIVP (4.63 ppm, *n* = 1/4); ^cCalculated via ¹H NMR spectroscopy by comparison of the –OTBDMS signals of the initiator at 0.14 ppm (*I* = 6H) and the CH₂ signals of DEVP (4.18 ppm, *m* = 1/4) and DAIVP (4.63 ppm, *n* = 1/4); ^dInitiator efficiency: IE = $M_{n,theo}/M_{n,NMR}$ with $M_{n,NMR}$ = 327.54 g/mol + $m \cdot 164.14$ g/mol + $n \cdot 188.16$ g/mol and $M_{n,theo}$ determined from the applied monomer to catalyst amounts; ^ePolydispersity index determined via size-exclusion chromatography multiangle light scattering (SEC-MALS) in THF:H₂O (1:1) with 340 mg/L 2,6-di-*tert*-butyl-4-methylphenol (BHT) and 9 g/L tetra-*n*-butylammonium bromide (TBAB).

displays a variation of the content of cross-linkable DAIVP, simultaneously targeting comparable molecular weights between 127 and 142 kg/mol in copolymers 1–4. The results for the copolymer microstructures and molecular weights were obtained via ¹H NMR spectroscopy (Figure S1), and ³¹P NMR spectroscopy (Figure S2) and ¹H DOSY NMR spectra (Figure S3) confirm successful copolymer synthesis. Furthermore, the polydispersities below 1.12 for entries 1–4 determined by SEC-MALS reflect a uniform molecular weight determination characteristic of catalytic REM-GTP. In a subsequent step, P(DEVP-*stat*-DAIVP) polymers 1–3 were subjected to side chain modification with 0.30 equiv of TMSBr, whereas polymer 4 was reacted with only 0.15 equiv of TMSBr (Scheme 1, Step 3). This polymer-analogous transformation is well-known for poly(vinylphosphonates), resulting in the formation of vinylphosphonic acid (VPA) units in the polymer backbone while maintaining the degree of polymerization.⁴³ After purification via dialysis against deionized water (MWCO = 8 kDa), lyophilization yielded pure P(DEVP-*stat*-DAIVP-*stat*-VPA) terpolymers, in which a statistical distribution of monomers is assumed. The degree of deprotection after each reaction, also reflected by the number of VPA units formed, was calculated via comparison of the ¹H NMR spectra of P(DEVP-*stat*-DAIVP) (Table 1, Entries 1–4) and P(DEVP-*stat*-DAIVP-*stat*-VPA) (Table 2, Entries 5–8), normalizing the signals of the polymer backbone (δ = 1.65–3.00 ppm). Notably, the side-chain hydrolysis of copolymers 1–4 (Table 1) toward terpolymers 5–8 (Table 2) resulted in a preference for DAIVP dealkylation compared to DEVP, as evidenced via ¹H NMR spectroscopy (Figure S4) and the compositions listed in Table 2. In this context, we hypothesize that this might be due to the proposed mechanism presented in Figure S4, agreeing with the literature and suggesting an allyl cleavage rather than ethyl cleavage for statistical reasons (different reaction pathways indicated by arrows) and due to better stabilization of the corresponding cation.^{1,46} In general, however, the compositions of P(DEVP-*stat*-DAIVP-*stat*-VPA)

Table 2. Calculated Compositions of P(DEVP-*stat*-DAIVP-*stat*-VPA) Terpolymers Obtained through Polymer-Analogous Transformation of P(DEVP-*stat*-DAIVP) with TMSBr and Water Uptake of the Corresponding Hydrogels, Followed by a Description of the Mechanical Properties of the Water-Swollen Hydrogel Samples

P(DEVP- <i>stat</i> -DAIVP- <i>stat</i> -VPA)	DEVP [%] ^a	DAIVP [%] ^a	VPA [%] ^a	Water uptake of corresponding hydrogel [g (H ₂ O)/g (HG)] ^b	Description of mechanical properties ^c
5	72.7	0.50	26.8	150 ± 27	No structural integrity
6	72.0	3.70	24.3	29 ± 4	Soft and brittle
7	65.6	6.80	27.6	28 ± 5	Stable specimen
8	72.1	8.20	19.7	19 ± 2	Stable specimen

^aPolymer composition of functionalized samples after purification as determined from ¹H NMR spectroscopy. ^bWater uptake of corresponding hydrogels with standard deviation: $Q = (M_s - M_d)/M_d$. ^cObtained from the handling of the water-swollen hydrogel samples during the swelling experiments.

terpolymers 5–7 presented in Table 2 suggest similar overall degrees of dealkylation, as evidenced by the extent of VPA formed, which aligns well with the application of equimolar amounts of TMSBr. Therefore, it can be concluded that controlling the amount of residual DAIVP units in the terpolymers available for cross-linking is only possible by adjusting the DEVP/DAIVP ratio during copolymer synthesis.

Hydrogel Synthesis and Characterization of Swelling Properties. The purified P(DEVP-*stat*-DAIVP-*stat*-VPA) terpolymers were subsequently subjected to a thiol–ene click reaction with 3,6-dioxo-1,8-octanedithiol using photochemical reaction conditions (λ = 365 nm) and 2,2-dimethoxy-2-phenylacetophenone (DMPA) as a photoinitiator (Scheme 1, Step 4). Each sample was cross-linked in a UV reactor for 60 min and dried to weight constancy in vacuo. After that, each dry sample was immersed in water for eight hours, and the water uptake was calculated by comparing the weight difference between the swollen and the dry sample according to Equation S1. In previous studies, P(DEVP-*stat*-DAIVP) copolymers were cross-linked without further modification, yielding relatively apolar materials with water uptakes of up to 2.22 g of water per gram of dry hydrogel. A hydrophilicity increase was possible by polymer modification via thiol–ene click chemistry with sodium 3-mercaptopropane-1-sulfonate before cross-linking, resulting in swelling ratios above 50. Here, we explored a different approach toward highly polar, cross-linked materials with the beneficial side-effect of introducing stimuli-responsiveness into these novel hydrogels.³⁷ The terpolymer compositions calculated via ¹H NMR spectroscopy (Figure S4), the results of the swelling experiments, as well as a description of the mechanical properties of the hydrogels are presented in Table 2. In this context, swelling experiments were performed at least in triplicate.

When comparing the terpolymer compositions presented in Table 2 with the initial compositions of P(DEVP-*stat*-DAIVP) 1–4 (Table 1), these results reflect the preference for DAIVP-side chain dealkylation over DEVP side chain deprotection, as discussed above and confirmed by ¹H NMR spectroscopy (Figure S4). However, treating copolymers 1–3, which display

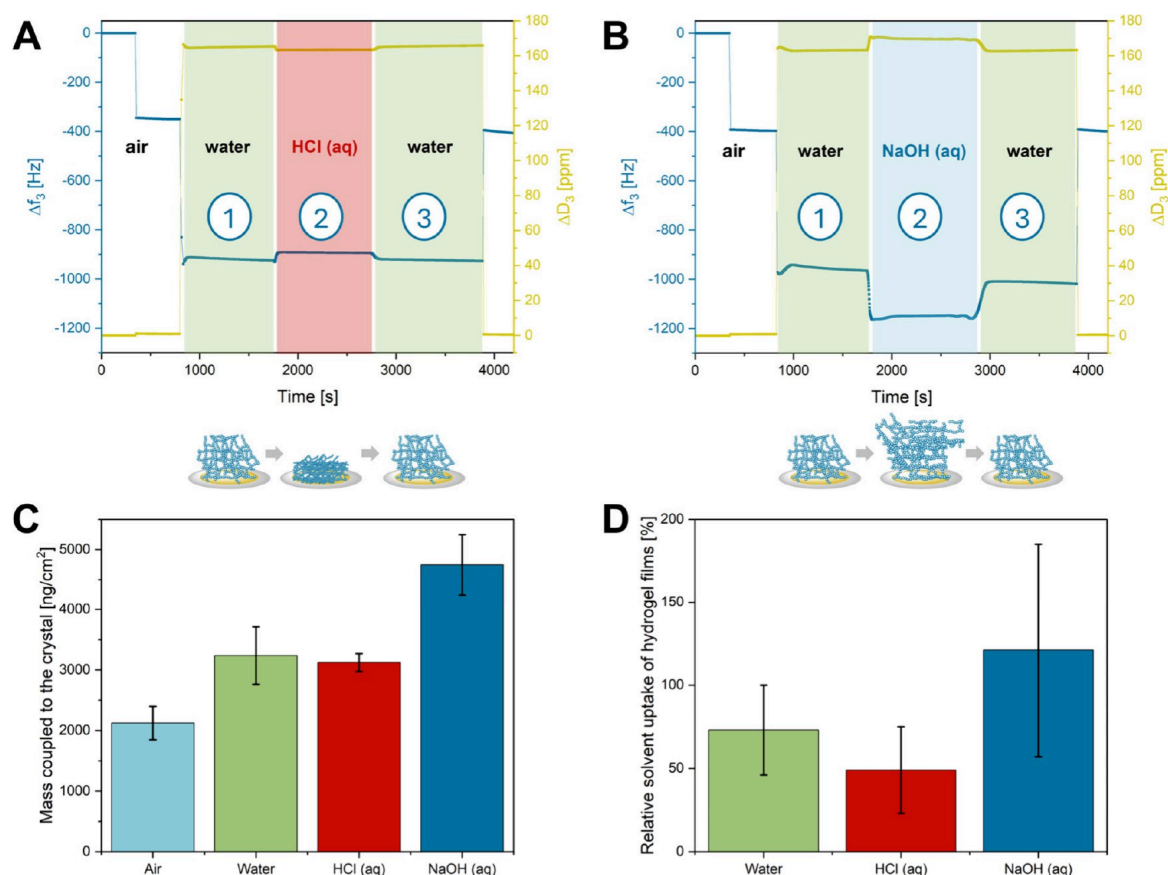


Figure 1. QCM-D measurements of thin films of cross-linked P(DEVP-*stat*-DAIVP-*stat*-VPA) in different aqueous media and measurements in ambient air before and after exposure to the liquids, checking for potential leaching of samples. (A) Investigation of sample behavior under acidic conditions (pH 1) and (B) investigation of sample behavior under alkaline conditions (pH 13). (C) Coupled hydrogel film masses in different environmental conditions obtained from the frequency changes of the third overtone and by subtracting the frequency decrease of each solvent on neat crystals. (D) Weight percentage of water in the films (mass of water per dry film mass) under different environmental conditions. Water masses were obtained from the coupled hydrogel film masses (water + hydrogel) by subtracting the masses obtained through the frequency decrease upon dry film deposition on the QCM-D sensors.

increasing numbers of DAIVP units with equimolar equivalents of TMSBr (0.30 equiv), gave access to terpolymers 5–7, which revealed residual DAIVP contents in the same sequence. Regarding the water uptake of the corresponding hydrogels, the high values of water absorption compared to those obtained in initial studies for the cross-linking of P(DEVP-*stat*-DAIVP) indicate an overall significant increase in the hydrophilicity of the gels induced by the polymer-analogous transformation.³⁷ Furthermore, relating the swelling ratio of the corresponding hydrogels to the polymer compositions, the water uptake is mainly governed by the cross-linking density given by the content of DAIVP in P(DEVP-*stat*-DAIVP-*stat*-VPA), which increases from polymer 5 to 8. This is particularly evident when polymers 5 and 6 are compared with very similar amounts of DEVP and VPA, mainly differing in the number of DAIVP units. While hydrogels from polymer 6 exhibited considerable swelling, the water absorption of polymer 5 indicated a superabsorbent material with a water uptake of about 150 g of water per gram of dry hydrogel, marking a high-performance material with significant potential, e.g., in

agricultural or hygienic applications.^{47–50} Comparing hydrogels from polymers 6 and 7, both materials show similar water uptake, despite notable differences in their DAIVP content. Therefore, we believe these examples illustrate an interplay between the cross-linking density and the polarity of the polymers. More specifically, polymer 7 contained 6.80% cross-linkable units, which exceeded the number of available sites in polymer 6. Nevertheless, polymer 7 also revealed the highest amount of vinylphosphonic acid units, which should yield the most polar cross-linked network and, thus, could explain the similar values for the water uptake of samples originating from polymers 6 and 7. Considering the mechanical properties of the hydrogels, an opposing trend compared to the water uptake regarding the DAIVP content was found. Whereas the swollen hydrogels arising from polymers 5 and 6 exhibited no or only poor mechanical stability, the specimen synthesized from polymers 7 and 8 remained mechanically stable in the swollen state and could be gently handled with tweezers (Figure S6). Apart from the description of the mechanical properties of the swollen states, exemplary frequency sweeps

conducted on hydrogels originating from polymers 6 and 8 accentuate these findings. In both cases, the hydrogels were formed from water between the rheometer plates in situ. The higher values of the storage and loss modulus of the more densely cross-linked polymer networks indicate a higher mechanical strength of the swollen specimen (Figure S7), aligning well with the findings from previous studies.³⁷

Investigations on the pH-Responsiveness of Thin Films. After investigating the water uptake of these novel P(DEVP-*stat*-DAIVP-*stat*-VPA)-based hydrogels, we aimed to understand their behavior in media with pH values other than water since the introduction of vinylphosphonic acid units should induce pH-responsive behavior. For this purpose, thin films of cross-linked, partially hydrolyzed poly(vinylphosphonates) were prepared on different substrates by applying a well-established spin-coating procedure reported for various biomaterials.^{44,45} In this context, a less than 0.01 wt % solution of polymer 8 in methanol/water (6/1) was applied to obtain thin hydrogel films on either silicon wafers or the Au electrodes of quartz-crystal microbalance (QCM-D) sensors. The processing of poly(vinylphosphonate)-based hydrogels by spin-coating has not been described before, and the fabrication of thin films of these materials could be relevant for various applications. The dry films of cross-linked, partially hydrolyzed poly(vinylphosphonates) were investigated by profilometry, light microscopy, QCM-D, and AFM. Characterization of the thin films by profilometry on cleaned silicon wafers revealed an average layer thickness of 39.4 ± 2.33 nm and a roughness average of 1.96 ± 0.75 nm determined from 12 measurements on 3 different substrates (Table S1), indicating relatively smooth and homogeneous coatings. An exemplary profilometry measurement is shown in Figure S8. Furthermore, the dry film mass was obtained from QCM-D measurements of crystals before and after spin coating and irradiation of the polymer film deposited on the quartz crystal resonator. Whereas the resonance frequency f decreased when the hydrogel was introduced, the dissipation factor D , which is the second measure of QCM-D and reflects the viscoelastic properties of the sample, increased simultaneously. This is due to the deposition of the hydrogel, resulting in an energy loss of the oscillating system due to its viscoelasticity. Given the frequency shifts of the third overtone upon spin coating, the mass coverage on the Au-surface was calculated using the Sauerbrey eq (Equation S2). Applying the average resonance frequency change Δf_3 of -360 ± 46 Hz obtained from 12 QCM-D measurements, the resulting mass per area on the resonators was calculated to be 2.12 ± 0.27 $\mu\text{g}/\text{cm}^2$. Finally, atomic force microscopy was applied to further explore the surface morphology of the hydrogels spin-coated onto the QCM-D sensor (Figure 3A). AFM indicated quantitative surface coverage of the crystals. However, the AFM images along with the recordings of the light microscope (Figure S9) revealed minor inhomogeneities on the substrate surfaces. This could either arise from a nonperfectly dissolved polymer in the spin coating solution, which was not assessable with the naked eye, or some unintended self-assembly processes on the surfaces. Nevertheless, we studied the behavior of these thin films of cross-linked P(DEVP-*stat*-DAIVP-*stat*-VPA) via QCM-D to gain insight into the pH-responsive behavior of the novel materials. First, a baseline corresponding to the resonance frequency of an uncoated sensor and, therefore, to $\Delta f_3 = 0$ Hz was established in ambient air. Subsequently, the same sensor was spin-coated with an 85 ppm (0.0085 wt %) solution of

polymer 8 (Table 2), containing the cross-linker and photoinitiator, and irradiated ($\lambda = 365$ nm, $t = 1$ min) to yield a cross-linked network on the Au-coated surface of the QCM-D sensor. Following this step, remeasurement of the crystals in air confirmed successful spin coating by a frequency change of -360 ± 46 Hz, which is also observable in the first decrease in Δf_3 highlighted in Figures 1A and 1B.

Transitioning from air to water, both measurements in Figure 1 reveal a significant decrease in the oscillation frequency of the third overtone of the crystals, dropping to frequencies around $\Delta f_3 = -940 \pm 80$ Hz, which is a commonly observed phenomenon due to density changes in the medium. However, a substantial contribution toward this frequency difference is caused by the swelling of the hydrogel film on the QCM-D resonator. Subtracting the frequency changes through dry film deposition ($\Delta f_3 = -360 \pm 46$ Hz) and water on an empty QCM-D crystal ($\Delta f_3 = -392$ Hz, Figure S10) would indicate a weight increase through hydrodynamically coupled water of roughly 1.11 $\mu\text{g}/\text{cm}^2$ as determined by the Sauerbrey equation, disregarding that this relation becomes nonlinear in swollen systems without full elastic coupling to the sensor. Once stable QCM-D signals were reached, indicating the equilibrium swelling state of the hydrogel films, the aqueous environments were altered to either 0.1 M hydrochloric acid (aq) (pH 1) or 0.1 M sodium hydroxide solution (aq) (pH 13), while the swelling behavior of each film. Switching to acidic measurement conditions (Figure 1A), a sharp frequency increase to $\Delta f_3 = -923 \pm 25$ Hz, along with a decrease of the dissipation to $\Delta D_3 = 164 \pm 1$ ppm, was observed. Both trends can be explained by a collapse of the formerly partially deprotonated hydrogel at pH 7 through protonation at pH 1 and, therefore, the loss of electrostatic repulsion. This hypothesis is supported by the titration curve of PVPA (Figure S5), revealing a gradual increase of the pH value, indicating a dynamic deprotonation/protonation of the polymers, and suggesting that parts of the PVPA might as well be deprotonated at a pH value of 7. Furthermore, the decrease in dissipation is explained by the lower viscoelasticity of the swollen hydrogel upon collapse, causing a smaller energy loss than in the initial state. The exact opposite trend in the frequency and dissipation values is observed for alkaline conditions (Figure 1B). Upon displacement of distilled water by NaOH (aq) in the measurement cell, a sharp decrease in the frequency to $\Delta f_3 = -1195 \pm 85$ Hz and an increase in the dissipation to $\Delta D_3 = 170 \pm 2$ ppm, followed by plateaus of either, was detected. In analogy to the explanation above, this, in turn, is accounted for by an extensive swelling of the hydrogel network due to electrostatic repulsion of the deprotonated vinylphosphonic acid units in the polymers, resulting in a higher mass of water coupled to the QCM-D sensor. With the aid of the titration curve of PVPA (Figure S5), displaying the behavior of a monoprotic acid and a gradual deprotonation, it becomes obvious that under the harsh conditions of pH 13, large parts of the VPA units in cross-linked P(DEVP-*stat*-DAIVP-*stat*-VPA) should be deprotonated. The strong electrostatic repulsion explains the more drastic changes in Δf_3 and ΔD_3 switching from pH 7 (partially deprotonated) to 13 (mostly deprotonated) than that from pH 7 (partially deprotonated) to 1 (mostly protonated). This trend is also reflected in the calculated coupled masses (hydrogel + water) in different environments (Figure 1C) and can also be seen in Figure 1D, which shows the mass of water per dry film mass for the different swelling states. Comparing

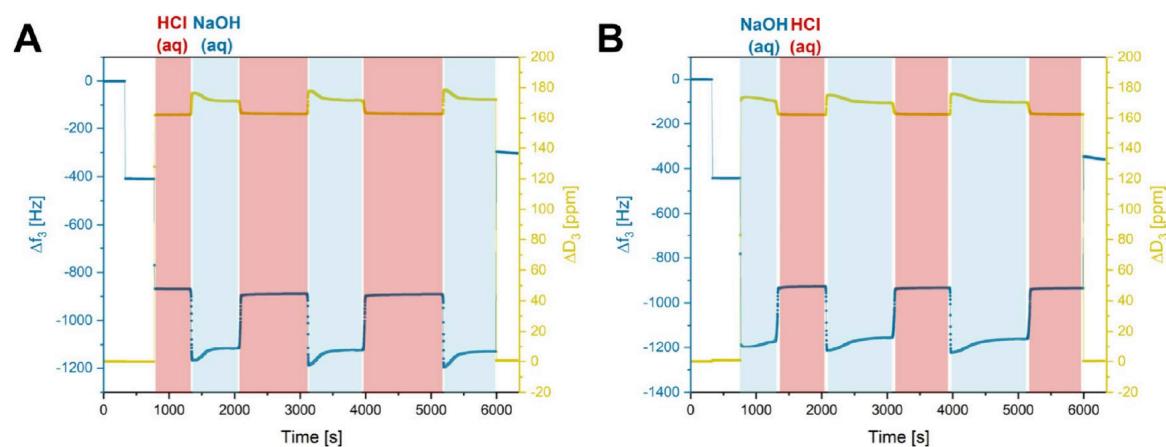


Figure 2. QCM-D measurements of thin films of cross-linked P(DEVP-*stat*-DAIVP-*stat*-VPA) in alternating aqueous media (two pH values) and measurements on air before and after exposure to the liquids. (A) Cycling of the pH value between pH 1 (0.1 M HCl solution) and pH 13 (0.1 M NaOH solution) over three cycles. (B) Cycling of the pH value between pH 13 (0.1 M NaOH solution) and pH 1 (0.1 M HCl solution) over three cycles.

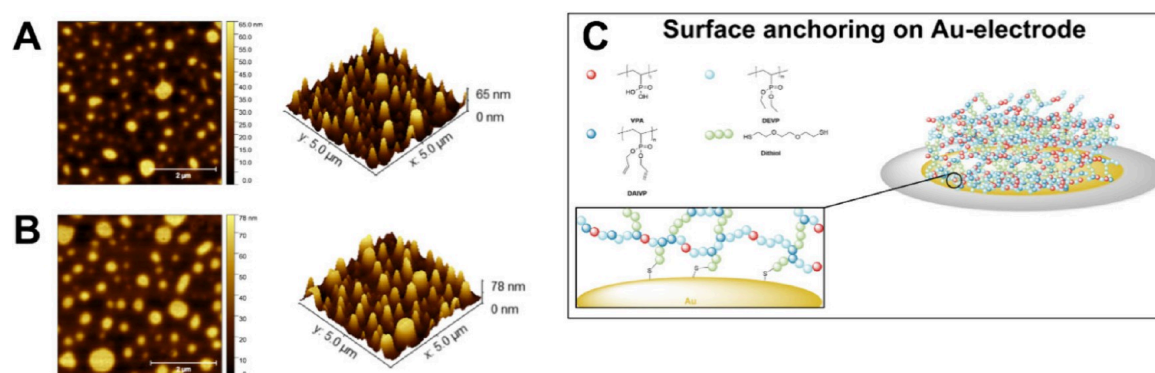


Figure 3. AFM images of the native hydrogel on the Au-surface of a QCM-D crystal (A), the hydrogel after QCM-D measurements with alternating pH values and subsequent drying of the crystals (B), and proposed surface anchoring of P(DEVP-*stat*-DAIVP-*stat*-VPA)-based hydrogels by the dithiol cross-linker via interaction with the gold electrode (C).

the water uptake found in the QCM-D studies for thin films of cross-linked polymer 8 (Figure 1D) with the water absorption of the macromolecular objects (Table 2), a significant reduction in hydrogel swelling can be observed. This could be attributed to the restrained chain mobility of the polymer chains due to the surface attachment, making the polymers more immobile for swelling and hindering water accessibility into the networks. Nevertheless, the results in Figure 1D reveal pH-dependent swelling of the thin hydrogel film. Notably, control experiments confirmed that the observed frequency and dissipation changes in aqueous environments, shown in Figure 1, arise exclusively from the film behavior on the QCM-D sensors since the density or other solvent effects had no impact on the values of frequency and dissipation when measuring uncoated sensors (Figure S10). Next, the reversibility toward the initial swelling state in water was confirmed by returning to pH 7 in both cases. This resulted in plateaus of the signals and yielded similar data for Δf_3 and ΔD_3 as initially determined, therefore not hinting toward any mass loss on the sensors. To confirm this assumption, the measurements were stopped and the crystals dried thoroughly

using nitrogen gas. Remeasurement of the dry crystals (final plateaus in Figures 1A and 1B) and comparison with the pristine masses confirmed that no detachment of the hydrogel films from the Au surfaces of the QCM-D resonators occurred despite exposing the films to the harsh conditions discussed above. To further explore the application potential of these materials in devices, the reversibility of swelling and collapse of thin films of P(DEVP-*stat*-DAIVP-*stat*-VPA)-based hydrogels at these extreme pH values was studied over the course of three cycles (Figures 2A and 2B).

In these experiments, QCM-D sensors spin-coated with a P(DEVP-*stat*-DAIVP-*stat*-VPA)-containing solution and subsequently cross-linked via UV irradiation were first investigated in air, resulting in the frequency and dissipation changes upon mass deposition mentioned previously. When exposing the films on the crystals to acidic conditions (pH 1), $\Delta f_3 = -923 \pm 25$ Hz and $\Delta D_3 = 164 \pm 1$ ppm were obtained (Figure 2A). Switching to alkaline conditions (pH 13) after reaching stable measurement values, a sharp decrease in the frequency to $\Delta f_3 = -1195 \pm 85$ Hz and an increase in the dissipation to $\Delta D_3 = 170 \pm 2$ ppm was obtained, indicating extensive swelling of the

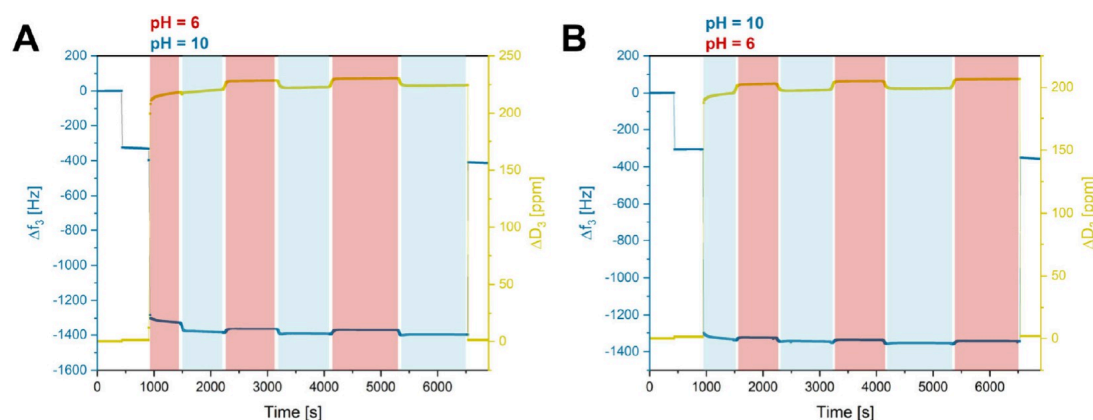


Figure 4. QCM-D measurements of thin films of cross-linked P(DEVP-*stat*-DAIVP-*stat*-VPA) in different buffers and measurements in air before and after exposure to the liquids. (A) Cycling of the pH value between pH 6 (0.1 M citrate buffer) and pH 10 (0.1 M carbonate buffer) over three cycles. (B) Cycling of the pH value between pH 10 (0.1 M carbonate buffer) and pH 6 (0.1 M citrate buffer) over three cycles.

hydrogel film as discussed above. These values were successfully reproduced when performing this solvent exchange for two subsequent cycles, indicating fully reversible swelling and deswelling of the film without detachment during the online monitoring of the f and D values. The opposite behavior was observed when starting the measurements at high pH values (Figure 2B). To confirm the preservation of the hydrogel layers on the QCM resonators, the crystals were dried and remeasured in air, yielding comparable data of Δf_3 and ΔD_3 as opposed to their initial values, suggesting no significant weight loss after three cycles. To further substantiate this assumption, AFM measurements of the coated sensors after QCM-D cycling experiments were conducted to investigate the surface topography. Comparing the AFM measurements before (Figure 3A) and after (Figure 3B), the QCM-D experiments revealed similar surface coverages of the hydrogel and did not hint toward any film loss caused by the harsh conditions. The excellent adhesion of the films on the gold substrates led to the hypothesis that the dithiol cross-linker applied in hydrogel synthesis might act as a surface anchor interconnecting the hydrogel network with the electrode surface (Figure 3C). This hypothesis is supported by numerous reports on the interaction thiol- or sulfur-containing polymers with Au electrodes in QCM-D,^{51–53} and by control experiments, in which exposing films of non-cross-linked polymers to different aqueous environments resulted in a significant sample loss (Figure S11).

To demonstrate the broader applicability of these novel materials, the pH-responsiveness was studied under milder conditions (2 pH units above and below the equivalence point of the titration of PVPA with NaOH, Figure S5) by investigating the thin film behavior of cross-linked P(DEVP-*stat*-DAIVP-*stat*-VPA) in 0.1 M citrate buffer (pH 6) and 0.1 M carbonate buffer (pH 10) (Figures 4A and 4B). Again, the Δf_3 values obtained in these experiments demonstrate high reversibility between the swelling states over three cycles regardless of the order in which the buffers were added to the samples. Each experiment was performed in triplicate, revealing excellent reproducibility and yielding $\Delta f_3 = -1395 \pm 47$ Hz for the collapsed state (pH 6) and $\Delta f_3 = -1427 \pm 38$ Hz for the swollen state (pH 10), allowing differentiation between the two pH values. The higher frequency decreases

compared to the measurements presented in Figure 3 might hint toward buffer interactions with the films or density effects. Unlike in the case of HCl (aq) and NaOH (aq) (Figure S10), measurements of uncoated QCM-D crystals in the buffered solutions indeed showed a dependence of the resonance frequency and the dissipation on the surrounding medium (Figure S12). In this context, the frequency increased switching to the carbonate buffer, counteracting the swelling-induced frequency decrease, and vice versa for the citrate buffer. Consequently, the frequency window for pH differentiation might effectively appear smaller than that for other solutions in the same pH window. In contrast to the measurements with NaOH (aq) and HCl (aq), the values for ΔD_3 do not inversely correlate with the frequency states but seem to be dominated by the viscoelastic properties of the buffers as evidenced by the corresponding control experiments (Figure S12).

Nevertheless, the results presented in Figures 2 and 4 reveal the pH-responsive behavior of cross-linked P(DEVP-*stat*-DAIVP-*stat*-VPA) polymers in different media, suggesting a high potential for implementing the material properties in various applications. In this context, the excellent adhesion of hydrogel films on gold surfaces combined with the photochemical cross-linking process allows photolithographic micropatterning, which is relevant not only in the biomedical field but also in optics and electronics.^{54,55} Further, the extensive swelling of these hydrogels; their ability to form thin, homogeneous films; and their pH-dependent volume changes render them ideal candidates for developing piezoelectric pH-sensors.^{56,57} For device fabrication, a more detailed study of the correlation between the water uptake and the film thickness is crucial, as the substrate polarity can dominate the swelling properties for very thin films.^{58,59} Very thin films further comprise layers with less mobile polymer chains due to the interaction with the solid Au substrate, leading to fewer degrees of freedom and therefore to less swelling and a lower relative mass increase. A fundamental understanding of this dependency, in turn, might help to adjust the sensor's sensitivity in future studies.

Surface Analysis of Thin Films on Gold Substrates. To further elucidate the interactions between the films of cross-linked P(DEVP-*stat*-DAIVP-*stat*-VPA) polymers and the Au

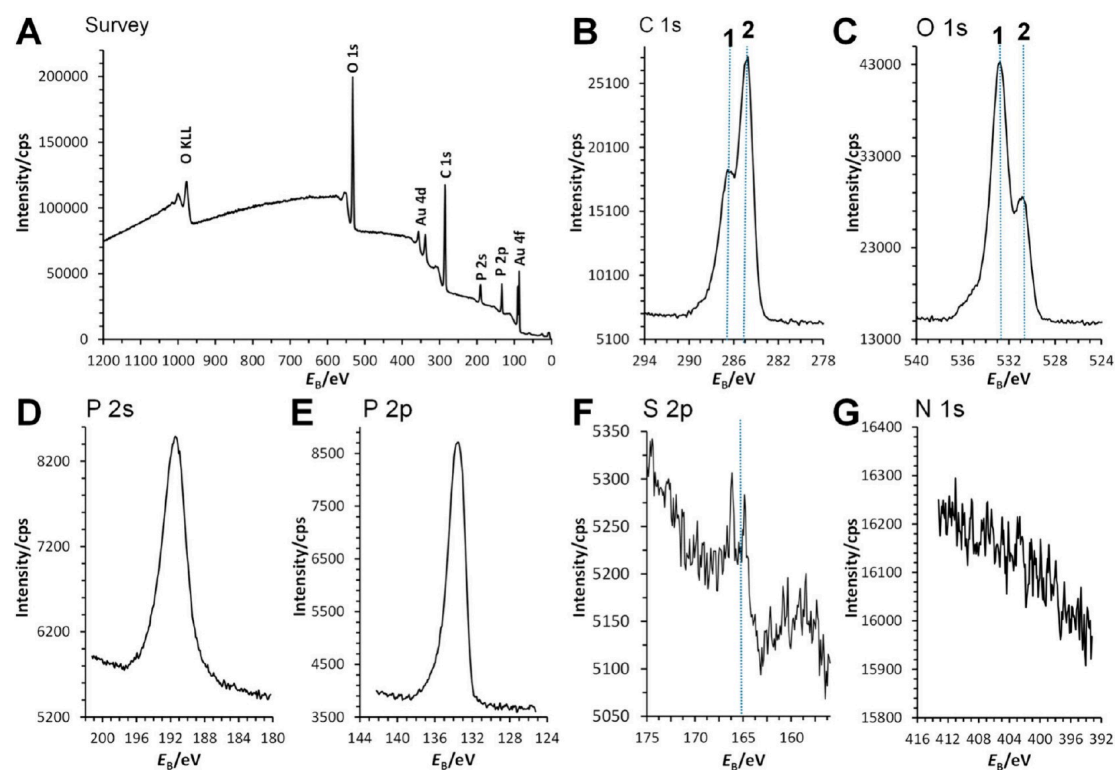


Figure 5. Survey (A) and high-resolution XPS spectra for (B) C 1s, (C) O 1s, (D) P 2s, (E) P 2p, (F) S 2p, and (G) N 1s.

surfaces of the QCM-D sensors, in-depth surface analysis of the spin-coated films was conducted via X-ray photoelectron spectroscopy (XPS) and time-of-flight secondary ion mass spectrometry (ToF-SIMS). Figure 5 presents the survey and high-resolution XPS spectra, providing an overview of the surface composition. The survey spectrum reveals the presence of O-, C-, Au-, and P-containing species on the surface. However, the S- and N-related signals, which could confirm the presence of the dithiol cross-linker and the polymer end-group, were not developed in the XPS spectra (Figures 5A, 5F, 5G).

Figure 5B displays the C 1s spectrum, which clearly identifies C–C/C–H containing species at 284.8 eV (dashed line 2) and C–O containing species at a distinct binding energy (dashed line 1). The O 1s spectrum (Figure 5C) indicates two distinct oxygen environments, marked at dashed lines 1 and 2, which could correspond to R-PO₃-R₂ and R-PO₃H₂ groups, respectively, consistent with the polymer's expected structure. The phosphorus signals are intense in the XPS spectra, as shown in Figures 5A, 5D, and 5E. The P 2p spectrum, in particular, confirms the presence of R-PO₃-R₂ moieties, as evidenced by the binding energy (E_b) position. This observation supports the conclusion that the polymer is present on the Au surface. The S 2p and N 1s spectra (Figures 5F and 5G) show no detectable signals, indicating that the sulfur and nitrogen concentrations are too low for this technique. While a peak begins to emerge in the S 2p spectrum (Figure 5F), its intensity remains below the threshold for confident detection, as it does not exceed three times the background noise. Sulfur should, however, be

incorporated into the hydrogel structure due to the cross-linker. N-containing species, in turn, might originate from the polymer end groups. The limitations of XPS were addressed using ToF-SIMS, which has a lower detection limit and successfully confirmed the presence of S-containing species, providing a more comprehensive surface characterization. The cross-linked films on the surfaces comprise R-PO₃-containing moieties (R being the aliphatic polymer backbone) and S-containing moieties. Using ToF-SIMS, the polymer was characterized by S⁻, PO⁻ and C₂H₄PO₃⁻ signals in negative polarity (Figures 6A–C) and PO⁺, C₂H₄PO₃⁺, and C₂H₆PO₃⁺ signals in positive polarity (Figures 7A–C). These signals provided high mass resolution and accuracy, as designated in these figures. Two-dimensional ToF-SIMS imaging based on these signals revealed the homogeneous distribution of the cross-linked polymers on the Au electrode of the QCM sensor surface (Figures 6D–L and 7D–L). Subsequent sputtering with a 2.5 keV Ar₁₃₀₀⁺ beam gradually removed the organic material, allowing the creation of three-dimensional images (Figure 8) and depth profiles (Figure 9). The S⁻ and PO⁻ signals demonstrated the polymer distribution in negative polarity, while the S⁺, S₂⁺, and PO⁺ signals were utilized in positive polarity. As expected, S⁺ and S₂⁺ signals were less intense in the positive polarity. Au⁻ and Au⁺ signals served to identify the Au substrate in negative and positive polarities, respectively. Both the three-dimensional ToF-SIMS images (Figure 8) and the depth profiles (Figure 9) confirmed the accumulation of sulfur atoms at the Au surface, as evidenced by increased S-related signal intensity at the polymer network/Au interface, supporting the hypothesis of surface anchoring

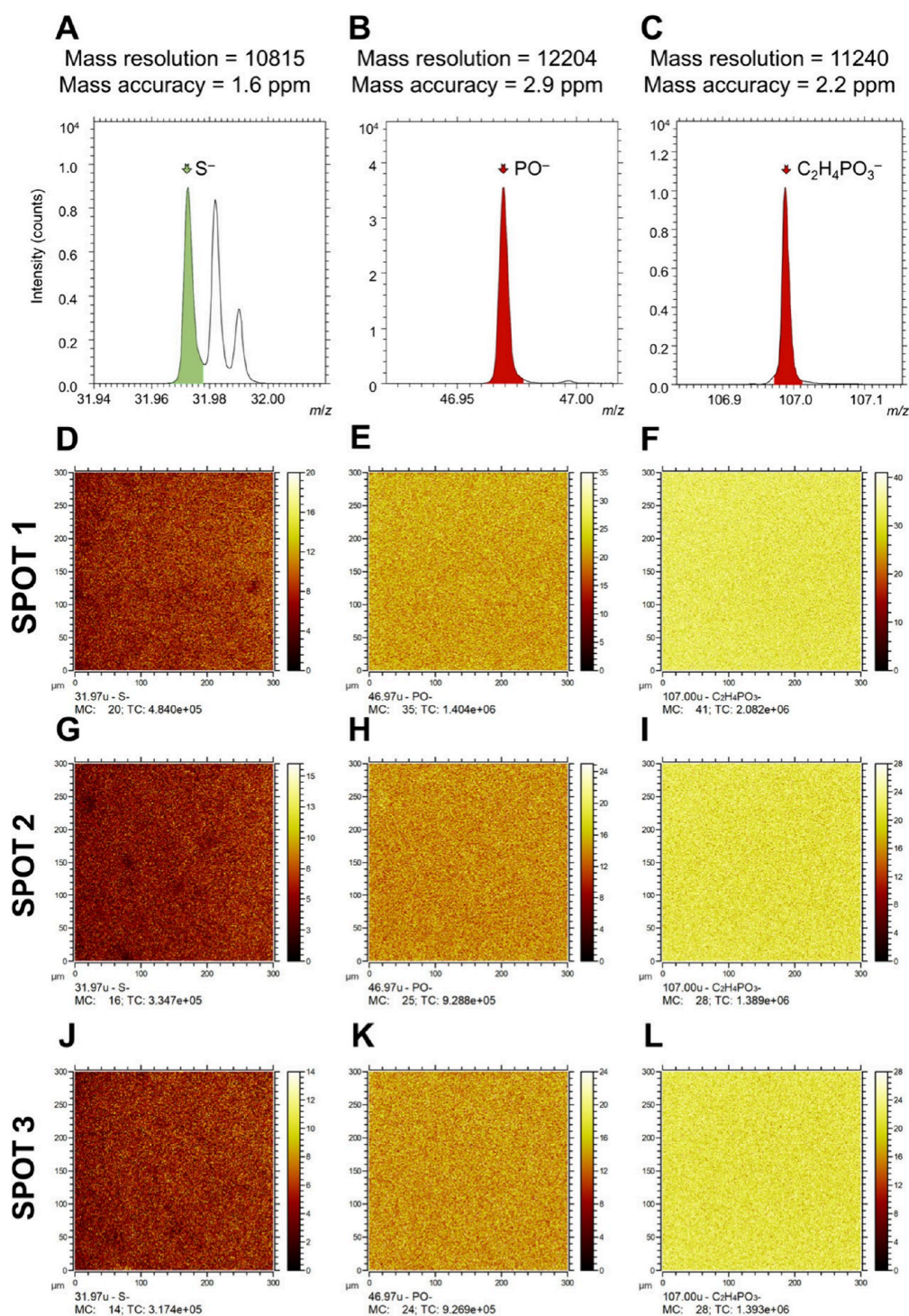


Figure 6. Negative ion ToF-SIMS spectra showing the peaks for (A) S^- , (B) PO^- , and (C) $C_2H_4PO_3^-$, along with corresponding two-dimensional ToF-SIMS images for spot 1 (D–F), spot 2 (G–I), and spot 3 (J–L) on the surface, illustrating the spatial distribution of S^- , PO^- , and $C_2H_4PO_3^-$ signals.

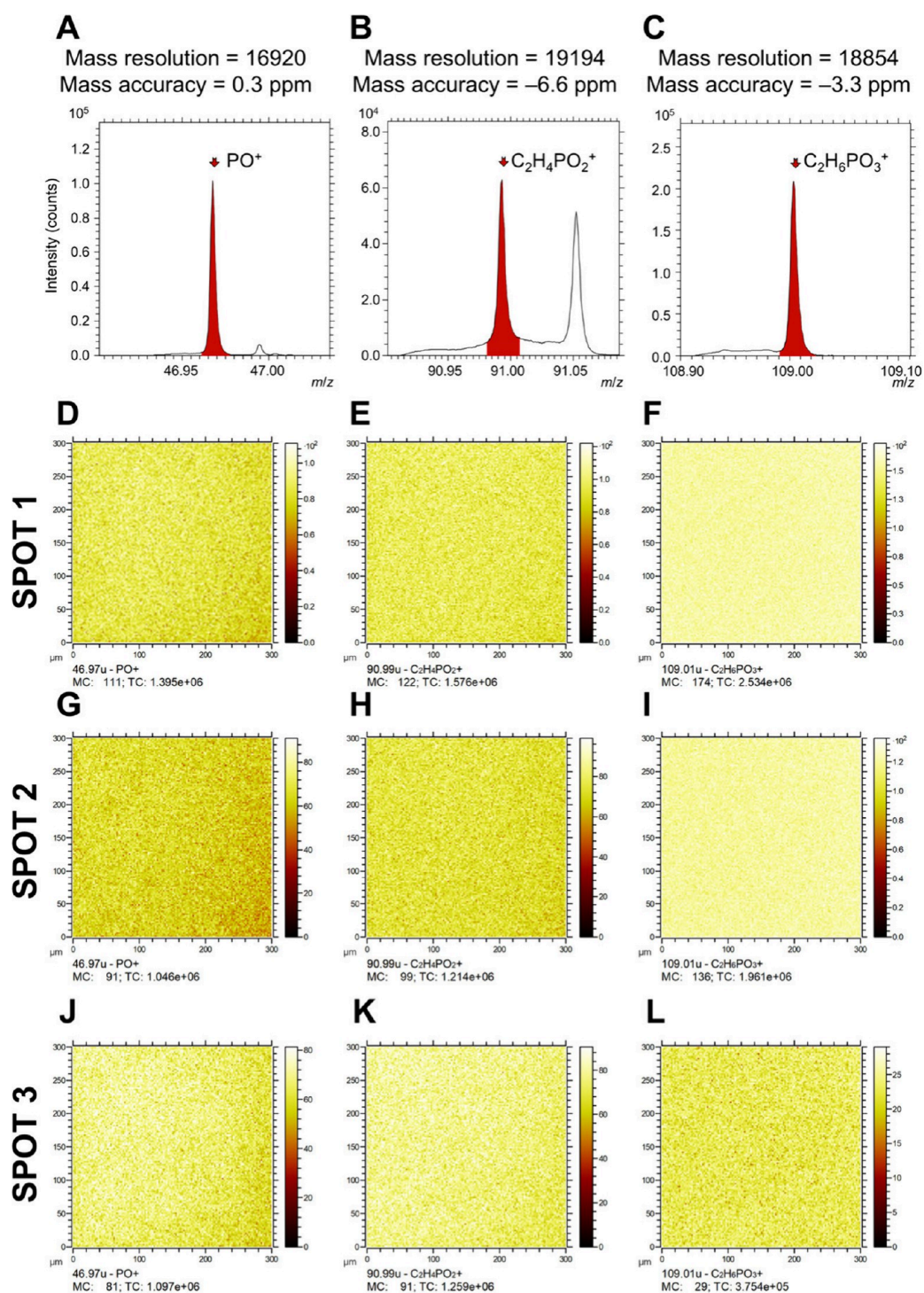


Figure 7. Positive ion ToF-SIMS spectra showing the peaks for (A) PO^+ , (B) $\text{C}_2\text{H}_4\text{PO}_2^+$, and (C) $\text{C}_2\text{H}_6\text{PO}_3^+$, along with corresponding two-dimensional ToF-SIMS images for spot 1 (D–F), spot 2 (G–I), and spot 3 (J–L) on the surface, illustrating the spatial distribution of PO^+ , $\text{C}_2\text{H}_4\text{PO}_2^+$, and $\text{C}_2\text{H}_6\text{PO}_3^+$ signals.

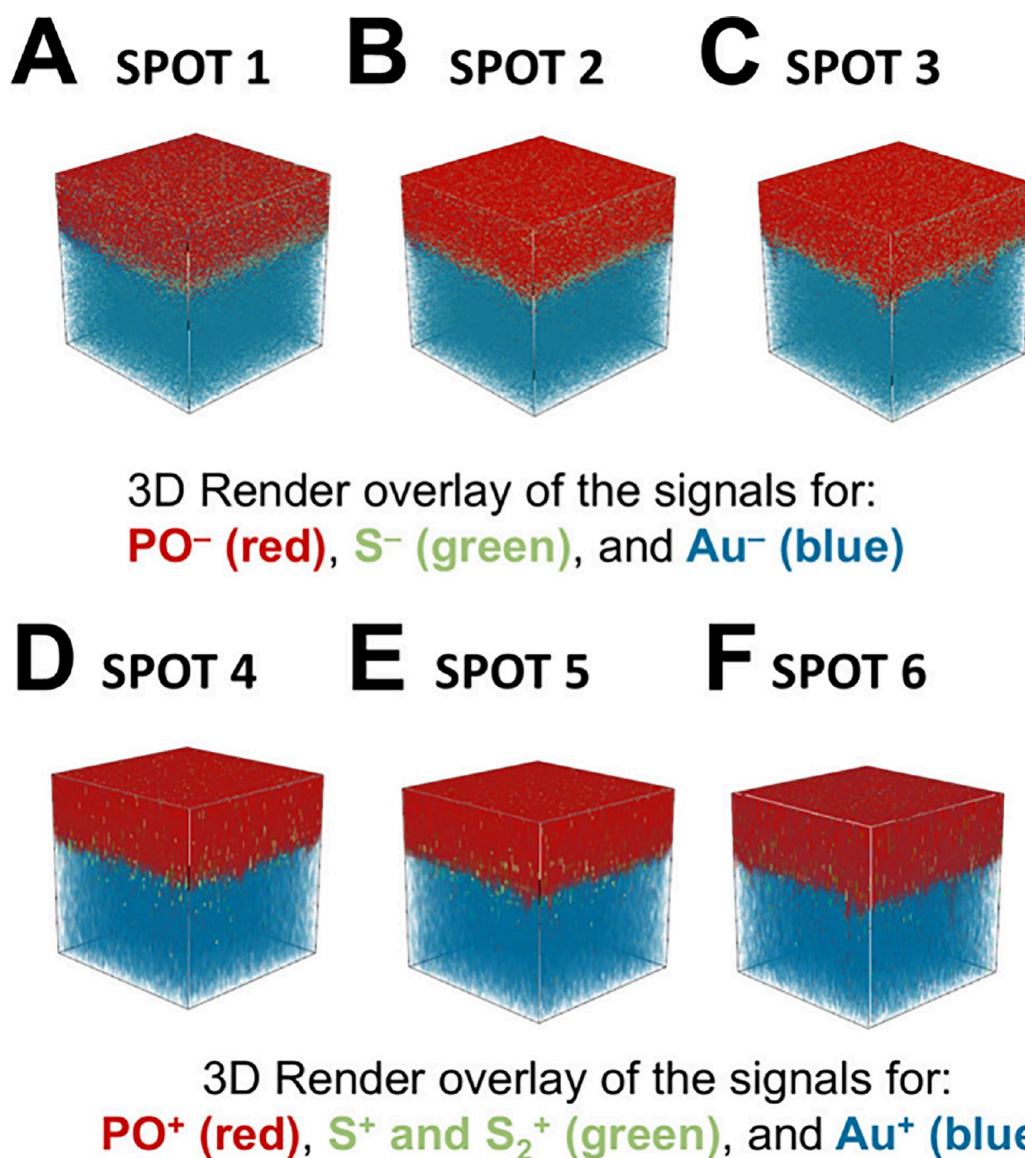


Figure 8. Three-dimensional ToF-SIMS images for 6 different spots of the surface showing the distribution of PO^- , S^- , Au^- signals (A–C), and PO^+ , S^+ , S_2^+ , and Au^+ signals (D–F). Sputtering was performed by using 2.5 keV Ar_{1300}^+ . x - and y -scales are $300 \mu\text{m} \times 300 \mu\text{m}$.

through Au-thiol interactions presented in Figure 3C. The three-dimensional ToF-SIMS images in Figure 8 further reveal the presence of the cross-linked polymers on the QCM-D sensors and a homogeneous distribution of the dithiol cross-linker within the P(DEVP-*stat*-DAIVP-*stat*-VPA) networks.

CONCLUSION

In this study, we introduced an innovative method to synthesize highly water-absorbing, pH-responsive hydrogels via photochemical cross-linking of allyl groups in P(DEVP-*stat*-DAIVP-*stat*-VPA). The hydrophilic and cross-linkable polymers were easily accessible by polymer-analogous hydrolysis of P(DEVP-*stat*-DAIVP) copolymers obtained via highly controlled catalytic polymerization (REM-GTP). Side-chain

dealkylation of poly(vinylphosphonates) using TMSBr preferentially targeted allylic over ethyl side chains, as confirmed via ^1H NMR spectroscopy. Photochemical cross-linking of P-(DEVP-*stat*-DAIVP-*stat*-VPA) yielded superabsorbent materials with water uptakes up to $150 \pm 27 \text{ g } (\text{H}_2\text{O})/\text{g}$ (hydrogel) and evident structure–property relationships between the cross-linking density and swelling behavior. In the second part, thin polymer films were successfully spin-coated on silicon wafers and gold electrodes of QCM-D sensors, followed by photo-cross-linking, yielding hydrogel films with a thickness of $39.4 \pm 2.33 \text{ nm}$ characterized via profilometry, QCM-D, and AFM. The hydrogel films exhibited pronounced pH-responsive behavior in QCM-D measurements when exposed to various aqueous media, displayed by the corresponding frequency and

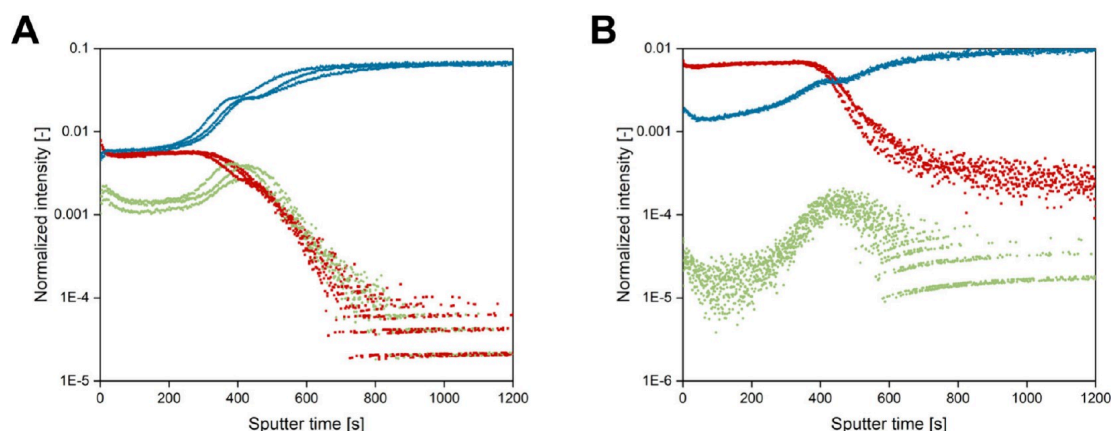


Figure 9. Depth profiles measured at three different spots on the surface in (A) negative polarity (Au^- in blue, PO^- in red, and S^-/S_2^+ in green) and (B) positive polarity (Au^+ in blue, PO^+ in red, and S^+/S_2^+ in green). Normalization was applied based on the total ion intensities.

dissipation values reflecting different swelling states of the samples. In addition, the high stability of films on the sensors under harsh conditions was explained by the surface anchoring of the hydrogels via interactions of the dithiol cross-linker with the gold surface of the electrode. In-depth XPS and ToF-SIMS studies confirmed this hypothesis and contributed to a more comprehensive surface characterization of cross-linked P-(DEVP-*stat*-DAIVP-*stat*-VPA) films on gold substrates. Overall, these novel materials were successfully applied as pH sensors in QCM-D experiments, and this study revealed great potential for these hydrogels to be implemented as super-absorbent networks or in photolithographic applications due to their excellent adhesion on gold surfaces. Most importantly, however, the pH-responsive properties of P-(DEVP-*stat*-DAIVP-*stat*-VPA) are currently being explored for potential utilization in pH-sensors and actuators, for which these novel stimuli-responsive materials are highly promising candidates.

■ ASSOCIATED CONTENT

SI Supporting Information

The Supporting Information is available free of charge at <https://pubs.acs.org/doi/10.1021/acsami.4c17704>.

Materials and methods; Experimental procedures; Polymer characterization; Titration curve of PVPA; Hydrogel swelling experiments; Rheological measurements; Macroscopic and microscopic images of hydrogel (films); Thin-film preparation and characterization; Calculations of the mass deposition by the Sauerbrey equation; Quartz crystal microbalance control experiments (PDF)

■ AUTHOR INFORMATION

Corresponding Authors

Bernhard Rieger – Technical University of Munich, TUM School of Natural Sciences, Department of Chemistry, WACKER-Chair of Macromolecular Chemistry, 85748 Garching, Germany; orcid.org/0000-0002-0023-884X; Email: rieger@tum.de

Rupert Kargl – Graz University of Technology, Institute for Chemistry and Technology of Biobased Systems (IBioSys), 8010 Graz, Austria; orcid.org/0000-0003-4327-7053; Email: rupert.kargl@tugraz.at

Authors

Anton S. Maier – Technical University of Munich, TUM School of Natural Sciences, Department of Chemistry, WACKER-Chair of Macromolecular Chemistry, 85748 Garching, Germany

Matjaž Finšgar – Faculty of Chemistry and Chemical Engineering, University of Maribor, 2000 Maribor, Slovenia; orcid.org/0000-0002-8302-9284

Beatrice De Chiara – Technical University of Munich, TUM School of Computation, Information and Technology, Munich Institute of Biomedical Engineering, Department of Electrical Engineering, Neuroelectronics, Hans-Piloty-Str. 1, 85748 Garching, Germany

Bernhard Wolfrum – Technical University of Munich, TUM School of Computation, Information and Technology, Munich Institute of Biomedical Engineering, Department of Electrical Engineering, Neuroelectronics, Hans-Piloty-Str. 1, 85748 Garching, Germany; orcid.org/0000-0003-4438-3755

Karin Stana Kleinschek – Graz University of Technology, Institute for Chemistry and Technology of Biobased Systems (IBioSys), 8010 Graz, Austria; orcid.org/0000-0002-9189-0242

Complete contact information is available at: <https://pubs.acs.org/doi/10.1021/acsami.4c17704>

Author Contributions

The manuscript was written through contributions of all authors. All authors have given approval to the final version of the manuscript.

Funding

A.S.M. is grateful for the generous funding within a Kekulé fellowship from the Fonds der Chemischen Industrie. B.D.C. acknowledges support from the TUM Innovation Network “Artificial Intelligence Powered Multifunctional Material Design” (ARTEMIS).

Notes

The authors declare no competing financial interest.

■ ACKNOWLEDGMENTS

The authors want to thank Tobias Steindorfer and Dr. Tamilselvan Mohan for their help with AFM measurements. Further, we are grateful for Philipp Weingarten’s help

proofreading this manuscript. Prof. Gregor Trimmel, Institute of Chemistry and Technology of Materials (ICTM) is acknowledged for access to the profilometer. The Slovenian Research Agency supported the work (Grant No. P2-0118). The project is co-financed by the Republic of Slovenia, the Ministry of Higher Education, Science and Innovation, and the European Union under the European Regional Development Fund.

ABBREVIATIONS

AFM, atomic force microscopy; DAIVP, diallyl vinylphosphonate; DEVP, diethyl vinylphosphonate; VPA, vinylphosphonic acid; REM-GTP, rare earth metal-mediated group-transfer polymerization; NMR, nuclear magnetic resonance; DMPA, 2,2-dimethoxy-2-phenylacetophenone; IE, initiator efficiency; D , polydispersity index; QCM-D, quartz crystal microbalance with dissipation monitoring; Δf_3 , frequency change of the third overtone of the QCM-D sensor; ΔD_3 , dissipation change of the third overtone of the QCM-D sensor; TMSBr, trimethylsilyl bromide; MWCO, molecular weight cutoff, r.t., room temperature; SEC-MALS, size-exclusion chromatography multiangle light scattering; ToF-SIMS, time-of-flight secondary ion mass spectrometry; XPS, X-ray photoelectron spectroscopy

REFERENCES

- Sood, N.; Bhardwaj, A.; Mehta, S.; Mehta, A. Stimuli-Responsive Hydrogels in Drug Delivery and Tissue Engineering. *Drug Delivery* **2016**, *23* (3), 748–770.
- Amirthalingam, S.; Rajendran, A. K.; Moon, Y. G.; Hwang, N. S. Stimuli-Responsive Dynamic Hydrogels: Design, Properties and Tissue Engineering Applications. *Mater. Horiz.* **2023**, *10* (9), 3325–3350.
- El-Husseiny, H. M.; Mady, E. A.; El-Dakrouy, W. A.; Zewail, M. B.; Noshay, M.; Abdelfatah, A. M.; Doghish, A. S. Smart/Stimuli-Responsive Hydrogels: State-of-the-Art Platforms for Bone Tissue Engineering. *Appl. Mater. Today* **2022**, *29*, No. 101560.
- Leach, J. B.; Schmidt, C. E. Characterization of Protein Release From Photocrosslinkable Hyaluronic Acid-Polyethylene Glycol Hydrogel Tissue Engineering Scaffolds. *Biomater.* **2005**, *26* (2), 125–135.
- Bhattarai, N.; Ramay, H. R.; Gunn, J.; Matsen, F. A.; Zhang, M. PEG-Grafted Chitosan as an Injectable Thermosensitive Hydrogel for Sustained Protein Release. *J. Controlled Release* **2005**, *103* (3), 609–624.
- Picchio, M. L.; Paredes, A. J.; Palma, S. D.; Passeggi, M. C.; Gugliotta, L. M.; Minari, R. J.; Igarzabal, C. I. A. pH-Responsive Casein-Based Films and Their Application As Functional Coatings in Solid Dosage Formulations. *Colloids Surf., A* **2018**, *541*, 1–9.
- Bilia, A.; Carelli, V.; Di Colo, G.; Nannipieri, E. In Vitro Evaluation of a pH-Sensitive Hydrogel for Control of GI Drug Delivery From Silicone-Based Matrices. *Int. J. Pharm.* **1996**, *130*, 83–92.
- Xu, L.; Qiu, L.; Sheng, Y.; Sun, Y.; Deng, L.; Li, X.; Bradley, M.; Zhang, R. Biodegradable pH-Responsive Hydrogels for Controlled Dual-Drug Release. *J. Mater. Chem. B* **2018**, *6* (3), 510–517.
- Dong, L.; Agarwal, A. K.; Beebe, D. J.; Jiang, H. Adaptive Liquid Microlenses Activated by Stimuli-Responsive Hydrogels. *Nature* **2006**, *442* (7102), 551–554.
- Gutowksa, A.; Bae, Y. H.; Feijen, J.; Kim, S. W. Heparin Release From Thermosensitive Hydrogels. *J. Controlled Release* **1992**, *22*, 95–104.
- Sershen, S. R.; Mensing, G. A.; Ng, M.; Halas, N. J.; Beebe, D. J.; West, J. L. Independent Optical Control of Microfluidic Valves Formed from Optomechanically Responsive Nanocomposite Hydrogels. *Adv. Mater.* **2005**, *17* (11), 1366–1368.
- Suzuki, A.; Tanaka, T. Phase Transition in Polymer Gels Induced by Visible Light. *Nature* **1990**, *346*, 345–347.
- Qiao, K.; Guo, S.; Zheng, Y.; Xu, X.; Meng, H.; Peng, J.; Fang, Z.; Xie, Y. Effects of Graphene on the Structure, Properties, Electro-Response Behaviors of GO/PAA Composite Hydrogels and Influence of Electro-Mechanical Coupling on BMSC Differentiation. *Mater. Sci. Eng., C* **2018**, *93*, 853–863.
- Ghasemi-Mobarakeh, L.; Prabhakaran, M. P.; Morshed, M.; Nasr-Esfahani, M. H.; Baharvand, H.; Kiani, S.; Al-Deyab, S. S.; Ramakrishna, S. Application of Conductive Polymers, Scaffolds and Electrical Stimulation for Nerve Tissue Engineering. *J. Tissue Eng. Regen. Med.* **2011**, *5* (4), e17–35.
- Miyata, T.; Asami, N.; Uragami, T. A Reversibly Antigen-Responsive Hydrogel. *Nature* **1999**, *399*, 766–769.
- Sheppard, N. F.; Lesho, M. J.; McNally, P.; Shaun Francomacaro, A. Microfabricated Conductometric pH Sensor. *Sens. Actuators B Chem.* **1995**, *28*, 95–102.
- Naficy, S.; Oveissi, F.; Patrick, B.; Schindeler, A.; Dehghani, F. Printed, Flexible pH Sensor Hydrogels for Wet Environments. *Adv. Mater. Technol.* **2018**, *3* (11), 1800137.
- Wang, J.; Chen, Z.; Mauk, M.; Hong, K.-S.; Li, M.; Yang, S.; Bau, H. H. Thermo-Responsive Hydrogel Valves for Lab on a Chip. *Biomed Microdevices* **2005**, *7*, 313–322.
- Han, Z.; Wang, P.; Mao, G.; Yin, T.; Zhong, D.; Yiming, B.; Hu, X.; Jia, Z.; Nian, G.; Qu, S.; Yang, W. Dual pH-Responsive Hydrogel Actuator for Lipophilic Drug Delivery. *ACS Appl. Mater. Interfaces* **2020**, *12* (10), 12010–12017.
- Fusi, G.; Del Giudice, D.; Skarsetz, O.; Di Stefano, S.; Walther, A. Autonomous Soft Robots Empowered by Chemical Reaction Networks. *Adv. Mater.* **2023**, *35* (7), No. e2209870.
- Jia, Y.; Zhang, X.; Yang, W.; Lin, C.; Tao, B.; Deng, Z.; Gao, P.; Yang, Y.; Cai, K. A pH-Responsive Hyaluronic Acid Hydrogel for Regulating the Inflammation and Remodeling of the ECM in Diabetic Wounds. *J. Mater. Chem. B* **2022**, *10* (15), 2875–2888.
- Zhang, L.; Ma, Y.; Zhao, C.; Zhu, X.; Chen, R.; Yang, W. Synthesis of pH-Responsive Hydrogel Thin Films Grafted on PCL Substrates for Protein Delivery. *J. Mater. Chem. B* **2015**, *3* (39), 7673–7681.
- Katan, T.; Kargl, R.; Mohan, T.; Steindorfer, T.; Mozetič, M.; Kovač, J.; Stana Kleinschek, K. Solid Phase Peptide Synthesis on Chitosan Thin Films. *Biomacromolecules* **2022**, *23* (3), 731–742.
- Miao, J.; Wu, X.; Fang, Y.; Zeng, M.; Huang, Z.; Ouyang, M.; Wang, R. Multifunctional Hydrogel Coatings With High Antimicrobial Loading Efficiency and pH-Responsive Properties for Urinary Catheter Applications. *J. Mater. Chem. B* **2023**, *11* (15), 3373–3386.
- Hu, J.; Hu, Q.; He, X.; Liu, C.; Kong, Y.; Cheng, Y.; Zhang, Y. Stimuli-Responsive Hydrogels with Antibacterial Activity Assembled from Guanosine, Aminoglycoside, and a Bifunctional Anchor. *Adv. Healthc. Mater.* **2020**, *9* (2), No. e1901329.
- Hu, J.; Zheng, Z.; Liu, C.; Hu, Q.; Cai, X.; Xiao, J.; Cheng, Y. A pH-Responsive Hydrogel With Potent Antibacterial Activity Against Both Aerobic and Anaerobic Pathogens. *Biomater. Sci.* **2019**, *7* (2), 581–584.
- Trad, M.; Miled, W.; Benltoufa, S.; Boughattas, A.; Benslama, R.; Fayala, F.; Bakhrouf, A. Chitosan Hydrogel-Coated Cotton Fabric: Antibacterial, pH-Responsiveness, and Physical Properties. *J. Appl. Polym. Sci.* **2018**, *135* (34), 46645.
- Silva-Pereira, M. C.; Teixeira, J. A.; Pereira-Júnior, V. A.; Stefani, R. Chitosan/Corn Starch Blend Films With Extract From Brassica Oleraceae (Red Cabbage) as a Visual Indicator of Fish Deterioration. *LWT* **2015**, *61* (1), 258–262.
- Bäcker, M.; Raue, M.; Schusser, S.; Jeitner, C.; Breuer, L.; Wagner, P.; Poghosian, A.; Förster, A.; Mang, T.; Schöning, M. J. Microfluidic Chip With Integrated Microvalves Based on Temperature- and pH-Responsive Hydrogel Thin Films. *Phys. Status Solidi* **2012**, *209* (5), 839–845.
- Howard, S. C.; Craig, V. S. J.; FitzGerald, P. A.; Wanless, E. J. Swelling and Collapse of an Adsorbed pH-Responsive Film-Forming

Microgel Measured by Optical Reflectometry and QCM. *Langmuir* **2010**, *26* (18), 14615–14623.

(31) Miras, J.; Liu, C.; Blomberg, E.; Thormann, E.; Vilchez, S.; Esquena, J. pH-Responsive Chitosan Nanofilms Crosslinked With Genipin. *Colloids Surf.* **2021**, *616*, No. 126229.

(32) Mohan, T.; Rathner, R.; Reishofer, D.; Koller, M.; Elschner, T.; Spirk, S.; Heinze, T.; Stana-Kleinschek, K.; Kargl, R. Designing Hydrophobically Modified Polysaccharide Derivatives for Highly Efficient Enzyme Immobilization. *Biomacromolecules* **2015**, *16* (8), 2403–2411.

(33) Drozdov, A. D.; deClaville Christiansen, J. The Effects of pH and Ionic Strength on Equilibrium Swelling of Polyampholyte Gels. *International Journal of Solids and Structures* **2017**, *110–111*, 192–208.

(34) Guvendiren, M.; Yang, S.; Burdick, J. A. Swelling-Induced Surface Patterns in Hydrogels with Gradient Crosslinking Density. *Adv. Funct. Mater.* **2009**, *19* (19), 3038–3045.

(35) Zhang, Y.; Won, C.-Y.; Chu, C.-C. Synthesis and Characterization of Biodegradable Hydrophobic-Hydrophilic Hydrogel Networks With a Controlled Swelling Property. *J. Polym. Sci., Part A: Polym. Chem.* **2000**, *38* (13), 2392–2404.

(36) Brelle, L.; Fay, F.; Ozturk, T.; Didier, N.; Renard, E.; Langlois, V. Hydrogel Based on Polyhydroxyalkanoate Sulfonate: Control of the Swelling Rate by the Ionic Group Content. *Biomacromolecules* **2023**, *24* (4), 1871–1880.

(37) Maier, A. S.; Mansi, S.; Halama, K.; Weingarten, P.; Mela, P.; Rieger, B. Cytocompatible Hydrogels With Tunable Mechanical Strength and Adjustable Swelling Properties Through Photo-Cross-Linking of Poly(vinylphosphonates). *ACS Appl. Mater. Interfaces* **2024**, *16* (43), 58135–58147.

(38) Zhang, N.; Salzinger, S.; Soller, B. S.; Rieger, B. Rare Earth Metal-Mediated Group-Transfer Polymerization: From Defined Polymer Microstructures to High-Precision Nano-Scaled Objects. *J. Am. Chem. Soc.* **2013**, *135* (24), 8810–8813.

(39) Soller, B. S.; Salzinger, S.; Jandl, C.; Pöthig, A.; Rieger, B. C–H Bond Activation by σ -Bond Metathesis as a Versatile Route Toward Highly Efficient Initiators for the Catalytic Precision Polymerization of Polar Monomers. *Organometallics* **2015**, *34* (11), 2703–2706.

(40) Salzinger, S.; Soller, B. S.; Plikhta, A.; Seemann, U. B.; Herdtweck, E.; Rieger, B. Mechanistic Studies on Initiation and Propagation of Rare Earth Metal-Mediated Group Transfer Polymerization of Vinylphosphonates. *J. Am. Chem. Soc.* **2013**, *135* (35), 13030–13040.

(41) Halama, K.; Schaffer, A.; Rieger, B. Allyl Group-Containing Polyvinylphosphonates as a Flexible Platform for the Selective Introduction of Functional Groups via Polymer-Analogous Transformations. *RSC Adv.* **2021**, *11* (61), 38555–38564.

(42) Halama, K.; Lin, M. T.-Y.; Schaffer, A.; Foith, M.; Adams, F.; Rieger, B. Cytocompatible Triblock Copolymers with Controlled Microstructure Enabling Orthogonally Functionalized Bio-polymer Conjugates. *Macromolecules* **2024**, *57* (4), 1438–1447.

(43) Salzinger, S.; Seemann, U. B.; Plikhta, A.; Rieger, B. Poly(vinylphosphonate)s Synthesized by Trivalent Cyclopentadienyl Lanthanide-Induced Group Transfer Polymerization. *Macromolecules* **2011**, *44* (15), 5920–5927.

(44) Mohan, T.; Niegelhell, K.; Nagaraj, C.; Reishofer, D.; Spirk, S.; Olschewski, A.; Stana-Kleinschek, K.; Kargl, R. Interaction of Tissue Engineering Substrates with Serum Proteins and Its Influence on Human Primary Endothelial Cells. *Biomacromolecules* **2017**, *18* (2), 413–421.

(45) Mohan, T.; Kargl, R.; Doliška, A.; Vesel, A.; Köstler, S.; Ribitsch, V.; Stana-Kleinschek, K. Wettability and Surface Composition of Partly and Fully Regenerated Cellulose Thin Films From Trimethylsilyl Cellulose. *J. Colloid Interface Sci.* **2011**, *358* (2), 604–610.

(46) Błażewska, K. M. McKenna Reaction—Which Oxygen Attacks Bromotrimethylsilane? *J. Org. Chem.* **2014**, *79* (1), 408–412.

(47) Abd Manan, T. S. B.; Beddu, S.; Mohamad, D.; Mohd Kamal, N. L.; Itam, Z.; Khan, T.; Jusoh, H.; Abdul Rahman, N. A.; Mohamed

Nazri, F.; Mohd Yapandi, M. F. K.; Wan Mohtar, W. H. M.; Isa, M. H.; Che Muda, Z.; Ahmad, A.; Wan Rasdi, N. Physicochemical Properties of Absorbent Hydrogel Polymers in Disposable Baby Diapers. *Chem. Phys. Lett.* **2021**, *774*, No. 138605.

(48) Zohuriaan-Mehr, M. J.; Omidian, H.; Doroudiani, S.; Kabiri, K. Advances in Non-Hygienic Applications of Superabsorbent Hydrogel Materials. *J. Mater. Sci.* **2010**, *45* (21), 5711–5735.

(49) Ismaelimgohadam, S.; Jonoobi, M.; Hamzeh, Y.; Azimi, B.; Mezzetta, A.; Guazzelli, L.; Cinelli, P.; Seggiani, M.; Danti, S. Development and Characterization of Sodium Alginate-Based Bio-hybrid Super Absorbent Polymer with High Retention Capacity Suitable for Baby Diapers. *J. Polym. Environ.* **2024**, *32*, S212.

(50) Guilherme, M. R.; Aouada, F. A.; Fajardo, A. R.; Martins, A. F.; Paulino, A. T.; Davi, M. F.; Rubira, A. F.; Muniz, E. C. Superabsorbent Hydrogels Based on Polysaccharides for Application in Agriculture As Soil Conditioner and Nutrient Carrier: A Review. *Eur. Polym. J.* **2015**, *72*, 365–385.

(51) Basit, H.; van der Heyden, A.; Gondran, C.; Nysten, B.; Dumy, P.; Labbé, P. Tethered Bilayer Lipid Membranes on Mixed Self-Assembled Monolayers of a Novel Anchoring Thiol: Impact of the Anchoring Thiol Density on Bilayer Formation. *Langmuir* **2011**, *27* (23), 14317–14328.

(52) Spagnolo, S.; Davoudian, K.; Ahmadi, S.; Chan, E.; Hianik, T.; Thompson, M. Thiol-Based Probe Linker with Antifouling Properties for Aptasensor Development. *Chemosensors* **2022**, *10* (10), 435.

(53) Slavin, S.; Soeriyadi, A. H.; Voorhaar, L.; Whittaker, M. R.; Becer, C. R.; Boyer, C.; Davis, T. P.; Haddleton, D. M. Adsorption Behaviour of Sulfur Containing Polymers to Gold Surfaces Using QCM-D. *Soft Matter* **2012**, *8* (1), 118–128.

(54) Batchelor, R. R.; Blasco, E.; Wuest, K. N. R.; Lu, H.; Wegener, M.; Barner-Kowollik, C.; Stenzel, M. H. Spatially Resolved Coding of λ -Orthogonal Hydrogels by Laser Lithography. *Chem. Commun.* **2018**, *54* (19), 2436–2439.

(55) Li, B.; He, M.; Ramirez, L.; George, J.; Wang, J. Multifunctional Hydrogel Microparticles by Polymer-Assisted Photolithography. *ACS Appl. Mater. Interfaces* **2016**, *8* (6), 4158–4164.

(56) Fu, R.; Zhong, X.; Xiao, C.; Lin, J.; Guan, Y.; Tian, Y.; Zhou, Z.; Tan, G.; Hu, H.; Zhou, L.; Ning, C. A Stretchable, Biocompatible, and Self-Powered Hydrogel Multichannel Wireless Sensor System Based on Piezoelectric Barium Titanate Nanoparticles for Health Monitoring. *Nano Energy* **2023**, *114*, No. 108617.

(57) Scarpa, E.; Mastronardi, V. M.; Guido, F.; Algieri, L.; Quattieri, A.; Fiammengio, R.; Rizzi, F.; De Vittorio, M. Wearable Piezoelectric Mass Sensor Based on pH Sensitive Hydrogels for Sweat pH Monitoring. *Sci. Rep.* **2020**, *10* (1), 10854.

(58) Hu, N.; Gao, D.; Song, F.; Yang, C.; Zhang, J.; Müller-Buschbaum, P.; Zhong, Q. Effect of Embedded G-C3N4 Nanosheets on the Hydration and Thermal Response Behavior of Cross-Linked Thermoresponsive Copolymer Films. *Langmuir* **2024**, *40* (28), 14663–14673.

(59) Zhong, Q.; Chen, C.; Mi, L.; Wang, J.-P.; Yang, J.; Wu, G.-P.; Xu, Z.-K.; Cubitt, R.; Müller-Buschbaum, P. Thermoresponsive Diblock Copolymer Films With a Linear Shrinkage Behavior and Its Potential Application in Temperature Sensors. *Langmuir* **2020**, *36* (3), 742–753.

5.5 Author contributions

Anton Maier synthesized the catalyst and monomers, performed the polymerization experiments, and characterized all polymers (NMR, SEC-MALS, etc.). A. M. synthesized all cross-linked materials and characterized the water uptake. Furthermore, A. M did the spin-coating, thin-film characterization (profilometry, AFM, light microscopy), and QCM-D measurements. A. M. conceptualized the project and initiated the collaborations with all other authors. A. M. analyzed the measurement results and wrote the original draft.

6 Additive manufacturing of poly(vinylphosphonate)-based hydrogels

6.1 Bibliographic data

Title: “High-Fidelity Direct Ink Writing of Poly(vinylphosphonate)-Reinforced Polysaccharide Inks With Tunable Properties”

Status: Paper, Publication date: 16.01.2025

Journal: ACS Applied Polymer Materials

Publisher: American Chemical Society (ACS)

DOI: 10.1021/acsapm.4c03517

Authors: Anton S. Maier, Florian Lackner, Julia Fink, Tobias Steindorfer, Elisabeth Hofmann, Karin Stana Kleinschek, and Bernhard Rieger

6.2 Table of content graphic

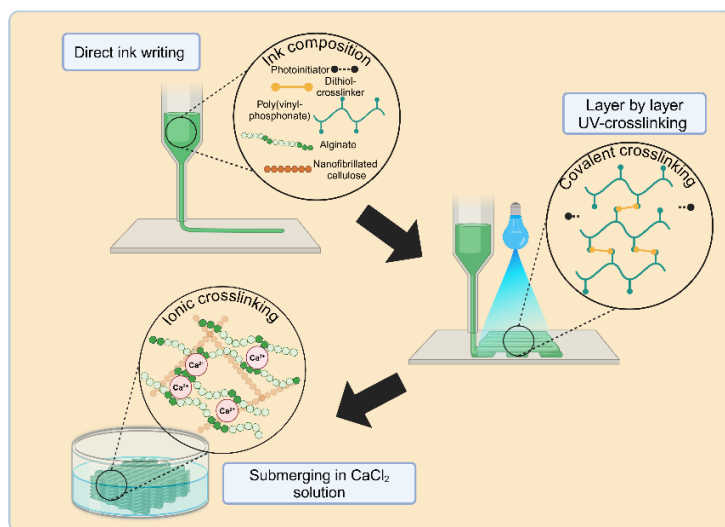


Figure 27: Table of content graphic for the manuscript entitled “High-Fidelity Direct Ink Writing of Poly(vinylphosphonate)-Reinforced Polysaccharide Inks With Tunable Properties”.

A. S. Maier and F. Lackner contributed equally to the manuscript. A. S. Maier and F. Lackner prepared the original draft. A. S. Maier performed all polymer-related experiments and polymer characterization. A. S. Maier and F. Lackner performed the additive manufacturing experiments. F. Lackner performed tensile testing and printed the samples for cytotoxicity testing. A. S. Maier and F. Lackner contributed to the original idea. All work was supervised by B. Rieger and K. Stana Kleinschek.

6.3 Content

This study leverages the photochemical cross-linking of P(DEVP-*stat*-DAIVP) for additive manufacturing via direct ink writing (DIW). Statistical poly(vinylphosphonate) copolymers are synthesized via REM-GTP, targeting different amounts of cross-linkable DAIVP units. Furthermore, a different dithiol cross-linker (1,6-hexanedithiol), other photoinitiators, and the solvent water are employed to enhance cytocompatibility and reduce purification efforts. Initial printing experiments with this emulsion result in poor resolutions and shape fidelities due to overextrusion caused by the low ink viscosities. Therefore, the ink rheology is modified by applying a 3 wt% nanofibrillated cellulose (NFC) suspension to dissolve the polymers and adding sodium alginate (Alg) as a thickener. The corresponding ink exhibits thixotropic behavior as confirmed by rotational rheology measurements, thus allowing the extrusion of continuous, free-standing strands facilitated by the shear-force alignment of NFC. The polymer-reinforced inks enable the printing of sophisticated structures through layer-by-layer deposition with intermediate photochemical cross-linking of P(DEVP-*stat*-DAIVP), resulting in high shape fidelity and printing stability. In this context, printing a 30-layered infill tube, an 89-layered free-standing tube, and an overhanging object with a 30° incline demonstrate the superiority of polymer-reinforced ink over standard NFC/Alg ink. Utilizing the optimized ink composition, specimens for evaluating the water uptake and the mechanical properties of different poly(vinylphosphonate)-reinforced inks are printed. Regarding water uptake, the synthetic polymers dictate the printed objects' swelling behavior in physiological NaCl solution and contribute to high swelling shape fidelity in CaCl₂-containing solutions applied to induce ionic Alg cross-linking, overcoming the issue of NFC/Alg inks regarding poor shape retention upon swelling. Whereas the polymer-reinforced inks do not exceed the mechanical strength of an NFC/Alg control in tensile testing as ionic cross-linking dominates, the tensile modulus correlates with the cross-linking degree of the polymer, and the mechanical strength of the inks is within the range of materials commonly used for tissue engineering applications. Finally, the pristine objects are subjected to cytotoxicity testing after ionic cross-linking, displaying only moderate cytotoxicity toward two cell lines, hence suggesting great potential for ink optimization and biomedical applications.

6.4 Manuscript

ACS APPLIED
POLYMER MATERIALS

Open Access

This article is licensed under [CC-BY 4.0](https://creativecommons.org/licenses/by/4.0/)pubs.acs.org/acsapm

Article

High-Fidelity Direct Ink Writing of Poly(vinylphosphonate)-Reinforced Polysaccharide Inks with Tunable Properties

Anton S. Maier,¹ Florian Lackner,¹ Julia Fink, Tobias Steindorfer, Elisabeth Hofmann, Karin Stana Kleinschek,* and Bernhard Rieger*Cite This: *ACS Appl. Polym. Mater.* 2025, 7, 1752–1762

Read Online

ACCESS |

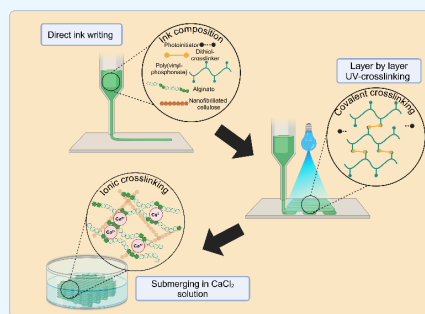
Metrics & More

Article Recommendations

Supporting Information

ABSTRACT: Herein, a concept for the structural reinforcement of nanofibrillated cellulose (NFC)/alginate (Alg) formulations for direct ink writing (DIW) applying photochemical cross-linking of poly(vinylphosphonate) copolymers is introduced. Ultraviolet (UV-A) irradiation (one second per layer) enables the covalent cross-linking of statistical copolymers consisting of diallyl vinylphosphonate (DAVP) and diethyl vinylphosphonate (DEVP) via thiol–ene click chemistry, giving access to high shape fidelities and sophisticated structures. The polymers were obtained via rare earth metal-mediated group-transfer polymerization (REM-GTP), allowing excellent control over molecular weights and copolymer composition with narrow polydispersities. Optimized ink formulations include 9 wt % P(DEVP-*stat*-DAVP) dissolved in a 3 wt % aqueous nanofibrillated cellulose (NFC) suspension with roughly 3 wt % of sodium alginate, 1,6-hexanedithiol as cross-linker, and a photoinitiator. The shear-thinning behavior of this formulation, confirmed by rotational rheology, allowed extrusion-based DIW to create various objects, demonstrating the high shape fidelity and printing stability of these inks. Specimens printed from polymer-containing NFC/Alg inks were investigated regarding water uptake and mechanical properties, revealing an improvement of the swelling shape fidelity of printed objects in CaCl₂-containing physiological NaCl solution by combining chemical cross-linking and ionic cross-linking. Furthermore, the respective material properties correlated with the cross-linking density induced by the reinforcement with synthetic polymers. Finally, the pristine printed objects revealed only slight cytotoxicities toward primary human umbilical vein endothelial cells (HUVECs) and immortalized human embryonic kidney cells (HEK293 cell line).

KEYWORDS: Hydrogels, biomaterials, catalytic polymerization, additive manufacturing, photochemical cross-linking



INTRODUCTION

Additive manufacturing and, in particular, direct ink writing (DIW) are important 3D printing techniques because they enable the creation of sophisticated 3D models from a broad range of materials exhibiting appropriate rheological behavior. These flow properties allow ink extrusion through a deposition nozzle, forming dimensionally stable objects through layer-by-layer deposition.^{1–6} One of the most abundant biobased polymeric structures with a high application potential in DIW are cellulose nanofibrils (NFC) due to their outstanding mechanical properties and useful morphology.^{7–9} NFC is obtained from bacteria,¹⁰ or as less defined structures by chemical and mechanical treatment of plant cellulose fibers^{11,12} and characterized by a high aspect (length/diameter) ratio resulting in significant strength and stiffness.¹³ However, the most notable feature of NFC for DIW is the shear-thinning behavior of aqueous suspensions of nanofibrillated cellulose. The shear-force alignment of fibers upon extrusion-based printing is caused by the high aspect ratio of NFC, the high hydration, and the absence of covalent cross-links.^{14–16} Nevertheless, the printed objects lack mechanical stability

without additional cross-linking. Therefore, NFC-based inks for DIW are often complemented with thickening agents, adding mechanical strength and flexibility and allowing network formation.¹⁶ One biopolymer for this purpose is alginate (Alg) obtained from the cell walls of brown algae. Alg is commonly used as a thickener or gelling agent in the food industry but attracts increasing interest in the biomedical field.^{17–19} The addition of alginate to aqueous NFC suspensions thus increases viscosity and further allows the ionic cross-linking of printed objects by adding solutions containing bivalent cations such as Ca²⁺.^{20–22} In the literature, there are numerous reports on the application of NFC/alginate inks in DIW, including the creation of objects with anisotropic mechanical properties, the printing of sophisticated structures, and extensive studies confirming the

Received: November 7, 2024

Revised: January 7, 2025

Accepted: January 8, 2025

Published: January 16, 2025



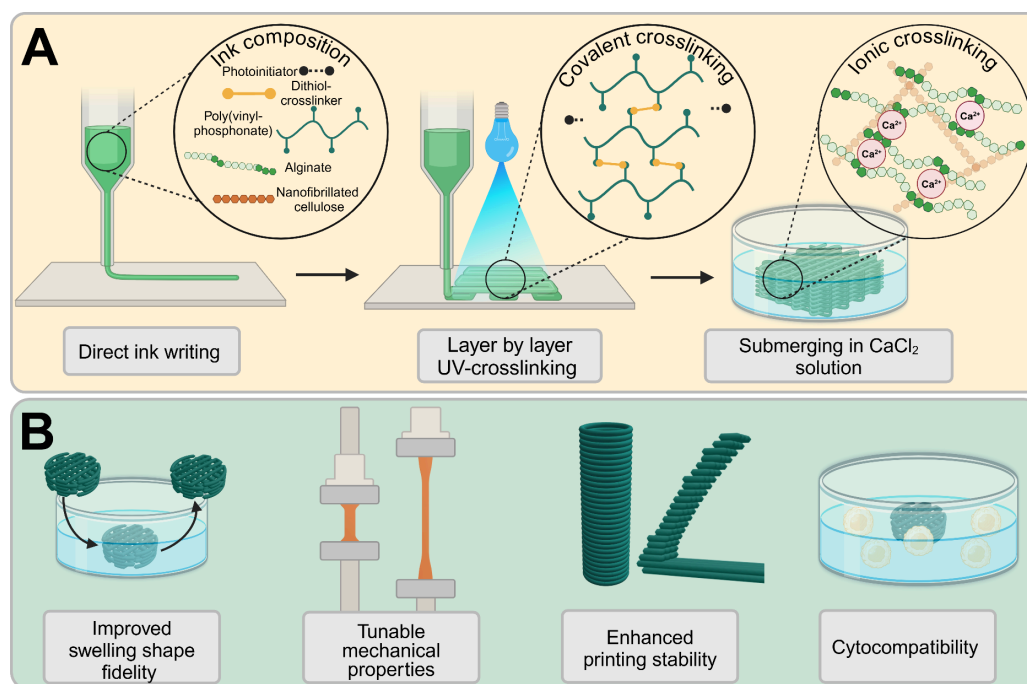
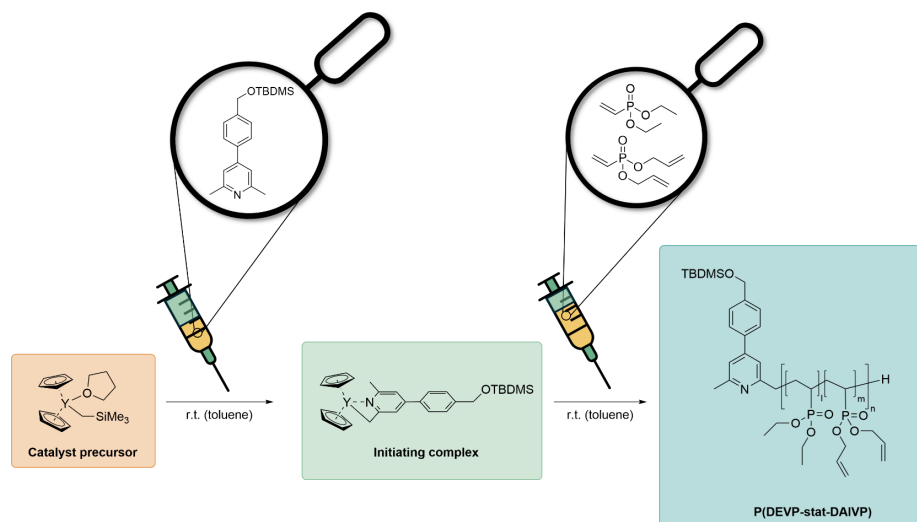


Figure 1. Schematic process overview of direct ink writing with polymer-reinforced NFC/Alg inks: (A) Extrusion-based 3D printing of NFC/Alg inks containing photo-cross-linkable poly(vinylphosphonates), photoinitiator, and dithiols as cross-linker via layer-by-layer deposition with intermediate UV-A-irradiation, followed by postcuring of the final objects in CaCl_2 solution and (B) advantages of novel, polymer-reinforced ink formulations over standard NFC/Alg inks with the same ink composition.

Scheme 1. Rare Earth Metal-Mediated Statistical Copolymerization of Diethyl Vinylphosphonate (DEVP) and Diallyl Vinylphosphonate (DAIVP) to P(DEVP-stat-DAIVP) with an In Situ Generated Species of $\text{Cp}_2\text{YCH}_2\text{TMS}(\text{thf})$



cytocompatibility of these ink formulations.^{23–26} However, there are some drawbacks concerning the uncontrolled ionic cross-linking of NFC/Alg inks by Ca^{2+} -cations. These include poor dimensional stability of objects upon swelling in the CaCl_2 cross-linking solution, leading to a loss of shape fidelity or the collapse of structures caused by the leaching of ions.^{27,28} To

overcome these issues, supramolecular hydrogels of biopolymers can additionally be reinforced through covalent cross-links, yielding increased mechanical strength while maintaining the dynamic properties of noncovalent networks.^{29,30} One class of synthetic polymers for this purpose is poly(vinylphosphonates) obtained via rare earth metal-mediated

group-transfer polymerization (REM-GTP).³¹ REM-GTP enables the synthesis of polymers through repeated 1,4-conjugate addition of Michael-type monomers, achieving excellent control over the polymer microstructure while maintaining narrow polydispersities.^{32,33} In this context, statistical copolymers from the monomers diallyl vinylphosphonate (DAIVP) and diethyl vinylphosphonate (DEVP) susceptible to postpolymerization functionalization by thiol–ene click reactions, e.g. with biologically active motifs, can be obtained with high precision.^{34,35} Applying photoinitiated thiol–ene click chemistry with dithiols and suitable photoinitiators allows cross-linking P(DEVP-*stat*-DAIVP) copolymers toward hydrogels. The corresponding materials exhibit widely tunable properties regarding water uptake and mechanical strength, and high cytocompatibility after purification, making them appealing candidates as scaffold materials for various cells.³⁶ Herein, we apply poly(vinylphosphonate)-based hydrogels to reinforce NFC/alginate inks in extrusion-based additive manufacturing. After optimization of the ink composition, the shear-thinning behavior of the inks combined with the photoinitiated cross-linking process provided by adding P(DEVP-*stat*-DAIVP) gives access to high shape fidelity and complex structures, which can additionally be postcured via ionic cross-linking in Ca²⁺-containing solutions. Further, investigations of the water uptake and mechanical properties reveal the benefits of adding synthetic polymers and demonstrate the control of material properties by adjusting the covalent cross-linking density (Figure 1). In the final part, the pristine printed objects are investigated regarding their cytotoxicity toward different cell types.

RESULTS AND DISCUSSION

Polymer Synthesis. The copolymerization of diethyl vinylphosphonate (DEVP) and diallyl vinylphosphonate (DAIVP) was performed according to a previously reported procedure.³⁶ After CH-bond activation of the initiator through σ -bond metathesis with the catalyst was confirmed via ¹H NMR spectroscopy as indicated by the absence of the CH₂-group signal (doublet, $\delta = -0.66$ ppm) of Cp₂YCH₂TMS(thf), a mixture of DEVP and the calculated amount of cross-linkable DAIVP was added (Scheme 1).

When quantitative conversion was confirmed via ³¹P NMR spectroscopy, the polymerization was stopped, and the copolymers precipitated in hexane and lyophilized from 1,4-dioxane (for experimental details, see the Supporting Information). Table 1 shows the polymerization results for copolymers 1–3, later used to reinforce NFC/Alg inks with photo-cross-linked, poly(vinylphosphonate)-based hydrogels.

As confirmed by the copolymerization results, we successfully applied the excellent control over copolymer composition and polydispersity provided by rare earth metal-mediated group-transfer polymerization (REM-GTP) to obtain copolymers 1–3. Table 1 displays a variation of the amount of cross-linkable DAIVP units while targeting similar amounts of repeats in the polymers, which is reflected in the similar molecular weights of the polymers ($M_{n,NMR} \approx 25$ – 26 kg/mol). These were determined via ¹H NMR spectroscopy by referring the DEVP and DAIVP signals in the copolymer spectrum to the distinct -OTBDMS end-group signal in each sample (Figures S1–S3). Without exception, the targeted ratio of DAIVP is met with high precision, and narrow polydispersities below 1.12 are achieved in all cases, as illustrated by the refractive index detector signals of gel permeation chromatography in Figure S4. Further, successful copolymerization of DEVP and DAIVP was

Table 1. Polymerization Results of Rare Earth Metal-Mediated Group-Transfer Polymerization of DEVP and DAIVP to Obtain Statistical Copolymers 1–3 Applied to Reinforce NFC/Alg Inks in Direct Ink Writing Experiments

Entry	DEVP/ DAIVP/ Cat. ^a	Targeted DAIVP content [%]	X [%] ^b	DAIVP content [%] ^c	M_n NMR ^d	IE ^e	\bar{D} ^f
1	95/5/1	5	>99%	4.8	25.9	57	1.07
2	90/10/1	10	>99%	9.2	24.7	60	1.12
3	80/20/1	20	>99%	19.1	26.0	59	1.10

^aReactant ratio desired. ^bConversion determined via ³¹P NMR spectroscopy in CD₃OD. ^cDetermined via ¹H NMR spectroscopy by comparison of the CH₂ signals of DEVP (4.18 ppm, $m = 1/4$) and DAIVP (4.63 ppm, $n = 1/4$). ^dCalculated via ¹H NMR spectroscopy by comparison of the -OTBDMS signals of the initiator at 0.14 ppm ($I = 6H$) and the CH₂ signals of DEVP (4.18 ppm, $m = 1/4$) and DAIVP (4.63 ppm, $n = 1/4$). ^eInitiator efficiency (IE): $IE = M_{n,calc}/M_{n,NMR}$ with $M_{n,NMR} = 327.54$ g/mol + $m^*164.14$ g/mol + $n^*188.16$ g/mol. ^fPolydispersity determined via size-exclusion chromatography multiangle light scattering (SEC-MALS) in THF:H₂O (1:1) with 340 mg/L 2,6-di-*tert*-butyl-4-methylphenol (BHT) and 9 g/L tetra-*n*-butylammonium bromide (TBAB).

confirmed via ³¹P NMR and ¹H DOSY NMR spectroscopy, as indicated by the presence of only one diffusion coefficient in the spectra (Figures S5–S10).

General Ink Composition and Initial Printing Experiments. To target biomedical applications, the P(DEVP-*stat*-DAIVP)-based hydrogel system reported in an initial study was altered, aiming for a more cytocompatible formulation that potentially reduces purification efforts before in vitro experiments with living microorganisms.³⁶ Therefore, the cytotoxic solvent 1,4-dioxane, capable of dissolving the polymers very well, was switched to water, which can dissolve the polymers and represents the base for most body fluids. Further, 3,6-dioxo-1,8-octanedithiol exhibiting low lethal doses according to safety data sheets, most likely due to its high hydrophilicity caused by the polyethylene glycol (PEG) chain, was replaced by food grade 1,6-hexanedithiol (higher lethal doses) as a cross-linker for the photochemical thiol–ene click reaction for hydrogel formation. Finally, the formerly applied photoinitiator 2,2-dimethoxy-2-phenylacetophenone (DMPA) was substituted by less toxic 2-hydroxy-2-methylpropiophenone as well as by the water-soluble, noncytotoxic and visible-light absorbing photoinitiator lithium phenyl(2,4,6-trimethylbenzoyl)phosphine (LAP). Overall, we switched from a formerly homogeneous solution (Figure 2A) to an emulsion with the cross-linker (and initiator) emulsified in an aqueous solution of P(DEVP-*stat*-DAIVP) (Figure 2B) with no considerable impact on the cross-linking process. After gel formation was successfully proven with the vial test (Figures 2A and 2B, bottom), initial printing tests were conducted to explore the printability of this new ink formulation (due to cost reasons, 2-hydroxy-2-methylpropiophenone was selected as cross-linker instead of rather expensive LAP). In this context, two different objects were chosen to evaluate the printability as well as the shape fidelity, which is considered a combination of extrudability and the capability to form wet, free-standing strains. Here, a grid, shown in Figure 2C, and a logo, presented in Figure 2D, were attempted with printing settings according to Table S1. By comparison of the model with the pictures during the printing process and the final object, the poor shape fidelity of this ink formulation is already observable. This can be attributed to the low viscosity of the emulsion causing

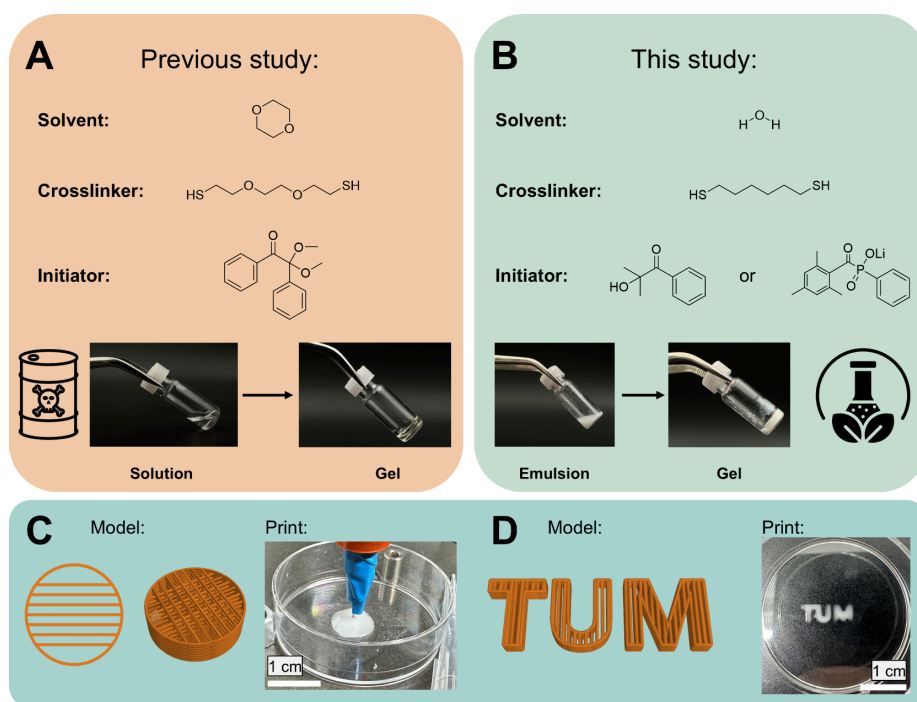


Figure 2. (A) Previously reported system for the synthesis of poly(vinylphosphonate)-based hydrogels from a solution of polymer in 1,4-dioxane with 3,6-dioxo-1,8-octanedithiol as cross-linker and 2,2-dimethoxy-2-phenylacetophenone as initiator.³⁶ (B) System introduced in this work consisting of an emulsion of 1,6-hexanedithiol as cross-linker in an aqueous P(DEVP-*stat*-DAVP) solution with either 2-hydroxy-2-methylpropiophenone or lithium phenyl(2,4,6-trimethylbenzoyl)phosphinate as photoinitiator. (C) Direct ink writing of the aqueous emulsion: model (left) and final object (right). (D) Direct ink writing of the aqueous emulsion: model (left) and final object (right).

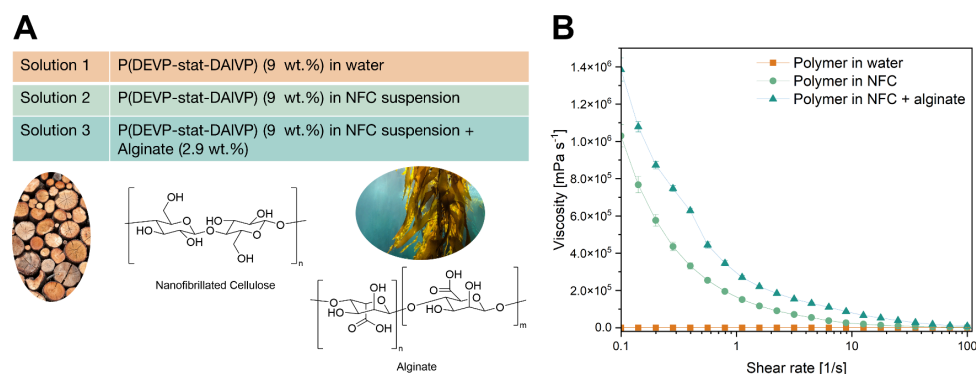


Figure 3. (A) Compositions of solutions 1–3 for the investigation of shear-thinning behavior by rotational rheology. (B) Viscosity curves for solutions 1–3 determined via rotational rheology at shear rates between 0.1 and 100 1/s.

overextrusion and therefore a very low resolution of the targeted structures. In addition, proceeding with this ink composition would most likely lead to poor reproducibility of the hydrogel synthesis and printed objects. Thus, a modification of ink rheology with well-established biopolymers was necessary, which will be discussed in the next section.

Optimization and Characterization of Inks Toward High Shape Fidelity. Given the poor shape fidelity of aqueous emulsions of poly(vinylphosphonates), 1,6-hexanedithiol, and 2-hydroxy-2-methylpropiophenone (Figures 2C and 2D), a modification of ink rheology by the addition of NFC and Alg was

targeted. As mentioned in the introduction, NFC introduces shear-thinning properties and can be processed via DIW due to the shear-force alignment of nanofibrils upon extrusion. However, aqueous suspensions of nanocellulose fibers lack covalent cross-links, resulting in low mechanical stability and rather poor shape fidelity of the printed objects. Therefore, Alg is often added as a thickening agent, further modifying the rheology and, in addition to that, introducing sites for ionic cross-linking by the addition of bivalent cations such as Ca²⁺. The chemical structures of NFC and Alg are displayed in Figure 3A. First, the rheology of three different inks was compared. In

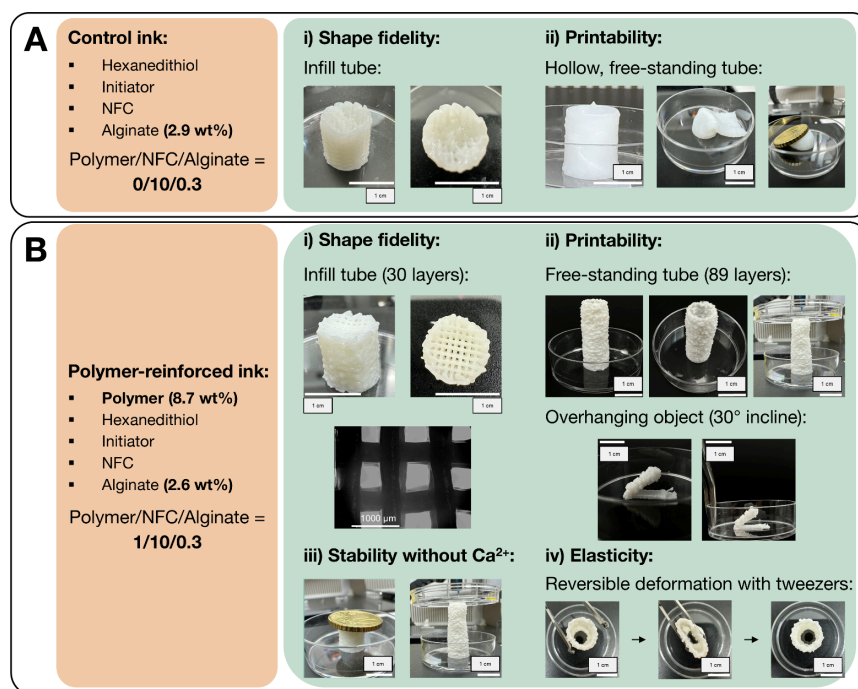


Figure 4. Ink composition and images of printed objects to evaluate the shape fidelity, printability, and mechanical properties of different NFC/Alg inks. Comparison of an NFC/Alg ink (A) with the corresponding ink reinforced through photochemical cross-linking of P(DEVP-*stat*-DAIVP) (B). The printed objects include an infill tube with excellent shape fidelity between the infill strands, a hollow, free-standing tube with 89 layers (machine maximum) without collapsing, and an overhanging object with a 30° incline. Further details regarding the printing models and printing parameters are provided in the Supporting Information, Table S1.

this context, the initial emulsion was compared to a system in which the polymer was dissolved in an aqueous suspension of NFC (3 wt %) and finally to a formulation, where additionally, Alg is added as a thickening agent (for the exact ink compositions, see Figure 3A). As expected, the rheological measurements confirm the introduction of shear-thinning behavior by switching to the NFC suspension as matrix and demonstrate a further increase in the gel character upon addition of alginate. Clear evidence of this is given by the rotational rheology measurements presented in Figure 3A, in which the viscosity of the polymer-containing NFC/alginate ink exceeds the viscosity obtained from the solution of P(DEVP-*stat*-DAIVP) in the NFC suspension as well as the polymer emulsion in water. Whereas the latter shows no notable response upon the increase of the shear rate, the NFC-containing inks reveal the shear-force alignment of the cellulose nanofibrils, leading to decreasing viscosities with higher shear stress. These shear thinning properties are essential for smooth extrusion through the deposition nozzle while maintaining a high storage modulus G' at lower shear deformation (Figure S11), allowing filament shape fidelity.¹⁶ The enhanced viscoelastic properties of the inks, particularly pronounced for those containing poly(vinylphosphonates), alginate, and NFC, prove the necessity of adding all three components. In addition to the rheological characterization, transmitted light microscopy pictures (Figure S14) of a P(DEVP-*stat*-DAIVP)-containing NFC/Alg ink directly after preparation revealed a homogeneous distribution of the 1,6-hexanedithiol cross-linker as droplets with diameters below 20 μm . Furthermore, as presented by the microscopic

images in Figure S14, the emulsion remained stable for 24 h of storage, ensuring no phase separation occurred during the printing process.

After the rheology of the three different inks was investigated, extrusion and printing tests were conducted with the NFC and NFC/Alg inks (Figure S12). Compared to the emulsion (Figure S12A), the polymer solution in NFC (3 wt % NFC in water, 9 wt % polymer in ink) showed significantly higher viscosity, which led to good extrudability. However, the viscosity of the corresponding polymer solution was too low to allow the extrusion of continuous filaments, causing only a moderate shape fidelity of the final object (Figure S12B). Upon addition of alginate to the polymer-containing NFC suspension, the viscosity was further increased to a level that allowed the extrusion of thin, continuous filaments, allowing printing of 30-layered grids with an infill distance of 1.0 mm with excellent resolution and proofing the outstanding shape fidelity of this ink formulation (Figure 4B, i) and Figure S12C). During the printing process, UV-A-curing for one second between each layer helped with the formation of this complex structure and did not lead to a noticeable loss of layer-to-layer adhesion, presumably due to nonquantitative cross-linking of each layer, enabling the connection of the next layer through thiol–ene click reaction at the interface. The 30-layered infill tube with uniform pore size revealed remarkable stability in carrying the weight of a coin even without ionic cross-linking after curing the final printed object by UV-irradiation for 120 s (Figure 4B, iii)). This confirms the necessity of covalent reinforcement for good shape fidelity and printing stability. To demonstrate this, we

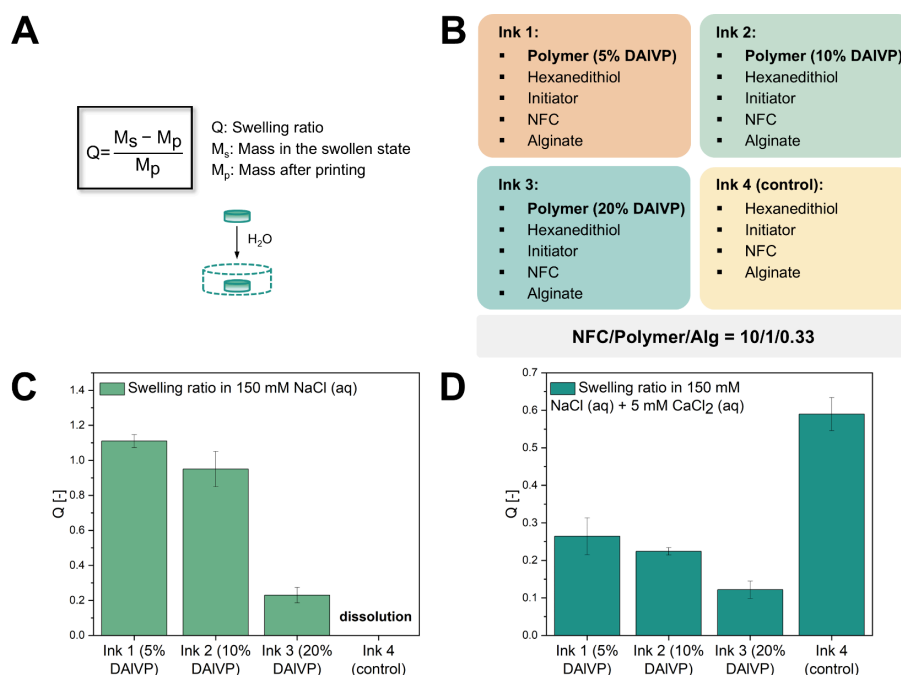


Figure 5. Investigation of the water uptake of different printed structures consisting of P(DEVP-*stat*-DAIVP)-reinforced NFC/Alg inks compared to a control. (A) Definition of the swelling ratio used to quantify the water uptake. (B) Composition of inks 1–4 applied to print specimens for swelling experiments. (C) Results of the swelling experiments of objects printed with inks 1–4 in physiological NaCl solution. (D) Results of the swelling experiments of objects printed with inks 1–4 in physiological NaCl (aq) upon the addition of 5 mM CaCl₂ (aq).

printed an infill tube with a varying number of layers ($n = 3, 13, 20, 30$) using a nozzle with a 0.41 mm diameter and an infill distance of 1.00 mm (Figure S13), ideally resulting in square-shaped gaps with 0.59 mm length, as described in the literature as a measure for desirable shape fidelity and ink stability.^{24,37} The P(DEVP-*stat*-DAIVP)-containing ink was able to extrude in a rod-like filament shape with a measured diameter of 0.50 ± 0.03 mm for 3 layers and 0.44 ± 0.04 mm for 30 layers with square-shaped gaps with a length of 0.46 ± 0.08 mm and a width of 0.55 ± 0.07 mm. This contrasted with the control ink, which did not contain poly(vinylphosphonates) and could not be covalently stabilized during printing. The control ink showed an insufficient storage modulus upon extrusion and continuous flow, leading to broader stands with 0.62 ± 0.04 mm diameter and smaller, round-edged pores with 0.27 ± 0.06 mm length after 3 printed layers. For structures with more layers ($n = 13, 20, 30$), no more top-to-bottom open pores were visible due to the sagging of the object. To further quantitatively describe the pore shape, we measured the angle of the infill gaps, which was $94 \pm 5^\circ$ for 3 layers and $91 \pm 2^\circ$ for 30 layers, which was close to the desired square shape with ideally 90° in the case of the P(DEVP-*stat*-DAIVP)-reinforced ink. The control ink without covalent cross-linking resembled a rather circular shape due to its flow properties, with an angle of $127 \pm 9^\circ$ after 3 layers, revealing the low printing resolution in the absence of poly(vinylphosphonates). A detailed comparison of the printing resolution for a polymer-reinforced ink and a control ink is presented in Figure S13. Further, a hollow tube with a diameter of 10 mm and 89 consecutive layers was printed. This was the maximum number of layers that could be printed by the device with a selected strand height of 0.4 mm. After curing the final

object for 120 s, the obtained tube exhibited relatively high mechanical strength and good flexibility, allowing the reversible deformation with tweezers (Figure 4B, ii–iv). In a final printing experiment, we were able to obtain overhanging objects with a 30° incline (Figure 4B, ii). The possibility of targeting such complex architectures is significant for various scaffold materials in tissue engineering, such as branched blood vessels or an aortic arch.²⁵ For comparison, the structures presented in Figure 4B were printed with an ink with the same NFC/Alg ratio but without reinforcement by P(DEVP-*stat*-DAIVP) (Figure 4A). In the case of the 30-layered infill tube, this led to a drastically reduced resolution and poor shape fidelity (Figure 4A, i). Further, the mechanical properties in the absence of ionic cross-linking were significantly lowered, causing a sagging of the object upon printing and the collapse of the structure under the weight of the coin. Similarly, the hollow tube exhibited a significant loss of mechanical stability, resulting in the collapse of the structure after 61 layers during the printing process (Figure 4A, ii). Therefore, it can be concluded that the addition of photo-cross-linkable P(DEVP-*stat*-DAIVP) yields polymer-reinforced inks which allow the cross-linking by UV-irradiation between each layer, creating a vast design space and giving access to a variety of complex architectures. For this purpose, poly(vinylphosphonates) are ideal candidates as they can be obtained via precision polymerization applying REM-GTP and present a class of water-soluble polymers with high cytocompatibility,^{35,36,38} which becomes crucial when DIW is, e.g., applied in biomedical contexts such as tissue engineering.

Water Uptake of Printed Objects. In the context of materials applied in a biomedical context, it is crucial to understand the behavior of objects tailored to a specific

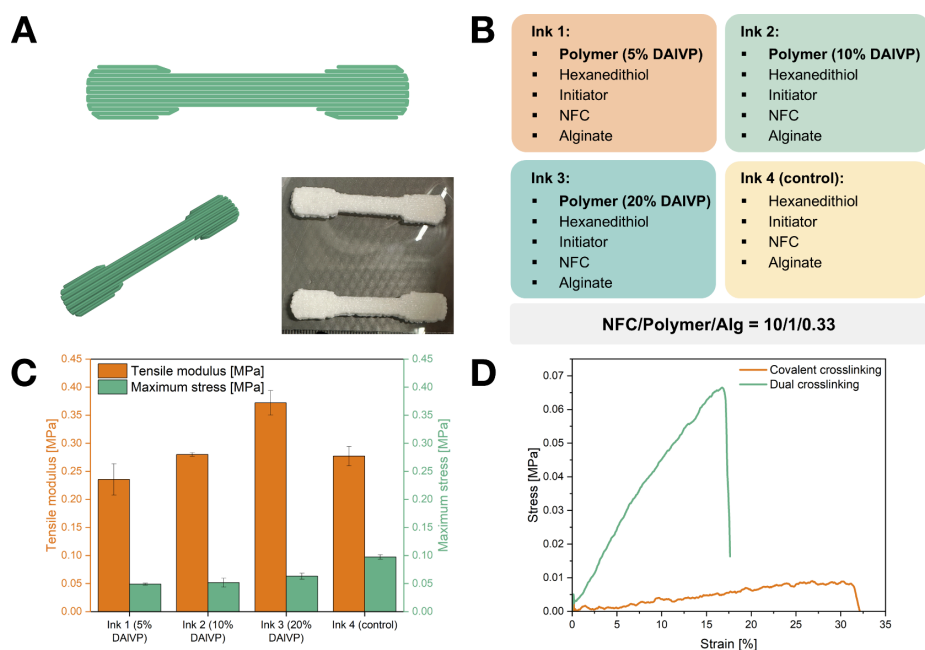


Figure 6. Investigation of the mechanical properties of different printed objects consisting of P(DEVP-*stat*-DAIVP)-reinforced NFC/Alg inks compared to a control. (A) Model and picture of the specimens printed for tensile testing. (B) Composition of inks 1–4 applied for printing specimens for stress–strain measurements. (C) Results of the stress–strain measurements of objects printed with inks 1–4 after swelling in CaCl₂-containing (5 mM) physiological NaCl solution (150 mM). (D) Comparison of specimens swollen in a physiological NaCl solution and specimens swollen in a CaCl₂-containing physiological NaCl solution.

application when subjected to an aqueous environment similar to *in vivo* conditions since aspects such as the loss of shape fidelity or structural breakdown due to pronounced swelling restrict application potential.^{27,28,36} Therefore, the swelling behavior of objects printed with different polymer-containing inks was compared to a “pure” NFC/alginate formulation to evaluate the effect of photochemically initiated, covalent reinforcement by P(DEVP-*stat*-DAIVP). Further, we investigated the influence of the covalent cross-linking density on the water absorption of 3D printed structures, which is governed by the number of cross-linking sites in the synthetic polymer. The swelling experiments described in the following were conducted with the specimens printed for the stress–strain measurements addressed later in this work. In this context, the water uptake was characterized by comparing the weight of the specimens after printing with the weight of the printed specimens immersed in different aqueous solutions for 16 h. The swelling ratio Q expresses the amount of water absorbed by the samples and is calculated from the weight of the swollen sample M_s and the weight M_p of the specimens after printing (Figure 5A). Unlike the traditional definition of the swelling ratio, the reference weight M_p does not represent a dry state but exhibits water contents between 79 and 84% already, depending on the ink composition (Figure 5B). The three different polymer-containing inks contain an increasing number of cross-linkable DAIVP units (polymers 1–3, Table 1) which are absent in the pure NFC/alginate ink (Figure 5B, ink 4). For a better evaluation of the effect of the polymer in inks 1–3, a fixed ratio of NFC (3 wt % suspension)/P(DEVP-*stat*-DAIVP)/Alg, as indicated in Figure 5B, was selected. The same weight ratio of the 3 wt % nanofibrillated cellulose suspension to alginate (3 wt

% NFC (aq)/Alg = 10/0.3) was also applied in the control (ink 4). The swelling of the printed specimens was investigated in a physiological 150 mM NaCl solution and a physiological NaCl solution containing 5 mM CaCl₂ (aq) to induce ionic cross-linking of the alginate chains. With respect to the water uptake in the physiological NaCl represented in Figure 5C, the samples exhibited weight increases between 0.23 and 1.11 g of water per gram of cross-linked material. Further, a clear correlation of the swelling ratio with cross-linking density dictated by the corresponding ink was observed. Whereas ink 1 was reinforced with a polymer containing around 5% of cross-linkable DAIVP units, ink 3 contains P(DEVP-*stat*-DAIVP) with roughly 20% DAIVP, which in turn leads to a much higher degree of cross-linking in samples printed with this formulation. This structure–property relationship is reflected in the corresponding hydrogel properties, as the water uptake of the specimens printed with ink 1 exceeded the water uptake of the respective samples from ink 3, which is in good agreement with the results reported in previous studies.³⁶ Another advantage of the reinforcement of NFC/Alg inks by poly(vinylphosphonate)-based hydrogels can be observed comparing samples printed with inks 1–3 and the control. Despite being able to create structures upon extrusion of ink 4, the objects are unsuitable to be subjected to *in vivo* conditions, as the corresponding specimens dissolved when immersed in physiological NaCl solution for several hours. Therefore, the results presented in Figure 5C nicely illustrate the beneficial reinforcing effect induced by covalently cross-linking P(DEVP-*stat*-DAIVP) in NFC/Alg inks. Finally, the water uptake of samples printed with inks 1–4 was investigated in a 5 mM CaCl₂-containing physiological NaCl solution (Figure 5D). Here, the same trend as described for Figure 5C was observed

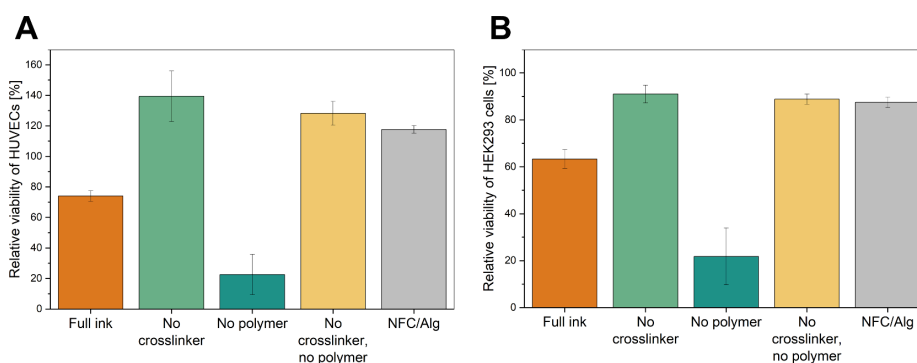


Figure 7. Relative cell viabilities of HUVECs (A) and HEK293 cells (B) after 48 h of indirect contact with different printed scaffolds determined by a PrestoBlue assay.

regarding the correlation between cross-linking density and swelling behavior. Notably, objects printed with ink 4 exhibited the highest swelling ratios of roughly 0.6 g of water per gram of material, twice the water absorption of the least covalently cross-linked sample (ink 1), and a 5-fold higher value than the most cross-linked object (ink 3). The high swelling ratio of the control specimens highlights the issue of a loss of shape fidelity upon ionic cross-linking of NFC/Alg hydrogels, leading to a loss of resolution. Therefore, the significantly lower water uptakes of polymer-reinforced inks 1–3 demonstrate that the corresponding objects exhibited high swelling shape fidelities, which are relevant for most biomedical applications. Overall, the effect of ionic cross-linking becomes evident when comparing the results presented in Figures 5C and 5D. The lower water uptake of samples in Figure 5D can be assigned to a higher cross-linking density due to a dual cross-linking in which covalent cross-links are complemented with Ca^{2+} -alginate interactions. This dual cross-linking mechanism, in combination with the intermediate photochemical, covalent cross-linking during printing described above, can be applied to form sophisticated structures that are subsequently postcured by adding Ca^{2+} ions.

Mechanical Properties. Finally, the specimens applied in the swelling experiments in physiological NaCl solution containing 5 mM CaCl_2 (aq) were subjected to tensile testing (Figure 6A). A well-studied feature of NFC-containing inks is the anisotropy of mechanical properties along and perpendicular to the fiber orientation of NFC.²⁴ To ensure the comparability of results, all specimens were fabricated following the same printing pathway, thus guaranteeing the same fiber orientation in each sample. In this context, the samples printed with inks 1–3 represented the dually cross-linked hydrogels combining covalent bonding and ionic interactions. In contrast, ink 4 was only cross-linked via Ca^{2+} ions (for ink compositions, see Figure 6B). Regarding the polymer-reinforced inks, an opposing trend for the tensile properties compared to the swelling behavior was observed. The tensile modulus and maximum stress increased with an increasing number of cross-linkable DAIVP units when switching from ink 1 to ink 3 (Figure 6C). This correlation is another structure–property relationship introduced by the synthetic polymers, and it can be assigned to the increasing covalent cross-linking density in these inks. With a tensile modulus between 0.24 ± 0.03 MPa for ink 1 and 0.37 ± 0.02 MPa for the stiffest ink 3, the tensile properties are comparable to methacrylated gelatin widely used for cartilage tissue engineering or poly(vinyl alcohol)/carrageenan used for skin

models.^{39,40} Notably, the samples printed with ink 4 exhibited a tensile modulus similar to that of ink 2 but exceeded the polymer-reinforced inks 1–3 in terms of maximum stress (Figures 6C and S15). Most likely, this is due to small imperfections in the prints with P(DEVP-*stat*-DAIVP) caused by ink inhomogeneities upon nonquantitative dissolution of the polymers or air-bubbles due to the surface-active properties of P(DEVP-*stat*-DAIVP) leading to foaming of the NFC suspension, which was hard to estimate due to the opaque color of the ink. Further, a comparison of the results of tensile testing to the ink composition was only performed for Ca^{2+} -cross-linked specimens as the covalently cross-linked samples originating from inks 1 and 2 kept in physiological 150 mM NaCl solution exhibited high elasticities and poor mechanical stabilities; thus, mostly rupturing upon sample preparation. Only specimens printed with ink 3, which induces the highest number of covalent cross-links due to the high DAIVP content in the polymers, were able to be measured after immersing them in 150 mM NaCl (aq) overnight. This indicates that the properties of NFC and Alg mostly dominate the mechanical features of these novel ink formulations. The polymer-reinforced inks are highly beneficial regarding the dimensional stability of printed objects (higher swelling shape fidelity and no more dissolution in NaCl solution), as discussed above. Nevertheless, the effects of poly(vinylphosphonate) addition on the mechanical properties are apparent, considering the correlation between the tensile modulus and the cross-linking degree of the synthetic polymers. To evaluate the effect of dual cross-linking on the printed structures, structures printed with ink 3 and kept in CaCl_2 -containing solution were compared with their nonionically cross-linked counterparts, as shown in Figure 6D. From these results, it becomes evident that postcuring with Ca^{2+} ions leads to a significant increase in the mechanical strength of objects created through direct ink writing as expressed by the higher maximum stress. Additionally, the higher slope of the exemplary curve for the dual cross-linked specimen shown in Figure 6D indicates a higher tensile modulus and, therefore, a less elastic sample. In conclusion, these results illustrate how postcuring with bivalent ions can be applied to reinforce objects that are printable with high shape fidelity due to intermediate photochemical cross-linking, as described in previous sections. Overall, the two cross-linking mechanisms possible in these systems mutually support each other. Whereas covalent cross-linking leads to high shape fidelities during printing, ionic cross-

linking can introduce additional strength into the final printed structures.

Cytocompatibility Studies. Finally, cytotoxicity investigations were conducted to investigate these novel materials' potential in biomedical applications. The cell viability of primary human umbilical vein endothelial cells (HUVECs) and immortalized human embryonic kidney cells (HEK293 cell line) was studied by performing a cell viability assay (PrestoBlue). It is well-known that the natural polysaccharides NFC and Alg are biocompatible materials that support cell viability in vivo.^{41–43} Furthermore, various in vitro studies with poly(vinylphosphonates) confirmed that these synthetic polymers have no adverse effects on the cell viability of different cell types.^{35,36,38} In the cytotoxicity tests, we studied five different sample compositions to potentially identify compounds in the inks that have harmful effects on the cells. The specimens for cytotoxicity testing were printed according to the model presented in Table S1 and Ca²⁺-cross-linked in 5 mM CaCl₂-containing 150 mM NaCl solution before the experiments. The five scaffolds for the PrestoBlue assay consisted of the regular poly(vinylphosphonate)-reinforced ink, an ink without 1,6-hexanedithiol, an ink without the synthetic polymer, an NFC/Alg mixture with only lithium phenyl(2,4,6-trimethylbenzoyl)-phosphinate (LAP) photoinitiator, and, finally, one formulation only containing NFC and Alg. The results presented in Figure 7A revealed a cell viability of HUVECs of 74.0 ± 3.51% relative to the control (equally cultured cells but without extracts of the inks), indicating a slight reduction in cell viability. Considering the threshold value of 70% given by EN ISO 10993–5, these materials could be declared nontoxic. Comparing the P(DEVP-*stat*-DAIVP)-reinforced inks (orange) to the second sample category (green) in Figure 7A, not containing the cross-linker and exhibiting high cell viabilities, the cytotoxic effect of 1,6-hexanedithiol, which is applied in excess in the polymer-reinforced inks, becomes evident. The lowest relative viability of HUVECs was found for the third formulation lacking the P(DEVP-*stat*-DAIVP) copolymers. In the absence of the poly(vinylphosphonates) and consequently, in the presence of significant amounts of unreacted 1,6-hexanedithiol, only 22.6 ± 13.2% relative cell viability was found. This demonstrates a positive effect of these polymers on the cytocompatibility (most likely due to a reduction of the free cross-linker by reaction with P(DEVP-*stat*-DAIVP)) as the same samples but with polymer (full ink, orange bars) performed better. Considering the NFC/Alg inks with and without LAP (yellow and green), both materials revealed no adverse effect on the cell viability relative to the control. This was expected as LAP is a standard cytocompatible photoinitiator and the biocompatibility of NFC and Alg is well-studied.^{41–43} Similar trends were observed for the second cell type. As with the HUVECs, the viabilities of HEK293 cells relative to the control assumed high values for all samples not containing 1,6-hexanedithiol (Figure 7B). The materials without P(DEVP-*stat*-DAIVP) performed the worst, and the cells in contact with the specimen printed with the standard polymer-reinforced ink (orange) displayed viabilities of 63.3 ± 3.95%. To sum up, the P(DEVP-*stat*-DAIVP)-reinforced inks exhibited slight decreases in the relative cell viability of both cell types, likely attributed to cytotoxic effects of the cross-linker. Nevertheless, the standard ink composition presented in this study contains an excess of the cross-linker concerning the cross-linkable groups to ensure quantitative cross-linking, which could be reduced. Additionally, purification of the cross-linked materials is possible, as reported previously,³⁶

highlighting the potential of P(DEVP-*stat*-DAIVP)-reinforced NFC/Alg inks for biomedical applications given their high shape fidelity and tunable material properties. Further, by applying water-insoluble 1,6-hexanedithiol as a cross-linker, we demonstrated that emulsion-based printing inks are applicable in DIW, which broadens the scope of potential, nontoxic hydrophobic dithiol cross-linkers.

CONCLUSION

To sum up, we introduced a novel approach applying poly(vinylphosphonate)-based hydrogels to reinforce well-established NFC/Alg inks for DIW, giving access to high shape fidelities and complex structures through intermediate photochemical cross-linking applying thiol–ene click chemistry. This combination of advanced material design, controlled polymer synthesis via REM-GTP, and dual cross-linking offers a versatile and scalable method to fabricate sophisticated structures with high fidelity and tunable properties in DIW. The optimized ink with an NFC (3 wt % suspension)/P(DEVP-*stat*-DAIVP)/Alg ratio of 10/1/0.3 was applied to print sophisticated structures like a 30-layered infill tube with uniform pore size and excellent resolution, a hollow tube consisting of 89 layers, and even overhanging objects with 30° incline. Furthermore, specimens were printed with three different polymer-containing inks and compared to a control without P(DEVP-*stat*-DAIVP) regarding the water uptake and mechanical properties. Here, an evident structure–property relationship was observable between the covalent cross-linking degree and the water absorption. The lower water absorption values in 5 mM CaCl₂-containing 150 mM NaCl solution were attributed to the additional ionic cross-links. Compared to the control, the polymer-reinforced prints exhibited significantly lower swelling values in the CaCl₂ solution, demonstrating the high swelling shape fidelity of the prints, which is crucial in all 3D printing applications. In the stress–strain measurements, a clear correlation between the tensile modulus and the number of cross-links in polymer-reinforced specimens was observed. A comparison of the mechanical properties of covalently cross-linked NFC/Alg inks with the corresponding analogs stored in 5 mM CaCl₂ (aq) revealed the reinforcing effect of ionic cross-linking on the printed structures. In conclusion, both cross-linking mechanisms presented in this study mutually support each other. Whereas covalent cross-linking ensures a high shape fidelity upon printing and swelling shape retention, ionic cross-linking can reinforce the sophisticated structures obtained by the printing process with intermediate cross-linking. Cytocompatibility studies of pristine prints revealed slightly cytotoxic effects of the cross-linker. However, the moderate cell viabilities of both tested cell types relative to the control revealed a clear potential for optimization toward higher cytocompatibility to proceed toward biomedical applications of these precisely printable objects. The applicability of both hydrophilic and hydrophobic dithiols broadens the scope of potential cross-linkers to reduce purification efforts.

ASSOCIATED CONTENT

Supporting Information

The Supporting Information is available free of charge at <https://pubs.acs.org/doi/10.1021/acsapm.4c03517>.

Printing of overhanging objects with a 30° incline through layer-by-layer deposition with intermediate photochemical cross-linking (MP4)

Materials and methods; Experimental procedures; Polymer characterization; Printing models and parameters; Extrudability of different ink compositions; Rheological measurements; Light microscopic images of the inks; Stress–strain measurements (PDF)

AUTHOR INFORMATION

Corresponding Authors

Bernhard Rieger – WACKER-Chair of Macromolecular Chemistry, Department of Chemistry, TUM School of Natural Sciences, Technical University of Munich, 85748 Garching, Germany; orcid.org/0000-0002-0023-884X; Email: rieger@tum.de

Karin Stana Kleinschek – Institute for Chemistry and Technology of Biobased Systems (IBioSys), Graz University of Technology, 8010 Graz, Austria; orcid.org/0000-0002-9189-0242; Email: karin.stanakleinschek@tugraz.at

Authors

Anton S. Maier – WACKER-Chair of Macromolecular Chemistry, Department of Chemistry, TUM School of Natural Sciences, Technical University of Munich, 85748 Garching, Germany

Florian Lackner – Institute for Chemistry and Technology of Biobased Systems (IBioSys), Graz University of Technology, 8010 Graz, Austria

Julia Fink – COREMED – Centre of Regenerative and Precision Medicine, JOANNEUM RESEARCH Forschungsgesellschaft GmbH, 8010 Graz, Austria; Research Unit for Tissue Regeneration, Repair and Reconstruction, Division of Plastic, Aesthetic and Reconstructive Surgery, Department of Surgery, Medical University of Graz, 8036 Graz, Austria

Tobias Steindorfer – Institute for Chemistry and Technology of Biobased Systems (IBioSys), Graz University of Technology, 8010 Graz, Austria

Elisabeth Hofmann – Research Unit for Tissue Regeneration, Repair and Reconstruction, Division of Plastic, Aesthetic and Reconstructive Surgery, Department of Surgery, Medical University of Graz, 8036 Graz, Austria

Complete contact information is available at: <https://pubs.acs.org/10.1021/acscapm.4c03517>

Author Contributions

¹The manuscript was written through contributions of all authors. All authors have given approval to the final version of the manuscript. A.S.M. and F.L. contributed equally.

Funding

A.S.M. is grateful for the generous funding within a Kekulé fellowship from the Fonds der Chemischen Industrie.

Notes

The authors declare no competing financial interest.

ACKNOWLEDGMENTS

The authors want to acknowledge the help of Dr. Tamilselvan Mohan in creating the graphical abstract and Figure ¹ with Biorender.com. Support from the TUM Innovation Network project ARTEMIS is acknowledged.

ABBREVIATIONS

Alg, alginate; DAIVP, diallyl vinylphosphonate; DEVP, diethyl vinylphosphonate; DIW, direct ink writing; REM-GTP, rare earth metal-mediated group-transfer polymerization; NMR,

nuclear magnetic resonance; DMPA, 2,2-dimethoxy-2-phenylacetophenone; IE, initiator efficiency; Đ, polydispersity index; r.t., room temperature; LAP, lithium phenyl(2,4,6-trimethylbenzoyl)phosphinate; NFC, nanofibrillated cellulose; SEC-MALS, size-exclusion chromatography multiangle light scattering; UV, ultraviolet; HUVECs, human umbilical vein endothelial cells; HEK293, immortalized human embryonic kidney cells

REFERENCES

- (1) Fischbach, C.; Chen, R.; Matsumoto, T.; Schmelzle, T.; Brugge, J. S.; Poverini, P. J.; Mooney, D. J. Engineering tumors with 3D scaffolds. *Nat. Methods* **2007**, *4* (10), 855–860.
- (2) Janarthanan, G.; Kim, J. H.; Kim, I.; Lee, C.; Chung, E.-J.; Noh, I. Manufacturing of self-standing multi-layered 3D-bioprinted alginate-hyaluronate constructs by controlling the cross-linking mechanisms for tissue engineering applications. *Biofabrication* **2022**, *14* (3), 035013.
- (3) Saadi, M. A. S. R.; Maguire, A.; Pottackal, N. T.; Thakur, M. S. H.; Ikram, M. M.; Hart, A. J.; Ajayan, P. M.; Rahman, M. M. Direct Ink Writing: A 3D Printing Technology for Diverse Materials. *Adv. Mater.* **2022**, *34* (28), 2108855.
- (4) Yang, G.; Sun, Y.; Qin, L.; Li, M.; Ou, K.; Fang, J.; Fu, Q. Direct-ink-writing (DIW) 3D printing functional composite materials based on supra-molecular interaction. *Compos. Sci. Technol.* **2021**, *215*, 109013.
- (5) Mohan, T.; Maver, T.; Štiglic, A. D.; Stana-Kleinschek, K.; Kargl, R. 3D bioprinting of polysaccharides and their derivatives: From characterization to application. *Fundamental Biomaterials: Polymers* **2018**, 105–141.
- (6) Rasekh, M.; Ahmad, Z.; Day, R.; Wickam, A.; Edirisinghe, M. Direct Writing of Polycaprolactone Polymer for Potential Biomedical Engineering Applications. *Adv. Eng. Mater.* **2011**, *13* (9), B296–B305.
- (7) Geurds, L.; Lauko, J.; Rowan, A. E.; Amiralian, N. Tailored nanocellulose-grafted polymer brush applications. *J. Mater. Chem. A* **2021**, *9* (32), 17173–17188.
- (8) Rol, F.; Belgacem, M. N.; Gandini, A.; Bras, J. Recent advances in surface-modified cellulose nanofibrils. *Prog. Polym. Sci.* **2019**, *88*, 241–264.
- (9) Klemm, D.; Kramer, F.; Moritz, S.; Lindström, T.; Ankerfors, M.; Gray, D.; Dorris, A. Nanocelluloses: a new family of nature-based materials. *Angew. Chem., Int. Ed.* **2011**, *50* (24), 5438–5466.
- (10) Gao, M.; Li, J.; Bao, Z.; Hu, M.; Nian, R.; Feng, D.; An, D.; Li, X.; Xian, M.; Zhang, H. A natural in situ fabrication method of functional bacterial cellulose using a microorganism. *Nat. Commun.* **2019**, *10* (1), 437.
- (11) Li, T.; Chen, C.; Brozena, A. H.; Zhu, J. Y.; Xu, L.; Driemeier, C.; Dai, J.; Rojas, O. J.; Isogai, A.; Wägberg, L.; Hu, L. Developing fibrillated cellulose as a sustainable technological material. *Nature* **2021**, *590* (7844), 47–56.
- (12) Isogai, A. Development of completely dispersed cellulose nanofibers. *Proc. Jpn. Acad. Ser. B Phys. Biol. Sci.* **2018**, *94* (4), 161–179.
- (13) Apelgren, P.; Karabulut, E.; Amoroso, M.; Mantas, A.; Martínez Ávila, H.; Kölby, L.; Kondo, T.; Toriz, G.; Gatenholm, P. In Vivo Human Cartilage Formation in Three-Dimensional Bioprinted Constructs with a Novel Bacterial Nanocellulose Bioink. *ACS Biomater. Sci. Eng.* **2019**, *5* (5), 2482–2490.
- (14) Fourmann, O.; Hausmann, M. K.; Neels, A.; Schubert, M.; Nyström, G.; Zimmermann, T.; Siqueira, G. 3D printing of shape-morphing and antibacterial anisotropic nanocellulose hydrogels. *Carbohydr. Polym.* **2021**, *259*, 117716.
- (15) Gladman, A. S.; Matsumoto, E. A.; Nuzzo, R. G.; Mahadevan, L.; Lewis, J. A. Biomimetic 4D printing. *Nat. Mater.* **2016**, *15* (4), 413–418.
- (16) Siqueira, G.; Kokkinis, D.; Libanori, R.; Hausmann, M. K.; Gladman, A. S.; Neels, A.; Tingaut, P.; Zimmermann, T.; Lewis, J. A.; Studart, A. R. Cellulose Nanocrystal Inks for 3D Printing of Textured Cellular Architectures. *Adv. Funct. Mater.* **2017**, *27* (12), 1604619.

- (17) Deng, X.; Huang, B.; Wang, Q.; Wu, W.; Coates, P.; Sefat, F.; Lu, C.; Zhang, W.; Zhang, X. A Mussel-Inspired Antibacterial Hydrogel with High Cell Affinity, Toughness, Self-Healing, and Recycling Properties for Wound Healing. *ACS Sustain. Chem. Eng.* **2021**, *9* (8), 3070–3082.
- (18) Benselfelt, T.; Engström, J.; Wågberg, L. Supramolecular double networks of cellulose nanofibrils and algal polysaccharides with excellent wet mechanical properties. *Green Chem.* **2018**, *20* (11), 2558–2570.
- (19) Yue, Y.; Han, J.; Han, G.; French, A. D.; Qi, Y.; Wu, Q. Cellulose nanofibers reinforced sodium alginate-polyvinyl alcohol hydrogels: Core-shell structure formation and property characterization. *Carbohydr. Polym.* **2016**, *147*, 155–164.
- (20) Ji, D.; Park, J. M.; Oh, M. S.; Nguyen, T. L.; Shin, H.; Kim, J. S.; Kim, D.; Park, H. S.; Kim, J. Superstrong, superstiff, and conductive alginate hydrogels. *Nat. Commun.* **2022**, *13* (1), 3019.
- (21) Kuo, C. K.; Ma, P. X. Maintaining dimensions and mechanical properties of ionically crosslinked alginate hydrogel scaffolds in vitro. *J. Biomed. Mater. Res., Part A* **2008**, *84A* (4), 899–907.
- (22) Doderò, A.; Pianella, L.; Vicini, S.; Alloisio, M.; Ottonelli, M.; Castellano, M. Alginate-based hydrogels prepared via ionic gelation: An experimental design approach to predict the crosslinking degree. *Eur. Polym. J.* **2019**, *118*, 586–594.
- (23) Bordoni, M.; Karabulut, E.; Kuzmenko, V.; Fantini, V.; Pansarasa, O.; Cereda, C.; Gatenholm, P. 3D Printed Conductive Nanocellulose Scaffolds for the Differentiation of Human Neuroblastoma Cells. *Cells* **2020**, *9* (3), 682.
- (24) Lackner, F.; Knecht, I.; Novak, M.; Nagaraj, C.; Dobaj Štiglic, A.; Kargl, R.; Olschewski, A.; Stana Kleinschek, K.; Mohan, T. 3D-Printed Anisotropic Nanofiber Composites with Gradual Mechanical Properties. *Adv. Mater. Technol.* **2023**, *8* (10), 2201708.
- (25) Lackner, F.; Surina, P.; Fink, J.; Kotzbeck, P.; Kolb, D.; Stana, J.; Grab, M.; Hagl, C.; Tsilimparis, N.; Mohan, T.; Stana Kleinschek, K.; Kargl, R. 4-Axis 3D-Printed Tubular Biomaterials Imitating the Anisotropic Nanofiber Orientation of Porcine Aortae. *Adv. Healthc. Mater.* **2024**, *13* (2), No. e2302348.
- (26) Jovic, T. H.; Nicholson, T.; Arora, H.; Nelson, K.; Doak, S. H.; Whitaker, I. S. A comparative analysis of pulp-derived nanocelluloses for 3D bioprinting facial cartilages. *Carbohydr. Polym.* **2023**, *321*, 121261.
- (27) Lee, K. Y.; Mooney, D. J. Alginate: properties and biomedical applications. *Prog. Polym. Sci.* **2012**, *37* (1), 106–126.
- (28) Lin, Z.; Wu, M.; He, H.; Liang, Q.; Hu, C.; Zeng, Z.; Cheng, D.; Wang, G.; Chen, D.; Pan, H.; Ruan, C. 3D Printing of Mechanically Stable Calcium-Free Alginate-Based Scaffolds with Tunable Surface Charge to Enable Cell Adhesion and Facile Biofunctionalization. *Adv. Funct. Mater.* **2019**, *29* (9), 1808439.
- (29) Cao, L.; Huang, J.; Chen, Y. Dual Cross-linked Epoxidized Natural Rubber Reinforced by Tunicate Cellulose Nanocrystals with Improved Strength and Extensibility. *ACS Sustainable Chem. Eng.* **2018**, *6* (11), 14802–14811.
- (30) Hafeez, S.; Decarli, M. C.; Aldana, A.; Ebrahimi, M.; Ruiter, F. A. A.; Duimel, H.; van Blitterswijk, C.; Pitet, L. M.; Moroni, L.; Baker, M. B. In Situ Covalent Reinforcement of a Benzene-1,3,5-Tricarboxamide Supramolecular Polymer Enables Biomimetic, Tough, and Fibrous Hydrogels and Bioinks. *Adv. Mater.* **2023**, *35* (35), No. e2301242.
- (31) Zhang, N.; Salzinger, S.; Soller, B. S.; Rieger, B. Rare earth metal-mediated group-transfer polymerization: from defined polymer microstructures to high-precision nano-scaled objects. *J. Am. Chem. Soc.* **2013**, *135* (24), 8810–8813.
- (32) Salzinger, S.; Soller, B. S.; Plikhta, A.; Seemann, U. B.; Herdtweck, E.; Rieger, B. Mechanistic studies on initiation and propagation of rare earth metal-mediated group transfer polymerization of vinylphosphonates. *J. Am. Chem. Soc.* **2013**, *135* (35), 13030–13040.
- (33) Soller, B. S.; Salzinger, S.; Jandl, C.; Pöthig, A.; Rieger, B. C-H Bond Activation by σ -Bond Metathesis as a Versatile Route toward Highly Efficient Initiators for the Catalytic Precision Polymerization of Polar Monomers. *Organometallics* **2015**, *34* (11), 2703–2706.
- (34) Halama, K.; Schaffer, A.; Rieger, B. Allyl group-containing polyvinylphosphonates as a flexible platform for the selective introduction of functional groups via polymer-analogous transformations. *RSC Adv.* **2021**, *11* (61), 38555–38564.
- (35) Halama, K.; Lin, M. T.-Y.; Schaffer, A.; Foith, M.; Adams, F.; Rieger, B. Cytocompatible Triblock Copolymers with Controlled Microstructure Enabling Orthogonally Functionalized Bio-polymer Conjugates. *Macromolecules* **2024**, *57* (4), 1438–1447.
- (36) Maier, A. S.; Mansi, S.; Halama, K.; Weingarten, P.; Mela, P.; Rieger, B. Cytocompatible Hydrogels with Tunable Mechanical Strength and Adjustable Swelling Properties through Photo-Cross-Linking of Poly(vinylphosphonates). *ACS Appl. Mater. Interfaces* **2024**, *16* (43), 58135–58147.
- (37) Schwab, A.; Levato, R.; D'Este, M.; Piluso, S.; Eglin, D.; Malda, J. Printability and Shape Fidelity of Bioinks in 3D Bioprinting. *Chem. Rev.* **2020**, *120* (19), 11028–11055.
- (38) Schwarzenböck, C.; Vagin, S. I.; Heinz, W. R.; Nelson, P. J.; Rieger, B. Studies on the Biocompatibility of Poly(diethyl vinylphosphonate) with a New Fluorescent Marker. *Macromol. Rapid Commun.* **2018**, *39* (15), 1800259.
- (39) Gao, F.; Xu, Z.; Liang, Q.; Li, H.; Peng, L.; Wu, M.; Zhao, X.; Cui, X.; Ruan, C.; Liu, W. Osteochondral Regeneration with 3D-Printed Biodegradable High-Strength Supramolecular Polymer Reinforced-Gelatin Hydrogel Scaffolds. *Adv. Sci.* **2019**, *6* (15), 1900867.
- (40) Jiang, P.; Yan, C.; Guo, Y.; Zhang, X.; Cai, M.; Jia, X.; Wang, X.; Zhou, F. Direct ink writing with high-strength and swelling-resistant biocompatible physically crosslinked hydrogels. *Biomater. Sci.* **2019**, *7* (5), 1805–1814.
- (41) Apelgren, P.; Amoroso, M.; Säljö, K.; Lindahl, A.; Brantsing, C.; Stridh Orrhult, L.; Markstedt, K.; Gatenholm, P.; Kölby, L. Long-term in vivo integrity and safety of 3D-bioprinted cartilaginous constructs. *J. Biomed. Mater. Res. B* **2021**, *109* (1), 126–136.
- (42) Park, M.; Lee, D.; Hyun, J. Nanocellulose-alginate hydrogel for cell encapsulation. *Carbohydr. Polym.* **2015**, *116*, 223–228.
- (43) Kjesbu, J. S.; Zaytseva-Zotova, D.; Sämfors, S.; Gatenholm, P.; Troedsson, C.; Thompson, E. M.; Strand, B. L. Alginate and tunicate nanocellulose composite microbeads - Preparation, characterization and cell encapsulation. *Carbohydr. Polym.* **2022**, *286*, 119284.

6.5 Author contributions

Anton Maier synthesized the catalyst and monomers, performed the polymerization experiments, and characterized all polymers (NMR, SEC-MALS, etc.). A. M. analyzed the extrudability of different ink compositions and performed the rheological measurements. Furthermore, A. M. prepared the inks for DIW and contributed to the printing and swelling experiments. A. M. conceptualized the project and initiated the collaborations with the coauthors. A. M. analyzed the measurement results and wrote the original draft.

7 Dynamic covalent networks

7.1 Bibliographic data

Title: “Modifications of Poly(vinylphosphonates) toward Dynamic Covalent Networks”

Status: Paper, Publication date: 26.02.2025

Journal: Macromolecules

Publisher: American Chemical Society (ACS)

DOI: 10.1021/acs.macromol.4c03063

Authors: Jana Knezevic, Anton S. Maier, Florian Lackner, Karin Stana Kleinschek, and Bernhard Rieger

7.2 Table of content graphic

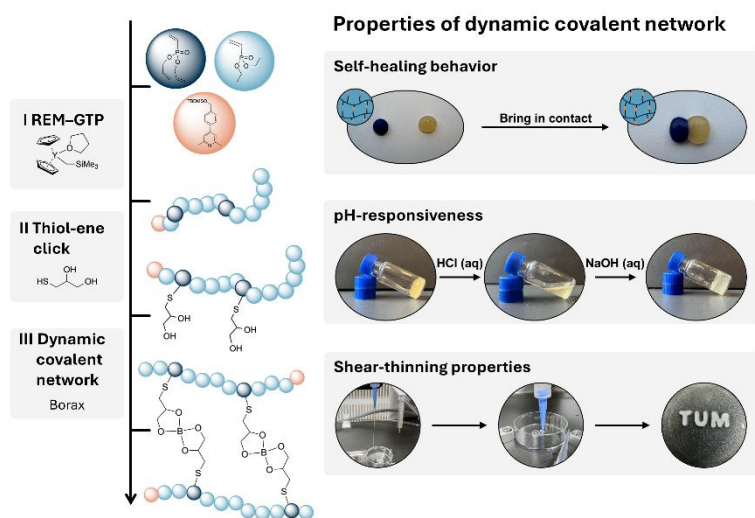


Figure 28: Table of content graphic for the manuscript entitled “Modifications of Poly(vinylphosphonates) Toward Dynamic Covalent Networks”.

J. Knezevic and A. S. Maier contributed equally to the manuscript. J. Knezevic and A. S. Maier prepared the original draft. A. S. Maier provided the original idea. J. Knezevic and A. S. Maier planned the experiments which J. Knezevic performed. F. Lackner performed the additive manufacturing experiments. J. Knezevic and A. S. Maier analyzed the data together with F. Lackner. All work was supervised by K. Stana Kleinschek and B. Rieger.

7.3 Content

This study introduces a synthetic approach toward dynamic covalent networks starting from statistical P(DEVP-*stat*-DAIVP) copolymers. Intending to leverage the dynamic covalent interactions between 1,2-diols and boronic acid derivatives, poly(vinylphosphonates) with variable ratios of allyl group-containing DAIVP units are synthesized applying REM-GTP, followed by the photochemical functionalization of the polymers with 1-thioglycerol via thiol-ene click chemistry. Detailed ^1H NMR and ^1H DOSY NMR analyses confirm the successful functionalization of the polymers, which are subsequently subjected to DCN formation experiments with different boronic acid derivatives. In this context, adding benzene-1,4-diboronic acid or sodium tetraborate (borax) solutions to the polymer solution allowed assembly toward DCNs. The resulting networks display tunable viscoelastic properties by varying the concentrations or the diol-functionalization degrees of the polymers, as confirmed by thorough characterization of the crossover frequencies, relaxation times, and equilibrium storage moduli in rheology. Furthermore, ramping strain sweeps display the self-healing behavior of the water-born systems with quantitative recovery of the material properties after the destruction of the hydrogels, complementing the observations regarding self-healing on a macroscopic level. The hydrogels exhibit pronounced pH-responsive behavior, enabling reversible decomposition and reformation of the DCNs from diol-functionalized poly(vinylphosphonates) and borax upon adding hydrochloric acid and sodium hydroxide solutions, alternating the pH value. Finally, rotational rheology and extrusion tests with a syringe confirm the shear-thinning behavior expected for this class of materials. Applying this feature of DCNs to extrusion-based additive manufacturing by direct ink writing enables the extrusion of continuous filaments, allowing the printing of simple objects. Summarizing, this study introduces a simplistic three-component system (polymer, borax, water) to yield attractive materials with tunable properties.

7.4 Manuscript

Macromolecules

Open Access

This article is licensed under [CC-BY 4.0](https://creativecommons.org/licenses/by/4.0/)pubs.acs.org/Macromolecules

Article

Modifications of Poly(vinylphosphonates) toward Dynamic Covalent Networks

Jana Knezevic,[#] Anton S. Maier,[#] Florian Lackner, Karin Stana Kleinschek, and Bernhard Rieger^{*}Cite This: *Macromolecules* 2025, 58, 2683–2693

Read Online

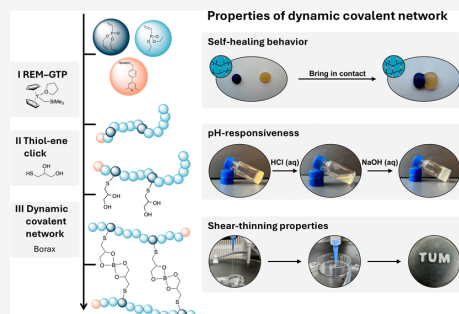
ACCESS |

Metrics & More

Article Recommendations

Supporting Information

ABSTRACT: Dynamic covalent networks (DCNs) are an attractive class of materials combining the beneficial properties of chemically and physically cross-linked networks. In this study, poly(vinylphosphonates) were functionalized toward precursors capable of forming DCNs with boronic acid derivatives. Statistical copolymers from diethyl vinylphosphonate (DEVVP) and diallyl vinylphosphonate (DAIVP) were obtained with high control over the polymer microstructure and narrow dispersities applying catalytic rare earth metal-mediated group-transfer polymerization (REM-GTP). Subsequent functionalization with 1-thioglycerol through photochemical thiol–ene click chemistry, confirmed via ¹H DOSY NMR spectroscopy, yielded water-soluble, diol-containing polymers that could undergo network formation with benzene-1,4-diboronic acid (DBA) in dimethyl sulfoxide and sodium tetraborate decahydrate (borax) in water. The aqueous system displayed tunable viscoelastic properties by varying the polymer functionalization degree and concentration, as evidenced by oscillatory rheology monitoring the plateau storage moduli G' and the crossover frequencies ω_c . The self-healing capability of the novel DCNs was demonstrated on the macroscopic level and rheologically by performing ramping strain sweeps between 1% and 500% deformation. Additionally, the poly(vinylphosphonate)-based hydrogels exhibited pronounced pH-responsive behavior, allowing network formation and dissolution upon alternations of the pH value. Finally, the shear-thinning behavior of the DCNs was confirmed via rotational rheology. The extrudability of this type of hydrogel allowed for initial additive manufacturing experiments applying extrusion-based direct ink writing to yield simple printed objects.



INTRODUCTION

Hydrogels are hydrophilic, three-dimensional polymer networks that can absorb and retain significant amounts of water without dissolving due to the cross-links present in these structures.^{1,2} These materials are typically formed through covalent junctions (chemical cross-linking)^{3,4} and/or supramolecular interactions, e.g., hydrogen bonds, ionic interactions, or host–guest chemistry (physical cross-linking) between the polymer chains.^{5–7} An elegant approach toward novel materials that combine beneficial properties of chemically and physically cross-linked hydrogels involves utilizing dynamic covalent networks (DCNs).

DCNs combine the strength of covalent cross-links with the reversibility of noncovalent interactions.⁸ Hydrogels formed via dynamic covalent chemistries exhibit an attractive set of material properties, such as shear-thinning behavior allowing injection and extrusion, self-healing through reversible covalent bond formation, and the possibility of facile processing via molding.^{9–12} Furthermore, the ability of DCNs to form and decay reversibly in response to changes in environmental conditions, e.g., temperature, pH value, or the presence of specific chemical motifs, along with the injectability of these materials, are reasons for their application as drug delivery systems.^{13–15} For dynamic covalent interactions, different

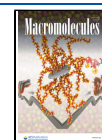
chemistries were reported. These include reversible Diels–Alder reactions,^{16,17} Schiff base reactions,¹⁸ transesterifications,^{19,20} disulfide bond formation,^{21,22} and dynamic phenylboronic ester complexation.^{9,23,24} DCNs based on phenylboronic ester complexation are formed through reactions of boronic acids with 1,2- and 1,3-diols, resulting in stable, cyclic five- or six-membered rings.²⁵ The condensation reaction proceeds at high rates without the addition of a catalyst, and the reaction rates depend on the types of boronic acid and diol substrates, leading to product formation under thermodynamic control.^{9,26–28} This binding specificity in the presence of different substrates allows the application of boronic ester DCNs as probes, e.g., for sugar sensing.²⁹ The highly dynamic character of boronic acid–diol networks further enables processing via extrusion-based additive manufacturing and is

Received: December 9, 2024

Revised: February 13, 2025

Accepted: February 14, 2025

Published: February 26, 2025



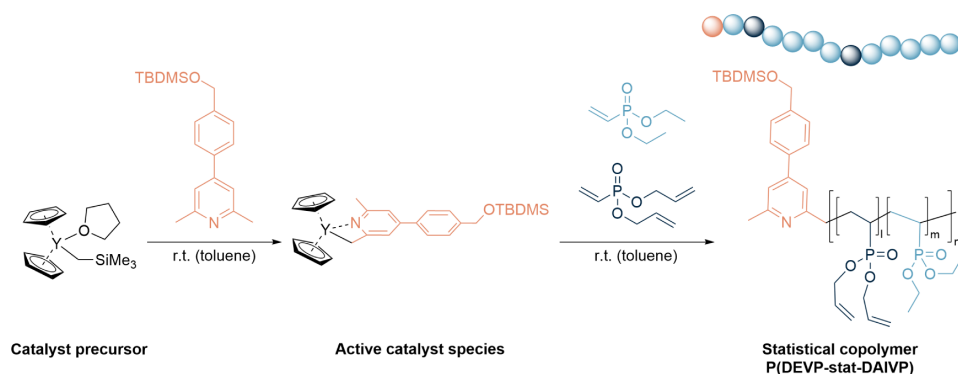


Figure 1. Statistical copolymerization of DEVP and DAIVP via REM-GTP applying an in situ generated yttrium catalyst.

the base for stimuli-responsive, injectable, biocompatible hydrogels for drug delivery.^{13,30,31}

In contrast to these highly flexible platforms, our group recently reported the synthesis of chemically cross-linked hydrogels obtained by photochemical cross-linking of poly(vinylphosphonates). The corresponding materials exhibited precisely tunable water uptakes, mechanical properties, and high cytocompatibility.³² In this context, the starting materials for cross-linking were obtained via rare earth metal-mediated group-transfer polymerization (REM-GTP), enabling the statistical copolymerization of the monomers diallyl vinylphosphonate (DAIVP) and diethyl vinylphosphonate (DEVP). By proceeding via a repeated 1,4-conjugated addition, the mechanism of REM-GTP allows precise control over the polymer microstructure (monomer ratio and sequence) while preserving narrow dispersities for polymerizations of Michael-type monomers.^{33–35} After polymerization, DAIVP-containing poly(vinylphosphonates) obtained via REM-GTP can be successfully converted with various substrates applying photochemically induced thiol–ene click chemistry to introduce different functionalities into the polymer side chains.^{36–38} A similar approach could be the initial step for combining the beneficial properties of poly(vinylphosphonates) obtained by high-precision polymerization via REM-GTP (excellent control over molecular weight and copolymer microstructure, narrow dispersities, cytocompatibility) with the advantageous features of DCNs, like self-healing and shear-thinning behavior.^{9,11,32,38}

To target the synthesis of DCNs based on poly(vinylphosphonates), statistical copolymers from DEVP and DAIVP, denoted as P(DEVP-*stat*-DAIVP), were synthesized via REM-GTP. Subsequently, different P(DEVP-*stat*-DAIVP) polymers were functionalized quantitatively with 1-thioglycerol by photoinitiated thiol–ene click chemistry, and different boronic acid derivative-containing solutions were added to obtain DCNs based on poly(vinylphosphonates). This approach leverages the precise tunability of the polymer microstructure provided by REM-GTP, enabling advanced material design with tailored properties of cross-linked materials. Further, the application of poly(vinylphosphonates) for DCN synthesis bears great potential in biomedical contexts due to the good water solubility and high cytocompatibility of this polymer class.^{32,38} The DCNs were subsequently characterized in detail via ¹H NMR spectroscopy, oscillatory rheology, and self-healing experiments. Finally, initial direct ink writing (DIW) tests were performed, revealing the potential for applying these novel DCNs as inks for additive manufacturing.

RESULTS AND DISCUSSION

Polymer Synthesis and Functionalization. The synthesis of statistical copolymers from DEVP and DAIVP was performed according to previously reported procedures.³² The calculated amount of precursor catalyst Cp₂YCH₂TMS(thf) was dissolved in dry toluene, and the addition of 4-(4-(((*tert*-butyldimethylsilyloxy)methyl)phenyl)-2,6-dimethylpyridine led to the in situ generation of the active catalyst species as illustrated in Figure 1. In this context, quantitative CH-bond activation of the initiator was confirmed via ¹H NMR spectroscopy by the aliquot method (0.1 mL of reaction mixture +0.4 mL of dry C₆D₆) by detecting the absence of the characteristic CH₂–group signal of the precursor catalyst (doublet, $\delta = -0.66$ ppm). Subsequently, the calculated mixture of DEVP and DAIVP was quickly added to the catalyst solution, and the reaction mixture was stirred at room temperature until complete monomer conversion was found via ³¹P NMR spectroscopy by withdrawing another aliquot in CD₃OD. The addition of 0.5 mL of MeOH, followed by precipitation in pentane, centrifugation, and lyophilization in 1,4-dioxane, yielded the purified P(DEVP-*stat*-DAIVP) copolymers. The corresponding polymerization results are summarized in Table 1.

As illustrated by the results given in Table 1, polymers with similar molecular weights but varying DEVP/DAIVP ratios were synthesized in the polymerization experiments. The copolymers' molecular weights were obtained via ¹H NMR spectroscopy using the distinct signals of the –OTBDMDS group of the initiator incorporated in each chain as a reference and range between 30 and 39 kg/mol. In this study, the desired molecular weights were rather low for the copolymers to exhibit high solubilities, which facilitated functionalization in the next step but also helped with the solubilization of the functionalized P(DEVP-*stat*-DAIVP) polymers to test DCN formation. Additionally, the targeted amounts of the allyl group-containing DAIVP units accessible for functionalization via thiol–ene click chemistry in copolymers 1–3 slightly exceeded their theoretical values, still controlling the monomer ratio upon polymer synthesis allowed adjusting the corresponding ratio in the copolymers. Besides the good control over molecular weights and monomer ratio given these results, the low dispersities below 1.17 presented in Table 1 demonstrate the high precision of REM-GTP. To confirm successful copolymerization, polymers 1–3 were characterized via ¹H-, ³¹P-, and ¹H DOSY NMR spectroscopy (Figures S1–

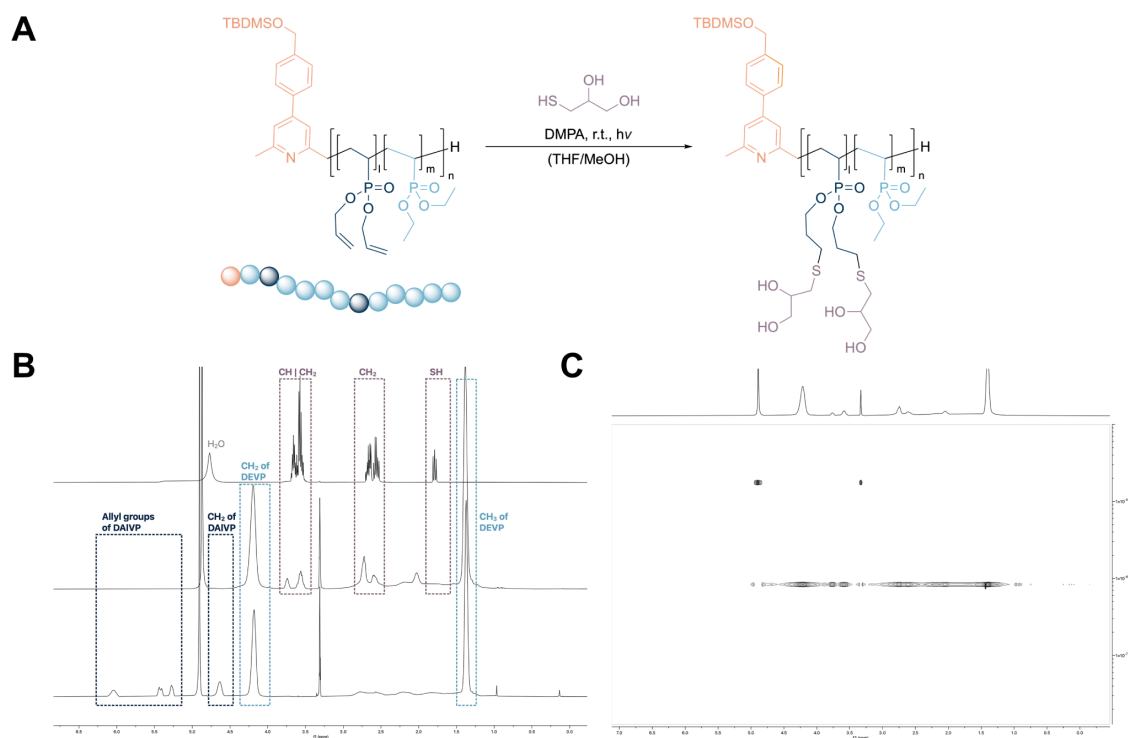


Figure 2. Functionalization of P(DEVP-*stat*-DAIVP) with 1-thioglycerol via photochemical thiol–ene click reaction (A), corresponding ^1H NMR spectra of 1-thioglycerol (top), P(DEVP-*stat*-DAIVP) (bottom), and functionalized copolymer (middle) (B), and ^1H DOSY NMR spectrum of purified, functionalized copolymer (C).

Table 1. Results for the Polymerization of DEVP and DAIVP via REM-GTP with the CH-Bond Activated Species of $\text{Cp}_2\text{YCH}_2\text{TMS}(\text{thf})^{\text{a}}$

Polymer	DEVP/DAIVP/Cat. ^b	Targeted DAIVP content [%]	X [%] ^c	DAIVP content [%] ^d	$M_{n,\text{NMR}}^e$ [kg mol ⁻¹]	IE ^f	Đ^g	Polymer designation after functionalization
1	92/11/1	10	>99%	13.3	30	59	1.17	4
2	86/15/1	15	>99%	17.5	39	45	1.13	5
3	81/21/1	20	>99%	24.6	33	53	1.09	6

^aAll polymerizations were performed at room temperature in toluene, with a monomer feed of 100 repetition units and varying the DEVP/DAIVP/Catalyst ratio. Quantitative conversions were determined via ^{31}P NMR spectroscopy in CD_3OD . ^bReactant ratio based on the monomer and catalyst weights in Table S2. ^cConversion determined via ^{31}P NMR spectroscopy in CD_3OD . ^dDetermined via ^1H NMR spectroscopy by comparison of the CH_2 signals of DEVP (4.18 ppm, $m = 1/4$) and DAIVP (4.63 ppm, $n = 1/4$). ^eCalculated via ^1H NMR spectroscopy by comparison of the $-\text{OTBDMS}$ signals of the initiator at 0.14 ppm ($I = 6\text{H}$) and the CH_2 signals of DEVP (4.18 ppm, $m = 1/4$) and DAIVP (4.63 ppm, $n = 1/4$). ^fInitiator efficiency (IE): $\text{IE} = M_{n,\text{calc}}/M_{n,\text{NMR}}$ with $M_{n,\text{NMR}} = 327.54 \text{ g/mol} + m \times 164.14 \text{ g/mol} + n \times 188.16 \text{ g/mol}$. ^gDispersity determined via size-exclusion chromatography multiangle light scattering (SEC-MALS) in $\text{THF:H}_2\text{O}$ (1:1) with 340 mg/L 2,6-di-*tert*-butyl-4-methylphenol (BHT) and 9 g/L tetra-*n*-butylammonium bromide (TBAB).

S3). The refractive index detector signal of SEC-MALS for each copolymer is shown in Figure S4. Furthermore, the copolymers exhibited the expected thermal behavior with a thermal decomposition onset of 306 °C and the absence of a melting point, as reported in previous studies, which is shown in Figures S5 and S6.³²

In our approach toward DCNs, we wanted to utilize the specific interaction between 1,2-diols and boronic acids, which are known to undergo reversible, uncatalyzed reactions forming 5-membered boronic esters.^{9,25–27} A promising step for realizing this type of interaction with poly(vinylphosphonates) involves the application of thiol–ene click chemistry. The functionalization of P(DEVP-*stat*-DAIVP)

with different thiol group-containing substrates was subject to numerous previous studies.^{32,36–38} Commercially available 1-thioglycerol was selected as a simple representative of 1,2-diols for the photochemical functionalization of copolymers 1–3 (Table 1) as illustrated in Figure 2A (for experimental details, see the Supporting Information).

The functionalized copolymers 4–6 were purified by dialysis against water (MWCO = 8 kDa). ^1H NMR spectroscopic analysis of the diol-functionalized compounds revealed the absence of the allyl group signals of DAIVP, as shown in Figure 2B. Therefore, full conversion of double bonds in the thiol–ene click reaction was assumed. Consequently, polymers 4–6 exhibited the same DEVP contents as their unfunctionalized

counterparts 1–3, and all DAIVP units were transformed into diol-containing moieties. These binding sites for boronic acids were statistically distributed throughout the polymers, as the microstructure of the unfunctionalized P(DEVP-*stat*-DAIVP) polymers 1–3 was expected to persist after the click reaction. Figure 2B additionally shows the successful incorporation of the 1-thioglycerol into P(DEVP-*stat*-DAIVP) by the corresponding aliphatic signals of the diol. Additional ^1H DOSY NMR spectra of the functionalized copolymers, as demonstrated by the exemplary spectrum in Figure 2C, were measured to confirm the absence of polymer degradation through the photochemical reaction. As only one diffusion coefficient could be detected, quantitative functionalization was assumed without any effects on the degree of polymerization. Additional thermal analysis of these functionalized P(DEVP-*stat*-DAIVP) copolymers via TGA and DSC revealed a similar decomposition behavior compared to unfunctionalized copolymers and the preservation of the amorphous character of the polymers (Figures S7 and S8).

Synthesis of Dynamic Covalent Networks. To induce DCN formation in solutions of functionalized poly(vinylphosphonates) 4–6, we searched for molecular, bifunctional boronic acid (derivatives), which allow the reversible cross-linking of polymer chains via boronic ester formation. Initially, benzene-1,4-diboronic acid (DBA) was selected to screen for DCN synthesis following numerous reports in the literature.^{39–41} Accordingly, the diol-functionalized P(DEVP-*stat*-DAIVP) copolymers were dissolved in dimethyl sulfoxide (DMSO), resulting in a homogeneous polymer solution. Considering the amounts of functionalized DAIVP units in the polymers (Table 1), the number of diol groups in the solution was calculated. Subsequently, a second solution of DBA in DMSO with the same concentration as the polymer solution, containing an equimolar amount of boronic acid units to the diols (ensuring a 1:1 ratio of 1,2-diol to boronic acid), was added. Table 2 displays some selected results of our experiments on DCN synthesis, including information on the functionalized P(DEVP-*stat*-DAIVP) with the designation from Table 1 that was utilized, the solvent, the cross-linker, and the polymer concentration expressed as a weight percentage. The additional columns reflect the corresponding diol concentration in the solution calculated from the functionalization degree, the polymer weight percentage in the solution, the density of the solvent, and whether a DCN was formed based on the tube inversion test.

Following the addition of DBA to copolymers 4–6, immediate sol–gel transition ($t < 1\text{ s}$) was observed, confirmed by the tube inversion test, as shown in Figure 3. Furthermore, ^1H NMR spectroscopic experiments confirmed the synthesis of DCNs in DMSO with DBA as a cross-linker by the incorporation of aromatic signals into the DCN spectrum and the disappearance of OH-group signals, as shown in Figure S9. For the combination of diol-functionalized poly(vinylphosphonates) and DBA in DMSO, successful DCN formation for different polymer concentrations and varying functionalization degrees was observed, as demonstrated by entries 1–4 in Table 2. However, it must be noted that copolymer 4, exhibiting the lowest functionalization degree due to the low number of DAIVP units in the initial copolymer 1, required higher weight percentages of polymer to achieve enough OH-groups in solution for sol–gel transition. Comparing entries 1 and 3, it becomes evident that by switching to a higher functionalization degree using polymer 5,

DCN synthesis succeeded due to an increased concentration of 1,2-diol units in the solution despite the same weight percentage of polymer. Entry 4 displays the successful DCN formation with polymer 6 and equimolar amounts of DBA at high weight percentages of 30 wt % polymer, which was selected as the upper limit in this study due to solubility issues of the polymers above this concentration. As DCNs are often applied in a biomedical context, e.g., as injectable drug delivery systems or biosensors,^{13,15,22} overcoming the drawback of using organic solvents such as DMSO and switching to aqueous systems is a first step toward developing novel DCNs for such applications. However, the use of DBA as a cross-linker is limited to organic solvents due to the poor water solubility of the compound. An alternative cross-linker often reported for the synthesis of hydrogels exhibiting dynamic covalent properties is sodium tetraborate (borax).^{42,43} In the literature, borax is broadly applied to develop biocompatible materials formed by the complexation between the borate and hydroxyl groups of a polymer. The resulting materials act as bone replacements, sensing platforms, or scaffolds for cell growth.^{44–46} Therefore, applying borax for the aqueous synthesis of DCNs is a promising step toward hydrogels that can be employed in biological settings. Despite exhibiting poor water solubility at room temperature, borax decahydrate dissolved well in water when heated to 80 °C rapidly without immediate recrystallization going back to room temperature. For borax, the approach toward DCN synthesis slightly differed from the previous procedure with DBA in DMSO. Due to solubility issues of borax at very high concentrations, a 1.20 M stock solution was prepared. Again, equimolar amounts of borax regarding the 1,2-diol units in the polymer solution were applied. However, the necessary volume of stock solution was added instead of dissolving the borax at the same solution concentration as the polymer, causing minor differences in the total water volumes applied for hydrogel synthesis. This allowed us to test the DCN synthesis as described above, but by dissolving the polymers and the cross-linker in water. The experiments with polymers 4–6 and borax as a cross-linker under the conditions presented in Table 2 successfully yielded hydrogels, which was additionally confirmed by the tube inversion method, as depicted in Figure 3. Considering entries 5–7 in Table 2, successful DCN synthesis with this approach required higher weight percentages of polymer in solution to guarantee sufficient amounts of diols for borax complexation. As for the organic system, switching to higher polymer functionalization degrees for DCN synthesis allowed the application of lower polymer concentrations, observable in entries 8–12. A second advantage of the aqueous system over its organic counterpart, besides applying a more biocompatible matrix (solvent and cross-linker), was the higher dimensional stability of these DCNs. Whereas the DMSO system exhibited pronounced flow and shape deformation, the hydrogels formed stable structures, as shown in Figure S10.

Thermogravimetric analysis of hydrogels formed by combining functionalized poly(vinylphosphonates) and borax displayed dehydration of the materials, followed by the transitions already observed for the polymers (Figure S11). In the DSC measurements of these materials, no temperature response could be detected, as the only observable transition was the melting point of water, which is illustrated in Figure S12. Remeasurement of the DSC curves after water removal did not reveal any additional transition, indicating the preservation of the amorphous character of the polymers

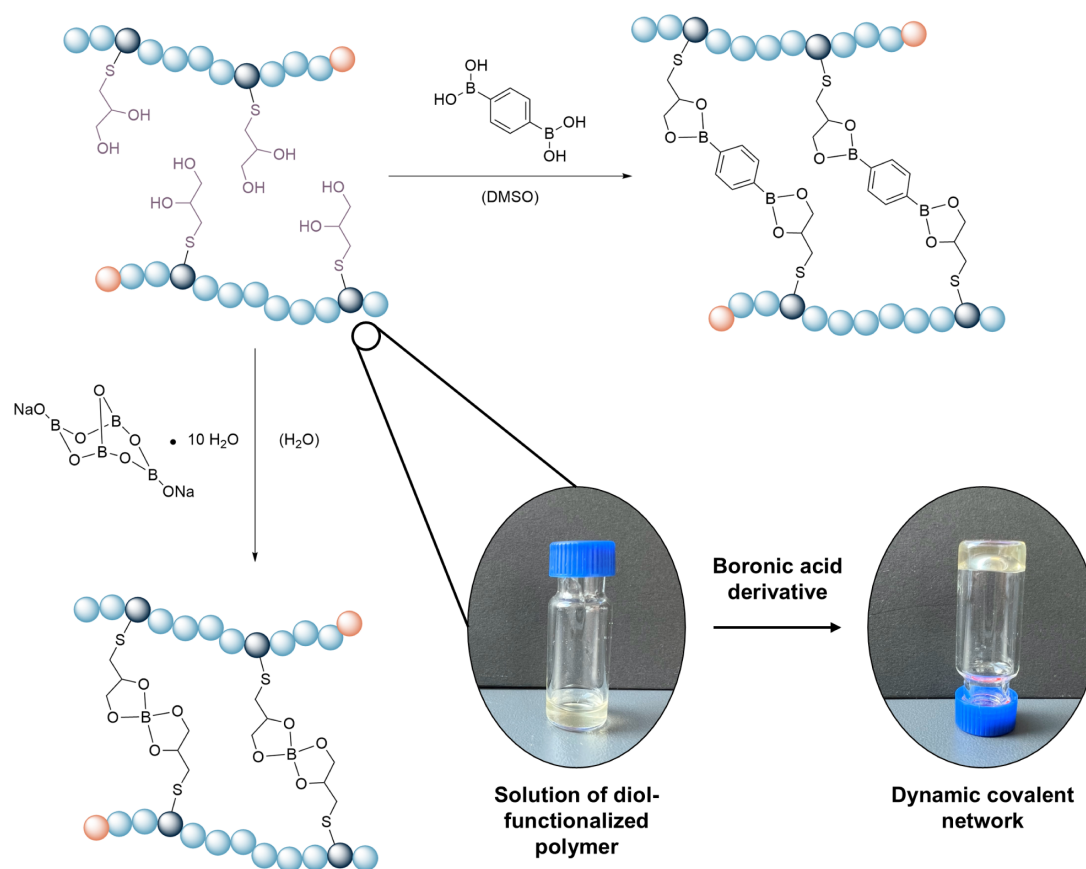


Figure 3. Synthesis of DCNs from diol-functionalized P(DEVP-*stat*-DAIVP) polymers by adding benzene-1,4-diboric acid (DBA) or sodium tetraborate. The tube inversion method confirmed the successful formation of DCNs.

(Figure S13). Due to the drawbacks of organic solvents, we decided to only pursue the further characterization of the aqueous system for the further course of this study. For the DCNs formed upon borax complexation, we quantified the sol and gel fraction of the hydrogels with different diol-functionalization degrees and weight percentages of polymer in the solution, revealing water contents in the networks between 69% and 84%, as particularized in Table S3.

Viscoelastic Properties of Dynamic Covalent Networks. Oscillatory shear rheology was applied to characterize the viscoelastic properties of the aqueous DCNs based on the interaction of diol-functionalized poly(vinylphosphonates) and borax. Frequency sweeps between 0.1 and 100 rad/s were performed on fully gelled samples to evaluate the viscoelastic properties. All hydrogels in this study exhibited frequency-dependent viscoelastic behavior, displaying viscous behavior at low frequencies, followed by a crossover of the storage modulus G' and the loss modulus G'' , resulting in a high-frequency plateau indicating elastic sample behavior. The plateau values for G' describe the energy stored within the networks.^{10,13} To evaluate the mechanical properties of different hydrogels, the plateau storage moduli at 100 rad/s were compared among all samples capable of forming hydrogels since all G' values were well within the high-frequency plateau at this frequency. A second measure of the

mechanical properties of DCNs accessible via oscillatory rheology is the crossover frequency ω_c . The crossover frequency in oscillatory rheology is an essential parameter for characterizing the viscoelastic behavior of DCNs. It is defined as the frequency at which the storage modulus equals the loss modulus, indicating a transition between predominantly elastic and viscous behavior.^{47,48} The crossover frequency inversely correlates with the material's relaxation time, describing the time scale over which the network reconfigures or dissipates stress due to the exchange of dynamic covalent bonds. In DCNs, ω_c is affected by the bond exchange dynamics. Thus, a faster bond exchange leads to a higher ω_c , while slower dynamics result in a lower ω_c .⁴⁹ Therefore, lower values of the crossover frequency are often related to a more solid-like behavior over a broader frequency range. The crossover frequency for DCNs is influenced by the number of cross-links in the material, as the cross-linking degree affects the network structure and the corresponding relaxation time. Consequently, more densely cross-linked networks exhibit slower relaxation dynamics, correlating with longer relaxation times and lower crossover frequencies.⁵⁰ In our experiments, we compared three different functionalization degrees at a fixed weight percentage of polymer in solution and four different concentrations of diol-functionalized polymer in solution for one functionalization degree. Equimolar ratios of diol units to

Table 2. Selected Results of Solvents, Crosslinkers, and Concentrations Tested for the Formation of DCNs from 1-Thioglycerol-Functionalized Poly(vinylphosphonates)

Entry	Polymer	Solvent	Cross-linker	Polymer concentration [wt %]	Diol concentration in solution [mol/L]	DCN formation?
1	4	DMSO	DBA	12.5	0.21	No
2	4	DMSO	DBA	20.0	0.37	Yes
3	5	DMSO	DBA	12.5	0.26	Yes
4	6	DMSO	DBA	30.0	1.02	Yes
5	4	Water	Borax	12.5	0.19	No
6	4	Water	Borax	20.0	0.34	No
7	4	Water	Borax	25.0	0.45	Yes
8	5	Water	Borax	12.5	0.24	Yes
9	5	Water	Borax	30.0	0.72	Yes
10	6	Water	Borax	12.5	0.31	Yes
11	6	Water	Borax	20.0	0.54	Yes
12	6	Water	Borax	30.0	0.93	Yes

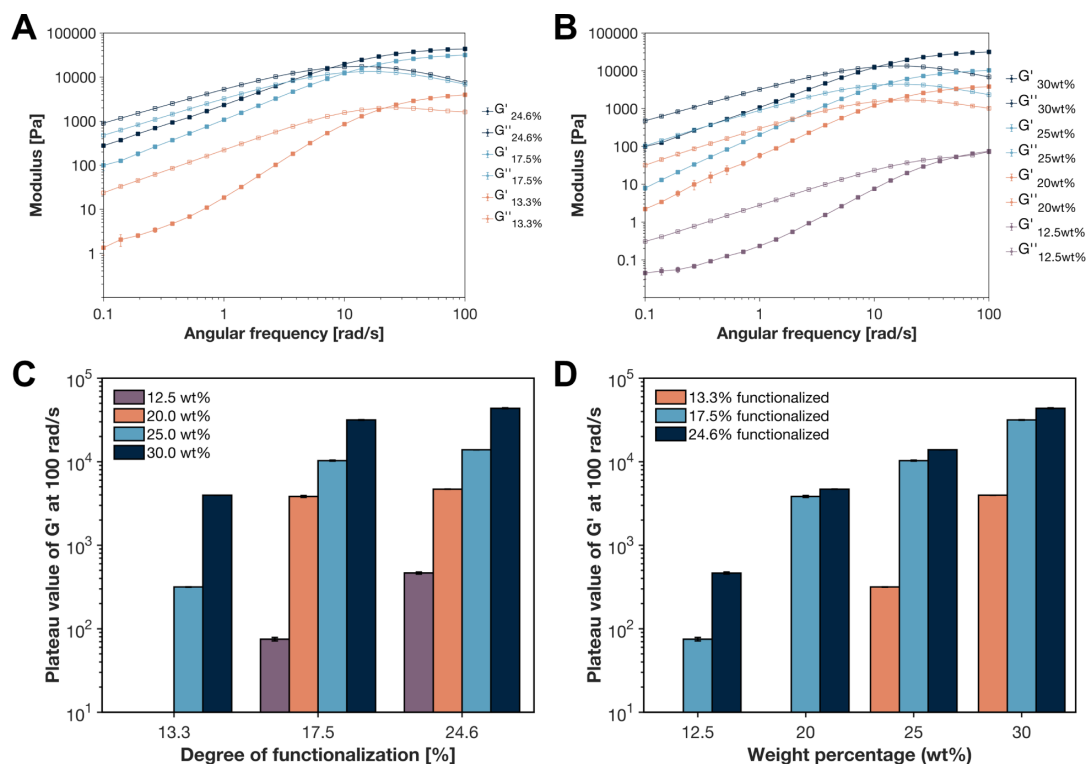


Figure 4. Comparison of the viscoelastic properties of DCNs formed from polymers with different functionalization degrees and concentrations in water. Oscillatory frequency sweeps between 0.1 and 100 rad/s at 1% strain for (A) polymers with different degrees of polymer functionalization with 1-thioglycerol at 30 wt % polymer concentration and (B) different weight percentages of a polymer with 17.5% 1-thioglycerol-functionalized units in solution. Comparison of the viscoelastic properties of DCNs formed from diol-functionalized poly(vinylphosphonates) by evaluation of the plateau values of the storage modulus at 100 rad/s for (C) different degrees of diol-functionalization of the polymer and (D) weight percentages of functionalized polymers in solution.

borax were applied in all cases to ensure comparable results. Figure 4A shows the frequency sweeps for DCNs formed from quantitatively 1-thioglycerol-functionalized polymers with increasing DAIVP-content at a fixed polymer weight percentage (30 wt %) in solution with the corresponding equimolar amounts of borax. Consequently, at a fixed polymer concentration, the increasing degree of functionalization results in a higher number of diol units available for cross-linking and, thus, a higher cross-linking degree. This is reflected in the

values of the plateau storage modulus as well as in the ω_c values. Whereas the polymer with a functionalization degree of 24.6% resulted in values of G' of 43.6 kPa and a crossover frequency of 7.20 rad/s, hinting toward a strong and stiff gel, a solution with the same weight percentage of a 13.3% functionalized polymer resulted in a hydrogel with G' of 3.97 kPa and ω_c of 19.5 rad/s as indicated by the results presented in Figure 4A. Complementing these results, stress-relaxation curves within the linear viscoelastic region of the networks

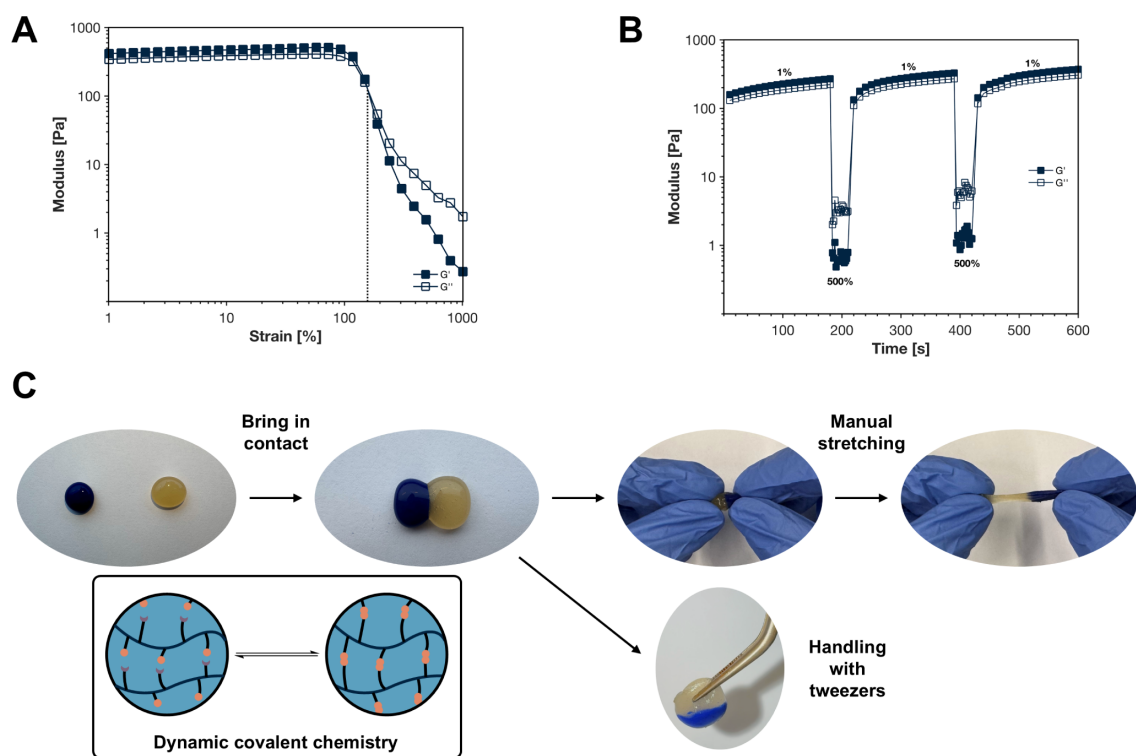


Figure 5. Amplitude sweep of poly(vinylphosphonate)-based DCNs at 10 rad/s (A), rheological self-healing experiments of poly(vinylphosphonate)-based DCNs formed in water at an angular frequency of 10 rad/s alternating between low ($\gamma = 1\%$) and high ($\gamma = 500\%$) shear forces (B), and images of the self-healing of two hydrogels (different colors for better visualization of the interface) with subsequent macroscopic sample handling (C).

were measured as provided in Figure S14. Comparing the time-dependent stress response of hydrogels with different cross-linking degrees formed from polymers 4–6 after applying a sudden deformation of $\gamma = 1\%$ yielded valuable insights into the network dynamics of poly(vinylphosphonate)-based DCNs. For all networks, the relaxation times τ were in the order of milliseconds to seconds, indicating a rapid bond exchange in these systems. Furthermore, a clear trend in the τ values was observed, aligning well with the findings on the viscoelastic properties presented above. Accordingly, the networks with the lowest cross-linking density exhibited the fastest relaxation ($\tau = 0.02$ s) with a sharp, exponential decay of the relaxation modulus, indicating few constraints on molecular motion and a low number of cross-links resisting stress dissipation. In contrast, the networks with the highest number of cross-links revealed the longest relaxation times ($\tau = 2.87$ s), corresponding to a slower dissipation of stress upon deformation due to increased material stiffness. Analogously, the measurements presented in Figure 4B show a similar trend. Fixing the degree of functionalization of P(DEVP-*stat*-DAIVP) by applying a polymer, in which the 17.5% DAIVP units are quantitatively functionalized with 1-thioglycerol, changes in the polymer concentrations applied in DCN synthesis affect the mechanical properties of the final materials. This is reflected in the results presented in Figure 4B. Applying a 30 wt % solution of functionalized P(DEVP-*stat*-DAIVP) and equimolar amounts of borax with respect to the diol units results in the formation of a hydrogel with an equilibrium storage modulus

at 100 rad/s of 31.6 kPa and ω_c of 10 rad/s. In contrast, a less concentrated 20 wt % solution, e.g., yields a weaker DCN with G' values of 3.83 kPa and a crossover frequency of 14.0 rad/s. Figure 4C,D shows the dependency of the plateau storage moduli at 100 rad/s on the degree of functionalization of the poly(vinylphosphonate) copolymers and the weight percentage of polymer in solution applied upon DCN synthesis. This overview of the data obtained from numerous frequency sweeps shown in Figures S15–S21 displays the tunability of mechanical properties of poly(vinylphosphonate)-based DCNs. Certain combinations of functionalization degree and concentration did not yield gel formation among the tested conditions, e.g., polymers with low functionalization degrees at low concentrations, likely due to an insufficient concentration of diol units for notable cross-linking. Polymers with a fixed concentration but increasing degree of functionalization, which is adjustable upon polymer synthesis via REM-GTP and the click reaction, displayed increasing elastic portions as illustrated by the blue series in Figure 4C. Highly functionalized polymers resulted in DCN formation for all tested concentrations with increasing G' at 100 rad/s with an increasing polymer weight percentage as indicated by the dark blue bars in Figure 4D. A similar tunability of the viscoelastic properties was demonstrated for the DCNs formed in DMSO with DBA as cross-linker (Figure S22).

Self-Healing Behavior and pH-Responsiveness. A well-known feature of DCNs is their capability to self-heal. First, an amplitude sweep was performed on a fully gelled

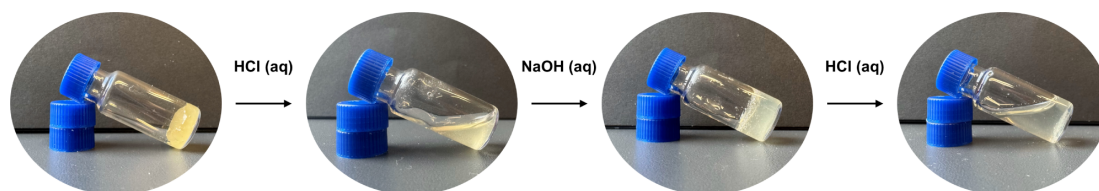


Figure 6. pH-induced decomposition and reformation of poly(vinylphosphonate)-based boronic ester networks.

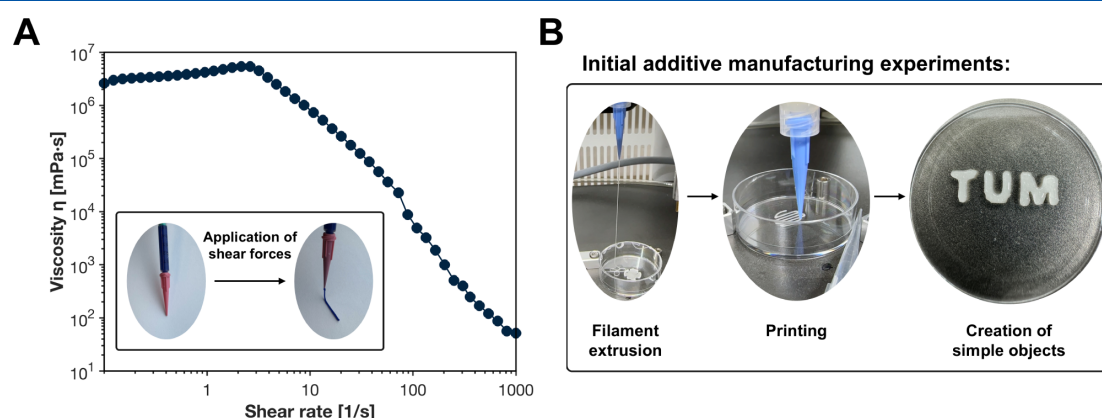


Figure 7. Viscosity curve of poly(vinylphosphonate)-based DCNs obtained via rotational rheology and extrusion of free-standing, continuous hydrogel filaments through a syringe (A) and initial extrusion-based additive manufacturing experiments of the novel hydrogel systems (B).

sample at a frequency of 10 rad/s to determine the strain values necessary for a structural breakdown of the sample. As illustrated by the measurement results in Figure 5A, the transition toward liquid-like behavior, indicated by the crossover of G' and G'' , followed by $G'' > G'$, occurs at deformations of 190%. Next, based on the results of Figure 5A, rheological self-healing experiments were conducted, in which 500% strain was applied to ensure the disruption of the gel network. The results of these experiments are shown in Figure 5B, in which self-healing was monitored over two cycles by conducting a ramping strain sweep applying deformations between 1% and 500%. In this context, G' and G'' assumed 265 and 218 Pa at low shear forces ($\gamma = 1\%$). Applying the high shear forces ($\gamma = 500\%$), these values immediately dropped to 0.72 and 3.33 Pa. Subsequent self-healing of the gel at low shear forces led to a quantitative recovery of the G' values within 10 s. A similar behavior could be repeated in a second cycle, again leading to a quantitative recovery of G' compared to its initial values, proving the recovery of material properties by self-healing. To evaluate the self-healing capability of these DCNs based on poly(vinylphosphonates) on a macroscopic level, two specimens of the same hydrogel were prepared, as shown in Figure 5C. One of the two specimens was dyed using blue watercolor to facilitate visualization of the interface between the samples after self-healing. As illustrated in Figure 5C, the two DCNs could fuse after bringing them in contact for less than 10 s at room temperature, allowing the formation of new boronic ester bonds at the interface. The self-healed samples could subsequently be handled with tweezers as they supported their own weight and displayed remarkable resistance when manually pulled apart. Performing ramping strain sweeps with the DCNs formed in DMSO, in turn, revealed a change in the viscoelastic properties after each cycle,

confirming the pronounced flow and shape deformation of the DMSO system, which was also observed in the corresponding macroscopic self-healing experiments (Figure S23).

Another feature of DCNs based on boronic acid complexation is the pH-responsive behavior of such materials, as the reversible boronic ester formation is strongly pH-dependent.^{43,51,52} Thus, the dissociation and reformation of poly(vinylphosphonate)-based DCNs introduced in this study was studied under different conditions. Matching reports in the literature,^{10,24,43} the addition of 1 M hydrochloric acid (HCl) solution led to a quick dissolution of the hydrogel. Subsequent addition of 1 M sodium hydroxide solution, followed by mild shaking, led to a reformation of the hydrogel, as illustrated by the images in Figure 6, which could once more be dissolved upon HCl (aq) addition, revealing the pH-responsiveness of these novel poly(vinylphosphonate)-based hydrogels. In this context, the system becomes too dilute for network reformation over time. However, applying more concentrated acid and base solutions should counteract the diluting effect and enable more iterations of this network formation and reformation process.

Shear-Thinning Behavior, Extrudability, and Initial Printing Tests. The reversibility of boronic ester formation induces shear-thinning behavior in materials formed by these interactions, meaning that networks composed of dynamic covalent linkages start to flow upon applying shear forces. Rheological experiments are commonly performed to monitor this behavior. In rotational rheology, experiments in which the shear rate is increased stepwise reveal shear-thinning behavior by a decrease in the DCN's viscosity. The measurement results in Figure 7A demonstrate a strong reduction of several orders of magnitude in the hydrogel's viscosity upon increasing the shear rate. This behavior allows the extrusion of materials

through a syringe, as illustrated by the images embedded in Figure 7A, enabling the extrusion of free-standing, continuous filaments. Therefore, the DCNs are promising candidates for extrusion-based additive manufacturing techniques. In our initial extrusion experiments, we utilized polymer 6 (Table 1) since it provides the highest functionalization degree and, therefore, the best mechanical properties of the hydrogels when applying high polymer concentrations (see the results presented in Figure 4), giving access to the stable, continuous filaments shown in Figure 7A. When performing initial additive manufacturing experiments, applying a more dilute solution of polymer 6 (22 wt %) was necessary to obtain reasonable amounts of ink for the larger-scale experiments. As indicated by the results in Figure 7B, employing the poly(vinylphosphonate)-based DCNs in direct ink writing (DIW) allowed the extrusion of continuous filaments, which is the prerequisite of material processing by DIW. The extrusion of the hydrogels further enabled the printing of simple objects with moderate shape fidelities, as illustrated by the printed logo in Figure 7B. Despite exhibiting improvable resolution in DIW, these experiments serve as a first proof of concept for further studies on the additive manufacturing of these hydrogels. In this context, applying higher weight percentages of diol-functionalized polymers for the ink preparation should give access to inks to create more sophisticated, highly resolved objects.

CONCLUSION

In summary, this study introduced a new synthetic approach toward DCNs based on poly(vinylphosphonates) utilizing reversible boronic ester chemistry. Different statistical P-(DEVP-*stat*-DAIVP) copolymers were obtained with high precision and narrow dispersities applying REM-GTP. Subsequent photochemical functionalization with 1-thioglycerol yielded diol-containing, water-soluble polymers as excellent precursors for complexation with borax toward DCNs. Besides water and borax, polymer solutions in DMSO enabled the formation of networks with DBA as a cross-linker. The hydrogels exhibited remarkable material properties, such as tunable viscoelastic properties by adjusting the polymer concentration upon DCN synthesis or employing different degrees of functionalization of the diol-containing polymers. Other noteworthy features of these networks include their ability to quickly self-heal ($t < 10$ s) due to the dynamic bond character in the hydrogels, their pH-responsiveness allowing reversible formation and decay upon adjusting the pH value, and the shear-thinning behavior of the DCNs. The viscosity decrease of poly(vinylphosphonate)-based DCNs upon application of shear forces enabled initial DIW tests in which simple shapes could be created. Overall, we developed a simplistic three-component system (polymer, borax, and water) to yield novel materials with tunable properties. The results presented in this study are the foundation for further research on optimizing these DCNs in additive manufacturing and their potential application as injectable hydrogels for biomedical applications. Furthermore, the highly dynamic character of boronic acid-diol networks and the binding specificity of this interaction could be utilized in sensing applications, e.g., sugar sensing.

ASSOCIATED CONTENT

Supporting Information

The Supporting Information is available free of charge at <https://pubs.acs.org/doi/10.1021/acs.macromol.4c03063>.

Materials and methods; printing model and parameters; experimental procedures; polymer characterization; thermal characterization of polymers and dynamic covalent networks; rheological measurements (PDF)

AUTHOR INFORMATION

Corresponding Author

Bernhard Rieger – TUM School of Natural Sciences, Department of Chemistry, WACKER-Chair of Macromolecular Chemistry, Technical University of Munich, Germany, Garching 85748, Germany; orcid.org/0000-0002-0023-884X; Email: rieger@tum.de

Authors

Jana Knezevic – TUM School of Natural Sciences, Department of Chemistry, WACKER-Chair of Macromolecular Chemistry, Technical University of Munich, Germany, Garching 85748, Germany

Anton S. Maier – TUM School of Natural Sciences, Department of Chemistry, WACKER-Chair of Macromolecular Chemistry, Technical University of Munich, Germany, Garching 85748, Germany

Florian Lackner – Institute for Chemistry and Technology of Biobased Systems (IBioSys), Graz University of Technology, Austria, Graz 8010, Austria

Karin Stana Kleinschek – Institute for Chemistry and Technology of Biobased Systems (IBioSys), Graz University of Technology, Austria, Graz 8010, Austria; orcid.org/0000-0002-9189-0242

Complete contact information is available at: <https://pubs.acs.org/10.1021/acs.macromol.4c03063>

Author Contributions

#J.K. and A.S.M. contributed equally to this manuscript. The manuscript was written through the contributions of all authors. All authors have given approval to the final version of the manuscript.

Funding

A.S.M. is grateful for the generous funding within the Kekulé Fellowship from the Fonds der Chemischen Industrie.

Notes

The authors declare no competing financial interest.

ACKNOWLEDGMENTS

The authors want to acknowledge the help of Marina Wittig and Philipp Weingarten in proofreading this manuscript. The authors thank Tobias Steindorfer for helping us with the additive manufacturing experiments.

ABBREVIATIONS

Borax, sodium tetraborate decahydrate; DAIVP, diallyl vinylphosphonate; DBA, benzene-1,4-diboronic acid; DCN, dynamic covalent network; DEVP, diethyl vinylphosphonate; DIW, direct ink writing; DMSO, dimethyl sulfoxide; REM-GTP, rare earth metal-mediated group-transfer polymerization

REFERENCES

- (1) Ross-Murphy, S. B.; McEvoy, H. Fundamentals of Hydrogels and Gelation. *Br. Poly. J.* **1986**, *18* (1), 2–7.
- (2) Peppas, N. A.; Bures, P.; Leobandung, W.; Ichikawa, H. Hydrogels in Pharmaceutical Formulations. *Eur. J. Pharm. Biopharm.* **2000**, *50* (1), 27–46.
- (3) Du, H.; Zha, G.; Gao, L.; Wang, H.; Li, X.; Shen, Z.; Zhu, W. Fully Biodegradable Antibacterial Hydrogels via Thiol–Ene “Click” Chemistry. *Polym. Chem.* **2014**, *5* (13), 4002–4008.
- (4) Rodell, C. B.; MacArthur, J. W.; Dorsey, S. M.; Wade, R. J.; Wang, L. L.; Woo, Y. J.; Burdick, J. A. Shear-Thinning Supramolecular Hydrogels with Secondary Autonomous Covalent Crosslinking to Modulate Viscoelastic Properties In Vivo. *Adv. Funct. Mater.* **2015**, *25* (4), 636–644.
- (5) Park, M.-R.; Seo, B.-B.; Song, S.-C. Dual Ionic Interaction System Based on Polyelectrolyte Complex and Ionic, Injectable, and Thermosensitive Hydrogel for Sustained Release of Human Growth Hormone. *Biomater* **2013**, *34* (4), 1327–1336.
- (6) Chen, J.; Peng, Q.; Thundat, T.; Zeng, H. Stretchable, Injectable, and Self-Healing Conductive Hydrogel Enabled by Multiple Hydrogen Bonding toward Wearable Electronics. *Chem. Mater.* **2019**, *31* (12), 4553–4563.
- (7) Takashima, Y.; Harada, A. Stimuli-Responsive Polymeric Materials Functioning via Host–Guest Interactions. *J. Incl. Phenom. Macrocycl. Chem.* **2017**, *88* (3–4), 85–104.
- (8) Wei, Z.; Yang, J. H.; Zhou, J.; Xu, F.; Zrínyi, M.; Dussault, P. H.; Osada, Y.; Chen, Y. M. Self-Healing Gels Based on Constitutional Dynamic Chemistry and Their Potential Applications. *Chem. Soc. Rev.* **2014**, *43* (23), 8114–8131.
- (9) Marco-Dufort, B.; Tibbitt, M. W. Design of Moldable Hydrogels for Biomedical Applications Using Dynamic Covalent Boronic Esters. *Mater. Today Chem.* **2019**, *12*, 16–33.
- (10) Marco-Dufort, B.; Iten, R.; Tibbitt, M. W. Linking Molecular Behavior to Macroscopic Properties in Ideal Dynamic Covalent Networks. *J. Am. Chem. Soc.* **2020**, *142* (36), 15371–15385.
- (11) Cromwell, O. R.; Chung, J.; Guan, Z. Malleable and Self-Healing Covalent Polymer Networks through Tunable Dynamic Boronic Ester Bonds. *J. Am. Chem. Soc.* **2015**, *137* (20), 6492–6495.
- (12) Zou, W.; Dong, J.; Luo, Y.; Zhao, Q.; Xie, T. Dynamic Covalent Polymer Networks: from Old Chemistry to Modern Day Innovations. *Adv. Mater.* **2017**, *29* (14), 1606100.
- (13) Marco-Dufort, B.; Willi, J.; Vielba-Gomez, F.; Gatti, F.; Tibbitt, M. W. Environment Controls Biomolecule Release from Dynamic Covalent Hydrogels. *Biomacromolecules* **2021**, *22* (1), 146–157.
- (14) Yesilyurt, V.; Webber, M. J.; Appel, E. A.; Godwin, C.; Langer, R.; Anderson, D. G. Injectable Self-Healing Glucose-Responsive Hydrogels with pH-Regulated Mechanical Properties. *Adv. Mater.* **2016**, *28* (1), 86–91.
- (15) Yu, J.; Wang, J.; Zhang, Y.; Chen, G.; Mao, W.; Ye, Y.; Kahkoska, A. R.; Buse, J. B.; Langer, R.; Gu, Z. Glucose-Responsive Insulin Patch for the Regulation of Blood Glucose in Mice and Minipigs. *Nat. Biomed. Eng.* **2020**, *4* (5), 499–506.
- (16) Adzima, B. J.; Aguirre, H. A.; Kloxin, C. J.; Scott, T. F.; Bowman, C. N. Rheological and Chemical Analysis of Reverse Gelation in a Covalently Cross-Linked Diels–Alder Polymer Network. *Macromolecules* **2008**, *41* (23), 9112–9117.
- (17) Chen, X.; Dam, M. A.; Ono, K.; Mal, A.; Shen, H.; Nutt, S. R.; Sheran, K.; Wudl, F. A Thermally Re-mendable Cross-Linked Polymeric Material. *Science* **2002**, *295* (5560), 1698–1702.
- (18) Liu, J.; Zhang, X.; Chen, X.; Qu, L.; Zhang, L.; Li, W.; Zhang, A. Stimuli-Responsive Dendronized Polymeric Hydrogels Through Schiff-Base Chemistry Showing Remarkable Topological Effects. *Polym. Chem.* **2018**, *9* (3), 378–387.
- (19) Corbett, P. T.; Leclaire, J.; Vial, L.; West, K. R.; Wietor, J.-L.; Sanders, J. K. M.; Otto, S. Dynamic combinatorial chemistry. *Chem. Rev.* **2006**, *106* (9), 3652–3711.
- (20) Montarnal, D.; Capelot, M.; Tournilhac, F.; Leibler, L. Silica-Like Malleable Materials From Permanent Organic Networks. *Science* **2011**, *334* (6058), 965–968.
- (21) Zhang, X.; Waymouth, R. M. 1,2-Dithiolane-Derived Dynamic, Covalent Materials: Cooperative Self-Assembly and Reversible Cross-Linking. *J. Am. Chem. Soc.* **2017**, *139* (10), 3822–3833.
- (22) Yu, H.; Wang, Y.; Yang, H.; Peng, K.; Zhang, X. Injectable self-healing hydrogels formed via thiol/disulfide exchange of thiol functionalized F127 and dithiolane modified PEG. *J. Mater. Chem. B* **2017**, *5* (22), 4121–4127.
- (23) Cash, J. J.; Kubo, T.; Bapat, A. P.; Sumerlin, B. S. Room-Temperature Self-Healing Polymers Based on Dynamic-Covalent Boronic Esters. *Macromolecules* **2015**, *48* (7), 2098–2106.
- (24) Chen, Y.; Tan, Z.; Wang, W.; Peng, Y.-Y.; Narain, R. Injectable, Self-Healing, and Multi-Responsive Hydrogels via Dynamic Covalent Bond Formation between Benzoxaborole and Hydroxyl Groups. *Biomacromolecules* **2019**, *20* (2), 1028–1035.
- (25) Kang, B.; Kalow, J. A. Internal and External Catalysis in Boronic Ester Networks. *ACS Macro Lett.* **2022**, *11* (3), 394–401.
- (26) Roy, C. D.; Brown, H. C. Stability of Boronic Esters – Structural Effects on the Relative Rates of Transesterification of 2-(Phenyl)-1,3, 2-Dioxaborolane. *J. Organomet. Chem.* **2007**, *692* (4), 784–790.
- (27) Brooks, W. L. A.; Deng, C. C.; Sumerlin, B. S. Structure-Reactivity Relationships in Boronic Acid-Diol Complexation. *ACS Omega* **2018**, *3* (12), 17863–17870.
- (28) Rowan, S. J.; Cantrill, S. J.; Cousins, G. R. L.; Sanders, J. K. M.; Stoddart, J. F. Dynamic Covalent Chemistry. *Angew. Chem., Int. Ed.* **2002**, *41* (6), 898–952.
- (29) Axthelm, J.; Askes, S. H. C.; Elstner, M.; Reddy, G. U.; Görls, H.; Bellstedt, P.; Schiller, A. Fluorinated Boronic Acid-Appended Pyridinium Salts and 19F NMR Spectroscopy for Diol Sensing. *J. Am. Chem. Soc.* **2017**, *139* (33), 11413–11420.
- (30) An, H.; Bo, Y.; Chen, D.; Wang, Y.; Wang, H.; He, Y.; Qin, J. Cellulose-based self-healing hydrogel through boronic ester bonds with excellent biocompatibility and conductivity. *RSC Adv.* **2020**, *10* (19), 11300–11310.
- (31) Robinson, L. L.; Self, J. L.; Fusi, A. D.; Bates, M. W.; Read de Alaniz, J.; Hawker, C. J.; Bates, C. M.; Sample, C. S. Chemical and Mechanical Tunability of 3D-Printed Dynamic Covalent Networks Based on Boronate Esters. *ACS Macro Lett.* **2021**, *10* (7), 857–863.
- (32) Maier, A. S.; Mansi, S.; Halama, K.; Weingarten, P.; Mela, P.; Rieger, B. Cytocompatible Hydrogels with Tunable Mechanical Strength and Adjustable Swelling Properties through Photo-Cross-Linking of Poly(vinylphosphonates). *ACS Appl. Mater. Interfaces* **2024**, *16* (43), 58135–58147.
- (33) Adams, F.; Machat, M. R.; Altenbuchner, P. T.; Ehrmaier, J.; Pöthig, A.; Karsili, T. N. V.; Rieger, B. Toolbox of Nonmetallocene Lanthanides: Multifunctional Catalysts in Group-Transfer Polymerization. *Inorg. Chem.* **2017**, *56* (16), 9754–9764.
- (34) Soller, B. S.; Salzinger, S.; Jandl, C.; Pöthig, A.; Rieger, B. C–H Bond Activation by σ -Bond Metathesis as a Versatile Route toward Highly Efficient Initiators for the Catalytic Precision Polymerization of Polar Monomers. *Organometallics* **2015**, *34* (11), 2703–2706.
- (35) Salzinger, S.; Soller, B. S.; Plikhta, A.; Seemann, U. B.; Herdtweck, E.; Rieger, B. Mechanistic Studies on Initiation and Propagation of Rare Earth Metal-Mediated Group Transfer Polymerization of Vinylphosphonates. *J. Am. Chem. Soc.* **2013**, *135* (35), 13030–13040.
- (36) Schwarzenböck, C.; Schaffer, A.; Pahl, P.; Nelson, P. J.; Huss, R.; Rieger, B. Precise Synthesis of Thermoresponsive Polyvinylphosphonate-Biomolecule Conjugates via Thiol–Ene Click Chemistry. *Polym. Chem.* **2018**, *9* (3), 284–290.
- (37) Halama, K.; Schaffer, A.; Rieger, B. Allyl Group-Containing Polyvinylphosphonates as a Flexible Platform for the Selective Introduction of Functional Groups via Polymer-Analogous Transformations. *RSC Adv.* **2021**, *11* (61), 38555–38564.
- (38) Halama, K.; Lin, M. T.-Y.; Schaffer, A.; Foith, M.; Adams, F.; Rieger, B. Cytocompatible Triblock Copolymers with Controlled Microstructure Enabling Orthogonally Functionalized Bio-polymer Conjugates. *Macromolecules* **2024**, *57* (4), 1438–1447.

- (39) Chen, Y.; Tang, Z.; Zhang, X.; Liu, Y.; Wu, S.; Guo, B. Covalently Cross-Linked Elastomers with Self-Healing and Malleable Abilities Enabled by Boronic Ester Bonds. *ACS Appl. Mater. Interfaces* **2018**, *10* (28), 24224–24231.
- (40) Nishiyabu, R.; Kobayashi, H.; Kubo, Y. Dansyl-Containing Boronate Hydrogel Film As Fluorescent Chemosensor of Copper Ions in Water. *RSC Adv.* **2012**, *2* (16), 6555.
- (41) Gosecki, M.; Gosecka, M. Boronic Acid Esters and Anhydrides as Dynamic Cross-Links in Vitrimers. *Polymers* **2022**, *14* (4), 842.
- (42) Liu, X.; Ren, Z.; Liu, F.; Zhao, L.; Ling, Q.; Gu, H. Multifunctional Self-Healing Dual Network Hydrogels Constructed via Host-Guest Interaction and Dynamic Covalent Bond as Wearable Strain Sensors for Monitoring Human and Organ Motions. *ACS Appl. Mater. Interfaces* **2021**, *13* (12), 14612–14622.
- (43) He, L.; Szopinski, D.; Wu, Y.; Luinstra, G. A.; Theato, P. Toward Self-Healing Hydrogels Using One-Pot Thiol-Ene Click and Borax-Diol Chemistry. *ACS Macro Lett.* **2015**, *4* (7), 673–678.
- (44) Medrano-David, D.; Lopera, A. M.; Londoño, M. E.; Araque-Marin, P. Formulation and Characterization of a New Injectable Bone Substitute Composed PVA/Borax/CaCO₃ and Demineralized Bone Matrix. *J. Funct. Biomater.* **2021**, *12* (3), 46.
- (45) Narita, T.; Hsieh, W.-C.; Ku, Y. T.; Su, Y.-C.; Inoguchi, H.; Takeno, H. Fracture Behavior and Biocompatibility of Cellulose Nanofiber-Reinforced Poly(vinyl alcohol) Composite Hydrogels Cross-Linked with Borax. *Biomacromolecules* **2025**, *26* (1), 374–386.
- (46) Yang, N.; Qi, P.; Ren, J.; Yu, H.; Liu, S.; Li, J.; Chen, W.; Kaplan, D. L.; Ling, S. Polyvinyl Alcohol/Silk Fibroin/Borax Hydrogel Ionotronics: A Highly Stretchable, Self-Healable, and Biocompatible Sensing Platform. *ACS Appl. Mater. Interfaces* **2019**, *11* (26), 23632–23638.
- (47) Accardo, J. V.; Kalow, J. A. Reversibly tuning hydrogel stiffness through photocontrolled dynamic covalent crosslinks. *Chem. Sci.* **2018**, *9* (27), 5987–5993.
- (48) Meng, F.; Saed, M. O.; Terentjev, E. M. Rheology of Vitrimers. *Nat. Commun.* **2022**, *13* (1), 5753.
- (49) Bischoff, D. J.; Lee, T.; Kang, K.-S.; Molineux, J.; O’Neil Parker, W.; Pyun, J.; Mackay, M. E. Unraveling the rheology of inverse vulcanized polymers. *Nat. Commun.* **2023**, *14* (1), 7553.
- (50) Dörr, D.; Kuhn, U.; Altstädt, V. Rheological Study of Gelation and Crosslinking in Chemical Modified Polyamide 12 Using a Multiwave Technique. *Polymers* **2020**, *12*, 855.
- (51) Yan, J.; Springsteen, G.; Deeter, S.; Wang, B. The Relationship Among pKa, pH, and Binding Constants in the Interactions Between Boronic Acids and Diols—It Is Not As Simple as It Appears. *Tetrahedron* **2004**, *60* (49), 11205–11209.
- (52) Huang, Z.; Delparastan, P.; Burch, P.; Cheng, J.; Cao, Y.; Messersmith, P. B. Injectable Dynamic Covalent Hydrogels of Boronic Acid Polymers Cross-Linked by Bioactive Plant-Derived Polyphenols. *Biomater. Sci.* **2018**, *6* (9), 2487–2495.

7.5 Author contributions

Anton Maier synthesized the catalyst and monomers and provided the original idea. A. M. carried out initial polymerization and functionalization experiments and supervised all further experimental work. Furthermore, A. M. conceptualized the project and initiated collaborations with the coauthors. A. M. analyzed the measurement results and contributed to writing the original draft.

8 Summary and Outlook

Within the scope of this thesis, the profound knowledge of the catalysis of REM-GTP, the copolymerization of vinylphosphonate monomers, and polymer-analogous transformations of poly(vinylphosphonates) gathered by several generations of researchers was successfully applied to develop functional, cross-linked polymer materials with significant application potential. Overall, this thesis was divided into four subprojects, all involving the cross-linking of poly(vinylphosphonates), which are summarized in Figure 29.

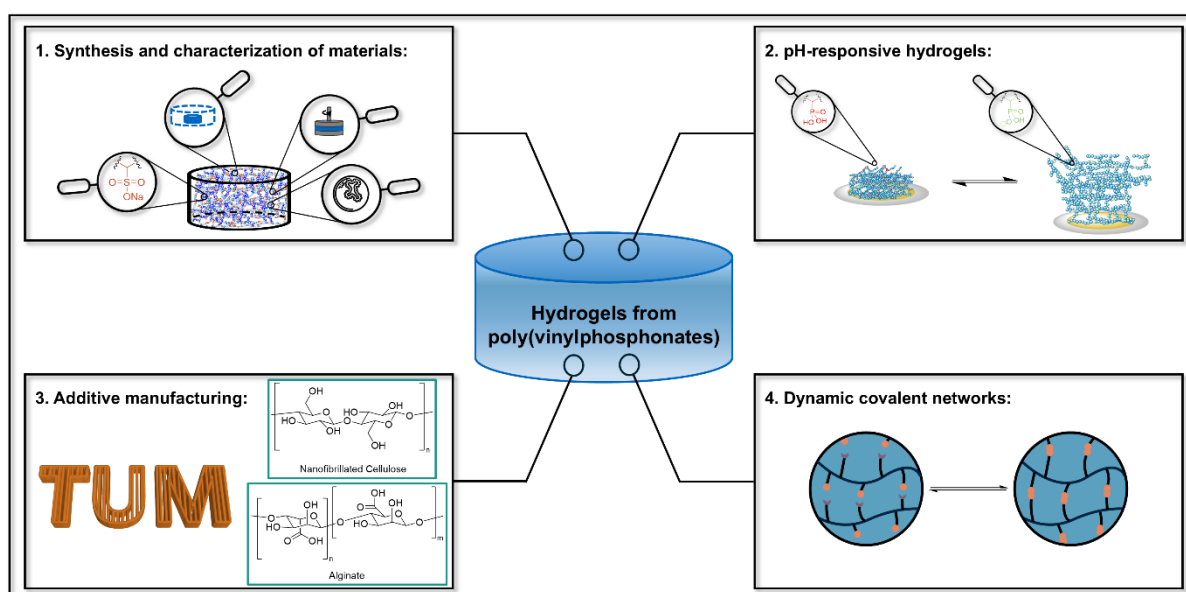


Figure 29: Overview of different projects addressed in this thesis: Synthesis and fundamental characterization of poly(vinylphosphonate)-based hydrogels, studies on the pH-responsiveness of thin films of poly(vinylphosphonate)-based hydrogels, reinforcement of NFC/Alg inks in DIW through photo-cross-linking of poly(vinylphosphonates), and modifications of poly(vinylphosphonates) to create dynamic covalent networks.

In the first part of the thesis, new polymeric materials were developed by covalent photochemical cross-linking of allyl group-containing P(DEVP-*stat*-DAIVP) copolymers with high rates ($t < 3$ s) by applying thiol-ene click chemistry. REM-GTP allowed a facile adjustment of the copolymer compositions while maintaining narrow polydispersities, thus enabling a straightforward modification of the mechanical properties by tuning the cross-linking density, as demonstrated by oscillatory rheology and nanoindentation experiments. As the cross-linking degree increased, the mechanical strength improved while the water uptake decreased. Nevertheless, the functionalization of the copolymers with 3-mercaptopropane-1-sulfonate yielded

significantly increased water uptakes, rendering the materials promising candidates as superabsorbent hydrogels. Finally, a thorough biological characterization revealed a high biomedical application potential. The purified hydrogels enabled cell growth and proliferation and supported endothelialization while displaying antibacterial properties and not inducing inflammation. Consequently, these materials were considered promising candidates for in vivo applications. Leveraging the same photochemical cross-linking process, a two-step synthetic process toward a highly hydrophilic polymer network was introduced in a second study. In this context, P(DEVP-*stat*-DAIVP) copolymers were subjected to polymer-analogous hydrolysis by reaction with TMSBr, followed by cross-linking with a dithiol cross-linker. Combining these steps gave access to VPA-containing, superabsorbent hydrogels with water uptakes of up to 150 ± 27 g (H₂O)/g (hydrogel). Thin layers of these hydrogels were successfully spin-coated onto different substrates as homogeneous films and analyzed by profilometry, light microscopy, AFM, and QCM-D. Real-time QCM-D measurements in different aqueous environments with alternating pH values displayed the fully reversible, pH-dependent swelling of the films, which sustained harsh conditions without erosion from the gold surfaces. Hypothesizing that this might be due to interactions of the dithiol cross-linkers with the Au-surfaces, anchoring the films on the substrate, detailed XPS and ToF-SIMS studies were conducted, confirming this assumption by an S-related signal increase at the polymer network/Au interface. This study demonstrated the application of thin, pH-responsive hydrogel films in QCM-D measurements as gravimetric pH-sensors. For the future, this concept of surface anchoring poly(vinylphosphonate)-based hydrogels on gold surfaces is an excellent starting point for developing more sophisticated piezoelectric pH-sensors. Devices applying pH-responsive hydrogels allow real-time pH-monitoring in diverse fields, including biomedicine (blood, sweat, and urine analysis), water quality assessment, or wearable sensors.^{335,336} Similarly, the excellent adhesion of the hydrogels on gold surfaces creates opportunities for photolithographic micropatterning, which should be explored since it is not only relevant for biomedicine but also finds application in optics and electronics.^{337,338} Finally, despite the rather tedious synthesis, the extraordinary water uptakes of VPA-containing hydrogels could be relevant for niche applications requiring superabsorbent properties. In the third project within the scope of this thesis, the

covalent cross-linking of P(DEVP-*stat*-DAIVP) copolymers was applied to reinforce NFC/Alg inks for DIW, allowing the printing of sophisticated objects with high shape fidelities through layer-by-layer deposition with intermediate photochemical-cross-linking. The polymer-reinforced objects exhibited tunable swelling behavior by adjusting the covalent cross-linking density of the poly(vinylphosphonates). Furthermore, they maintained high swelling shape fidelities in CaCl₂-containing solutions (utilized for ionic cross-linking of Alg), overcoming limitations of standard NFC/Alg inks. While the mechanical properties were mainly dominated by the effects of Ca²⁺-cross-linking of Alg, the tensile moduli correlated with the covalent cross-linking density, and the mechanical strengths of the materials were within the range of selected examples of tissue engineering materials. In the last step, the poly(vinylphosphonate)-reinforced prints were evaluated for cell compatibility, displaying only moderate cytotoxicities toward two relevant cell lines, primarily attributed to the cytotoxicity of the dithiol cross-linker. Nevertheless, this study suggested the application potential of this approach in tissue engineering as DIW of the modified NFC/Alg inks enabled the precise creation of highly resolved structures with tunable properties controlled by the DAIVP extents in the poly(vinylphosphonates) complementing the inks. Future steps should, therefore, involve research on even less cytotoxic cross-linkers to further increase biocompatibility or purification of the printed structures to decrease harmful effects on the cells. Additionally, this study demonstrated that applying DIW as a processing method for poly(vinylphosphonate)-based hydrogels (with or without natural polymers in inks) is possible. Considering the highly hydrophilic, pH-responsive hydrogel materials found in the previous study, the concepts of both studies could be combined as follows: DIW could enable the selective incorporation of pH-responsive regions within printed structures (utilization of two different inks), allowing for localized differences in the swelling behavior, thereby paving the way for developing pH-responsive actuators and smart materials. A different hydrogel system enabling the processing via DIW was presented in the final part of this thesis. Functionalization of P(DEVP-*stat*-DAIVP) copolymers with 1-thioglycerol by applying thiol-ene click chemistry gave access to polymers with 1,2-diol motifs, facilitating cross-linking with different appropriate boronic acid derivatives by leveraging dynamic boronic ester chemistry. These systems displayed tunable

viscoelastic properties by changing the concentrations of functionalized polymers and varying the degree of diol-functionalization, which could be controlled by adjusting the DAIVP content upon copolymerization. The poly(vinylphosphonate)-based DCNs further exhibited self-healing behavior and pH-responsiveness and facilitated the extrusion of continuous filaments due to their shear-thinning properties. Therefore, initial DIW experiments with these hydrogels allowed the creation of simple structures like logos. For the future, the DIW should be optimized for printing more sophisticated structures by increasing the functionalization degree of the poly(vinylphosphonates) and their concentration to yield stronger networks. Considering the cytocompatibility of each of the three ink compounds (water, polymer, borax),^{104,105,339,340} the findings in this study suggest a high application potential as injectable hydrogels for targeted drug delivery. Finally, the DCNs could be promising candidates for developing biosensors based on poly(vinylphosphonates) due to the binding affinity of different diols to a boronic acid, allowing the detection of sugars like glucose, which is relevant to treating chronic diseases like diabetes.^{226,227}

9 References

- (1) Abd-El-Aziz, A. S.; Antonietti, M.; Barner-Kowollik, C.; Binder, W. H.; Böker, A.; Boyer, C.; Buchmeiser, M. R.; Cheng, S. Z. D.; D'Agosto, F.; Floudas, G.; Frey, H.; Galli, G.; Genzer, J.; Hartmann, L.; Hoogenboom, R.; Ishizone, T.; Kaplan, D. L.; Leclerc, M.; Lendlein, A.; Liu, B.; Long, T. E.; Ludwigs, S.; Lutz, J.-F.; Matyjaszewski, K.; Meier, M. A. R.; Müllen, K.; Müllner, M.; Rieger, B.; Russell, T. P.; Savin, D. A.; Schlüter, A. D.; Schubert, U. S.; Seiffert, S.; Severing, K.; Soares, J. B. P.; Staffilani, M.; Sumerlin, B. S.; Sun, Y.; Tang, B. Z.; Tang, C.; Théato, P.; Tirelli, N.; Tsui, O. K. C.; Unterlass, M. M.; Vana, P.; Voit, B.; Vyazovkin, S.; Weder, C.; Wiesner, U.; Wong, W.-Y.; Wu, C.; Yagci, Y.; Yuan, J.; Zhang, G. The Next 100 Years of Polymer Science. *Macromol. Chem. Phys.* **2020**, *221* (16).
- (2) Zhang, Y. S.; Khademhosseini, A. Advances in Engineering Hydrogels. *Science* **2017**, *356* (6337).
- (3) Ullah, F.; Othman, M. B. H.; Javed, F.; Ahmad, Z.; Md Akil, H. Classification, Processing and Application of Hydrogels: A Review. *Mater. Sci. Eng. C* **2015**, *57*, 414–433.
- (4) Ionov, L. Hydrogel-Based Actuators: Possibilities and Limitations. *Mater. Today* **2014**, *17* (10), 494–503.
- (5) Zhou, Y.-N.; Li, J.-J.; Wang, T.-T.; Wu, Y.-Y.; Luo, Z.-H. Precision Polymer Synthesis by Controlled Radical Polymerization: Fusing the Progress From Polymer Chemistry and Reaction Engineering. *Prog. Polym. Sci.* **2022**, *130*, 101555.
- (6) Soller, B. S.; Zhang, N.; Rieger, B. Catalytic Precision Polymerization: Rare Earth Metal-Mediated Synthesis of Homopolymers, Block Copolymers, and Polymer Brushes. *Macromol. Chem. Phys.* **2014**, *215* (20), 1946–1962.
- (7) Adams, F.; Pahl, P.; Rieger, B. Metal-Catalyzed Group-Transfer Polymerization: A Versatile Tool for Tailor-Made Functional (Co)Polymers. *Chemistry* **2018**, *24* (3), 509–518.
- (8) Adams, F. Merging σ -Bond Metathesis with Polymerization Catalysis: Insights into Rare-Earth Metal Complexes, End-Group Functionalization, and Application Prospects. *Macromol. Rapid Commun.* **2024**, *45* (15), e2400122.

- (9) Szwarc, M.; Levy, M.; Milkovich, R. Polymerization Initiated by Electron Transfer to Monomer. A New Method of Formation of Block Polymers. *J. Am. Chem. Soc.* **1956**, *78*, 2656.
- (10) Szwarc, M. 'Living' Polymers. *Nature* **1956**, *178*, 1168–1169.
- (11) Szwarc, M. Living Polymers. Their Discovery, Characterization, and Properties. *J. Polym. Sci. A Polym. Chem.* **1998**, *36* (1), ix–xv.
- (12) Donald, P. E.; Lipkin, D.; Weissman, S. I. Reaction of Sodium Metal with Aromatic Hydrocarbons. *J. Am. Chem. Soc.* **1956** (78), 116–120.
- (13) Smid, J.; van Beylen, M.; Hogen-Esch, T. E. Perspectives on the Contributions of Michael Szwarc to Living Polymerization. *Prog. Polym. Sci.* **2006**, *31* (12), 1041–1067.
- (14) Waack, R.; Rembaum, A.; Coombes, J. D.; Szwarc, M. Molecular Weights of "Living" Polymers. *J. Am. Chem. Soc.* **1957**, *79*, 2026.
- (15) Flory, P. J. *Principles of Polymer Chemistry*, 1. publ. 1953, 20. print; Cornell Univ. Press, ca. 2010.
- (16) Flory, P. J. Molecular Size Distribution in Ethylene Oxide Polymers. *J. Am. Chem. Soc.* **1940**, *62*, 1561.
- (17) Webster, O. W. Living Polymerization Methods. *Science* **1991**, *251* (4996), 887–893.
- (18) Braunecker, W. A.; Matyjaszewski, K. Controlled/Living Radical Polymerization: Features, Developments, and Perspectives. *Prog. Polym. Sci.* **2007**, *32* (1), 93–146.
- (19) Matyjaszewski, K. Ranking Living Systems. *Macromolecules* **1993**, *26*, 1787–1788.
- (20) Matyjaszewski, K. Introduction to Living Polymeriz. Living and/or Controlled Polymerization. *J. Phys. Org. Chem.* **1995**, *8* (4), 197–207.
- (21) Fellows, C. M.; Jones, R. G.; Keddie, D. J.; Luscombe, C. K.; Matson, J. B.; Matyjaszewski, K.; Merna, J.; Moad, G.; Nakano, T.; Penczek, S.; Russell, G. T.; Topham, P. D. Terminology for Chain Polymerization (IUPAC Recommendations 2021). *Pure Appl. Chem.* **2022**, *94* (9), 1093–1147.
- (22) Matyjaszewski, K. Macromolecular Engineering: From Rational Design Through Precise Macromolecular Synthesis and Processing to Targeted Macroscopic Material Properties. *Prog. Polym. Sci.* **2005**, *30* (8-9), 858–875.

- (23) Bauer, B. J.; Fetters, L. J. Synthesis and Dilute-Solution Behavior of Model Star-Branched Polymers. *Rubber Chem. Technol.* **1978**, *51* (3), 406–436.
- (24) Hirao, A.; Goseki, R.; Ishizone, T. Advances in Living Anionic Polymerization: From Functional Monomers, Polymerization Systems, to Macromolecular Architectures. *Macromolecules* **2014**, *47* (6), 1883–1905.
- (25) Hong, K.; Uhrig, D.; Mays, J. W. Living Anionic Polymerization. *Curr. Opin. Solid State Mater. Sci.* **1999**, *4* (6), 531–538.
- (26) Aoshima, S.; Kanaoka, S. A Renaissance in Living Cationic Polymerization. *Chem. Rev.* **2009**, *109* (11), 5245–5287.
- (27) Miyamoto, M.; Sawamoto, M.; Higashimura, T. Living Polymerization of Isobutyl Vinyl Ether With Hydrogen Iodide/Iodine Initiating System. *Macromolecules* **1984**, *17* (3), 265–268.
- (28) Fantin, M.; Isse, A. A.; Gennaro, A.; Matyjaszewski, K. Understanding the Fundamentals of Aqueous ATRP and Defining Conditions for Better Control. *Macromolecules* **2015**, *48* (19), 6862–6875.
- (29) Weingarten, P.; Adams, F. Silver-Mediated ARGET-ATRP of Reactive Acrylates Using TPMANMe₂ Ligand: A Universal Strategy for Controlled Copolymerization. *ACS Macro Lett.* **2024**, *13* (10), 1318–1324.
- (30) Nothling, M. D.; Fu, Q.; Reyhani, A.; Allison-Logan, S.; Jung, K.; Zhu, J.; Kamigaito, M.; Boyer, C.; Qiao, G. G. Progress and Perspectives Beyond Traditional RAFT Polymerization. *Adv. Sci.* **2020**, *7* (20), 2001656.
- (31) Chiefari, J.; Chong, Y. K.; Ercole, F.; Krstina, J.; Jeffery, J.; Le, T. P. T.; Mayadunne, R. T. A.; Meijs, G. F.; Moad, C. L.; Moad, G.; Rizzardo, E.; Thang, S. H. Living Free-Radical Polymerization by Reversible Addition–Fragmentation Chain Transfer: The RAFT Process. *Macromolecules* **1998**, *31* (16), 5559–5562.
- (32) Gregory, A.; Stenzel, M. H. Complex Polymer Architectures via RAFT Polymerization: From Fundamental Process to Extending the Scope Using Click Chemistry and Nature’s Building Blocks. *Prog. Polym. Sci.* **2012**, *37* (1), 38–105.
- (33) Nakabayashi, K.; Mori, H. Recent Progress in Controlled Radical Polymerization of N-Vinyl Monomers. *Eur. Polym. J.* **2013**, *49* (10), 2808–2838.

- (34) Rosselgong, J.; Armes, S. P.; Barton, W. R. S.; Price, D. Synthesis of Branched Methacrylic Copolymers: Comparison between RAFT and ATRP and Effect of Varying the Monomer Concentration. *Macromolecules* **2010**, *43* (5), 2145–2156.
- (35) Kränzlein, M.; Pehl, T. M.; Adams, F.; Rieger, B. Uniting Group-Transfer and Ring-Opening Polymerization—Block Copolymers from Functional Michael-Type Monomers and Lactones. *Macromolecules* **2021**, *54* (23), 10860–10869.
- (36) Ajellal, N.; Carpentier, J.-F.; Guillaume, C.; Guillaume, S. M.; Helou, M.; Poirier, V.; Sarazin, Y.; Trifonov, A. Metal-Catalyzed Immortal Ring-Opening Polymerization of Lactones, Lactides and Cyclic Carbonates. *Dalton Trans.* **2010**, *39* (36), 8363–8376.
- (37) Klavetter, F. L.; Grubbs, R. H. Polycyclooctatetraene (Polyacetylene): Synthesis and Properties. *J. Am. Chem. Soc.* **1988**, *110*, 7807–7813.
- (38) Schrock, R. R. Living Ring-Opening Metathesis Polymerization Catalyzed by Well-Characterized Transition-Metal Alkylidene Complexes. *Acc. Chem. Res.* **1990**, *23*, 158–165.
- (39) Grubbs, R. H.; Tumas, W. Polymer Synthesis and Organotransition Metal Chemistry. *Science* **1989**, *243* (4893), 907–915.
- (40) Böhm, L. L. The Ethylene Polymerization With Ziegler Catalysts: Fifty Years After the Discovery. *Angew. Chem. Int. Ed. Engl.* **2003**, *42* (41), 5010–5030.
- (41) Brintzinger, H. H.; Fischer, D.; Mülhaupt, R.; Rieger, B.; Waymouth, R. M. Stereospecific Olefin Polymerization with Chiral Metallocene Catalysts. *Angew. Chem. Int. Ed. Engl.* **1995**, *34* (11), 1143–1170.
- (42) Zhang, W.; Sita, L. R. Highly Efficient, Living Coordinative Chain-Transfer Polymerization of Propene With ZnEt₂: Practical Production of Ultrahigh to Very Low Molecular Weight Amorphous Atactic Polypropenes of Extremely Narrow Polydispersity. *J. Am. Chem. Soc.* **2008**, *130* (2), 442–443.
- (43) Webster, O. W.; Hertler, W. R.; Sogah, D. Y.; Farnham, W. B.; RajanBabu, T. V. Group-Transfer Polymerization. 1. A New Concept for Addition Polymerization With Organosilicon Initiators. *J. Am. Chem. Soc.* **1983**, *105* (17), 5706–5708.
- (44) Webster, O. W. Group Transfer Polymerization: A Critical Review of Its Mechanism and Comparison with Other Methods for Controlled Polymerization of

- Acrylic Monomers. In *New Synthetic Methods; Advances in Polymer Science*; Springer Berlin Heidelberg, 2004; pp 1–34. DOI: 10.1007/b12303.
- (45) Webster, O. W. The Discovery and Commercialization of Group Transfer Polymerization. *J. Polym. Sci. A Polym. Chem.* **2000**, *38* (16), 2855–2860.
- (46) Quirk, R. P.; Kim, J.-S. Mechanistic Aspects of Silicon-Mediated Polymerization (Group Transfer Polymerization) of Methyl Methacrylate With Ester Enolate Anions As Nucleophilic Catalysts. *J. Phys. Org. Chem.* **1995**, *8* (4), 242–248.
- (47) Quirk, R. P.; Bidinger, G. P. Mechanistic Role of Enolate Ions in “Group Transfer Polymerization”. *Polym. Bull.* **1989**, *22*, 63–70.
- (48) Mueller, A. H. E. Kinetic Discrimination between Various Mechanisms in Group-Transfer Polymerization. *Macromolecules* **1994**, *27* (7), 1685–1690.
- (49) Litvinenko, G.; Müller, A. H. E. General Kinetic Analysis and Comparison of Molecular Weight Distributions for Various Mechanisms of Activity Exchange in Living Polymerizations. *Macromolecules* **1997**, *30* (5), 1253–1266.
- (50) Doherty, M. A.; Müller, A. H. E. Kinetics of Group Transfer Polymerization of Tert -Butyl Methacrylate in Tetrahydrofuran. *Makromol. Chem.* **1989**, *190* (3), 527–539.
- (51) Chen, J.; Gowda, R. R.; He, J.; Zhang, Y.; Chen, E. Y.-X. Controlled or High-Speed Group Transfer Polymerization by Silyl Ketene Acetals without Catalyst. *Macromolecules* **2016**, *49* (21), 8075–8087.
- (52) Chen, Y.; Fuchise, K.; Narumi, A.; Kawaguchi, S.; Satoh, T.; Kakuchi, T. Core-First Synthesis of Three-, Four-, and Six-Armed Star-Shaped Poly(methyl methacrylate)s by Group Transfer Polymerization Using Phosphazene Base. *Macromolecules* **2011**, *44* (23), 9091–9098.
- (53) Fevre, M.; Vignolle, J.; Heroguez, V.; Taton, D. Tris(2,4,6-trimethoxyphenyl)phosphine (TTMPP) as Potent Organocatalyst for Group Transfer Polymerization of Alkyl (Meth)acrylates. *Macromolecules* **2012**, *45* (19), 7711–7718.
- (54) Fuchise, K.; Sakai, R.; Satoh, T.; Sato, S.; Narumi, A.; Kawaguchi, S.; Kakuchi, T. Group Transfer Polymerization of N , N -Dimethylacrylamide Using Nobel Efficient System Consisting of Dialkylamino Silyl Enol Ether as an Initiator and Strong Brønsted Acid as an Organocatalyst. *Macromolecules* **2010**, *43* (13), 5589–5594.

- (55) Takada, K.; Ito, T.; Kitano, K.; Tsuchida, S.; Takagi, Y.; Chen, Y.; Satoh, T.; Kakuchi, T. Synthesis of Homopolymers, Diblock Copolymers, and Multiblock Polymers by Organocatalyzed Group Transfer Polymerization of Various Acrylate Monomers. *Macromolecules* **2015**, *48* (3), 511–519.
- (56) McCahill, J. S. J.; Welch, G. C.; Stephan, D. W. Reactivity of “Frustrated Lewis Pairs”: Three-Component Reactions of Phosphines, a Borane, and Olefins. *Angew. Chem. Int. Ed. Engl.* **2007**, *46* (26), 4968–4971.
- (57) Zhang, Y.; Miyake, G. M.; Chen, E. Y.-X. Alane-Based Classical and Frustrated Lewis Pairs in Polymer Synthesis: Rapid Polymerization of MMA and Naturally Renewable Methylene Butyrolactones into High-Molecular-Weight Polymers. *Angew. Chem.* **2010**, *122* (52), 10356–10360.
- (58) Zhang, Y.; Miyake, G. M.; John, M. G.; Falivene, L.; Caporaso, L.; Cavallo, L.; Chen, E. Y.-X. Lewis Pair Polymerization by Classical and Frustrated Lewis Pairs: Acid, Base and Monomer Scope and Polymerization Mechanism. *Dalton Trans.* **2012**, *41* (30), 9119–9134.
- (59) He, J.; Zhang, Y.; Chen, E. Synthesis of Pyridine- and 2-Oxazoline-Functionalized Vinyl Polymers by Alane-Based Frustrated Lewis Pairs. *Synlett* **2014**, *25* (11), 1534–1538.
- (60) Knaus, M. G. M.; Giuman, M. M.; Pöthig, A.; Rieger, B. End of Frustration: Catalytic Precision Polymerization with Highly Interacting Lewis Pairs. *J. Am. Chem. Soc.* **2016**, *138* (24), 7776–7781.
- (61) Maier, A. S.; Thomas, C.; Kränzlein, M.; Pehl, T. M.; Rieger, B. Macromolecular Rhenium–Ruthenium Complexes for Photocatalytic CO₂ Conversion: From Catalytic Lewis Pair Polymerization to Well-Defined Poly(vinyl bipyridine)–Metal Complexes. *Macromolecules* **2022**, *55* (16), 7039–7048.
- (62) Collins, S.; Ward, D. G. Group-Transfer Polymerization Using Cationic Zirconocene Compounds. *J. Am. Chem. Soc.* **1992**, *114* (13), 5460–5462.
- (63) Yasuda, H.; Yamamoto, H.; Yokota, K.; Miyake, S.; Nakamura, A. Synthesis of Monodispersed High Molecular Weight Polymers and Isolation of an organolanthanide(III) Intermediate Coordinated by a Penultimate poly(MMA) Unit. *J. Am. Chem. Soc.* **1992**, *114* (12), 4908–4910.

- (64) Seemann, U. B.; Dengler, J. E.; Rieger, B. High-Molecular-Weight Poly(vinylphosphonate)s by Single-Component Living Polymerization Initiated by Rare-Earth-Metal Complexes. *Angew. Chem. Int. Ed. Engl.* **2010**, *49* (20), 3489–3491.
- (65) Salzinger, S.; Soller, B. S.; Plikhta, A.; Seemann, U. B.; Herdtweck, E.; Rieger, B. Mechanistic Studies on Initiation and Propagation of Rare Earth Metal-Mediated Group Transfer Polymerization of Vinylphosphonates. *J. Am. Chem. Soc.* **2013**, *135* (35), 13030–13040.
- (66) Adams, F.; Machat, M. R.; Altenbuchner, P. T.; Ehrmaier, J.; Pöthig, A.; Karsili, T. N. V.; Rieger, B. Toolbox of Nonmetallocene Lanthanides: Multifunctional Catalysts in Group-Transfer Polymerization. *Inorg. Chem.* **2017**, *56* (16), 9754–9764.
- (67) Chen, E. Y.-X. Coordination Polymerization of Polar Vinyl Monomers by Single-Site Metal Catalysts. *Chem. Rev.* **2009**, *109* (11), 5157–5214.
- (68) Altenbuchner, P. T.; Soller, B. S.; Kissling, S.; Bachmann, T.; Kronast, A.; Vagin, S. I.; Rieger, B. Versatile 2-Methoxyethylaminobis(phenolate)yttrium Catalysts: Catalytic Precision Polymerization of Polar Monomers via Rare Earth Metal-Mediated Group Transfer Polymerization. *Macromolecules* **2014**, *47* (22), 7742–7749.
- (69) Kronast, A.; Reiter, D.; Altenbuchner, P. T.; Vagin, S. I.; Rieger, B. 2-Methoxyethylamino-bis(phenolate)yttrium Catalysts for the Synthesis of Highly Isotactic Poly(2-vinylpyridine) by Rare-Earth Metal-Mediated Group Transfer Polymerization. *Macromolecules* **2016**, *49* (17), 6260–6267.
- (70) Salzinger, S.; Seemann, U. B.; Plikhta, A.; Rieger, B. Poly(vinylphosphonate)s Synthesized by Trivalent Cyclopentadienyl Lanthanide-Induced Group Transfer Polymerization. *Macromolecules* **2011**, *44* (15), 5920–5927.
- (71) Hultsch, K. C.; Spaniol, T. P.; Okuda, J. Half-Sandwich Alkyl and Hydrido Complexes of Yttrium: Convenient Synthesis and Polymerization Catalysis of Polar Monomers. *Angew. Chem. Int. Ed.* **1999**, *38* (1-2), 227–230.
- (72) Yasuda, H.; Ihara, E. Rare Earth Metal Initiated Polymerizations of Polar and Nonpolar Monomers To Give High Molecular Weight Polymers With Extremely Narrow Molecular Weight Distribution. *Macromol. Chem. Phys.* **1995**, *196* (8), 2417–2441.

- (73) Boffa, L. S.; Novak, B. M. Bimetallic samarium(III) Catalysts via Electron Transfer Initiation: The Facile Synthesis of Well-Defined (Meth)acrylate Triblock Copolymers. *Tetrahedron* **1997**, *53* (45), 15367–15396.
- (74) Boffa, L. S.; Novak, B. M. Bimetallic Samarium (III) Initiators for the Living Polymerization of Methacrylates and Lactones. A New Route into Telechelic, Triblock, and "Link-Functionalized" ... *Macromolecules* **1994**, *27*, 6993–6995.
- (75) Zhang, N.; Salzinger, S.; Soller, B. S.; Rieger, B. Rare Earth Metal-Mediated Group-Transfer Polymerization: From Defined Polymer Microstructures to High-Precision Nano-Scaled Objects. *J. Am. Chem. Soc.* **2013**, *135* (24), 8810–8813.
- (76) Duchateau, R.; van Wee, C. T.; Teuben, J. H. Insertion and C–H Bond Activation of Unsaturated Substrates by Bis(benzamidinato)yttrium Alkyl, $[\text{PhC}(\text{NSiMe}_3)_2]_2\text{YR}$ (R = CH₂Ph·THF, CH(SiMe₃)₂), and Hydrido, $\{[\text{PhC}(\text{NSiMe}_3)_2]_2\text{Y}(\mu\text{-H})\}_2$, Compounds. *Organometallics* **1996**, *15* (9), 2291–2302.
- (77) Duchateau, R.; Brussee, E. A. C.; Meetsma, A.; Teuben, J. H. Synthesis and Reactivity of Bis(alkoxysilylamido)yttrium η^2 -Pyridyl and η^2 - α -Picolyll Compounds. *Organometallics* **1997**, *16* (25), 5506–5516.
- (78) Labinger, J. A.; Bercaw, J. E. Understanding and Exploiting C–H Bond Activation. *Nature* **2002**, *417* (6888), 507–514.
- (79) Waterman, R. σ -Bond Metathesis: A 30-Year Retrospective. *Organometallics* **2013**, *32* (24), 7249–7263.
- (80) Thompson, M. E.; Baxter, S. M.; Bulls, A. R.; Burger, B. J.; Nolan, M. C.; Santarsiero, B. D.; Schaefer, W. P.; Bercaw, J. E. σ -Bond Metathesis for Carbon-Hydrogen Bonds of Hydrocarbons and SC-R (R = H, Alkyl, Aryl) Bonds of Permethylscandocene Derivatives. Evidence for Noninvolvement of the π System in Electrophilic Activation of Aromatic and Vinylic C–H Bonds. *J. Am. Chem. Soc.* **1987**, *109*, 203–219.
- (81) Kaneko, H.; Nagae, H.; Tsurugi, H.; Mashima, K. End-Functionalized Polymerization of 2-Vinylpyridine Through Initial C–H Bond Activation of N-Heteroaromatics and Internal Alkynes by Yttrium Ene-Diamido Complexes. *J. Am. Chem. Soc.* **2011**, *133* (49), 19626–19629.

- (82) Soller, B. S.; Salzinger, S.; Jandl, C.; Pöthig, A.; Rieger, B. C–H Bond Activation by σ -Bond Metathesis as a Versatile Route toward Highly Efficient Initiators for the Catalytic Precision Polymerization of Polar Monomers. *Organometallics* **2015**, *34* (11), 2703–2706.
- (83) Altenbuchner, P. T.; Werz, P. D. L.; Schöppner, P.; Adams, F.; Kronast, A.; Schwarzenböck, C.; Pöthig, A.; Jandl, C.; Haslbeck, M.; Rieger, B. Next Generation Multiresponsive Nanocarriers for Targeted Drug Delivery to Cancer Cells. *Chemistry* **2016**, *22* (41), 14576–14584.
- (84) Xu, T.; Liu, J.; Lu, X.-B. Highly Active Half-Metallocene Yttrium Catalysts for Living and Chemoselective Polymerization of Allyl Methacrylate. *Macromolecules* **2015**, *48* (20), 7428–7434.
- (85) Xu, T.-Q.; Liu, J.-H.; Liu, Y. Half-Metallocene Complexes of Yttrium With Amidinate Ligands: Monoalkyl Yttrium Formation and C–H Bond Activation. *Polyhedron* **2016**, *113*, 50–54.
- (86) Weger, M.; Pahl, P.; Schmidt, F.; Soller, B. S.; Altmann, P. J.; Pöthig, A.; Gemmecker, G.; Eisenreich, W.; Rieger, B. Isospecific Group-Transfer Polymerization of Diethyl Vinylphosphonate and Multidimensional NMR Analysis of the Polymer Microstructure. *Macromolecules* **2019**, *52* (18), 7073–7080.
- (87) Cai, C.-X.; Toupet, L.; Lehmann, C. W.; Carpentier, J.-F. Synthesis, Structure and Reactivity of New Yttrium Bis(dimethylsilyl)amido and Bis(trimethylsilyl)methyl Complexes of a Tetradentate Bis(phenoxide) Ligand. *J. Organomet. Chem.* **2003**, *683* (1), 131–136.
- (88) Cui, C.; Shafir, A.; Reeder, C. L.; Arnold, J. Highly Isospecific Polymerization of Methyl Methacrylate with a Bis(pyrrolylaldiminato)samarium Hydrocarbyl Complex. *Organometallics* **2003**, *22* (17), 3357–3359.
- (89) Guillaume, S. M.; Brignou, P.; Susperregui, N.; Maron, L.; Kuzdrowska, M.; Roesky, P. W. Bis(phosphinimino)methanide Borohydride Complexes of the Rare-Earth Elements as Initiators for the Polymerization of Methyl Methacrylate: Combined Experimental and Computational Investigations. *Polym. Chem.* **2011**, *2* (8), 1728.
- (90) Xu, T.-Q.; Yang, G.-W.; Lu, X.-B. Highly Isotactic and High-Molecular-Weight Poly(2-vinylpyridine) by Coordination Polymerization with Yttrium Bis(phenolate) Ether Catalysts. *ACS Catal.* **2016**, *6* (8), 4907–4913.

- (91) Ihara, E.; Morimoto, M.; Yasuda, H. Living Polymerizations and Copolymerizations of Alkyl Acrylates by the Unique Catalysis of Rare Earth Metal Complexes. *Macromolecules* **1995**, *28* (23), 7886–7892.
- (92) Yasuda, H.; Yamamoto, H.; Yamashita, M.; Yokota, K.; Nakamura, A.; Miyake, S.; Kai, Y.; Kanehisa, N. Synthesis of High Molecular Weight Poly(methyl Methacrylate) With Extremely Low Polydispersity by the Unique Function of organolanthanide(III) Complexes. *Macromolecules* **1993**, *26* (26), 7134–7143.
- (93) Zhang, N.; Salzinger, S.; Rieger, B. Poly(vinylphosphonate)s with Widely Tunable LCST: A Promising Alternative to Conventional Thermoresponsive Polymers. *Macromolecules* **2012**, *45* (24), 9751–9758.
- (94) Tomasi, S.; Weiss, H.; Ziegler, T. Group Transfer Polymerizations of Acrylates Catalyzed by Mononuclear Early d-Block and f-Block Metallocenes: A DFT Study. *Organometallics* **2006**, *25* (15), 3619–3630.
- (95) Soller, B. S.; Sun, Q.; Salzinger, S.; Jandl, C.; Pöthig, A.; Rieger, B. Ligand Induced Steric Crowding in Rare Earth Metal-Mediated Group Transfer Polymerization of Vinylphosphonates: Does Enthalpy Matter? *Macromolecules* **2016**, *49* (5), 1582–1589.
- (96) Halama, K.; Schaffer, A.; Rieger, B. Allyl Group-Containing Polyvinylphosphonates as a Flexible Platform for the Selective Introduction of Functional Groups via Polymer-Analogous Transformations. *RSC Adv.* **2021**, *11* (61), 38555–38564.
- (97) Soller, B. S.; Salzinger, S.; Rieger, B. Rare Earth Metal-Mediated Precision Polymerization of Vinylphosphonates and Conjugated Nitrogen-Containing Vinyl Monomers. *Chem. Rev.* **2016**, *116* (4), 1993–2022.
- (98) Lanzinger, D.; Salzinger, S.; Soller, B. S.; Rieger, B. Poly(vinylphosphonate)s as Macromolecular Flame Retardants for Polycarbonate. *Ind. Eng. Chem. Res.* **2015**, *54* (6), 1703–1712.
- (99) Mariott, W. R.; Chen, E. Y.-X. Mechanism and Scope of Stereospecific, Coordinative-Anionic Polymerization of Acrylamides by Chiral Zirconocenium Ester and Amide Enolates. *Macromolecules* **2005**, *38* (16), 6822–6832.
- (100) Adams, F.; Altenbuchner, P. T.; Werz, P. D. L.; Rieger, B. Multiresponsive Micellar Block Copolymers From 2-Vinylpyridine and Dialkylvinylphosphonates With

a Tunable Lower Critical Solution Temperature. *RSC Adv.* **2016**, 6 (82), 78750–78754.

(101) Saurwein, A.; Schaffer, A.; Wieser, C.; Rieger, B. Synthesis, Characterisation and Functionalisation of BAB-Type Dual-Responsive Nanocarriers for Targeted Drug Delivery: Evolution of Nanoparticles Based on 2-Vinylpyridine and Diethyl Vinylphosphonate. *RSC Adv.* **2021**, 11 (3), 1586–1594.

(102) Schwarzenböck, C.; Nelson, P. J.; Huss, R.; Rieger, B. Synthesis of Next Generation Dual-Responsive Cross-Linked Nanoparticles and Their Application to Anti-Cancer Drug Delivery. *Nanoscale* **2018**, 10 (34), 16062–16068.

(103) Weingarten, P.; Lin, M. T.-Y.; Kränzlein, M.; Fietz, A.; Kachel, I.; Hurst, J.; Schnichels, S.; Adams, F. Phosphorous-Containing, Amphiphilic ABB' Copolymers As siRNA Nanocarriers With Enhanced Stability, Reduced In Vitro Cytotoxicity, and Efficient Knockdown Ability for the Treatment of Ocular Diseases. *RSC Appl. Polym.* **2025**.

(104) Halama, K.; Lin, M. T.-Y.; Schaffer, A.; Foith, M.; Adams, F.; Rieger, B. Cytocompatible Triblock Copolymers with Controlled Microstructure Enabling Orthogonally Functionalized Bio-polymer Conjugates. *Macromolecules* **2024**, 57 (4), 1438–1447.

(105) Schwarzenböck, C.; Vagin, S. I.; Heinz, W. R.; Nelson, P. J.; Rieger, B. Studies on the Biocompatibility of Poly(diethyl vinyl-phosphonate) with a New Fluorescent Marker. *Macromol. Rapid Commun.* **2018**, 39 (15), e1800259.

(106) Adams, F.; Pschenitzka, M.; Rieger, B. Yttrium-Catalyzed Synthesis of Bipyridine-Functionalized AB-Block Copolymers: Micellar Support for Photocatalytic Active Rhenium-Complexes. *ChemCatChem* **2018**, 10 (19), 4309–4316.

(107) Lovison, D.; Weingarten, P.; Sebeschuk, A.; Rieger, B.; Casini, A. Micellar Transfer Hydrogenation Catalysis in Water with Monocarbonyl Ruthenium(II)-poly(vinylphosphonate)-Containing Polymers: Achieving Reduction of Biomass-Derived Aldehydes. *ACS Appl. Polym. Mater.* **2024**, 6 (22), 13855–13864.

(108) Kränzlein, M.; Pehl, T. M.; Halama, K.; Großmann, P. F.; Kratky, T.; Mühlbach, A. M.; Rieger, B. Azide-Modified Poly(diethyl vinylphosphonate) for Straightforward Graft-to Carbon Nanotube Functionalization. *Macromol. Mater. Eng.* **2023**, 308 (6).

- (109) Schwarzenböck, C.; Schaffer, A.; Pahl, P.; Nelson, P. J.; Huss, R.; Rieger, B. Precise Synthesis of Thermoresponsive Polyvinylphosphonate-Biomolecule Conjugates via Thiol–Ene Click Chemistry. *Polym. Chem.* **2018**, *9* (3), 284–290.
- (110) Schaffer, A.; Kränzlein, M.; Rieger, B. Precise Synthesis of Poly(dimethylsiloxane) Copolymers through C–H Bond-Activated Macroinitiators via Yttrium-Mediated Group Transfer Polymerization and Ring-Opening Polymerization. *Macromolecules* **2020**, *53* (19), 8382–8392.
- (111) Schaffer, A.; Kränzlein, M.; Rieger, B. Synthesis and Application of Functional Group-Bearing Pyridyl-Based Initiators in Rare Earth Metal-Mediated Group Transfer Polymerization. *Macromolecules* **2020**, *53* (11), 4345–4354.
- (112) Pehl, T. M.; Kränzlein, M.; Adams, F.; Schaffer, A.; Rieger, B. C–H Bond Activation of Silyl-Substituted Pyridines with Bis(Phenolate)Yttrium Catalysts as a Facile Tool towards Hydroxyl-Terminated Michael-Type Polymers. *Catalysts* **2020**, *10* (4), 448.
- (113) Weingarten, P.; Thomas, S. R.; Luiza de Andrade Querino, A.; Halama, K.; Kränzlein, M.; Casini, A.; Rieger, B. A Graft-To Strategy of Poly(vinylphosphonates) on Dopazide-Coated Gold Nanoparticles Using In Situ Catalyst Activation. *RSC Adv.* **2024**, *14* (12), 8145–8149.
- (114) Gauthier, M. A.; Gibson, M. I.; Klok, H.-A. Synthesis of Functional Polymers by Post-Polymerization Modification. *Angew. Chem. Int. Ed.* **2009**, *48* (1), 48–58.
- (115) Posner, T. Beiträge zur Kenntniss der ungesättigten Verbindungen. II. Ueber die Addition von Mercaptanen an ungesättigte Kohlenwasserstoffe. *Ber. Dtsch. Chem. Ges.* **1905**, *38* (1), 646–657.
- (116) Morgan, C. R.; Magnotta, F.; Ketley, A. D. Thiol/Ene Photocurable Polymers. *J. Polym. Sci. Polym. Chem. Ed.* **1977**, *15* (3), 627–645.
- (117) Kade, M. J.; Burke, D. J.; Hawker, C. J. The Power of Thiol-Ene Chemistry. *J. Polym. Sci. A Polym. Chem.* **2010**, *48* (4), 743–750.
- (118) Hoyle, C. E.; Lee, T. Y.; Roper, T. Thiol–Enes: Chemistry of the Past With Promise for the Future. *J. Polym. Sci. A Polym. Chem.* **2004**, *42* (21), 5301–5338.
- (119) Hoyle, C. E.; Bowman, C. N. Thiol-Ene Click Chemistry. *Angew. Chem., Int. Ed.* **2010**, *49* (9), 1540–1573.

- (120) Lowe, A. B. Thiol–Ene “Click” Reactions and Recent Applications in Polymer and Materials Synthesis: A First Update. *Polym. Chem.* **2014**, *5* (17), 4820–4870.
- (121) Lowe, A. B. Thiol-Ene “Click” Reactions and Recent Applications in Polymer and Materials Synthesis. *Polym. Chem.* **2010**, *1* (1), 17–36.
- (122) Błażewska, K. M. McKenna Reaction–Which Oxygen Attacks Bromotrimethylsilane? *J. Org. Chem.* **2014**, *79* (1), 408–412.
- (123) Späth, F.; Maier, A. S.; Stasi, M.; Bergmann, A. M.; Halama, K.; Wenisch, M.; Rieger, B.; Boekhoven, J. The Role of Chemically Innocent Polyanions in Active, Chemically Fueled Complex Coacervate Droplets. *Angew. Chem., Int. Ed.* **2023**, *62* (41), e202309318.
- (124) Sing, C. E.; Perry, S. L. Recent Progress in the Science of Complex Coacervation. *Soft matter* **2020**, *16* (12), 2885–2914.
- (125) Zhou, L.; Shi, H.; Li, Z.; He, C. Recent Advances in Complex Coacervation Design from Macromolecular Assemblies and Emerging Applications. *Macromol. Rapid Commun.* **2020**, *41* (21), e2000149.
- (126) Jin, F.-L.; Li, X.; Park, S.-J. Synthesis and Application of Epoxy Resins: A Review. *J. Ind. Eng. Chem.* **2015**, *29*, 1–11.
- (127) Chruściel, J. J. Modifications of Textile Materials with Functional Silanes, Liquid Silicone Softeners, and Silicone Rubbers-A Review. *Polymers* **2022**, *14* (20).
- (128) Akindoyo, J. O.; Beg, M. D. H.; Ghazali, S.; Islam, M. R.; Jeyaratnam, N.; Yuvaraj, A. R. Polyurethane Types, Synthesis and Applications – a Review. *RSC Adv.* **2016**, *6* (115), 114453–114482.
- (129) Catoira, M. C.; Fusaro, L.; Di Francesco, D.; Ramella, M.; Boccafoschi, F. Overview of Natural Hydrogels for Regenerative Medicine Applications. *J. Mater. Sci.: Mater. Med.* **2019**, *30* (10), 115.
- (130) Hamerton, I.; Mooring, L. The Use of Thermosets in Aerospace Applications. In *Thermosets*; Elsevier, 2012; pp 189–227. DOI: 10.1533/9780857097637.2.189.
- (131) Hennink, W. E.; van Nostrum, C. F. Novel crosslinking methods to design Novel Crosslinking Methods To Design Hydrogels. *Adv. Drug Deliv. Rev.* **2012**, *64*, 223–236.

- (132) Ho, T.-C.; Chang, C.-C.; Chan, H.-P.; Chung, T.-W.; Shu, C.-W.; Chuang, K.-P.; Duh, T.-H.; Yang, M.-H.; Tyan, Y.-C. Hydrogels: Properties and Applications in Biomedicine. *Molecules* **2022**, *27* (9).
- (133) Kloxin, C. J.; Bowman, C. N. Covalent Adaptable Networks: Smart, Reconfigurable and Responsive Network Systems. *Chem. Soc. Rev.* **2013**, *42* (17), 7161–7173.
- (134) Madduma-Bandarage, U. S. K.; Madihally, S. V. Synthetic Hydrogels: Synthesis, Novel Trends, and Applications. *J. Appl. Polym. Sci.* **2021**, *138* (19).
- (135) Rowan, S. J.; Cantrill, S. J.; Cousins, G. R. L.; Sanders, J. K. M.; Stoddart, J. F. Dynamic Covalent Chemistry. *Angew. Chem. Int. Ed.* **2002**, *41* (6), 898–952.
- (136) Scheutz, G. M.; Lessard, J. J.; Sims, M. B.; Sumerlin, B. S. Adaptable Crosslinks in Polymeric Materials: Resolving the Intersection of Thermoplastics and Thermosets. *J. Am. Chem. Soc.* **2019**, *141* (41), 16181–16196.
- (137) Tang, Y.; Xu, W.; Niu, S.; Zhang, Z.; Zhang, Y.; Jiang, Z. Crosslinked Dielectric Materials for High-Temperature Capacitive Energy Storage. *J. Mater. Chem. A* **2021**, *9* (16), 10000–10011.
- (138) Wemyss, A. M.; Bowen, C.; Plesse, C.; Vancaeyzeele, C.; Nguyen, G. T.; Vidal, F.; Wan, C. Dynamic Crosslinked Rubbers for a Green Future: A Material Perspective. *Mater. Sci. Eng. R Rep.* **2020**, *141*, 100561.
- (139) Fu, J.; Het Panhuis, M. in Hydrogel Properties and Applications. *J. Mater. Chem. B* **2019**, *7* (10), 1523–1525.
- (140) Chang, C.; Duan, B.; Cai, J.; Zhang, L. Superabsorbent Hydrogels Based on Cellulose for Smart Swelling and Controllable Delivery. *Eur. Polym. J.* **2010**, *46* (1), 92–100.
- (141) Chen, F.; Lu, S.; Zhu, L.; Tang, Z.; Wang, Q.; Qin, G.; Yang, J.; Sun, G.; Zhang, Q.; Chen, Q. Conductive Regenerated Silk-Fibroin-Based Hydrogels With Integrated High Mechanical Performances. *J. Mater. Chem. B* **2019**, *7* (10), 1708–1715.
- (142) Du, H.; Zha, G.; Gao, L.; Wang, H.; Li, X.; Shen, Z.; Zhu, W. Fully Biodegradable Antibacterial Hydrogels via Thiol–Ene “Click” Chemistry. *Polym. Chem.* **2014**, *5* (13), 4002–4008.

- (143) Ibrahim, S. M.; El Salmawi, K. M.; Zahran, A. H. Synthesis of Crosslinked Superabsorbent Carboxymethyl Cellulose/Acrylamide Hydrogels Through Electron-Beam Irradiation. *J. Appl. Polym. Sci.* **2007**, *104* (3), 2003–2008.
- (144) Koetting, M. C.; Peters, J. T.; Steichen, S. D.; Peppas, N. A. Stimulus-Responsive Hydrogels: Theory, Modern Advances, and Applications. *Mater. Sci. Eng. R Rep.* **2015**, *93*, 1–49.
- (145) Li, P.; Poon, Y. F.; Li, W.; Zhu, H.-Y.; Yeap, S. H.; Cao, Y.; Qi, X.; Zhou, C.; Lamrani, M.; Beuerman, R. W.; Kang, E.-T.; Mu, Y.; Li, C. M.; Chang, M. W.; Leong, S. S. J.; Chan-Park, M. B. A Polycationic Antimicrobial and Biocompatible Hydrogel With Microbe Membrane Suctioning Ability. *Nat. Mater.* **2011**, *10* (2), 149–156.
- (146) Augst, A. D.; Kong, H. J.; Mooney, D. J. Alginate Hydrogels As Biomaterials. *Macromol. Biosci.* **2006**, *6* (8), 623–633.
- (147) Fu, J.; Yang, F.; Guo, Z. The Chitosan Hydrogels: From Structure To Function. *New J. Chem.* **2018**, *42* (21), 17162–17180.
- (148) Zarrintaj, P.; Manouchehri, S.; Ahmadi, Z.; Saeb, M. R.; Urbanska, A. M.; Kaplan, D. L.; Mozafari, M. Agarose-Based Biomaterials for Tissue Engineering. *Carbohydr. Polym.* **2018**, *187*, 66–84.
- (149) Burdick, J. A.; Prestwich, G. D. Hyaluronic Acid Hydrogels for Biomedical Applications. *Adv. Mater.* **2011**, *23* (12), H41-56.
- (150) Chang, C.; Zhang, L. Cellulose-Based Hydrogels: Present Status and Application Prospects. *Carbohydr. Polym.* **2011**, *84* (1), 40–53.
- (151) Tan, H.; DeFail, A. J.; Rubin, J. P.; Chu, C. R.; Marra, K. G. Novel Multiarm PEG-Based Hydrogels for Tissue Engineering. *J. Biomed. Mater. Res. A* **2010**, *92* (3), 979–987.
- (152) Yang, T.; Malkoch, M.; Hult, A. Sequential Interpenetrating Poly(ethylene Glycol) Hydrogels Prepared by UV-Initiated Thiol–Ene Coupling Chemistry. *J. Polym. Sci. A Polym. Chem.* **2013**, *51* (2), 363–371.
- (153) Millon, L. E.; Mohammadi, H.; Wan, W. K. Anisotropic Polyvinyl Alcohol Hydrogel for Cardiovascular Applications. *J. Biomed. Mater. Res. B* **2006**, *79* (2), 305–311.

- (154) Wang, M.; Bai, J.; Shao, K.; Tang, W.; Zhao, X.; Lin, D.; Huang, S.; Chen, C.; Ding, Z.; Ye, J. Poly(vinyl alcohol) Hydrogels: The Old and New Functional Materials. *Int. J. Polym. Sci.* **2021**, *2021*, 1–16.
- (155) Nho, Y.-C.; Park, J.-S.; Lim, Y.-M. Preparation of Poly(acrylic acid) Hydrogel by Radiation Crosslinking and Its Application for Mucoadhesives. *Polymers* **2014**, *6* (3), 890–898.
- (156) Zhou, X.; Weng, L.; Chen, Q.; Zhang, J.; Shen, D.; Li, Z.; Shao, M.; Xu, J. Investigation of pH Sensitivity of Poly(acrylic Acid- Co -Acrylamide) Hydrogel. *Polym. Int.* **2003**, *52* (7), 1153–1157.
- (157) Patenaude, M.; Hoare, T. Injectable, Degradable Thermoresponsive Poly(N-isopropylacrylamide) Hydrogels. *ACS Macro Lett.* **2012**, *1* (3), 409–413.
- (158) Lanzalaco, S.; Mingot, J.; Torras, J.; Alemán, C.; Armelin, E. Recent Advances in Poly(N -isopropylacrylamide) Hydrogels and Derivatives as Promising Materials for Biomedical and Engineering Emerging Applications. *Adv. Eng. Mater.* **2023**, *25* (4).
- (159) Kolb, H. C.; Finn, M. G.; Sharpless, K. B. Click Chemistry: Diverse Chemical Function from a Few Good Reactions. *Angew. Chem. Int. Ed.* **2001**, *40* (11), 2004–2021.
- (160) Jiang, Y.; Chen, J.; Deng, C.; Suuronen, E. J.; Zhong, Z. Click Hydrogels, Microgels and Nanogels: Emerging Platforms for Drug Delivery and Tissue Engineering. *Biomaterials* **2014**, *35* (18), 4969–4985.
- (161) Reddy, S. K.; Anseth, K. S.; Bowman, C. N. Modeling of Network Degradation in Mixed Step-Chain Growth Polymerizations. *Polymer* **2005**, *46* (12), 4212–4222.
- (162) Rydholm, A. E.; Bowman, C. N.; Anseth, K. S. Degradable Thiol-Acrylate Photopolymers: Polymerization and Degradation Behavior of an In Situ Forming Biomaterial. *Biomaterials* **2005**, *26* (22), 4495–4506.
- (163) Zhu, L.; Zimudzi, T. J.; Li, N.; Pan, J.; Lin, B.; Hickner, M. A. Crosslinking of Comb-Shaped Polymer Anion Exchange Membranes via Thiol–Ene Click Chemistry. *Polym. Chem.* **2016**, *7* (14), 2464–2475.
- (164) Li, K. W.; Cen, L.; Zhou, C.; Zhang, A. K.; Yao, F.; Tan, L. H.; Xu, L. Q.; Fu, G. D. Well-Defined Poly(ethylene glycol) Hydrogels with Enhanced Mechanical Performance Prepared by Thermally Induced Copper-Catalyzed Azide–Alkyne Cycloaddition. *Macromol. Mater. Eng.* **2016**, *301* (11), 1374–1382.

- (165) Singh, G.; Majeed, A.; Singh, R.; George, N.; Singh, G.; Gupta, S.; Singh, H.; Kaur, G.; Singh, J. CuAAC Ensembled 1,2, 3-Triazole Linked Nanogels for Targeted Drug Delivery: A Review. *RSC Adv.* **2023**, *13* (5), 2912–2936.
- (166) Kuru, E. A.; Orakdogan, N.; Okay, O. Preparation of Homogeneous Polyacrylamide Hydrogels by Free-Radical Crosslinking Copolymerization. *Eur. Polym. J.* **2007**, *43* (7), 2913–2921.
- (167) Dai, X.; Chen, X.; Yang, L.; Foster, S.; Coury, A. J.; Jozefiak, T. H. Free Radical Polymerization of Poly(ethylene Glycol) Diacrylate Macromers: Impact of Macromer Hydrophobicity and Initiator Chemistry on Polymerization Efficiency. *Acta Biomater.* **2011**, *7* (5), 1965–1972.
- (168) Bencherif, S. A.; Siegwart, D. J.; Srinivasan, A.; Horkay, F.; Hollinger, J. O.; Washburn, N. R.; Matyjaszewski, K. Nanostructured hybrid hydrogels prepared by a combination of atom transfer radical polymerization and free radical polymerization. *Biomaterials* **2009**, *30* (29), 5270–5278.
- (169) Wilems, T. S.; Lu, X.; Kurosu, Y. E.; Khan, Z.; Lim, H. J.; Smith Callahan, L. A. Effects of Free Radical Initiators on Polyethylene Glycol Dimethacrylate Hydrogel Properties and Biocompatibility. *J. Biomed. Mater. Res. A* **2017**, *105* (11), 3059–3068.
- (170) Han, C.; Cao, M.; Yu, J.; Wang, S.; Zhou, X.; Chen, Y.; Yang, F. Carboxymethyl Cellulose-Based Composite Polymer Hydrogels Cross-Linked with Epichlorohydrin and Application for Cu(II) Removal. *ACS Appl. Polym. Mater.* **2023**, *5* (3), 2070–2078.
- (171) Bo, J. Study on PVA Hydrogel Crosslinked by Epichlorohydrin. *J. Appl. Polym. Sci.* **1992**, *46* (5), 783–786.
- (172) Mansur, H. S.; Sadahira, C. M.; Souza, A. N.; Mansur, A. A. FTIR Spectroscopy Characterization of Poly (Vinyl Alcohol) Hydrogel With Different Hydrolysis Degree and Chemically Crosslinked With Glutaraldehyde. *Mater. Sci. Eng. C* **2008**, *28* (4), 539–548.
- (173) Tian, Z.; Liu, W.; Li, G. The Microstructure and Stability of Collagen Hydrogel Cross-Linked by Glutaraldehyde. *Polym. Degrad. Stab.* **2016**, *130*, 264–270.

- (174) Yang, J.; Ding, C.; Huang, L.; Zhang, M.; Chen, L. The Preparation of Poly(γ -Glutamic Acid)-NHS Ester as a Natural Cross-Linking Agent of Collagen. *Int. J. Biol. Macromol.* **2017**, *97*, 1–7.
- (175) Wang, P.; Zhu, Y.; Feng, L.; Wang, Y.; Bu, Y. Rapidly Self-Deactivating and Injectable Succinyl Ester-Based Bioadhesives for Postoperative Antiadhesion. *ACS Appl. Mater. Interfaces* **2022**, *14* (1), 373–382.
- (176) Badali, E.; Hosseini, M.; Mohajer, M.; Hassanzadeh, S.; Saghati, S.; Hilborn, J.; Khanmohammadi, M. Enzymatic Crosslinked Hydrogels for Biomedical Application. *Polym. Sci. Ser. A* **2021**, *63* (S1), S1-S22.
- (177) Hu, B.-H.; Messersmith, P. B. Rational Design of Transglutaminase Substrate Peptides for Rapid Enzymatic Formation of Hydrogels. *J. Am. Chem. Soc.* **2003**, *125* (47), 14298–14299.
- (178) Yang, Z.; Liang, G.; Wang, L.; Xu, B. Using a Kinase/Phosphatase Switch To Regulate a Supramolecular Hydrogel and Forming the Supramolecular Hydrogel In Vivo. *J. Am. Chem. Soc.* **2006**, *128* (9), 3038–3043.
- (179) Khan, M. J.; Zhang, J.; Guo, Q. Covalent/Crystallite Cross-Linked Co-Network Hydrogels: An Efficient and Simple Strategy for Mechanically Strong and Tough Hydrogels. *Chem. Eng. J.* **2016**, *301*, 92–102.
- (180) Yang, Y.; Wang, X.; Yang, F.; Wang, L.; Wu, D. Highly Elastic and Ultratough Hybrid Ionic-Covalent Hydrogels with Tunable Structures and Mechanics. *Adv. Mater.* **2018**, *30* (18), e1707071.
- (181) Elnashar, M. M. M.; Yassin, M. A.; Kahil, T. Novel Thermally and Mechanically Stable Hydrogel for Enzyme Immobilization of Penicillin G Acylase via Covalent Technique. *J. Appl. Polym. Sci.* **2008**, *109* (6), 4105–4111.
- (182) Han, Z.; Lu, Y.; Qu, S. Design of Fatigue-Resistant Hydrogels. *Adv. Funct. Mater.* **2024**, *34* (21).
- (183) Lee, F.; Chung, J. E.; Xu, K.; Kurisawa, M. Injectable Degradation-Resistant Hyaluronic Acid Hydrogels Cross-Linked via the Oxidative Coupling of Green Tea Catechin. *ACS Macro Lett.* **2015**, *4* (9), 957–960.
- (184) Zhai, Y.; Meng, X.; Duan, H.; Ding, Z.; Liu, Y.; Lucia, L. Super Stable and Tough Hydrogel Containing Covalent, Crystalline, and Ionic Cross-Links. *Macromol. Chem. Phys.* **2016**, *217* (1), 32–38.

- (185) Siboro, S. A. P.; Anugrah, D. S. B.; Ramesh, K.; Park, S.-H.; Kim, H.-R.; Lim, K. T. Tunable Porosity of Covalently Crosslinked Alginate-Based Hydrogels and Its Significance in Drug Release Behavior. *Carbohydr. Polym.* **2021**, *260*, 117779.
- (186) Yang, Q.; Feng, S.; Guo, J.; Guan, F.; Zhang, S.; Sun, J.; Zhang, Y.; Xu, Y.; Zhang, X.; Da Bao; He, J. Construction of Chitosan/Alginate Aerogels With Three-Dimensional Hierarchical Pore Network Structure via Hydrogen Bonding Dissolution and Covalent Crosslinking Synergistic Strategy for Thermal Management Systems. *Int. J. Biol. Macromol.* **2024**, *275* (Pt 2), 133367.
- (187) Bi, L.; Godwin, B.; Baran, M. J.; Nazir, R.; Wulff, J. E. A Cleavable Crosslinking Strategy for Commodity Polymer Functionalization and Generation of Reprocessable Thermosets. *Angew. Chem.* **2023**, *135* (30).
- (188) Shahi, S.; Roghani-Mamaqani, H.; Talebi, S.; Mardani, H. Chemical Stimuli-Induced Reversible Bond Cleavage in Covalently Crosslinked Hydrogels. *Coord. Chem. Rev.* **2022**, *455*, 214368.
- (189) Shahi, S.; Roghani-Mamaqani, H.; Talebi, S.; Mardani, H. Stimuli-Responsive Destructible Polymeric Hydrogels Based on Irreversible Covalent Bond Dissociation. *Polym. Chem.* **2022**, *13* (2), 161–192.
- (190) Hu, X.; Vatankhah-Varnoosfaderani, M.; Zhou, J.; Li, Q.; Sheiko, S. S. Weak Hydrogen Bonding Enables Hard, Strong, Tough, and Elastic Hydrogels. *Adv. Mater.* **2015**, *27* (43), 6899–6905.
- (191) Song, G.; Zhang, L.; He, C.; Fang, D.-C.; Whitten, P. G.; Wang, H. Facile Fabrication of Tough Hydrogels Physically Cross-Linked by Strong Cooperative Hydrogen Bonding. *Macromolecules* **2013**, *46* (18), 7423–7435.
- (192) Kwon, H. J.; Yasuda, K.; Gong, J. P.; Ohmiya, Y. Polyelectrolyte Hydrogels for Replacement and Regeneration of Biological Tissues. *Macromol. Res.* **2014**, *22* (3), 227–235.
- (193) Lee, C.-J.; Wu, H.; Hu, Y.; Young, M.; Wang, H.; Lynch, D.; Xu, F.; Cong, H.; Cheng, G. Ionic Conductivity of Polyelectrolyte Hydrogels. *ACS Appl. Mater. Interfaces* **2018**, *10* (6), 5845–5852.
- (194) Wang, G.; Liu, Y.; Zu, B.; Da Lei; Guo, Y.; Wang, M.; Dou, X. Reversible Adhesive Hydrogel With Enhanced Sampling Efficiency Boosted by Hydrogen Bond

- and Van der Waals Force for Visualized Detection. *Chem. Eng. J.* **2023**, *455*, 140493.
- (195) Tuncaboylu, D. C.; Sari, M.; Oppermann, W.; Okay, O. Tough and Self-Healing Hydrogels Formed via Hydrophobic Interactions. *Macromolecules* **2011**, *44* (12), 4997–5005.
- (196) Tuncaboylu, D. C.; Argun, A.; Sahin, M.; Sari, M.; Okay, O. Structure Optimization of Self-Healing Hydrogels Formed via Hydrophobic Interactions. *Polymer* **2012**, *53* (24), 5513–5522.
- (197) Chen, Y.; Pang, X.-H.; Dong, C.-M. Dual Stimuli-Responsive Supramolecular Polypeptide-Based Hydrogel and Reverse Micellar Hydrogel Mediated by Host–Guest Chemistry. *Adv. Funct. Mater.* **2010**, *20* (4), 579–586.
- (198) Mantooth, S. M.; Munoz-Robles, B. G.; Webber, M. J. Dynamic Hydrogels from Host-Guest Supramolecular Interactions. *Macromol. Biosci.* **2019**, *19* (1), e1800281.
- (199) Ji, S.; Li, X.; Wang, S.; Li, H.; Duan, H.; Yang, X.; Lv, P. Physically Entangled Antiswelling Hydrogels with High Stiffness. *Macromol. Rapid Commun.* **2022**, *43* (19), e2200272.
- (200) Puza, F.; Zheng, Y.; Han, L.; Xue, L.; Cui, J. Physical Entanglement Hydrogels: Ultrahigh Water Content but Good Toughness and Stretchability. *Polym. Chem.* **2020**, *11* (13), 2339–2345.
- (201) Shao, C.; Chang, H.; Wang, M.; Xu, F.; Yang, J. High-Strength, Tough, and Self-Healing Nanocomposite Physical Hydrogels Based on the Synergistic Effects of Dynamic Hydrogen Bond and Dual Coordination Bonds. *ACS Appl. Mater. Interfaces* **2017**, *9* (34), 28305–28318.
- (202) Chang, X.; Geng, Y.; Cao, H.; Zhou, J.; Tian, Y.; Shan, G.; Bao, Y.; Wu, Z. L.; Pan, P. Dual-Crosslink Physical Hydrogels with High Toughness Based on Synergistic Hydrogen Bonding and Hydrophobic Interactions. *Macromol. Rapid Commun.* **2018**, *39* (14), e1700806.
- (203) Bernhard, S.; Tibbitt, M. W. Supramolecular Engineering of Hydrogels for Drug Delivery. *Adv. Drug Deliv. Rev.* **2021**, *171*, 240–256.
- (204) Lim, J.; Lin, Q.; Xue, K.; Loh, X. J. Recent Advances in Supramolecular Hydrogels for Biomedical Applications. *Mater. Today Adv.* **2019**, *3*, 100021.

- (205) Taylor, D. L.; Het Panhuis, M. in. Self-Healing Hydrogels. *Adv. Mater.* **2016**, *28* (41), 9060–9093.
- (206) Yang, Y.; Ding, X.; Urban, M. W. Chemical and Physical Aspects of Self-Healing Materials. *Prog. Polym. Sci.* **2015**, *49-50*, 34–59.
- (207) Wang, D.; Xia, Y.; Zhang, D.; Sun, X.; Chen, X.; Oliver, S.; Shi, S.; Lei, L. Hydrogen-Bonding Reinforced Injectable Hydrogels: Application As a Thermo-Triggered Drug Controlled-Release System. *ACS Appl. Polym. Mater.* **2020**, *2* (4), 1587–1596.
- (208) Zhang, G.; Ngai, T.; Deng, Y.; Wang, C. An Injectable Hydrogel with Excellent Self-Healing Property Based on Quadruple Hydrogen Bonding. *Macromol. Chem. Phys.* **2016**, *217* (19), 2172–2181.
- (209) Shigemitsu, H.; Fujisaku, T.; Onogi, S.; Yoshii, T.; Ikeda, M.; Hamachi, I. Preparation of Supramolecular Hydrogel-Enzyme Hybrids Exhibiting Biomolecule-Responsive Gel Degradation. *Nat. Protoc.* **2016**, *11* (9), 1744–1756.
- (210) Tran, N. Q.; Joung, Y. K.; Lih, E.; Park, K. M.; Park, K. D. Supramolecular Hydrogels Exhibiting Fast In Situ Gel Forming and Adjustable Degradation Properties. *Biomacromolecules* **2010**, *11* (3), 617–625.
- (211) Appel, E. A.; Loh, X. J.; Jones, S. T.; Dreiss, C. A.; Scherman, O. A. Sustained Release of Proteins From High Water Content Supramolecular Polymer Hydrogels. *Biomaterials* **2012**, *33* (18), 4646–4652.
- (212) Appel, E. A.; Loh, X. J.; Jones, S. T.; Biedermann, F.; Dreiss, C. A.; Scherman, O. A. Ultrahigh-Water-Content Supramolecular Hydrogels Exhibiting Multistimuli Responsiveness. *J. Am. Chem. Soc.* **2012**, *134* (28), 11767–11773.
- (213) Lu, H.; Li, M.; Wang, X.; Wang, Z.; Pi, M.; Cui, W.; Ran, R. Recyclable Physical Hydrogels As Durable and Efficient Solar-Driven Evaporators. *Chem. Eng. J.* **2022**, *450*, 138257.
- (214) Liu, X.; Li, Y.; Fang, X.; Zhang, Z.; Li, S.; Sun, J. Healable and Recyclable Polymeric Materials with High Mechanical Robustness. *ACS Mater. Lett.* **2022**, *4* (4), 554–571.
- (215) Ghobril, C.; Grinstaff, M. W. The Chemistry and Engineering of Polymeric Hydrogel Adhesives for Wound Closure: A Tutorial. *Chem. Soc. Rev.* **2015**, *44* (7), 1820–1835.

- (216) Koshenaj, K.; Ferrari, G. A Comprehensive Review on Starch-Based Hydrogels: From Tradition to Innovation, Opportunities, and Drawbacks. *Polymers* **2024**, *16* (14).
- (217) Jain, M.; Nowak, B. P.; Ravoo, B. J. Supramolecular Hydrogels Based on Cyclodextrins: Progress and Perspectives. *ChemNanoMat* **2022**, *8* (5).
- (218) Egan, G.; Phuagkhaopong, S.; Matthew, S. A. L.; Connolly, P.; Seib, F. P. Impact of Silk Hydrogel Secondary Structure on Hydrogel Formation, Silk Leaching and In Vitro Response. *Sci. Rep.* **2022**, *12* (1), 3729.
- (219) Wei, Z.; Yang, J. H.; Zhou, J.; Xu, F.; Zrínyi, M.; Dussault, P. H.; Osada, Y.; Chen, Y. M. Self-Healing Gels Based on Constitutional Dynamic Chemistry and Their Potential Applications. *Chem. Soc. Rev.* **2014**, *43* (23), 8114–8131.
- (220) Cromwell, O. R.; Chung, J.; Guan, Z. Malleable and Self-Healing Covalent Polymer Networks through Tunable Dynamic Boronic Ester Bonds. *J. Am. Chem. Soc.* **2015**, *137* (20), 6492–6495.
- (221) Marco-Dufort, B.; Tibbitt, M. W. Design of Moldable Hydrogels for Biomedical Applications Using Dynamic Covalent Boronic Esters. *Mater. Today Chem.* **2019**, *12*, 16–33.
- (222) Marco-Dufort, B.; Iten, R.; Tibbitt, M. W. Linking Molecular Behavior to Macroscopic Properties in Ideal Dynamic Covalent Networks. *J. Am. Chem. Soc.* **2020**, *142* (36), 15371–15385.
- (223) Zou, W.; Dong, J.; Luo, Y.; Zhao, Q.; Xie, T. Dynamic Covalent Polymer Networks: from Old Chemistry to Modern Day Innovations. *Adv. Mater.* **2017**, *29* (14).
- (224) Hatai, J.; Hirschhäuser, C.; Niemeyer, J.; Schmuck, C. Multi-Stimuli-Responsive Supramolecular Polymers Based on Noncovalent and Dynamic Covalent Bonds. *ACS Appl. Mater. Interfaces* **2020**, *12* (2), 2107–2115.
- (225) Marco-Dufort, B.; Willi, J.; Vielba-Gomez, F.; Gatti, F.; Tibbitt, M. W. Environment Controls Biomolecule Release from Dynamic Covalent Hydrogels. *Biomacromolecules* **2021**, *22* (1), 146–157.
- (226) Yesilyurt, V.; Webber, M. J.; Appel, E. A.; Godwin, C.; Langer, R.; Anderson, D. G. Injectable Self-Healing Glucose-Responsive Hydrogels with pH-Regulated Mechanical Properties. *Adv. Mater.* **2016**, *28* (1), 86–91.

- (227) Yu, J.; Wang, J.; Zhang, Y.; Chen, G.; Mao, W.; Ye, Y.; Kahkoska, A. R.; Buse, J. B.; Langer, R.; Gu, Z. Glucose-Responsive Insulin Patch for the Regulation of Blood Glucose in Mice and Minipigs. *Nat. Biomed. Eng.* **2020**, *4* (5), 499–506.
- (228) Lin, Y.; Chen, Y.; Yu, Z.; Huang, Z.; Lai, J.-C.; Tok, J. B.-H.; Cui, Y.; Bao, Z. Reprocessable and Recyclable Polymer Network Electrolytes via Incorporation of Dynamic Covalent Bonds. *Chem. Mater.* **2022**, *34* (5), 2393–2399.
- (229) Zhao, H.; Li, Z.; Zhan, S.; Yue, T.; Qu, J.; Li, H.; Zhang, L.; Ganesan, V.; Liu, J. Role of Dynamic Covalent Bond Density on the Structure and Properties of Vitrimers. *Macromolecules* **2024**, *57* (23), 11296–11310.
- (230) Niu, W.; Cao, X.; Wang, Y.; Yao, B.; Zhao, Y.; Cheng, J.; Wu, S.; Zhang, S.; He, X. Photonic Vitriimer Elastomer with Self-Healing, High Toughness, Mechanochromism, and Excellent Durability based on Dynamic Covalent Bond. *Adv. Funct. Mater.* **2021**, *31* (13).
- (231) Zou, Z.; Zhu, C.; Li, Y.; Lei, X.; Zhang, W.; Xiao, J. Rehealable, Fully Recyclable, and Malleable Electronic Skin Enabled by Dynamic Covalent Thermoset Nanocomposite. *Sci. Adv.* **2018**, *4* (2), eaaq0508.
- (232) Xing, Z.; Jia, X.; Li, X.; Yang, J.; Wang, S.; Li, Y.; Shao, D.; Feng, L.; Song, H. Novel Green Reversible Humidity-Responsive Hemiaminal Dynamic Covalent Network for Smart Window. *ACS Appl. Mater. Interfaces* **2023**, *15* (8), 11053–11061.
- (233) Chen, X.; Dam, M. A.; Ono, K.; Mal, A.; Shen, H.; Nutt, S. R.; Sheran, K.; Wudl, F. A Thermally Re-Mendable Cross-Linked Polymeric Material. *Science* **2002**, *295* (5560), 1698–1702.
- (234) Adzima, B. J.; Aguirre, H. A.; Kloxin, C. J.; Scott, T. F.; Bowman, C. N. Rheological and Chemical Analysis of Reverse Gelation in a Covalently Crosslinked Diels-Alder Polymer Network. *Macromolecules* **2008**, *41* (23), 9112–9117.
- (235) Liu, J.; Zhang, X.; Chen, X.; Qu, L.; Zhang, L.; Li, W.; Zhang, A. Stimuli-Responsive Dendronized Polymeric Hydrogels Through Schiff-Base Chemistry Showing Remarkable Topological Effects. *Polym. Chem.* **2018**, *9* (3), 378–387.
- (236) Zhao, S.; Liu, Y.; Zhao, H.; Ma, K.; Fu, Y.; Dong, Y.; Li, J.; Pang, C. Catalyst-Free Dynamic Covalent Polyester Networks with Dissociative Transesterification. *Macromolecules* **2024**, *57* (24), 11417–11428.

- (237) Zhang, X.; Waymouth, R. M. 1,2-Dithiolane-Derived Dynamic, Covalent Materials: Cooperative Self-Assembly and Reversible Cross-Linking. *J. Am. Chem. Soc.* **2017**, *139* (10), 3822–3833.
- (238) Yu, H.; Wang, Y.; Yang, H.; Peng, K.; Zhang, X. Injectable Self-Healing Hydrogels Formed via Thiol/Disulfide Exchange of Thiol Functionalized F127 and Dithiolane Modified PEG. *J. Mater. Chem. B* **2017**, *5* (22), 4121–4127.
- (239) Kang, B.; Kalow, J. A. Internal and External Catalysis in Boronic Ester Networks. *ACS Macro Lett.* **2022**, *11* (3), 394–401.
- (240) Brooks, W. L. A.; Deng, C. C.; Sumerlin, B. S. Structure-Reactivity Relationships in Boronic Acid-Diol Complexation. *ACS omega* **2018**, *3* (12), 17863–17870.
- (241) Roy, C. D.; Brown, H. C. Stability of Boronic Esters – Structural Effects on the Relative Rates of Transesterification of 2-(Phenyl)-1,3, 2-Dioxaborolane. *J. Organomet. Chem.* **2007**, *692* (4), 784–790.
- (242) An, H.; Bo, Y.; Chen, D.; Wang, Y.; Wang, H.; He, Y.; Qin, J. Cellulose-Based Self-Healing Hydrogel Through Boronic Ester Bonds With Excellent Biocompatibility and Conductivity. *RSC Adv.* **2020**, *10* (19), 11300–11310.
- (243) Axthelm, J.; Askes, S. H. C.; Elstner, M.; G, U. R.; Görls, H.; Bellstedt, P.; Schiller, A. Fluorinated Boronic Acid-Appended Pyridinium Salts and ¹⁹F NMR Spectroscopy for Diol Sensing. *J. Am. Chem. Soc.* **2017**, *139* (33), 11413–11420.
- (244) Bian, L.; Hou, C.; Tous, E.; Rai, R.; Mauck, R. L.; Burdick, J. A. The Influence of Hyaluronic Acid Hydrogel Crosslinking Density and Macromolecular Diffusivity on Human MSC Chondrogenesis and Hypertrophy. *Biomaterials* **2013**, *34* (2), 413–421.
- (245) Lee, K. Y.; Rowley, J. A.; Eiselt, P.; Moy, E. M.; Bouhadir, K. H.; Mooney, D. J. Controlling Mechanical and Swelling Properties of Alginate Hydrogels Independently by Cross-Linker Type and Cross-Linking Density. *Macromolecules* **2000**, *33* (11), 4291–4294.
- (246) Lin, Y.-H.; Lou, J.; Xia, Y.; Chaudhuri, O. Cross-Linker Architectures Impact Viscoelasticity in Dynamic Covalent Hydrogels. *Adv. Healthc. Mater.* **2024**, *13* (30), e2402059.

- (247) Jiang, X.; Li, C.; Han, Q. Modulation of Spatial and Topological Inhomogeneities of Linear Polymer Hydrogel. *Mater. Today Commun.* **2022**, *31*, 103700.
- (248) Meng, Z.; Thakur, T.; Chitrakar, C.; Jaiswal, M. K.; Gaharwar, A. K.; Yakovlev, V. V. Assessment of Local Heterogeneity in Mechanical Properties of Nanostructured Hydrogel Networks. *ACS nano* **2017**, *11* (8), 7690–7696.
- (249) Holt, S. E.; Rakoski, A.; Jivan, F.; Pérez, L. M.; Alge, D. L. Hydrogel Synthesis and Stabilization via Tetrazine Click-Induced Secondary Interactions. *Macromol. Rapid Commun.* **2020**, *41* (14), e2000287.
- (250) Sun, W.; Xue, B.; Li, Y.; Qin, M.; Wu, J.; Lu, K.; Wu, J.; Cao, Y.; Jiang, Q.; Wang, W. Polymer-Supramolecular Polymer Double-Network Hydrogel. *Adv. Funct. Mater.* **2016**, *26* (48), 9044–9052.
- (251) Cui, H.; Jiang, W.; Wang, C.; Ji, X.; Liu, Y.; Yang, G.; Chen, J.; Lyu, G.; Ni, Y. Lignin Nanofiller-Reinforced Composites Hydrogels With Long-Lasting Adhesiveness, Toughness, Excellent Self-Healing, Conducting, Ultraviolet-Blocking and Antibacterial Properties. *Compos. B Eng.* **2021**, *225*, 109316.
- (252) Meng, X.; Qiao, Y.; Do, C.; Bras, W.; He, C.; Ke, Y.; Russell, T. P.; Qiu, D. Hysteresis-Free Nanoparticle-Reinforced Hydrogels. *Adv. Mater.* **2022**, *34* (7), e2108243.
- (253) Barbucci, R.; Consumi, M.; Magnani, A. Dependence of Water Uptake and Morphology of Hyaluronan- and Alginate-Based Hydrogels on pH and Degree of Crosslinking. *Macromol. Chem. Phys.* **2002**, *203* (10-11), 1292–1300.
- (254) Marcombe, R.; Cai, S.; Hong, W.; Zhao, X.; Lapusta, Y.; Suo, Z. A Theory of Constrained Swelling of a pH-Sensitive Hydrogel. *Soft matter* **2010**, *6* (4), 784.
- (255) Gemeinhart, R. A.; Park, H.; Park, K. Pore Structure of Superporous Hydrogels. *Polym. Adv. Technol.* **2000**, *11* (8-12), 617–625.
- (256) Guilherme, M. R.; Aouada, F. A.; Fajardo, A. R.; Martins, A. F.; Paulino, A. T.; Davi, M. F.; Rubira, A. F.; Muniz, E. C. Superabsorbent Hydrogels Based on Polysaccharides for Application in Agriculture As Soil Conditioner and Nutrient Carrier: A Review. *Eur. Polym. J.* **2015**, *72*, 365–385.
- (257) Ismaeilimoghadam, S.; Jonoobi, M.; Hamzeh, Y.; Azimi, B.; Mezzetta, A.; Guazzelli, L.; Cinelli, P.; Seggiani, M.; Danti, S. Development and Characterization of

Sodium Alginate-Based Bio-hybrid Super Absorbent Polymer with High Retention Capacity Suitable for Baby Diapers. *J. Polym. Environ.* **2024**.

(258) Brelle, L.; Faÿ, F.; Ozturk, T.; Didier, N.; Renard, E.; Langlois, V. Hydrogel Based on Polyhydroxyalkanoate Sulfonate: Control of the Swelling Rate by the Ionic Group Content. *Biomacromolecules* **2023**, *24* (4), 1871–1880.

(259) Katan, T.; Kargl, R.; Mohan, T.; Steindorfer, T.; Mozetič, M.; Kovač, J.; Stana Kleinschek, K. Solid Phase Peptide Synthesis on Chitosan Thin Films. *Biomacromolecules* **2022**, *23* (3), 731–742.

(260) Wang, W.; Hu, J.; Zhang, R.; Yan, C.; Cui, L.; Zhu, J. A pH-Responsive Carboxymethyl Cellulose/Chitosan Hydrogel for Adsorption and Desorption of Anionic and Cationic Dyes. *Cellulose* **2021**, *28* (2), 897–909.

(261) Jurak, M.; Wiącek, A. E.; Ładniak, A.; Przykaza, K.; Szafran, K. What Affects the Biocompatibility of Polymers? *Adv. Colloid Interface Sci.* **2021**, *294*, 102451.

(262) Lu, P.; Ruan, D.; Huang, M.; Tian, M.; Zhu, K.; Gan, Z.; Xiao, Z. Harnessing the Potential of Hydrogels for Advanced Therapeutic Applications: Current Achievements and Future Directions. *Signal Transduct. Target. Ther.* **2024**, *9* (1), 166.

(263) Vogler, E. A. Protein Adsorption in Three Dimensions. *Biomaterials* **2012**, *33* (5), 1201–1237.

(264) Wonski, B. T.; Fisher, B.; Lam, M. T. Hydrogel Coating Optimization to Augment Engineered Soft Tissue Mechanics in Tissue-Engineered Blood Vessels. *Bioengineering* **2023**, *10* (7).

(265) Hu, B.; Ouyang, Y.; Zhao, T.; Wang, Z.; Yan, Q.; Qian, Q.; Wang, W.; Wang, S. Antioxidant Hydrogels: Antioxidant Mechanisms, Design Strategies, and Applications in the Treatment of Oxidative Stress-Related Diseases. *Adv. Healthc. Mater.* **2024**, *13* (11), e2303817.

(266) Morwood, A. J.; El-Karim, I. A.; Clarke, S. A.; Lundy, F. T. The Role of Extracellular Matrix (ECM) Adhesion Motifs in Functionalised Hydrogels. *Molecules* **2023**, *28* (12).

(267) Luo, C.; Huang, M.; Sun, X.; Wei, N.; Shi, H.; Li, H.; Lin, M.; Sun, J. Super-Strong, Nonswellable, and Biocompatible Hydrogels Inspired by Human Tendons. *ACS Appl. Mater. Interfaces* **2022**, *14* (2), 2638–2649.

- (268) Liu, Y.; Dong, T.; Chen, Y.; Sun, N.; Liu, Q.; Huang, Z.; Yang, Y.; Cheng, H.; Yue, K. Biodegradable and Cytocompatible Hydrogel Coating with Antibacterial Activity for the Prevention of Implant-Associated Infection. *ACS Appl. Mater. Interfaces* **2023**, *15* (9), 11507–11519.
- (269) Hernandez, J. L.; Woodrow, K. A. Medical Applications of Porous Biomaterials: Features of Porosity and Tissue-Specific Implications for Biocompatibility. *Adv. Healthc. Mater.* **2022**, *11* (9), e2102087.
- (270) Ross, A. M.; Jiang, Z.; Bastmeyer, M.; Lahann, J. Physical Aspects of Cell Culture Substrates: Topography, Roughness, and Elasticity. *Small* **2012**, *8* (3), 336–355.
- (271) Zheng, W. J.; An, N.; Yang, J. H.; Zhou, J.; Chen, Y. M. Tough Al-Alginate/Poly(N-Isopropylacrylamide) Hydrogel With Tunable LCST for Soft Robotics. *ACS Appl. Mater. Interfaces* **2015**, *7* (3), 1758–1764.
- (272) Cha, C.; Kohman, R. H.; Kong, H. Biodegradable Polymer Crosslinker: Independent Control of Stiffness, Toughness, and Hydrogel Degradation Rate. *Adv. Funct. Mater.* **2009**, *19* (19), 3056–3062.
- (273) Roth-Konforti, M. E.; Comune, M.; Halperin-Sternfeld, M.; Grigoriants, I.; Shabat, D.; Adler-Abramovich, L. UV Light-Responsive Peptide-Based Supramolecular Hydrogel for Controlled Drug Delivery. *Macromol. Rapid Commun.* **2018**, *39* (24), e1800588.
- (274) Zhao, Y.-L.; Stoddart, J. F. Azobenzene-Based Light-Responsive Hydrogel System. *Langmuir* **2009**, *25* (15), 8442–8446.
- (275) Rodon Fores, J.; Criado-Gonzalez, M.; Chaumont, A.; Carvalho, A.; Blanck, C.; Schmutz, M.; Serra, C. A.; Boulmedais, F.; Schaaf, P.; Jierry, L. Supported Catalytically Active Supramolecular Hydrogels for Continuous Flow Chemistry. *Angew. Chem.* **2019**, *131* (52), 18993–18998.
- (276) Zhao, T.; Chen, S.; Kang, K.; Ren, J.; Yu, X. Self-Assembled Copper Metallogel Bearing Terpyridine and Its Application as a Catalyst for the Click Reaction in Water. *Langmuir* **2022**, *38* (4), 1398–1405.
- (277) Zhang, W.; Feng, P.; Chen, J.; Sun, Z.; Zhao, B. Electrically Conductive Hydrogels for Flexible Energy Storage Systems. *Prog. Polym. Sci.* **2019**, *88*, 220–240.

- (278) Miras, J.; Liu, C.; Blomberg, E.; Thormann, E.; Vílchez, S.; Esquena, J. pH-Responsive Chitosan Nanofilms Crosslinked With Genipin. *Colloids Surf. A* **2021**, *616*, 126229.
- (279) Howard, S. C.; Craig, V. S. J.; FitzGerald, P. A.; Wanless, E. J. Swelling and Collapse of an Adsorbed pH-Responsive Film-Forming Microgel Measured by Optical Reflectometry and QCM. *Langmuir* **2010**, *26* (18), 14615–14623.
- (280) Yang, T.; Ji, R.; Deng, X.-X.; Du, F.-S.; Li, Z.-C. Glucose-Responsive Hydrogels Based on Dynamic Covalent Chemistry and Inclusion Complexation. *Soft matter* **2014**, *10* (15), 2671–2678.
- (281) Lee, I.-N.; Dobre, O.; Richards, D.; Ballestrem, C.; Curran, J. M.; Hunt, J. A.; Richardson, S. M.; Swift, J.; Wong, L. S. Photoresponsive Hydrogels with Photoswitchable Mechanical Properties Allow Time-Resolved Analysis of Cellular Responses to Matrix Stiffening. *ACS Appl. Mater. Interfaces* **2018**, *10* (9), 7765–7776.
- (282) Li, L.; Scheiger, J. M.; Levkin, P. A. Design and Applications of Photoresponsive Hydrogels. *Adv. Mater.* **2019**, *31* (26), e1807333.
- (283) Gumuscu, B.; Bomer, J. G.; van den Berg, A.; Eijkel, J. C. T. Photopatterning of Hydrogel Microarrays in Closed Microchips. *Biomacromolecules* **2015**, *16* (12), 3802–3810.
- (284) Hahn, M. S.; Taite, L. J.; Moon, J. J.; Rowland, M. C.; Ruffino, K. A.; West, J. L. Photolithographic Patterning of Polyethylene Glycol Hydrogels. *Biomaterials* **2006**, *27* (12), 2519–2524.
- (285) Revzin, A.; Russell, R. J.; Yadavalli, V. K.; Koh, W. G.; Deister, C.; Hile, D. D.; Mellott, M. B.; Pishko, M. V. Fabrication of Poly(ethylene Glycol) Hydrogel Microstructures Using Photolithography. *Langmuir* **2001**, *17* (18), 5440–5447.
- (286) O'Grady, M. L.; Kuo, P.; Parker, K. K. Optimization of Electroactive Hydrogel Actuators. *ACS Appl. Mater. Interfaces* **2010**, *2* (2), 343–346.
- (287) Li, J.; Ma, Q.; Xu, Y.; Yang, M.; Wu, Q.; Wang, F.; Sun, P. Highly Bidirectional Bendable Actuator Engineered by LCST-UCST Bilayer Hydrogel with Enhanced Interface. *ACS Appl. Mater. Interfaces* **2020**, *12* (49), 55290–55298.
- (288) Hu, Z.; Zhang, X.; Li, Y. Synthesis and Application of Modulated Polymer Gels. *Science* **1995**, *269* (5223), 525–527.

- (289) Fusi, G.; Del Giudice, D.; Skarsetz, O.; Di Stefano, S.; Walther, A. Autonomous Soft Robots Empowered by Chemical Reaction Networks. *Adv. Mater.* **2023**, *35* (7), e2209870.
- (290) Han, Z.; Wang, P.; Mao, G.; Yin, T.; Zhong, D.; Yiming, B.; Hu, X.; Jia, Z.; Nian, G.; Qu, S.; Yang, W. Dual pH-Responsive Hydrogel Actuator for Lipophilic Drug Delivery. *ACS Appl. Mater. Interfaces* **2020**, *12* (10), 12010–12017.
- (291) Jiang, Z.; Tan, M. L.; Taheri, M.; Yan, Q.; Tsuzuki, T.; Gardiner, M. G.; Diggle, B.; Connal, L. A. Strong, Self-Healable, and Recyclable Visible-Light-Responsive Hydrogel Actuators. *Angew. Chem.* **2020**, *132* (18), 7115–7122.
- (292) Li, M.; Wang, X.; Dong, B.; Sitti, M. In-Air Fast Response and High Speed Jumping and Rolling of a Light-Driven Hydrogel Actuator. *Nat. Commun.* **2020**, *11* (1), 3988.
- (293) Vermonden, T.; Fedorovich, N. E.; van Geemen, D.; Alblas, J.; van Nostrum, C. F.; Dhert, W. J. A.; Hennink, W. E. Photopolymerized Thermosensitive Hydrogels: Synthesis, Degradation, and Cytocompatibility. *Biomacromolecules* **2008**, *9* (3), 919–926.
- (294) Lee, B. H.; West, B.; McLemore, R.; Pauken, C.; Vernon, B. L. In-Situ Injectable Physically and Chemically Gelling NIPAAm-Based Copolymer System for Embolization. *Biomacromolecules* **2006**, *7* (6), 2059–2064.
- (295) Chen, F.; Lu, G.; Yuan, H.; Li, R.; Nie, J.; Zhao, Y.; Shu, X.; Zhu, X. Mechanism and Regulation of LCST Behavior in Poly(hydroxypropyl Acrylate)-Based Temperature-Sensitive Hydrogels. *J. Mater. Chem. A* **2022**, *10* (35), 18235–18247.
- (296) Li, J.; Mooney, D. J. Designing Hydrogels for Controlled Drug Delivery. *Nat. Rev. Mater.* **2016**, *1* (12).
- (297) Ghosh, S.; Parker, S. T.; Wang, X.; Kaplan, D. L.; Lewis, J. A. Direct-Write Assembly of Microperiodic Silk Fibroin Scaffolds for Tissue Engineering Applications. *Adv. Funct. Mater.* **2008**, *18* (13), 1883–1889.
- (298) Slaughter, B. V.; Khurshid, S. S.; Fisher, O. Z.; Khademhosseini, A.; Peppas, N. A. Hydrogels in Regenerative Medicine. *Adv. Mater.* **2009**, *21* (32-33), 3307–3329.
- (299) Lee, K. Y.; Mooney, D. J. Hydrogels for Tissue Engineering. *Chem. Rev.* **2001**, *101* (7), 1869–1879.

- (300) Wang, F.; Gao, Y.; Li, H.; Zhou, L.; Shi, H.; Feng, S.; Chen, J.; Mei, Z. Effect of Natural-Based Biological Hydrogels Combined With Growth Factors on Skin Wound Healing. *Nanotechnol. Rev.* **2022**, *11* (1), 2493–2512.
- (301) Liang, Y.; He, J.; Guo, B. Functional Hydrogels as Wound Dressing to Enhance Wound Healing. *ACS nano* **2021**, *15* (8), 12687–12722.
- (302) Del Andrade Olmo, J.; Pérez-Álvarez, L.; Sáez Martínez, V.; Benito Cid, S.; Ruiz-Rubio, L.; Pérez González, R.; Vilas-Vilela, J. L.; Alonso, J. M. Multifunctional Antibacterial Chitosan-Based Hydrogel Coatings on Ti6Al4V Biomaterial for Biomedical Implant Applications. *Int. J. Biol. Macromol.* **2023**, *231*, 123328.
- (303) Compañ, V.; Andrio, A.; López-Aleman, A.; Riande, E.; Refojo, M. F. Oxygen Permeability of Hydrogel Contact Lenses With Organosilicon Moieties. *Biomaterials* **2002**, *23* (13), 2767–2772.
- (304) Childs, A.; Li, H.; Lewittes, D. M.; Dong, B.; Liu, W.; Shu, X.; Sun, C.; Zhang, H. F. Fabricating Customized Hydrogel Contact Lens. *Sci. Rep.* **2016**, *6*, 34905.
- (305) Rasekh, M.; Ahmad, Z.; Day, R.; Wickam, A.; Edirisinghe, M. Direct Writing of Polycaprolactone Polymer for Potential Biomedical Engineering Applications. *Adv. Eng. Mater.* **2011**, *13* (9).
- (306) Fischbach, C.; Chen, R.; Matsumoto, T.; Schmelzle, T.; Brugge, J. S.; Poverini, P. J.; Mooney, D. J. Engineering Tumors With 3D Scaffolds. *Nat. Methods* **2007**, *4* (10), 855–860.
- (307) Yang, G.; Sun, Y.; Qin, L.; Li, M.; Ou, K.; Fang, J.; Fu, Q. Direct-Ink-Writing (DIW) 3D Printing Functional Composite Materials Based on Supra-Molecular Interaction. *Compos. Sci. Technol.* **2021**, *215*, 109013.
- (308) Saadi, M. A. S. R.; Maguire, A.; Pottackal, N. T.; Thakur, M. S. H.; Ikram, M. M.; Hart, A. J.; Ajayan, P. M.; Rahman, M. M. Direct Ink Writing: A 3D Printing Technology for Diverse Materials. *Adv. Mater.* **2022**, *34* (28), e2108855.
- (309) Geurds, L.; Lauko, J.; Rowan, A. E.; Amiralian, N. Tailored Nanocellulose-Grafted Polymer Brush Applications. *J. Mater. Chem. A* **2021**, *9* (32), 17173–17188.
- (310) Klemm, D.; Kramer, F.; Moritz, S.; Lindström, T.; Ankerfors, M.; Gray, D.; Dorris, A. Nanocelluloses: A New Family of Nature-Based Materials. *Angew. Chem.* **2011**, *50* (24), 5438–5466.

- (311) Rol, F.; Belgacem, M. N.; Gandini, A.; Bras, J. Recent Advances in Surface-Modified Cellulose Nanofibrils. *Prog. Polym. Sci.* **2019**, *88*, 241–264.
- (312) Gao, M.; Li, J.; Bao, Z.; Hu, M.; Nian, R.; Feng, D.; An, D.; Li, X.; Xian, M.; Zhang, H. A Natural In Situ Fabrication Method of Functional Bacterial Cellulose Using a Microorganism. *Nat. Commun.* **2019**, *10* (1), 437.
- (313) Isogai, A. Development of Completely Dispersed Cellulose Nanofibers. *Proc. Jpn. Acad. Ser. B Phys. Biol. Sci.* **2018**, *94* (4), 161–179.
- (314) Li, T.; Chen, C.; Brozena, A. H.; Zhu, J. Y.; Xu, L.; Driemeier, C.; Dai, J.; Rojas, O. J.; Isogai, A.; Wågberg, L.; Hu, L. Developing Fibrillated Cellulose as a Sustainable Technological Material. *Nature* **2021**, *590* (7844), 47–56.
- (315) Fourmann, O.; Hausmann, M. K.; Neels, A.; Schubert, M.; Nyström, G.; Zimmermann, T.; Siqueira, G. 3D Printing of Shape-Morphing and Antibacterial Anisotropic Nanocellulose Hydrogels. *Carbohydr. Polym.* **2021**, *259*, 117716.
- (316) Gladman, A. S.; Matsumoto, E. A.; Nuzzo, R. G.; Mahadevan, L.; Lewis, J. A. Biomimetic 4D Printing. *Nat. Mater.* **2016**, *15* (4), 413–418.
- (317) Siqueira, G.; Kokkinis, D.; Libanori, R.; Hausmann, M. K.; Gladman, A. S.; Neels, A.; Tingaut, P.; Zimmermann, T.; Lewis, J. A.; Studart, A. R. Cellulose Nanocrystal Inks for 3D Printing of Textured Cellular Architectures. *Adv. Funct. Mater.* **2017**, *27* (12).
- (318) Bensefelt, T.; Engström, J.; Wågberg, L. Supramolecular Double Networks of Cellulose Nanofibrils and Algal Polysaccharides With Excellent Wet Mechanical Properties. *Green Chem.* **2018**, *20* (11), 2558–2570.
- (319) Ji, D.; Park, J. M.; Oh, M. S.; Nguyen, T. L.; Shin, H.; Kim, J. S.; Kim, D.; Park, H. S.; Kim, J. Superstrong, Superstiff, and Conductive Alginate Hydrogels. *Nat. Commun.* **2022**, *13* (1), 3019.
- (320) Kuo, C. K.; Ma, P. X. Maintaining Dimensions and Mechanical Properties of Ionically Crosslinked Alginate Hydrogel Scaffolds In Vitro. *J. Biomed. Mater. Res. A* **2008**, *84* (4), 899–907.
- (321) Bordoni, M.; Karabulut, E.; Kuzmenko, V.; Fantini, V.; Pansarasa, O.; Cereda, C.; Gatenholm, P. 3D Printed Conductive Nanocellulose Scaffolds for the Differentiation of Human Neuroblastoma Cells. *Cells* **2020**, *9* (3).

- (322) Lackner, F.; Knechtl, I.; Novak, M.; Nagaraj, C.; Dobaj Štiglic, A.; Kargl, R.; Olschewski, A.; Stana Kleinschek, K.; Mohan, T. 3D-Printed Anisotropic Nanofiber Composites with Gradual Mechanical Properties. *Adv. Mater. Technol.* **2023**, *8* (10).
- (323) Lackner, F.; Šurina, P.; Fink, J.; Kotzbeck, P.; Kolb, D.; Stana, J.; Grab, M.; Hagl, C.; Tsilimparis, N.; Mohan, T.; Stana Kleinschek, K.; Kargl, R. 4-Axis 3D-Printed Tubular Biomaterials Imitating the Anisotropic Nanofiber Orientation of Porcine Aortae. *Adv. Healthc. Mater.* **2024**, *13* (2), e2302348.
- (324) Li, F.; Miao, G.; Gao, Z.; Xu, T.; Zhu, X.; Miao, X.; Song, Y.; Ren, G.; Li, X. A Versatile Hydrogel Platform for Oil/Water Separation, Dye Adsorption, and Wastewater Purification. *Cellulose* **2022**, *29* (8), 4427–4438.
- (325) Godiya, C. B.; Cheng, X.; Li, D.; Chen, Z.; Lu, X. Carboxymethyl Cellulose/Polyacrylamide Composite Hydrogel for Cascaded Treatment/Reuse of Heavy Metal Ions in Wastewater. *J. Hazard. Mat.* **2019**, *364*, 28–38.
- (326) Abd Manan, T. S. B.; Beddu, S.; Mohamad, D.; Mohd Kamal, N. L.; Itam, Z.; Khan, T.; Jusoh, H.; Abdul Rahman, N. A.; Mohamed Nazri, F.; Mohd Yapandi, M. F. K.; Wan Mohtar, W. H. M.; Isa, M. H.; Che Muda, Z.; Ahmad, A.; Wan Rasdi, N. Physicochemical Properties of Absorbent Hydrogel Polymers in Disposable Baby Diapers. *Chem. Phys. Lett.* **2021**, *774*, 138605.
- (327) Zhang, H.; Zhang, F.; Yuan, R. Applications of Natural Polymer-Based Hydrogels in the Food Industry. In *Hydrogels Based on Natural Polymers*; pp 357–410. DOI: 10.1016/B978-0-12-816421-1.00015-X.
- (328) Zohuriaan-Mehr, M. J.; Omidian, H.; Doroudiani, S.; Kabiri, K. Advances in Non-Hygienic Applications of Superabsorbent Hydrogel Materials. *J. Mater. Sci.* **2010**, *45* (21), 5711–5735.
- (329) Silva-Pereira, M. C.; Teixeira, J. A.; Pereira-Júnior, V. A.; Stefani, R. Chitosan/Corn Starch Blend Films With Extract From Brassica Oleraceae (Red Cabbage) as a Visual Indicator of Fish Deterioration. *LWT* **2015**, *61* (1), 258–262.
- (330) Bäcker, M.; Raue, M.; Schusser, S.; Jeitner, C.; Breuer, L.; Wagner, P.; Poghosian, A.; Förster, A.; Mang, T.; Schöning, M. J. Microfluidic Chip With Integrated Microvalves Based on Temperature- and pH-Responsive Hydrogel Thin Films. *Phys. Status Solidi* **2012**, *209* (5), 839–845.

- (331) Lee, K. Y.; Mooney, D. J. Alginate: Properties and Biomedical Applications. *Prog. Polym. Sci.* **2012**, *37* (1), 106–126.
- (332) Lin, Z.; Wu, M.; He, H.; Liang, Q.; Hu, C.; Zeng, Z.; Cheng, D.; Wang, G.; Chen, D.; Pan, H.; Ruan, C. 3D Printing of Mechanically Stable Calcium-Free Alginate-Based Scaffolds with Tunable Surface Charge to Enable Cell Adhesion and Facile Biofunctionalization. *Adv. Funct. Mater.* **2019**, *29* (9).
- (333) Hafeez, S.; Decarli, M. C.; Aldana, A.; Ebrahimi, M.; Ruitter, F. A. A.; Duimel, H.; van Blitterswijk, C.; Pitet, L. M.; Moroni, L.; Baker, M. B. In Situ Covalent Reinforcement of a Benzene-1,3,5-Tricarboxamide Supramolecular Polymer Enables Biomimetic, Tough, and Fibrous Hydrogels and Bioinks. *Adv. Mater.* **2023**, *35* (35), e2301242.
- (334) Cao, L.; Huang, J.; Chen, Y. Dual Cross-linked Epoxidized Natural Rubber Reinforced by Tunicate Cellulose Nanocrystals with Improved Strength and Extensibility. *ACS Sustainable Chem. Eng.* **2018**, *6* (11), 14802–14811.
- (335) Richter, A.; Paschew, G.; Klatt, S.; Lienig, J.; Arndt, K.-F.; Adler, H.-J. P. Review on Hydrogel-based pH Sensors and Microsensors. *Sensors* **2008**, *8* (1), 561–581.
- (336) Scarpa, E.; Mastronardi, V. M.; Guido, F.; Algieri, L.; Qualtieri, A.; Fiammengo, R.; Rizzi, F.; Vittorio, M. de. Wearable Piezoelectric Mass Sensor Based on pH Sensitive Hydrogels for Sweat pH Monitoring. *Sci. Rep.* **2020**, *10* (1), 10854.
- (337) Batchelor, R. R.; Blasco, E.; Wuest, K. N. R.; Lu, H.; Wegener, M.; Barner-Kowollik, C.; Stenzel, M. H. Spatially Resolved Coding of λ -Orthogonal Hydrogels by Laser Lithography. *Chem. Commun.* **2018**, *54* (19), 2436–2439.
- (338) Li, B.; He, M.; Ramirez, L.; George, J.; Wang, J. Multifunctional Hydrogel Microparticles by Polymer-Assisted Photolithography. *ACS Appl. Mater. Interfaces* **2016**, *8* (6), 4158–4164.
- (339) Medrano-David, D.; Lopera, A. M.; Londoño, M. E.; Araque-Marín, P. Formulation and Characterization of a New Injectable Bone Substitute Composed PVA/Borax/CaCO₃ and Demineralized Bone Matrix. *J. Funct. Biomater.* **2021**, *12* (3).
- (340) Narita, T.; Hsieh, W.-C.; Ku, Y. T.; Su, Y.-C.; Inoguchi, H.; Takeno, H. Fracture Behavior and Biocompatibility of Cellulose Nanofiber-Reinforced Poly(vinyl alcohol)

References

Composite Hydrogels Cross-Linked with Borax. *Biomacromolecules* **2025**, 26 (1), 374–386.

10 Appendix

10.1 List of figures

Figure 1: Sodium naphthalenide-initiated anionic ‘living’ polymerization of styrene. ^{9,10}	5
Figure 2: Degree of polymerization with monomer conversion for different polymerization types. Free radical polymerization (dotted line), living-type polymerization (solid line), and step-growth polymerization (dashed line).....	6
Figure 3: Mechanistic pathways of the SKA-GTP of MMA. ⁴⁴	9
Figure 4: Overview of exemplary Lewis acids, Lewis bases, propagation step, and monomers of group-transfer polymerization with frustrated and highly interacting Lewis pairs. ^{57,59–61}	11
Figure 5: Mechanism of initiation and propagation of the polymerization of MMA via REM-GTP with $[\text{Cp}^*_2\text{SmH}]_2$. ⁶³	12
Figure 6: Possible initiation pathways of DAVP polymerization with $\text{Cp}_2\text{LnX}(\text{THF})$ or $[\text{Cp}_2\text{LnX}]_2$ catalysts via REM-GTP. ⁶⁵	13
Figure 7: CH-bond activation of 2,4,6-trimethylpyridine with $\text{Cp}_2\text{YCH}_2\text{TMS}(\text{THF})$ generating $\text{Cp}_2\text{Y}(\text{sym-col})$ in situ and transition state of the σ -bond metathesis reaction. Subsequent addition of DEVP initiates polymerization via the indicated transition state.	14
Figure 8: Yasuda-type, monometallic propagation mechanism of REM-GTP of vinylphosphonate monomers with key intermediates and transition states. ⁶⁵	15
Figure 9: Overview of different catalyst classes for REM-GTP with exemplary structures for each group: Metallocenes, half-metallocenes, and non-metallocene catalysts. ^{65,66,68–71,77,81,84–90}	17
Figure 10: General reaction scheme of GTP and steric configurations of different Michael-type monomers (top). General resonance structure of α,β -unsaturated monomers for REM-GTP and examples of different Michael acceptor monomers (bottom).	19
Figure 11: Coordination strength of different Michael-type monomers to the catalyst metal center.....	20

Figure 12: Overview of different 2,6-dimethyl pyridine derivatives introduced as initiators into rare earth metal complexes via CH-bond activation: Native initiators without the necessity for post-polymerization modification and protected initiators requiring end-group deprotection under appropriate conditions. ^{83,106–112}	22
Figure 13: Mechanisms of the thiol-ene click reaction: Anionic thiol-Michael addition, free-radical mechanism and termination reactions.	24
Figure 14: Polymer-analogous hydrolysis of poly(vinylphosphonates) to poly(vinylphosphonic acid). ^{70,122}	25
Figure 15: Overview of selected examples of natural and synthetic polymers for hydrogel synthesis.	27
Figure 16: Advantages and drawbacks of chemically cross-linked hydrogels.	29
Figure 17: Advantages of physically cross-linked hydrogels compared to the advantages of chemically cross-linked hydrogels.	31
Figure 18: Overview of different dynamic covalent chemistries.	33
Figure 19: Summary of structure-property relationships in hydrogels providing design considerations for developing innovative materials.	37
Figure 20: Operating principle of QCM-D.	38
Figure 21: Workflow for the synthesis and characterization of hydrogel materials obtained by photochemical cross-linking of poly(vinylphosphonates) applying thiol-ene click chemistry.	43
Figure 22: Two-step synthetic procedure toward highly hydrophilic, VPA-containing hydrogels with application potential as stimuli-responsive materials and superabsorbers.	44
Figure 23: Combination of photochemical cross-linking of poly(vinylphosphonates) with DIW of NFC/Alg inks to access printed objects with high dimensional stability upon swelling.	45
Figure 24: Self-healing of hydrogel materials facilitated by dynamic boronic ester complexation.	46
Figure 25: Table of content graphic for the manuscript entitled “Cytocompatible Hydrogels with Tunable Mechanical Strength and Adjustable Swelling Properties through Photo-Cross-Linking of Poly(vinylphosphonates)”	47

Figure 26: Table of content graphic for the manuscript entitled “Water Uptake, Thin-Film Characterization, and Gravimetric pH-Sensing of Poly(vinylphosphonate)-Based Hydrogels”. 63

Figure 27: Table of content graphic for the manuscript entitled “High-Fidelity Direct Ink Writing of Poly(vinylphosphonate)-Reinforced Polysaccharide Inks With Tunable Properties”. 81

Figure 28: Table of content graphic for the manuscript entitled “Modifications of Poly(vinylphosphonates) Toward Dynamic Covalent Networks” 95

Figure 29: Overview of different projects addressed in this thesis: Synthesis and fundamental characterization of poly(vinylphosphonate)-based hydrogels, studies on the pH-responsiveness of thin films of poly(vinylphosphonate)-based hydrogels, reinforcement of NFC/Alg inks in DIW through photo-cross-linking of poly(vinylphosphonates), and modifications of poly(vinylphosphonates) to create dynamic covalent networks..... 109

10.2 Supporting information

10.2.1 Supporting information for chapter 4

Supporting Information

Cytocompatible Hydrogels with Tunable Mechanical Strength and Adjustable Swelling Properties through Photo-Cross-Linking of Poly(vinylphosphonates)

Anton S. Maier,[†] Salma Mansi,[‡] Kerstin Halama,[†] Philipp Weingarten,[†] Petra Mela,[‡] and Bernhard Rieger^{†}*

[†] Technical University of Munich, Germany, TUM School of Natural Sciences, Department of Chemistry, WACKER-Chair of Macromolecular Chemistry, Lichtenbergstraße 4, 85748 Garching, Germany

[‡] Technical University of Munich, Germany, TUM School of Engineering and Design, Department of Mechanical Engineering, Chair of Medical Materials and Implants, Munich Institute of Biomedical Engineering, Munich Institute of Integrated Materials, Energy and Process Engineering, Boltzmannstraße 15, 85748 Garching, Germany

Corresponding Authors

* rieger@tum.de

TABLE OF CONTENTS

1. Materials and Methods	3
2. Statistical Copolymerization of Diethylvinylphosphonate (DEVPh) and Diallylvinylphosphonate (DAIVPh)	8
3. Hydrogel Synthesis and Characterization	18
4. Hydrogel Purification and Cytotoxicity Testing	34
5. Additional biocompatibility studies	39
6. References	42

1. MATERIALS AND METHODS

General Experimental

All air and moisture-sensitive compounds were prepared using standard Schlenk techniques or in a glovebox with argon (99.996 vol.-%) from Westfalen as an inert gas. All glass instruments were oven-dried prior to use. Unless otherwise stated, all chemicals and solvents were purchased from Sigma-Aldrich, ABCR GmbH, or TCI Chemicals and used without further purification. Dry solvents were obtained from an MBraun MB-SPS-800 solvent purification system or by drying over activated alumina and stored over activated 3 Å molecular sieves. Deuterated solvents were purchased from Sigma-Aldrich and dried over activated 3 Å molecular sieves. The monomers diethyl vinylphosphonate (DEVP), diallyl vinylphosphonate (DAIVP), the complex $\text{Cp}_2\text{YCH}_2\text{TMS}(\text{thf})$ and the initiator 4-(4-(((tert-butyl)dimethylsilyloxy)methyl)phenyl)-2,6-dimethylpyridine were synthesized according to literature-known procedures.¹⁻³ The monomers were dried over calcium hydride and distilled prior to polymerization.

Elemental analysis

All elemental analyses were performed by the Laboratory for Microanalysis at the Institute of Inorganic Chemistry at the Technical University of Munich.

LCST determination

The LCST was determined via DLS analysis on a Litesizer 500 particle size analyzer equipped with a 658 nm 40 mW laser diode. The samples were transferred into a 45 μL low volume quartz cuvette (3x3 mm light path, Hellma Analytics). The lower critical solution temperature was determined by measuring the transmittance of the sample between 20°C and 60 °C over one heating and one cooling cycle. Each temperature was equilibrated for 4 minutes, and the

transmittance was measured over 6 seconds. The sample concentration of polymer was 2 mg mL^{-1} in distilled water, and the sample was passed through a $0.45 \text{ }\mu\text{m}$ syringe filter before measuring. The cloud point was determined at a 10% decrease of the transmittance compared to the initial value.

Thermogravimetric analysis (TGA)

Thermogravimetric analyses were recorded on a Q5000 SA from TA Instruments. The samples were applied in tared platinum crucibles and heated from room temperature to 800 or 1000 °C under synthetic air, applying a continuous heating ramp of 10 K/min. The measurement data were analyzed using the TA Universal Analysis software.

Differential scanning calorimetry (DSC)

DSC measurements were recorded on a DSC Q2000 from TA Instruments in exo down mode. The temperature program consisted of three consecutive heating and cooling cycles with a continuous heating ramp of 5 K min^{-1} between $-70 \text{ }^{\circ}\text{C}$ and $170 \text{ }^{\circ}\text{C}$. The measurement data was analyzed using the TA Universal Analysis software.

Infrared spectroscopy (FT-IR)

The IR-spectra were recorded on a Vertex-70 FT-IR spectrometer from Bruker at room temperature.

Oscillatory rheology

Rheological characterizations were performed on an MCR 302 controlled-stress rheometer from Anton Paar with an upper plate (25 mm diameter) and a glass plate as counterpart (gap size 0.5 mm). The samples were applied in a liquid state ($250 \text{ }\mu\text{L}$) and tempered to $25 \text{ }^{\circ}\text{C}$ through an

upper and lower Peltier system. Additionally, a protective hood was used. To prevent solvent evaporation during the measurements, a circular, moisturized sponge was placed around the sample under the protective hood while avoiding contact with the sample. A MAX-302 lamp from Asahi Spectra with a cutoff wavelength below 400 nm was used for irradiation through the bottom glass plate. Measurements were performed every 10 seconds, and the data was monitored via the Rheoplus software. Additional parameters are specified in the description of the corresponding measurement result.

Nanoindentation

To measure the surface mechanical properties of the crosslinked samples, nanoindentation was performed in air and after swelling in distilled water with a Bioindenter (UNHT³) from Anton Paar (Graz, Austria) with a ruby spherical indenter of 500 μm radius. The loading rate was set from 40 $\mu\text{N min}^{-1}$ to a maximum of 20 $\mu\text{N min}^{-1}$ with a 30-second hold at the maximum load followed by unloading at 40 $\mu\text{N min}^{-1}$. The maximum indentation depth was fixed to 100 μm . For the experiments in water, the specimen was fixed on the Petri dish surface using duct tape and swollen for 120 minutes. The indentation modulus was calculated using a Hertzian fit to the loading data. For each sample, 6 measurements were performed with a sideward displacement of 500 μm .

Photochemical reactions

To induce photochemical crosslinking, the samples were irradiated at a 20 mm distance, resulting in a light power intensity of 150 mW cm^{-2} , applying a current of 700 mA and a forward voltage of 15.2 V.

Lyophilization

Lyophilization was performed on a VaCo 5-II-D from Zirbus Technology GmbH with a pressure of 2 mbar and a condenser temperature of -90 °C. Polymers subjected to freeze-drying were dissolved in 1,4-dioxane or distilled water before freezing in liquid nitrogen under constant rotation.

Size-exclusion chromatography multi-angle light scattering (SEC-MALS)

Polydispersities of the polymers were determined via size-exclusion chromatography (SEC) with sample concentrations of 4 mg mL⁻¹ on two PL Polargel-M columns (Agilent) at 40 °C. A mixture of water and THF (1:1), treated with tetrabutylammonium bromide (9 g L⁻¹) and 3,5-di-tert-butyl-4-hydroxytoluene (340 mg L⁻¹) was used as eluent. Samples were analyzed using a Wyatt Dawn Heleos II light scattering unit in combination with a Wyatt Optilab rEX as RI detector unit.

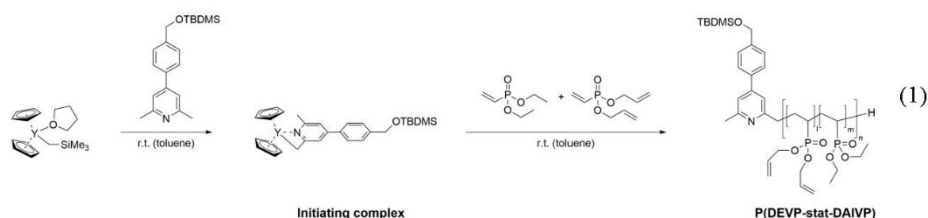
Nuclear magnetic resonance spectroscopy (NMR)

¹H-NMR- and ³¹P-NMR spectra of polymers were recorded on a Bruker AV-400HD, AV-500HD, or AV-II-500 spectrometer at 400 or 500 MHz (¹H) and 203 MHz (³¹P), respectively. All chemical shifts are given in parts per million (ppm) and referenced to the residual proton signal of the respective solvent (Benzene-d₆: δ = 7.16 ppm, Methanol-d₄: δ = 3.31 ppm). Deuterated solvents were purchased from Sigma-Aldrich or Deutero and dried over activated 3 Å molecular sieves. The NMR spectra were analyzed using the MestReNova software. ¹H DOSY NMR experiments were performed to characterize copolymers and functionalized copolymers.

Statistical analysis

The results of the cytotoxicity tests are expressed as the mean \pm standard deviation. The Shapiro-Wilk test was used to test normal distribution. When homogeneity of variances was fulfilled, the unpaired two-sided t-test between the groups with normal distribution was conducted. The unpaired two-sided t-test with Welch's correction was conducted for samples with unequal variances. The Mann-Whitney test was applied for samples without normal distribution. A statistically significant level was determined at $p < 0.05$. Data were analyzed using GraphPad Prism 10.

2. STATISTICAL COPOLYMERIZATION OF DIETHYLVINYLPHOSPHONATE (DEVP) AND DIALLYLVINYLPHOSPHONATE (DALVP)



The statistical copolymerization of DEVP and DAIVP was performed according to literature-known procedures.^{1,4} In a regular copolymerization experiment, the calculated amount of the catalyst precursor $\text{Cp}_2\text{ZrCH}_2\text{TMS}(\text{thf})$ is dissolved in dry toluene, and the corresponding amount of 4-(4-(((tert-butyldimethylsilyl)oxy)methyl)phenyl)-2,6-dimethylpyridine (1.10 eq.) added resulting in a yellow coloration of the solution upon formation of the initiating complex. The solution is stirred for two hours at room temperature before an aliquot (0.1 mL of the reaction mixture + 0.4 mL of dry benzene- d_6) is removed from the reaction mixture to ensure quantitative conversion of the catalyst precursor via $^1\text{H-NMR}$ spectroscopy. To initiate polymerization, the monomers DEVP and DAIVP are weighed into a syringe, mixed, and added to the reaction mixture in one motion. Upon confirmation of quantitative conversion via $^{31}\text{P-NMR}$ spectroscopy by withdrawing another aliquot (0.1 mL of the reaction mixture + 0.4 mL of undried methanol- d_4) from the reaction mixture, the polymerization is quenched by the addition of 0.5 mL of undried methanol. Subsequently, the polymer is precipitated from pentane. After centrifugation and decanting of the supernatant, the residual polymer was dissolved in 1,4-dioxane and subjected to freeze-drying, yielding the purified polymer.

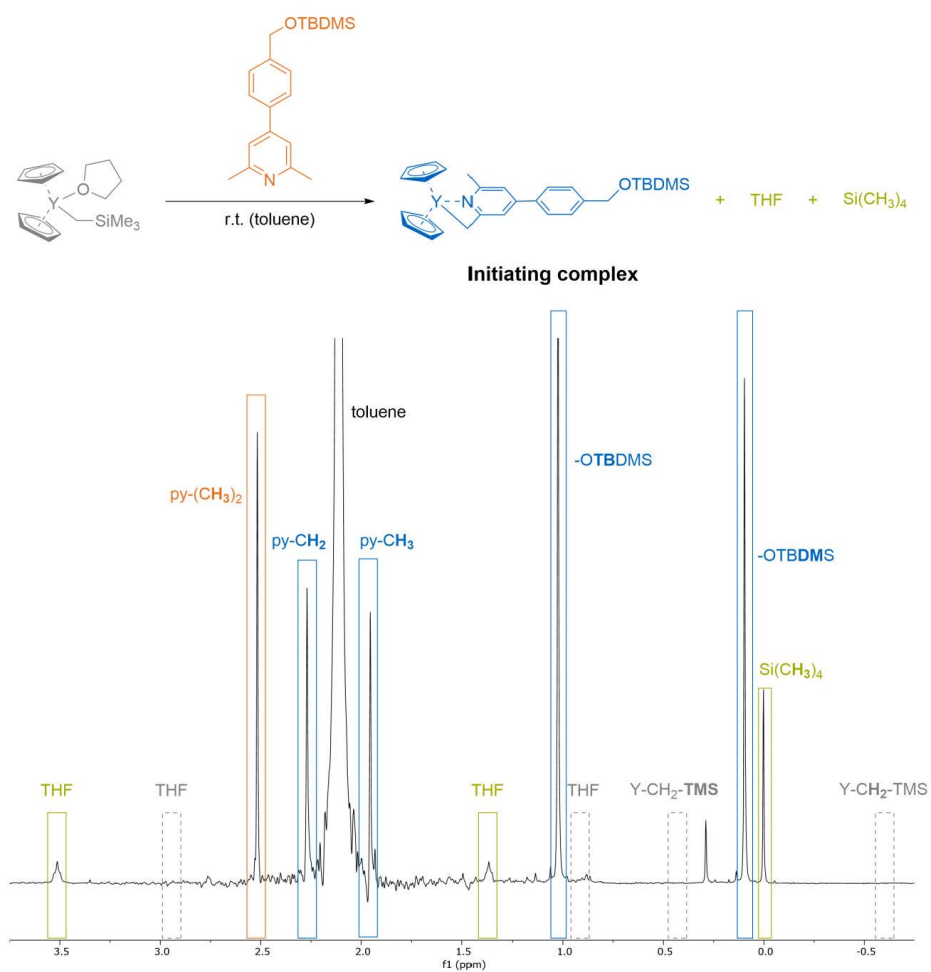


Figure S1: CH-bond activation of the initiator 4-(4-(((tert-butyl)dimethylsilyl)oxy)methyl)phenyl)-2,6-dimethylpyridine (orange) with Cp₂ZrCH₂TMS(thf) (grey) to yield the initiating complex (blue) and side products (green) and extract of the corresponding ¹H-NMR spectrum (Table 1, Entry 1). Dashed lines: catalyst signals prior to σ -bond metathesis.

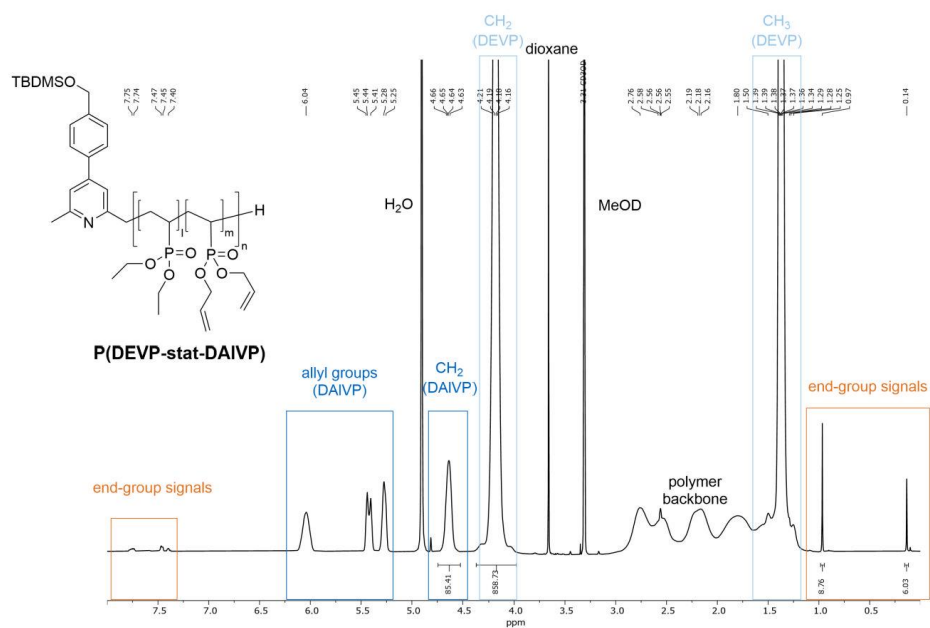


Figure S2: Exemplary copolymer ¹H-NMR spectrum of P(DEVP-stat-DAIVP) (Table 1, Entry 1) in MeOD with assignment of signals with relevant integrals for the determination of the molecular weight via ¹H-NMR spectroscopy.

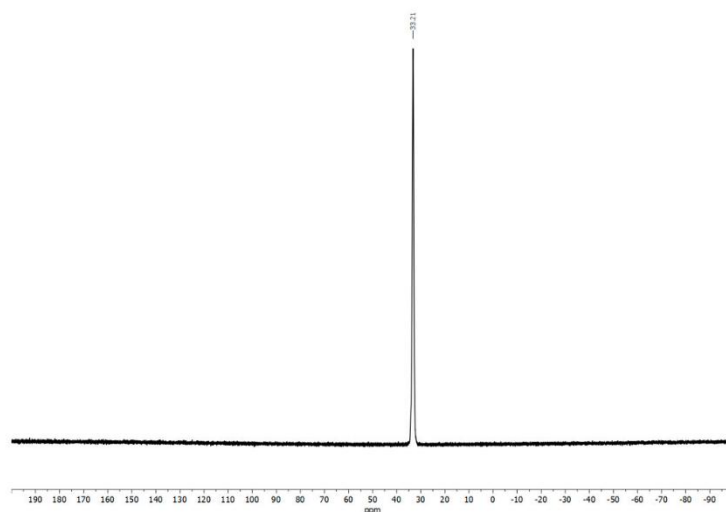


Figure S3: Exemplary ^{31}P -NMR spectrum of P(DEVP-stat-DAIVP) (Table 1, Entry 1) in MeOD.

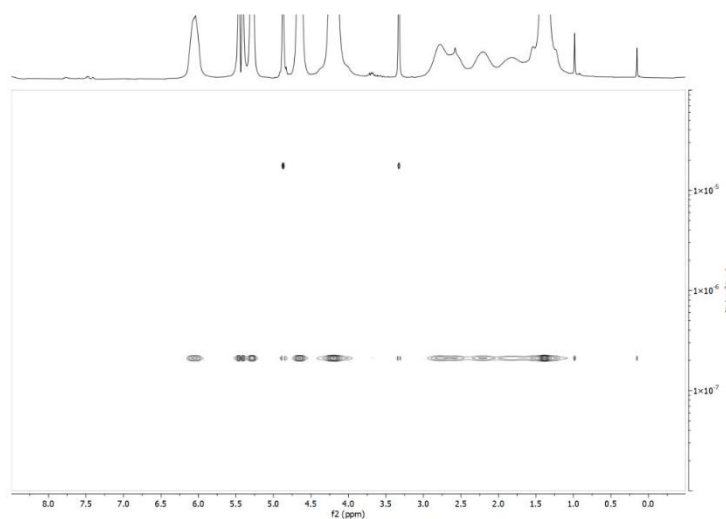


Figure S4: Exemplary ^1H DOSY NMR spectrum of P(DEVP-stat-DAIVP) (Table 1, Entry 6) in MeOD.

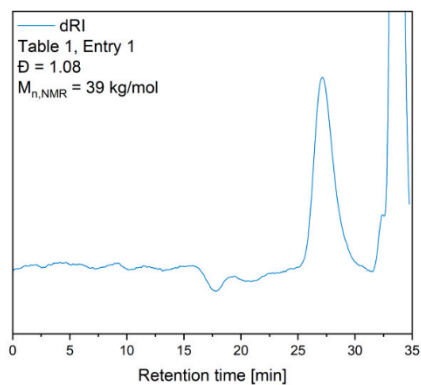


Figure S5: Refractive index detector signal of P(DEVP-stat-DAIVP) (Table 1, Entry 1) determined via SEC-MALS in THF/water (1:1) with tetrabutylammonium bromide (9 g L^{-1}) and 3,5-di-tert-butyl-4-hydroxytoluene (340 mg L^{-1}).

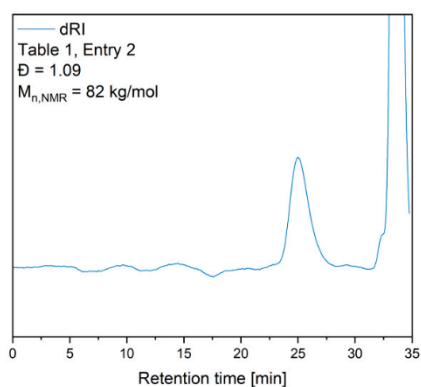


Figure S6: Refractive index detector signal of P(DEVP-stat-DAIVP) (Table 1, Entry 2) determined via SEC-MALS in THF/water (1:1) with tetrabutylammonium bromide (9 g L^{-1}) and 3,5-di-tert-butyl-4-hydroxytoluene (340 mg L^{-1}).

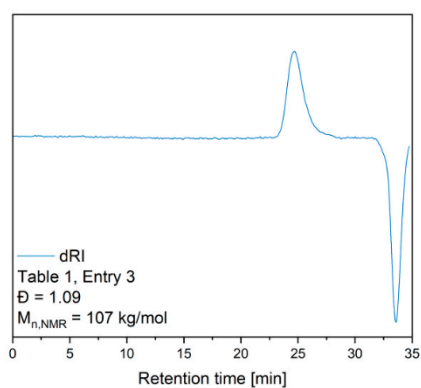


Figure S7: Refractive index detector signal of P(DEVP-stat-DAIVP) (Table 1, Entry 3) determined via SEC-MALS in THF/water (1:1) with tetrabutylammonium bromide (9 g L^{-1}) and 3,5-di-tert-butyl-4-hydroxytoluene (340 mg L^{-1}).

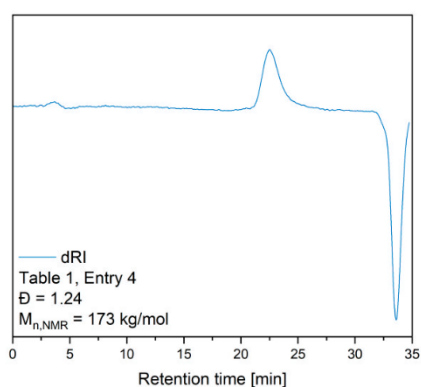


Figure S8: Refractive index detector signal of P(DEVP-stat-DAIVP) (Table 1, Entry 4) determined via SEC-MALS in THF/water (1:1) with tetrabutylammonium bromide (9 g L^{-1}) and 3,5-di-tert-butyl-4-hydroxytoluene (340 mg L^{-1}).

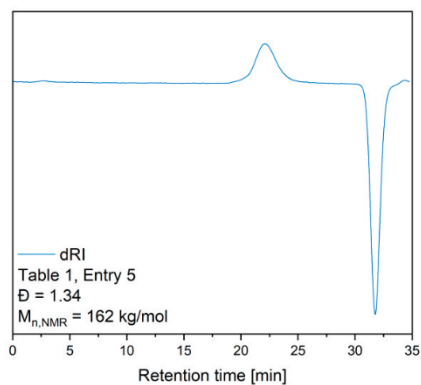


Figure S9: Refractive index detector signal of P(DEVP-stat-DAIVP) (Table 1, Entry 5) determined via SEC-MALS in THF/water (1:1) with tetrabutylammonium bromide (9 g L^{-1}) and 3,5-di-tert-butyl-4-hydroxytoluene (340 mg L^{-1}).

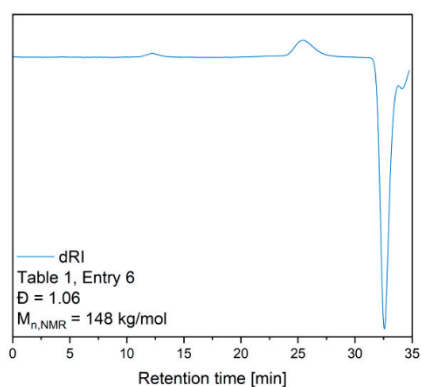


Figure S10: Refractive index detector signal of P(DEVP-stat-DAIVP) (Table 1, Entry 6) determined via SEC-MALS in THF/water (1:1) with tetrabutylammonium bromide (9 g L^{-1}) and 3,5-di-tert-butyl-4-hydroxytoluene (340 mg L^{-1}).

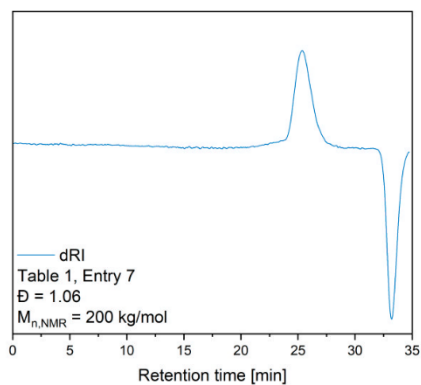


Figure S11: Refractive index detector signal of P(DEVP-stat-DAIVP) (Table 1, Entry 7) determined via SEC-MALS in THF/water (1:1) with tetrabutylammonium bromide (9 g L^{-1}) and 3,5-di-tert-butyl-4-hydroxytoluene (340 mg L^{-1}).

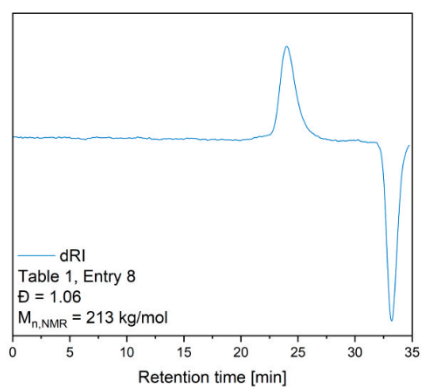


Figure S12: Refractive index detector signal of P(DEVP-stat-DAIVP) (Table 1, Entry 8) determined via SEC-MALS in THF/water (1:1) with tetrabutylammonium bromide (9 g L^{-1}) and 3,5-di-tert-butyl-4-hydroxytoluene (340 mg L^{-1}).

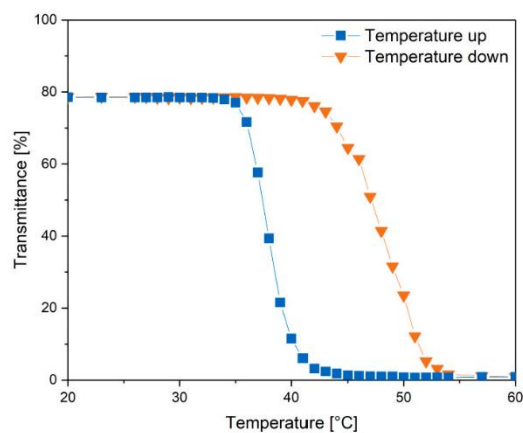


Figure S13: Determination of the cloud point of an aqueous solution of Entry 1, Table 1 via measurement of the transmittance of a 2 mg mL^{-1} solution of the polymer with increasing (blue symbols) and decreasing (orange symbols) temperature.

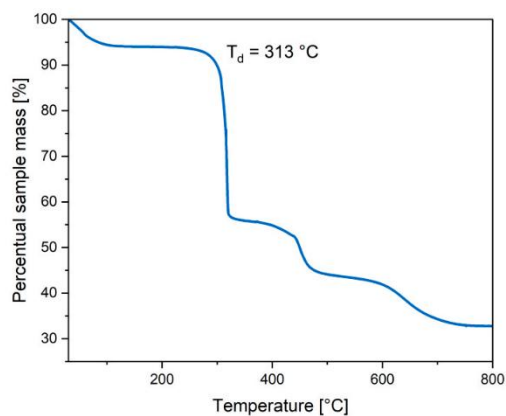


Figure S14: TGA measurement of Entry 3, Table 1 from room temperature to $800 \text{ }^\circ\text{C}$ under synthetic air with a heating rate of 10 K min^{-1} .

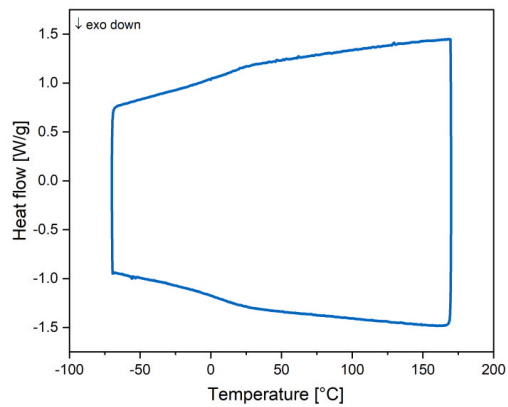


Figure S15: DSC measurement of Entry 3, Table 1 in the range of -70 to 170 °C measured in exo down mode.

3. HYDROGEL SYNTHESIS AND CHARACTERIZATION

Screening for hydrogel formation

Table S1: Screening of different reaction conditions and curing procedures for the formation of hydrogels from P(DEVP-stat-DAIVP) applying thiol-ene click chemistry with 3,6-dioxa-1,8-octanedithiol.

Entry	Reaction time	Curing procedure	Solvent	c (polymer) [mg/mL]	Degassed?	Gelation?
1	23 h	irradiation	THF/MeOH (5/1)	10	yes	yes
2	30 min	irradiation	THF/MeOH (5/1)	33	yes	yes
3	120 min	irradiation	H₂O	70	no	yes
4	120 min	irradiation	1,4-dioxane	160	no	yes
5	40 min	irradiation	1,4-dioxane	160	yes	yes
6	30 min	irradiation	1,4-dioxane	666	no	yes
7	60 min	heating (AIBN)	1,4-dioxane	160	no	yes

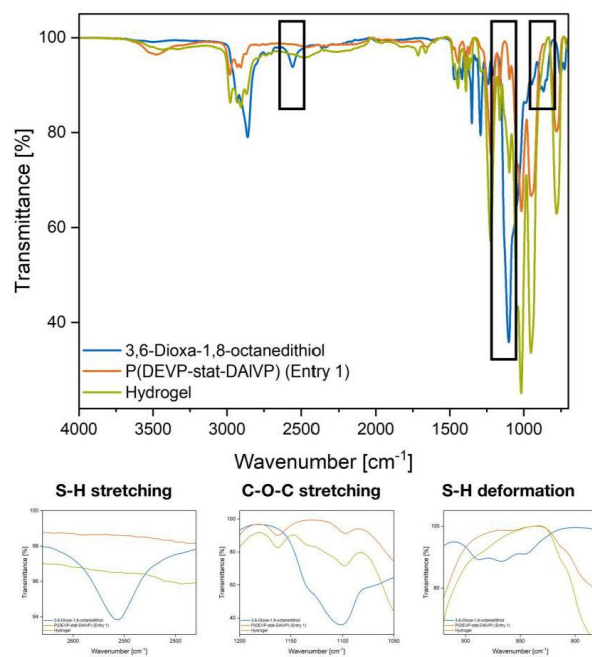


Figure S16: FT-IR spectra of the crosslinker (blue), the polymer (orange, Entry 1, Table 1), and the hydrogel (green): full spectra (top) and magnifications of the relevant regions in the full spectrum with assignments of signals (bottom).

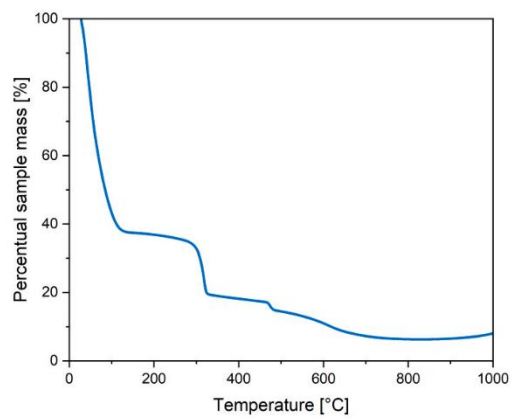


Figure S17: TGA measurement of a water-swollen hydrogel synthesized from Entry 8, Table 1 from room temperature to 1000 °C under synthetic air with a heating rate of 10 K min⁻¹.

Hydrogel synthesis for rheological experiments

In the rheological experiments described in the manuscript, gel samples subjected to characterization via oscillatory rheology were formed between the rheometer plates in situ. In a typical experiment, 100 mg of P(DEVP-stat-DAIVP) were dissolved in 0.3 mL of dioxane using a vortex mixer. Subsequently, the calculated amounts of 3,6-dioxa-1,8-octanedithiol (2.50 eq. with respect to the allyl groups of the polymer) and 2,2-dimethoxy-2-phenylacetophenone (0.40 eq. with respect to the allyl groups of the polymer) were added under light exclusion. Then, 0.25 mL of this stock solution was transferred onto the glass bottom plate of the rheometer, and the top plate was lowered. Next, the measurement was started, and irradiation of the sample from below ($\lambda = 365$ nm) was initiated at the desired time. In most cases, the sample behavior was studied for 5 minutes in the dark before measuring the rheological behavior upon irradiation for 5 minutes. As denoted in the manuscript, amplitude and frequency sweeps (Figures S13 and S14) on fully gelled samples to determine the linear viscoelastic region (LVR) were performed after irradiation of the polymer solutions between the plates for 5 minutes.

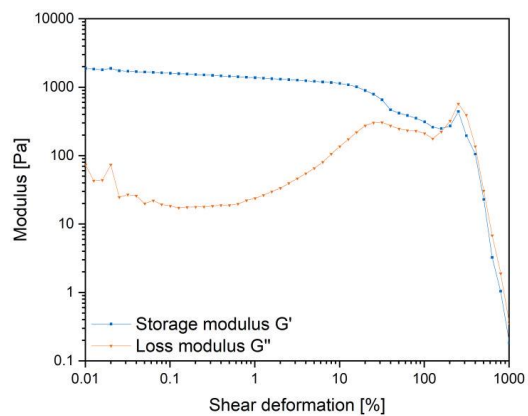


Figure S18: Amplitude sweep on a fully gelled sample with a frequency of 1 Hz and deformations between 0.01 and 1000%.

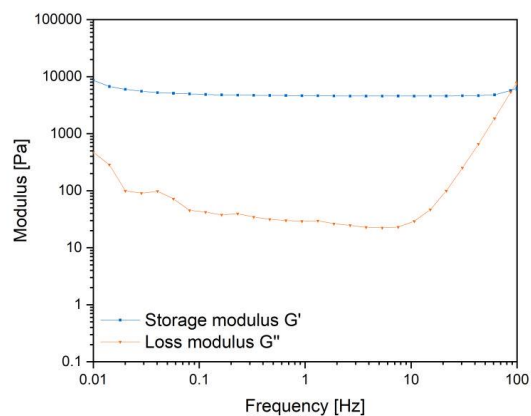


Figure S19: Frequency sweep on a fully gelled sample with a deformation of $\gamma = 1\%$ and frequencies between 0.01 and 100 Hz.

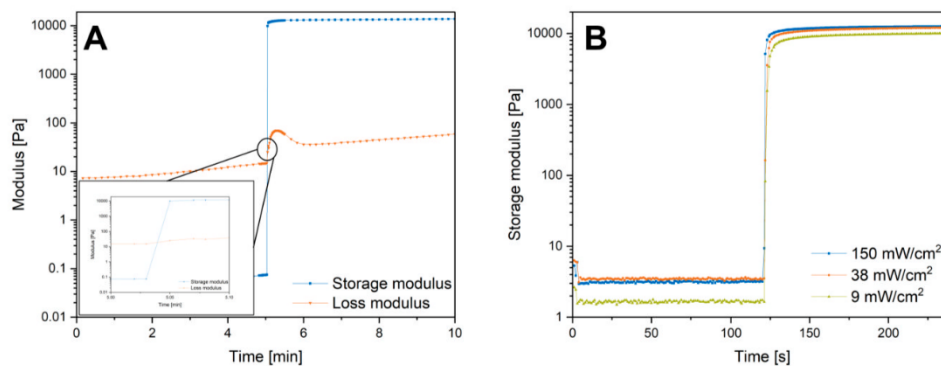


Figure S20: Kinetic investigation of the photochemical crosslinking of P(DEVP-stat-DAIVP) (Table 1, Entry 1) via photoinitiated thiol-ene click chemistry. Behavior of G' and G'' over time ($\gamma = 1\%$, $f = 5$ Hz) with irradiation ($\lambda = 365$ nm) after 5 minutes and a shorter measurement interval ($t = 1$ s) in the range of the sol-gel transition (A). Effect of the light intensity on the reaction rate of the thiol-ene reaction visualized by the development of the storage moduli upon crosslinking (light source activated after 120 seconds) (B).

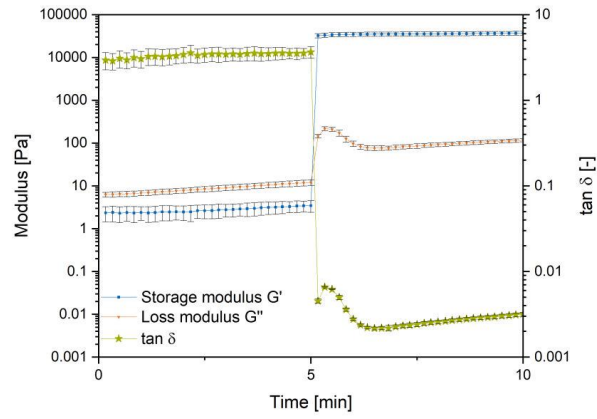


Figure S21: Rheological investigation of gelation process: behavior of G' , G'' and $\tan \delta$ over time ($\gamma = 1\%$, $f = 5$ Hz) with irradiation ($\lambda = 365$ nm) after 5 minutes.

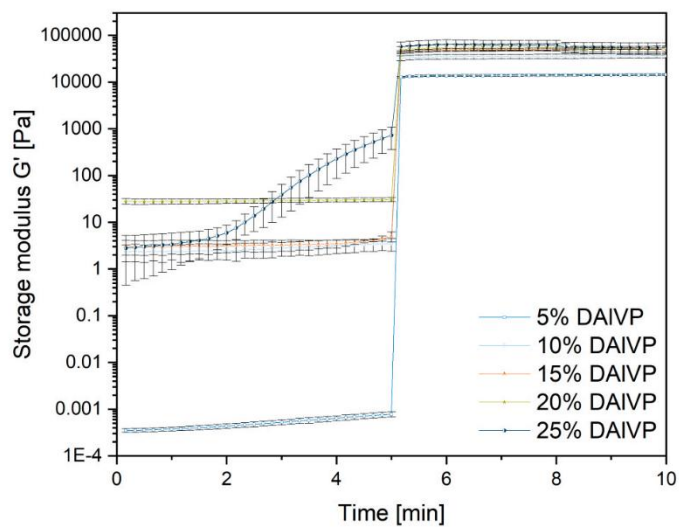


Figure S22: Behavior of the storage modulus over time and standard deviation for the evaluation of the mechanical strength of hydrogels formed from different P(DEVP-stat-DAIVP) copolymers at standard measurement conditions ($\gamma = 1\%$, $f = 5$ Hz). Start of irradiation ($\lambda = 365$ nm) after 5 minutes to give the plateau values of G' displayed in Figure 2A of the manuscript.

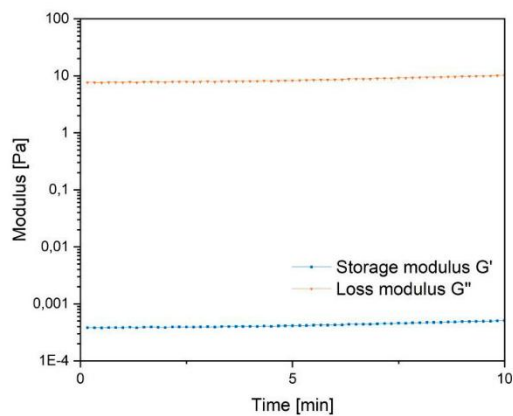


Figure S23: Rheological control experiment at standard measurement conditions ($\gamma = 1\%$, $f = 5$ Hz) without irradiation of the sample.

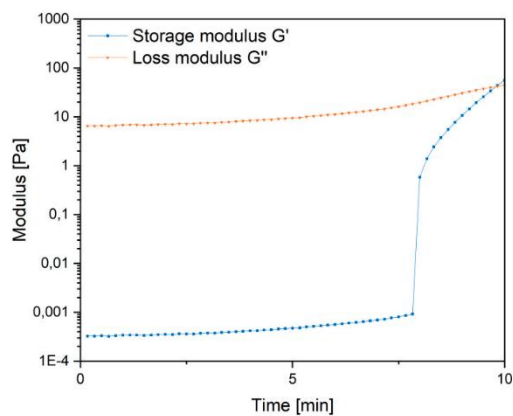


Figure S24: Rheological control experiment at standard measurement conditions ($\gamma = 1\%$, $f = 5$ Hz) with irradiation after 5 minutes and no initiator.

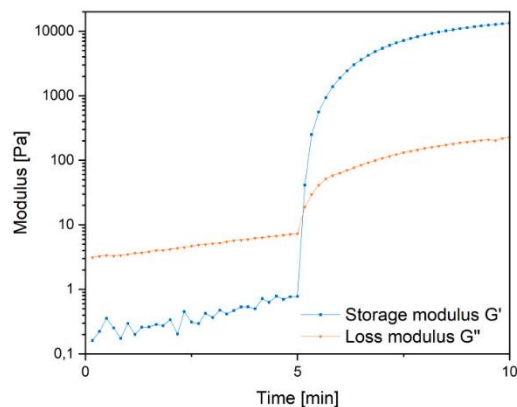


Figure S25: Rheological control experiment at standard measurement conditions ($\gamma = 1\%$, $f = 5$ Hz) with irradiation after 5 minutes without crosslinker.

Hydrogel synthesis for swelling experiments

To obtain crosslinked polymers for swelling experiments, 100 mg of respective P(DEVP-stat-DAIVP) copolymer were dissolved in 0.3 mL of dioxane in a polypropylene cup using a vortex mixer. Subsequently, calculated amounts of 3,6-dioxa-1,8-octanedithiol (2.50 eq. with respect to the allyl groups of the polymer) and 2,2-dimethoxy-2-phenylacetophenone (0.40 eq. with respect to the allyl groups of the polymer) were added under light exclusion. Then, the mixture was homogenized by vortexing and subjected to UV-irradiation ($\lambda = 365$ nm) for 60 minutes. Further, the solvent-swollen hydrogel chips obtained with this were dried in vacuo ($p = 6 \cdot 10^{-3}$ mbar) for 16 hours to remove residual solvent and excess crosslinker. Finally, after determining the weight of the dry samples, the dry gels were immersed in distilled water and swollen to constant mass for approximately 7 hours. To quantify the water uptake, the hydrogels were removed from the

solvent, and excess water was removed using paper tissue. The swelling ratio was calculated by comparing the weight of the swollen sample and the weight of the dry sample, as described in the manuscript.

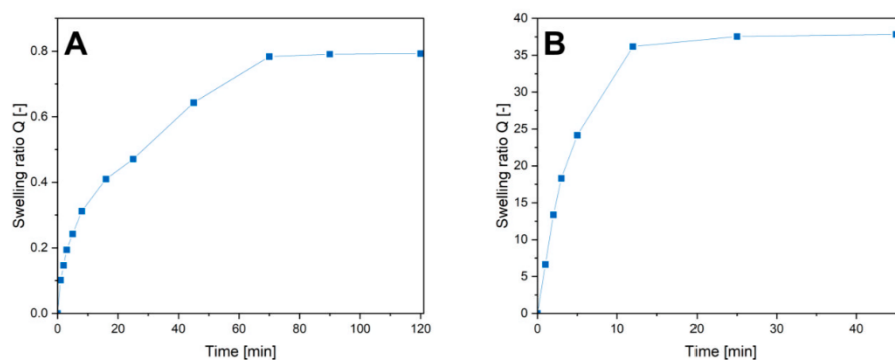


Figure S26: Water uptake kinetics of hydrogels originating from an unfunctionalized polymer (Table 1, Entry 4) (A) and a sulfonate-modified polymer (Table 2, Entry 11) (B).

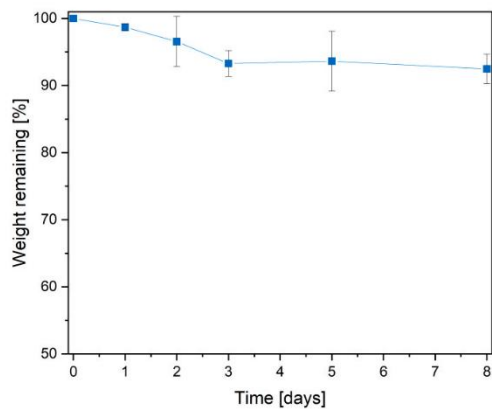
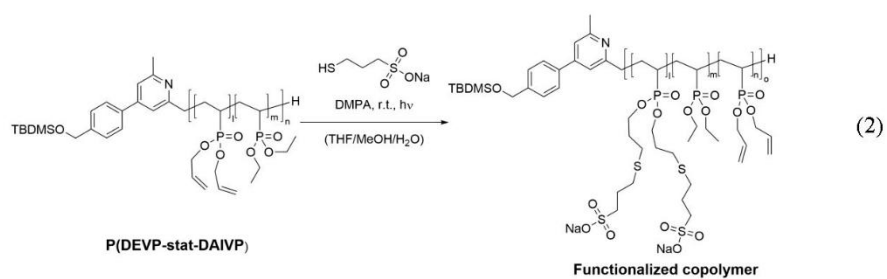


Figure S27: Investigation of the hydrolytic stability of hydrogels synthesized from Entry 1 (Table 1) under physiological conditions by determining the remaining weight relative to the weight of the swollen state over eight days in phosphate-buffered saline solution (pH 7.4) at 37 °C.

Functionalization of P(DEVP-stat-DAIVP) copolymers with sodium 3-mercaptopropane-1-sulfonate



The functionalization of P(DEVP-stat-DAIVP) with sodium 3-mercaptopropane-1-sulfonate was carried out according to a literature-known procedure.¹ In an oven-dried Schlenk flask, P(DEVP-

stat-DAIVP) was dissolved in a mixture of tetrahydrofuran, methanol, and water (THF/MeOH/H₂O = 5/1/1) (10 mL solvent per 100 mg of polymer). Subsequently, the calculated amounts of sodium 3-mercaptopropane-1-sulfonate (0.30 eq. with respect to the allyl groups of the polymer) and 2,2-dimethoxy-2-phenylacetophenone (DMPA) (0.10 eq. with respect to the allyl groups of the polymer) were added. The resulting clear solution was degassed through repeated application of vacuum and flooding with argon (15 iterations) and irradiated ($\lambda = 365$ nm) at room temperature for 15 hours. After the photoreaction, the solvent was removed in vacuo, and the residue was taken up in small amounts of distilled water. The functionalized polymer was then purified via dialysis (MWCO = 8 kDa) against distilled water and finally freeze-dried to afford the pure, functionalized polymers.

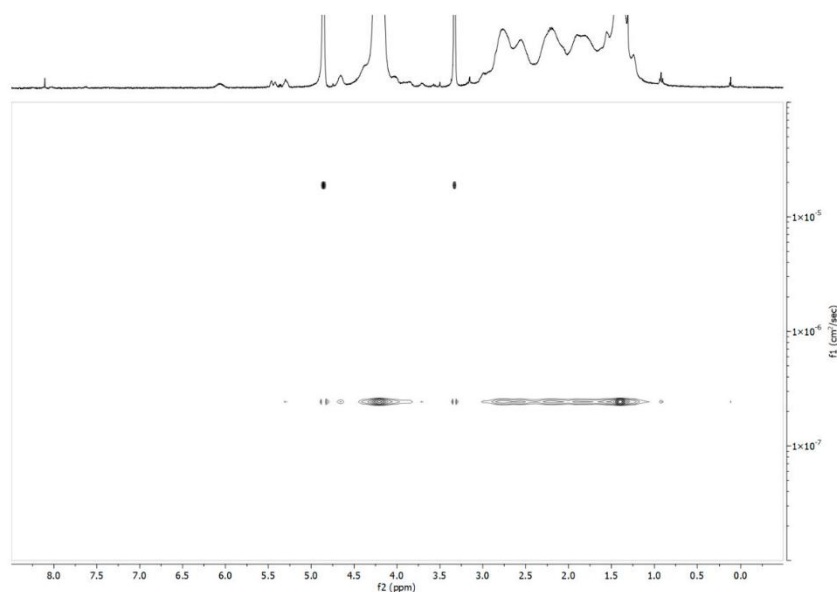


Figure S28: Exemplary ¹H DOSY NMR spectrum of functionalized P(DEVP-stat-DAIVP) in MeOD (Table 2, Entry 9).

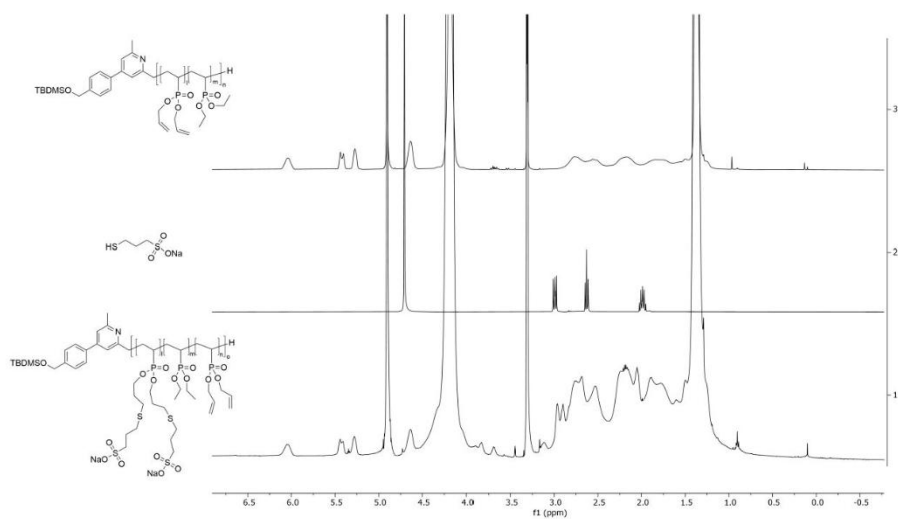


Figure S29: Functionalization of P(DEVP-stat-DAIVP) with sodium 3-mercaptopropane-1-sulfonate: ^1H -NMR spectrum of P(DEVP-stat-DAIVP) in MeOD (top), ^1H -NMR spectrum of sodium 3-mercaptopropane-1-sulfonate in D_2O (middle) and ^1H -NMR spectrum of functionalized P(DEVP-stat-DAIVP) (Table 2, Entry 10) in MeOD (bottom).

Table S2: Copolymer compositions determined via ¹H-NMR spectroscopy prior to click reaction and results of elemental analysis of functionalized polymers representing the calculation basis for the polymer compositions in the functionalization of P(DEVP-stat-DAIVP) with sodium 3-mercaptopropane-1-sulfonate.

Entry	DEVP unfunctionalized polymer [%]	DAIVP unfunctionalized polymer [%]	Equivalents of sulfonate with respect to allyl groups [-]	Theoretical sulfur content [wt.%]	Sulfur weight percentage via elemental analysis [wt.%]	Percentage of targeted functionalization degree of allyl groups [%]
9	96.2	3.8	0.30	0.87	0.53	60
10	90.1	9.9	0.30	2.15	1.51	70
11	84.7	15.3	0.30	3.19	2.72	85
12	79.4	20.6	0.30	4.15	2.74	66

Hydrogel synthesis and swelling with functionalized P(DEVP-stat-DAIVP)

The synthesis of hydrogels starting from functionalized P(DEVP-stat-DAIVP) was carried out similarly as described above. Unlike for the unfunctionalized copolymers, additional small amounts of water were added for polymers with high degrees of functionalization to help with solubilization of these highly hydrophilic compounds and achieve homogenous solutions for

crosslinking. The crosslinking and the determination of the water uptake were performed in the same way as for unfunctionalized polymers.



Figure S30: Images of hydrogel samples obtained from functionalized polymers: hydrogel in the dry state (left), highly swollen hydrogel without structural integrity (Table 2, Entry 9) (middle) and swollen hydrogel forming a soft and brittle chip (Table 2, Entry 11).

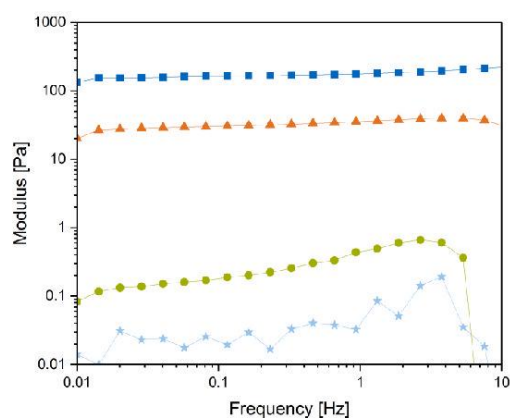


Figure S31: Frequency sweeps on fully gelled samples synthesized from sulfonate-functionalized polymers (83 mg mL^{-1}) with a deformation of $\gamma = 1\%$ and frequencies between 0.01 and 10 Hz: Entry 9 (light blue), entry 10 (green), entry 11 (orange), and entry 12 (blue).

4. HYDROGEL PURIFICATION AND CYTOTOXICITY TESTING

Hydrogel purification by Soxhlet extraction

Table S3: Sample descriptions, purification procedures, and fractions of extractable compounds and gel for hydrogels used in the extract test performed according to ISO 10993.

Hydrogel	Description	Solvent	Temperature (distillation flask)	Duration	Extractable fraction [%]	Gel Fraction [%]
1	P(DEVP-stat-DAIVP) (5% DAIVP), standard crosslinker (excess during synthesis)	EtOH, H ₂ O	140 °C (EtOH) 150 °C (H ₂ O)	9 h (EtOH) 18 h (water)	23	77
2	P(DEVP-stat-DAIVP) (5% DAIVP), standard crosslinker (excess during synthesis)	EtOH, H ₂ O	140 °C (EtOH) 150 °C (H ₂ O)	9 h (EtOH) 18 h (water)	14	86
3	P(DEVP-stat-DAIVP) (5% DAIVP), standard crosslinker (stoichiometric amounts)	EtOH, H ₂ O	140 °C (EtOH) 150 °C (H ₂ O)	9 h (EtOH) 18 h (water)	13	87
4	P(DEVP-stat-DAIVP) (10% DAIVP), standard crosslinker (excess during synthesis)	H ₂ O	150 °C	25 h	33	67
5	P(DEVP-stat-DAIVP) (10% DAIVP) standard crosslinker (stoichiometric amounts)	H ₂ O	150 °C	25 h	26	74

In the first step, the weight of dry samples subjected to Soxhlet extraction was determined for the calculation of sol and gel fractions. Subsequently, the dry gels were transferred into the thimble, and the Soxhlet apparatus was assembled. Soxhlet extraction was either carried out with ethanol followed by water or with water exclusively (for experimental details, see Table S3). After

complete purification, the hydrogels were dried in vacuo ($p = 6 \cdot 10^{-3}$ mbar) for 16 hours and the weight determined for comparison with the initial weight.

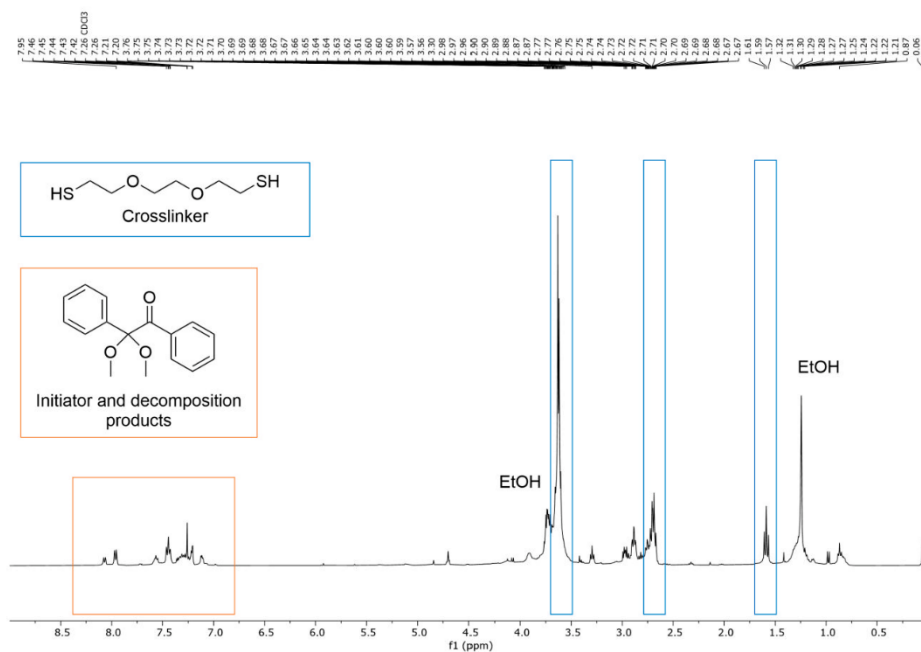


Figure S32: $^1\text{H-NMR}$ spectrum (solvent: CDCl_3) of the residue in the distillation flask after removal of the solvent from the Soxhlet extraction of Hydrogel 2, Table S2.

Cytotoxicity test

The cytotoxicity testing of hydrogels was conducted based on the extract test according to the ISO 10993. Human umbilical artery smooth muscle cells (HUASMCs) were cultured in Dulbecco's modified Eagle medium (DMEM, Gibco) supplemented with 10% v/v fetal bovine serum (FBS, Gibco) and 1% antibiotics/antimycotics (ABM, Gibco) at 37°C in a humidified atmosphere containing 5% CO₂. The developed hydrogels were first washed twice using 70% ethanol for 30 minutes each, subsequently rinsed with phosphate-buffered saline solution (PBS, Gibco), and then incubated in DMEM for 72 h at 37°C to create the eluates according to the defined weight/volume extraction ratios defined by the ISO. Untreated DMEM (Gibco, USA) was used as the negative control, and the eluate of a latex glove was incubated in DMEM for 72 h at 37°C as the positive control. HUASMCs were cultured in untreated medium in 96 wells at a cell density of 10 000 cells cm⁻² for 24 h, then the medium was aspirated before the eluates of the samples and controls were transferred to the corresponding wells. After 72 hours at 37°C and 5 % CO₂, the XTT proliferation assay (Invitrogen) was performed according to the manufacturer's instructions, and the absorbance at 450 nm was measured using the microplate reader (Spark, Tecan). The relative absorbance was calculated by normalizing the absorbance values to that of the negative control. Hydrogels exhibiting cell viability above 70 %, which is the threshold defined by the ISO, were considered non-cytotoxic.

Cell adhesion test

The hydrogels were washed with 70 % ethanol for 1 hour, rinsed with phosphate-buffered saline solution (PBS, Gibco), dried for 20 minutes, and transferred into 96 well plates (Greiner Bio-One). Human umbilical artery smooth muscle cells (HUASMCs) were seeded at a density of

10 000 cells cm^{-2} on the hydrogel surface and incubated in DMEM (Gibco, USA), supplemented with 10 % fetal bovine serum (Gibco, USA) and 1 % antibiotic-antimycotic (Gibco, USA) for 72 hours. The surface of a well plate (Greiner Bio, Germany) was used as the control. The XTT proliferation assay (Invitrogen) was performed according to the manufacturer's instructions, and the absorbance at 450 nm was measured using the microplate reader (Spark, Tecan). The relative absorbance was calculated by normalizing the absorbance values to that of the control (well surface). Subsequently, the cells were fixed in a 4 % formaldehyde solution (Carl Roth, Germany) in PBS for 15 minutes at room temperature and stained for fluorescence imaging. Briefly, the samples were blocked and permeabilized with PBS containing 5 % normal goat serum (Dako, Germany) and 0.1 % Triton X-100 (Sigma, Germany) for 60 min at room temperature. Staining for actin was performed with Acti-stain phalloidin 488 (Biozol, Germany) for 1 hour at 37 °C, and nuclei staining subsequently with DAPI (Invitrogen, USA) for 5 minutes at room temperature. Fluorescence images were taken with the BZ-X800 microscope (Keyence, Japan).

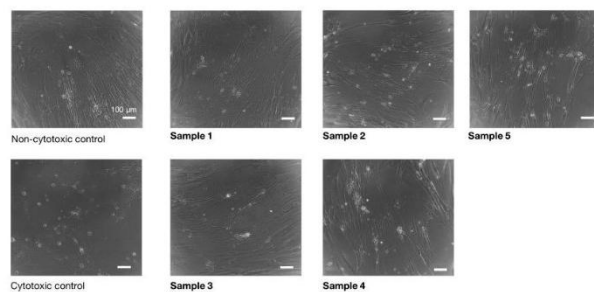


Figure S33: Qualitative evaluation of the cytotoxicity test based on the extract test according to ISO 10993. Microscopic images of human umbilical artery smooth muscle cells (HUASMCs) incubated for 72 h in presence of the eluates of Hydrogels 1-5 as well as of untreated cell culture medium as the negative control (NC) and of the eluate of a latex glove as the positive control (PC). Scale bar: 100 μm .

5. ADDITIONAL BIOCOMPATIBILITY STUDIES

Immune response via ELISA THP-1 cytokine release

The immune response to the hydrogels was evaluated by quantifying the cytokine release of monocyte-derived macrophages. The human cell line THP-1 (ATCC) was cultured in RPMI 1640 medium (Gibco, Life Technologies, Paisely, UK) supplemented with 10% fetal calf serum (Gibco), 2 mM l-glutamine (Gibco), 1 mM sodium pyruvate (Gibco), 1 U mL⁻¹ penicillin and 1 µg mL⁻¹ streptomycin (Gibco). The cells were differentiated into M0 macrophages using 100 µM phorbol 12-myristate 13-acetate for 72 h and were allowed to rest in a complete culture medium for 24 h. Prior to the assay, circular hydrogel discs with a surface area of 1 cm² were incubated in RPMI medium overnight to reach an equilibrium in their liquid uptake. The cells were then seeded at a density of 250 000 cells cm⁻¹ onto the samples, and the released cytokine concentration in the cell culture supernatant was evaluated after 72 h of incubation at 37 °C with 5% CO₂. The released pro-inflammatory (interleukin-6, tumor necrosis factor- α) and anti-inflammatory (transforming growth factor β , interleukin-10) cytokines were quantified with the DuoSet ELISA Development System (R&D Systems, Minneapolis, MN, USA) following the manufacturer's instructions using a multimode microplate reader (Spark, Tecan, Männedorf, Switzerland).

Bacterial adhesion

Determination of the bacterial adhesion was conducted with the strains *S. aureus* NCTC 8325-4 and *E. coli* ATCC 25922. Circular hydrogel discs with a diameter of 6 mm were sterilized in 70% ethanol for 1 h and then washed in phosphate-buffered saline (PBS) for 1 h. 10 µl of the bacterial suspensions with a concentration of 10⁹ CFU mL⁻¹ were subsequently seeded onto the hydrogel samples. After incubating the samples at 37 °C for 3 h, non-adherent bacteria were removed by

washing the samples thrice in 5 mL sterile PBS. The samples were then vortexed in PBS for 1 min to remove the adherent bacteria, which were quantified by plating serial dilutions on Chapman agar. The agar plates were incubated at 37 °C for 48 h, and the colonies were counted to quantify the number of adherent bacteria. Log reduction is calculated by determining the log₁₀ of the ratio of the initial seeding concentration to the final adherent bacterial concentration.

Endothelialization

To evaluate the ability of the hydrogels to support endothelialization, human umbilical vein endothelial cells (HUVECs) were used to investigate the formation of an endothelial layer on the hydrogel sample surface. HUVECs were cultured in endothelial cell basal medium (EBM-2, Lonza Group AG, Basel, Switzerland) supplemented with the endothelial growth medium 2 kit. Supplements included 0.1% insulin, 0.1% gentamicin, 0.1% ascorbic acid, 0.4% human fibroblast growth factor, 2% fetal bovine serum (FBS), 0.1% endothelial growth factor, 0.04% hydrocortisone, 0.1% epidermal growth factor, and 0.1% heparin. Prior to the assay, circular hydrogel discs with a diameter of 6 mm were incubated in EGM-2 medium overnight to reach an equilibrium in their liquid uptake. The cells were then seeded at a density of 10 000 cells cm⁻¹ onto the samples. After incubation for 24 hours at 37 °C, the samples were rinsed with PBS and fixed in 4% paraformaldehyde (Thermo Fisher Scientific Inc., USA) at room temperature for 15 min. Then, the samples were washed three times in PBS and blocked in a PBS solution (Gibco) with 5% normal goat serum (DAKO GmbH, Jena, Germany) for 1 h at room temperature. CD31 primary antibody (Sigma) 1:100 diluted in 0.1 % bovine serum albumin solution (BSA, Sigma, Germany) was added for 1 h at room temperature and followed by three washing steps for 5 min in PBS. Alexa 647 secondary antibody (Molecular Probes) 1:400 diluted in 0.1 % BSA solution was subsequently added. After 1 h incubation at room temperature, the samples were washed 3x

for 5 min in PBS. DAPI diluted in PBS (0.2 $\mu\text{g}/\text{ml}$) was added for nuclei staining (Thermo Fisher Scientific Inc, USA). Finally, the samples were imaged under the fluorescence microscope BZ-X800 (Keyence, Japan).

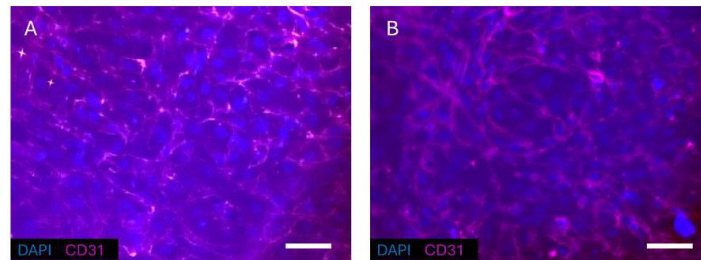


Figure S34: Immunohistochemical analysis of the endothelialization of the hydrogel samples. Immunohistochemical staining for CD31 of seeded endothelial cells on HG1 (A) and HG2 (B). 4',6-diamidino-2-phenylindole (DAPI) was used as cell nuclear counterstain (blue). Scale bar: 50 μm .

6. REFERENCES

- (1) Halama, K.; Schaffer, A.; Rieger, B. Allyl Group-Containing Polyvinylphosphonates as a Flexible Platform for the Selective Introduction of Functional Groups via Polymer-Analogous Transformations. *RSC Adv.* **2021**, *11* (61), 38555–38564.
- (2) Salzinger, S.; Soller, B. S.; Plikhta, A.; Seemann, U. B.; Herdtweck, E.; Rieger, B. Mechanistic Studies on Initiation and Propagation of Rare Earth Metal-Mediated Group Transfer Polymerization of Vinylphosphonates. *J. Am. Chem. Soc.* **2013**, *135* (35), 13030–13040.
- (3) Schaffer, A.; Kränzlein, M.; Rieger, B. Synthesis and Application of Functional Group-Bearing Pyridyl-Based Initiators in Rare Earth Metal-Mediated Group Transfer Polymerization. *Macromolecules* **2020**, *53* (11), 4345–4354.
- (4) Soller, B. S.; Salzinger, S.; Jandl, C.; Pöthig, A.; Rieger, B. C–H Bond Activation by σ -Bond Metathesis as a Versatile Route toward Highly Efficient Initiators for the Catalytic Precision Polymerization of Polar Monomers. *Organometallics* **2015**, *34* (11), 2703–2706.

10.2.2 Supporting information for chapter 5

Supporting Information

Water Uptake, Thin-Film Characterization, and Gravimetric pH-Sensing of Poly(vinylphosphonate)-Based Hydrogels

Anton S. Maier¹, Matjaž Finšgar², Beatrice De Chiara³, Rupert Kargl^{4,}, Bernhard Wolfrum³, Karin Stana Kleinschek⁴, and Bernhard Rieger^{1,*}*

¹Technical University of Munich, TUM School of Natural Sciences, Department of Chemistry, WACKER-Chair of Macromolecular Chemistry, Lichtenbergstraße 4, 85748 Garching, Germany

²Faculty of Chemistry and Chemical Engineering, University of Maribor, 2000 Maribor, Slovenia

³Technical University of Munich, TUM School of Computation, Information and Technology, Munich Institute of Biomedical Engineering, Department of Electrical Engineering, Neuroelectronics, Hans-Piloty-Str. 1, 85748 Garching, Germany

⁴Graz University of Technology, Institute for Chemistry and Technology of Biobased Systems (IBioSys), Stremayrgasse 9, 8010 Graz, Austria

Corresponding Authors

* rieger@tum.de

*rupert.kargl@tugraz.at

TABLE OF CONTENTS

1. Materials and Methods	3
2. Polymer and hydrogel synthesis	9
3. Thin-film preparation and characterization	15
4. Quartz crystal microbalance measurements	17
5. References	20

1. MATERIALS AND METHODS

General Experimental

All air and moisture-sensitive compounds were prepared using standard Schlenk techniques or in a glovebox with argon (99.996 vol.-%) from Westfalen as inert gas. All glass instruments were oven-dried prior to use. Unless otherwise stated, all chemicals and solvents were purchased from Sigma-Aldrich, ABCR GmbH, or TCI Chemicals and used without further purification. Dry solvents were obtained from an MBraun MB-SPS-800 solvent purification system or by drying over activated alumina and stored over activated 3 Å molecular sieves. Deuterated solvents were purchased from Sigma-Aldrich and dried over activated 3 Å molecular sieves. The monomers diethyl vinylphosphonate (DEVP), diallyl vinylphosphonate (DAIVP), the complex $\text{Cp}_2\text{YCH}_2\text{TMS}(\text{thf})$ and the initiator 4-(4-(((tert-butyl)dimethylsilyloxy)methyl)phenyl)-2,6-dimethylpyridine were synthesized according to literature-known procedures.¹⁻³ The monomers were dried over calcium hydride and distilled prior to polymerization.

Atomic force microscopy (AFM)

The surface morphology of thin hydrogel films coated onto the gold surfaces of QCM resonators was investigated using an atomic force microscope Tosca 400 from Anton Paar (Graz, Austria). The images were scanned in tapping mode with a silicon SPM-sensor (Arrow-NCR-50) from Nanoworld (Switzerland) with a resonance frequency of 285 kHz and a force constant of 42 N/m. Image sizes of $10\ \mu\text{m} \times 10\ \mu\text{m}$, $5\ \mu\text{m} \times 5\ \mu\text{m}$, and $1\ \mu\text{m} \times 1\ \mu\text{m}$ were scanned at a speed of 0.9 lines/second at room temperature. Image processing was done using the Gwyddion software.

Preparation of quartz crystal microbalance sensors

QCM 5 MHz 14 mm Cr/Au sensors were purchased from Quartz Pro AB, Sweden. Before the measurements, the QCM-D crystals were cleaned in several steps. First, the substrates were immersed in a solution containing 50 mL distilled water, 10 mL ammonia (25% in water), and 10 mL hydrogen peroxide (30% in water) and heated to 70 °C for 15 minutes. Subsequently, the crystals were dipped into distilled water for 15 minutes. After drying, the crystals were brought into contact with “piranha” solution containing H₂O₂ (30%) and H₂SO₄ (85%) in a ratio of 1:3 (v/v) for 60 seconds. Finally, the previous solution was removed by placing the QCM sensors in Milli-Q water for 15 minutes before drying them with nitrogen gas. In case of residual remains on the crystals front or backside, these were carefully removed with an acetone-soaked cotton swab, and the sensors dried again.

Cleaning of silicon wafers

Silicon wafers from Topsil (Germany) with (100) surface orientation were cut into pieces of 15 × 15 mm² and used for spin-coating, followed by layer thickness determination via profilometry. First, the substrates were rinsed with distilled water, followed by ethanol and distilled water. Subsequently, the wafers were immersed in “piranha” solution containing H₂O₂ (30%) and H₂SO₄ (85%) in a ratio of 1:3 (v/v) for 30 minutes. After removing them from the acidic solution, the silicon plates were placed in Milli-Q water for 30 minutes. Finally, each substrate was dried with nitrogen gas and thoroughly cleaned with an acetone-soaked cotton swab.

Lyophilization

Lyophilization was performed on a VaCo 5-II-D from Zirbus Technology GmbH with a pressure of 2 mbar and a condenser temperature of -90 °C. Polymers subjected to freeze-drying were

dissolved in 1,4-dioxane or distilled water before freezing in liquid nitrogen under constant rotation.

Nuclear magnetic resonance spectroscopy (NMR)

¹H-NMR- and ³¹P-NMR spectra of polymers were recorded on a Bruker AV-400HD, AV-500HD, or AV-II-500 spectrometer at 400 or 500 MHz (¹H) and 203 MHz (³¹P), respectively. All chemical shifts are given in parts per million (ppm) and referenced to the residual proton signal of the respective solvent (Benzene-d₆: δ = 7.16 ppm, Methanol-d₄: δ = 3.31 ppm). Deuterated solvents were purchased from Sigma-Aldrich or Deutero and dried over activated 3 Å molecular sieves. The NMR spectra were analyzed using the MestReNova software. ¹H DOSY NMR experiments were performed to characterize copolymers and functionalized copolymers.

Oscillatory Rheology

Rheological characterizations were performed on an MCR 302 rheometer from Anton Paar with an upper plate (25 mm diameter), a glass plate as a counterpart, and a gap size of 0.5 mm. The samples were applied in a liquid state (250 μL) and tempered to 25 °C through an upper and lower Peltier system. Additionally, a protective hood was used. A MAX-302 lamp from Asahi Spectra with a cutoff wavelength below 400 nm was used for irradiation through the bottom glass plate to form the hydrogels in situ before the measurements. Data acquisition took place every 10 seconds, and the data was monitored via the Rheoplus software. Frequency sweeps were performed at 1% deformation between 0.01 and 10 Hz.

Profilometry

The thickness of hydrogel thin films on cleaned silicon wafers was determined via profilometry using a DektakXT from Bruker. Therefore, the scan profile was set to hills and valleys with a scan length of 2000 μm in 10 seconds. Further, the Stylus radius was 12.5 μm with a force of 3 mg and a resolution of 0.666 $\mu\text{m}/\text{pt}$. Before analyzing the height profile, each sample was scratched to the substrate surface multiple times with a small razor blade to remove the films and obtain film heights with a step-height profile. In this context, film thickness determinations were carried out with 4 different substrates and at various positions on each substrate to calculate standard deviations.

Quartz crystal microbalance with dissipation monitoring (QCM-D)

QCM-D measurements were performed on cleaned quartz crystals on a QCM-D model E4 instrument from Q-Sense (Gothenburg, Sweden). The instrument simultaneously detects changes in the resonance frequency (Δf) and the energy dissipation (ΔD) caused by mass deposition or removal on an oscillating piezoelectric crystal. In this context, ΔD is applied to describe the viscoelastic properties of the material on the crystal as it refers to energy losses due to friction, causing a damping of the oscillation. Mass depositions on the crystals were calculated using the Sauerbrey equation, which correlates frequency changes Δf_n of certain overtones to the mass deposition on the crystals. A more detailed mathematical description can be found below.

Size-exclusion chromatography multi-angle light scattering (SEC-MALS)

Polydispersities of the polymers were determined via size-exclusion chromatography (SEC) with sample concentrations of 4 mg mL^{-1} on two PL Polargel-M columns (Agilent) at 40 $^{\circ}\text{C}$. A mixture of water and THF (1:1), treated with tetrabutylammonium bromide (9 g L^{-1}) and 3,5-di-tert-butyl-

4-hydroxytoluene (340 mg L⁻¹) was used as eluent. Samples were analyzed using a Wyatt Dawn Heleos II light scattering unit in combination with a Wyatt Optilab rEX as RI detector unit.

Spin-coating of quartz crystals and silicon wafers

The spin-coating of quartz crystals and silicon wafers was performed according to well-established procedures.^{4,5} The P(DEVP-stat-DAIVP-stat-VPA)-containing films were deposited on the static substrates by pipetting 50 μ L of a 85 ppm (0.0085 wt.%) polymer-containing stock solution in methanol/water (6/1) onto the surfaces of either the QCM-D crystals or the silicon wafers. Immediately after adding the stock solution, the substrates were rotated at a spinning speed of 4000 rpm with an acceleration of 2500 rpm/s for 60 seconds.

Time-of-flight secondary ion mass spectrometry (ToF-SIMS)

Time-of-flight secondary ion mass spectrometry (ToF-SIMS) measurements were performed using an M6 instrument (Iontof, Münster, Germany) with a 30 keV Bi₃⁺ primary ion beam operating at a target current of 0.6 pA. Spectra were calibrated using signals at known *m/z* values. Depth profiling was performed with a 2.5 keV Ar₁₃₀₀⁺ gas cluster ion beam (GCIB), applying a target current of 1 nA. Sputtering was carried out over a 500 by 500 μ m area, while the analysis was conducted in the central 300 by 300 μ m of the sputtered crater.

X-ray photoelectron spectroscopy (XPS)

X-ray photoelectron spectroscopy (XPS) analyses were conducted using a Supra+ system (Kratos, Manchester, UK) equipped with an Al K α excitation source. The spectra were calibrated using the C 1s peak corresponding to C-C/C-H at 284.8 eV. The spin-coated QCM-D sensor sample was mounted on the sample holder using a silicone-free double-sided tape. Measurements were

performed at a 90° take-off angle, with a spot size of 300 by 700 μm and a pass energy of 20 eV for high-resolution spectra and 160 eV for survey spectrum. Data collection and analysis were performed using Kratos' ESCApe 1.5 software.

2. POLYMER AND HYDROGEL SYNTHESIS

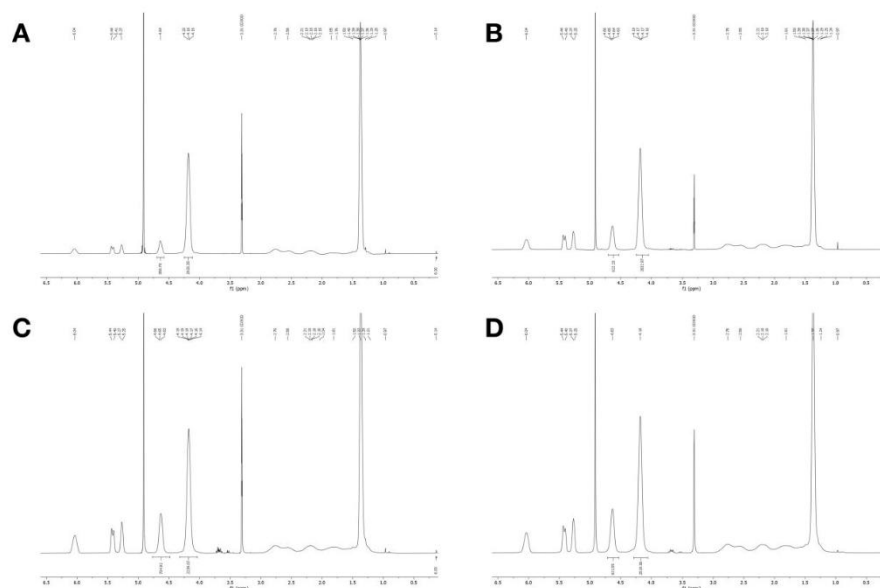


Figure S1: $^1\text{H-NMR}$ spectra of P(DEVP-stat-DAIVP) copolymers (Table 1, Entries 1-4) in CD_3OD with signals relevant for the molecular weight determination via $^1\text{H-NMR}$ spectroscopy (order A-D of the spectra corresponds to the order 1-4 in Table 1 of the manuscript).

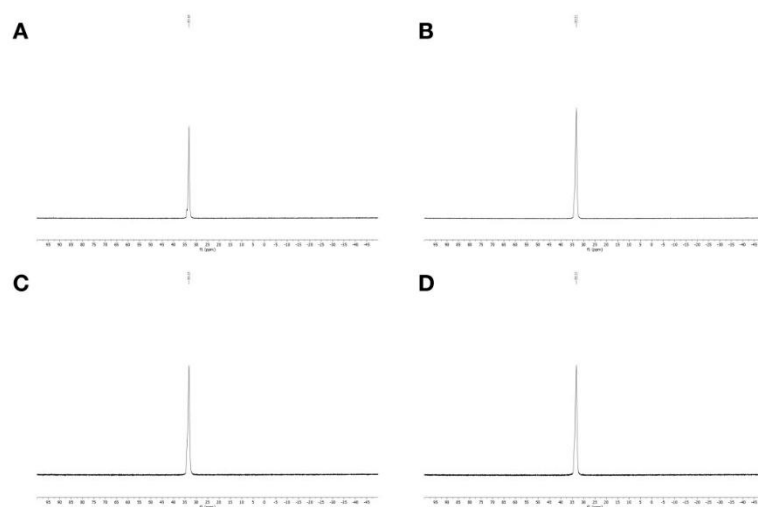


Figure S2: ^{31}P -NMR spectra of P(DEVP-stat-DAIVP) copolymers (Table 1, Entries 1-4) in CD_3OD (order A-D of the spectra corresponds to the order 1-4 in Table 1 of the manuscript).

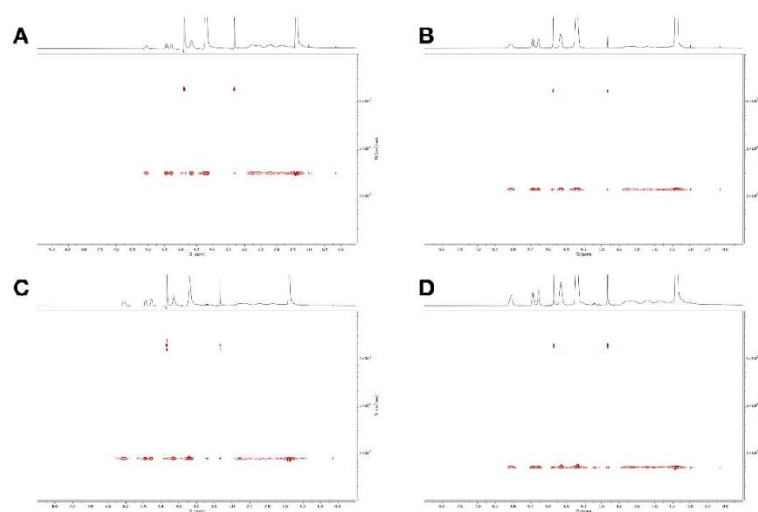


Figure S3: ^1H DOSY NMR spectra of P(DEVP-stat-DAIVP) copolymers (Table 1, Entries 1-4) in CD_3OD (order A-D of the spectra corresponds to the order 1-4 in Table 1 of the manuscript).

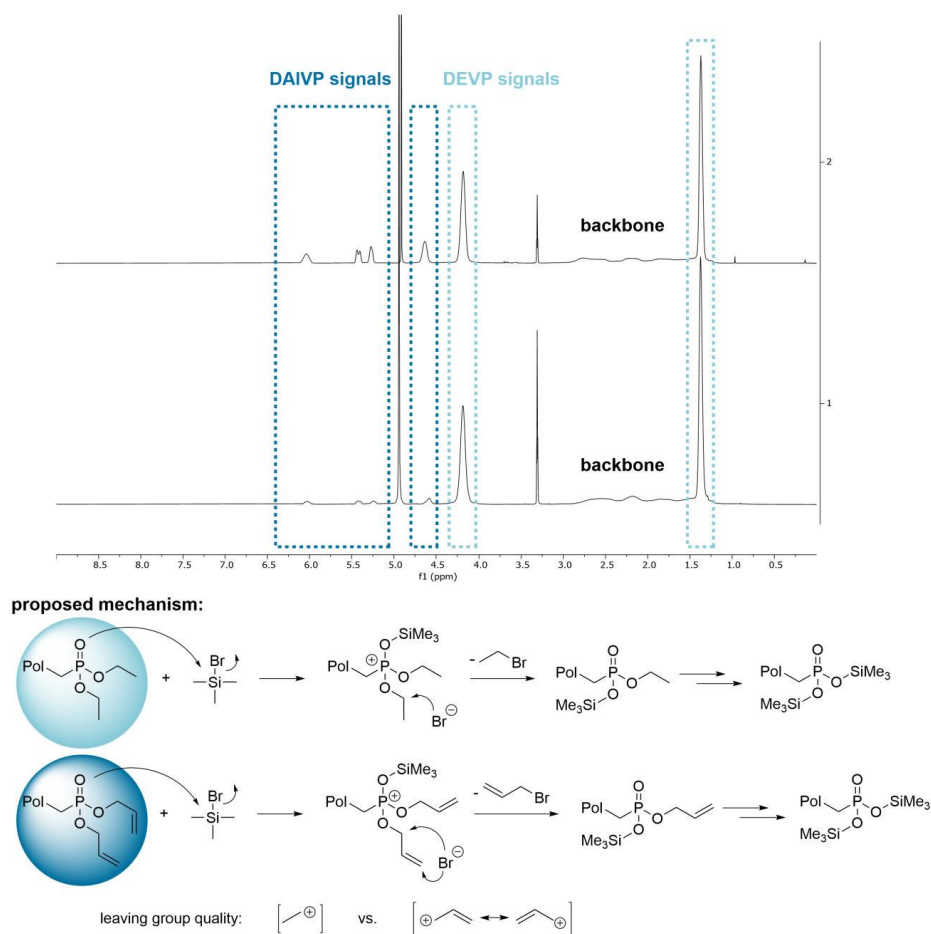


Figure S4: Comparison of ¹H-NMR spectra of P(DEVP-stat-DAIVP) (Table 1, polymer 2) (top spectrum) and P(DEVP-stat-DAIVP-stat-VPA) (Table 2, polymer 6) (bottom spectrum) in CD₃OD (top) and proposed reaction mechanism for the polymer analogous transformation of copolymers by reaction with TMSBr (bottom).⁶

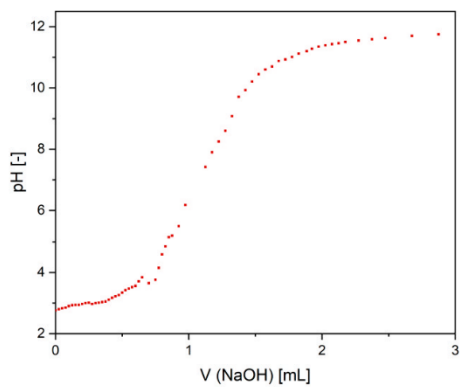


Figure S5: Titration of 10 mL of an aqueous solution poly(vinylphosphonic acid) (PVPA) (1 g L^{-1} polymer in H_2O , 9.3 mM VPA units) with 0.1 M NaOH (aq).

Hydrogel swelling experiments

For the determination of the water uptake, first, the dry weight of specimen subject to swelling experiments was determined after drying to weight constancy in vacuo. Subsequently, the samples were immersed in water for 8 hours. The swelling ratio given by Equation S1 was calculated by comparing the weight of the swollen specimen with the weight of the dry samples to obtain the water contents of each sample. Here, Q corresponds to the swelling ratio, M_s denotes the sample weight in the swollen state, and M_d refers to the weight of the specimen in the dry state. Further, standard deviations of the experiments were determined by performing the swelling experiments at least in triplicates.

$$Q = \frac{M_s - M_d}{M_d} \quad (\text{S1})$$

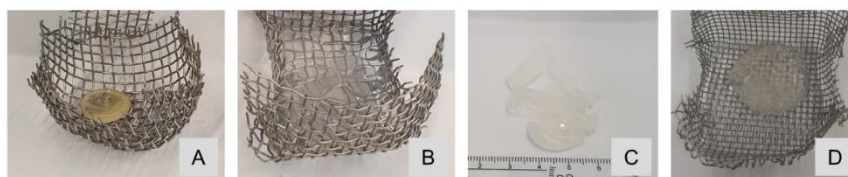


Figure S6: Images of hydrogel swelling (distilled water) of specimen obtained by photo-crosslinking of P(DEVP-stat-DAIVP-stat-VPA): hydrogel in the dry state (**A**), highly swollen hydrogel without structural integrity (Table 2, Entry 5) (**B**), swollen hydrogel forming a soft and brittle chip (Table 2, Entry 6) (**C**), and stable specimen after swelling (Table 2, Entry 8) (**D**).

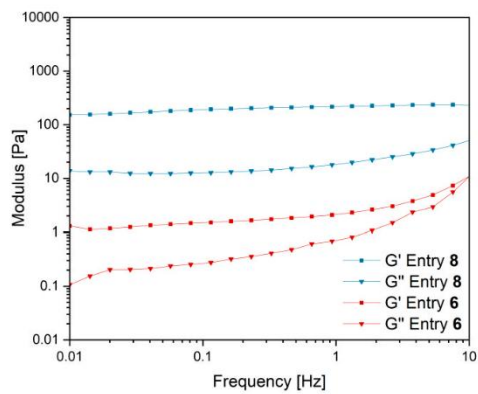


Figure S7: Comparison of the mechanical properties of hydrogels from polymers 6 (red curves) and 8 (blue curves) (Table 2) by frequency sweeps between 0.01 and 10 Hz at $\gamma = 1\%$.

3. THIN-FILM PREPARATION AND CHARACTERIZATION

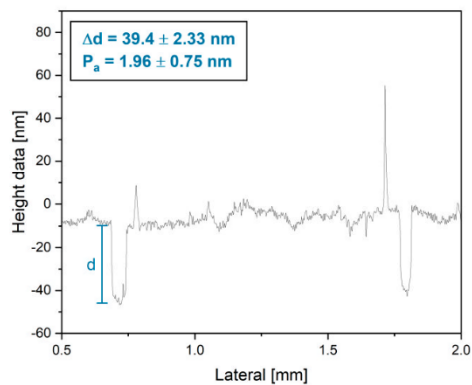


Figure S8: Exemplary profilometric measurement of a thin film of crosslinked P(DEVP-stat-DAIVP-stat-VPA) spin-coated on a silicon wafer and scratched twice with a thin razor blade.

Table S1: Summary of profilometric measurements to determine the dry film thickness and surface roughness of substrates spin-coated with crosslinked P(DEVP-stat-DAIVP-stat-VPA).

Substrate	1					
Δd [nm]	37.27	40.77	39.17	36.60	40.98	41.90
P_a [nm]	1.358		3.091		2.556	
Substrate	2			3		
Δd [nm]	37.577	38.234	35.136	41.522	41.841	42.386
P_a [nm]	1.110			1.671		

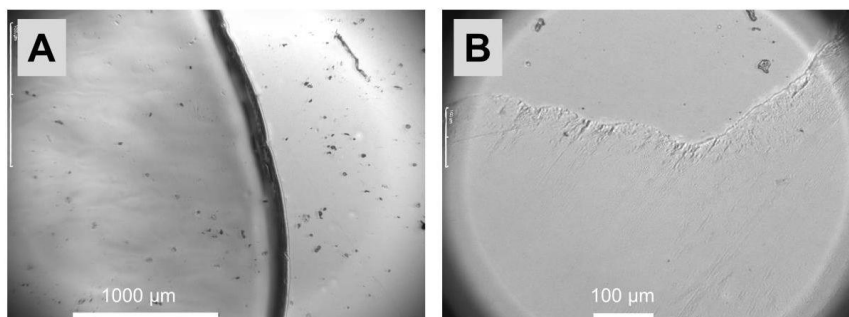


Figure S9: Light microscopic images of P(DEVP-stat-DAIVP-stat-VPA) spin-coated onto silicon wafers from an 85 ppm (0.0085 wt.%) solution in MeOH/H₂O (6/1) in two different magnifications: 5-fold magnification (A), and 20-fold magnification (B).

4. QUARTZ CRYSTAL MICROBALANCE MEASUREMENTS

Calculations of the mass deposition by the Sauerbrey equation

During the QCM-D measurements, the instrument simultaneously detects changes in the resonance frequency (Δf) and the energy dissipation (ΔD) caused by mass deposition or removal on an oscillating piezoelectric crystal. Dry film masses and masses of hydrogels coupled to the crystal during QCM-D experiments were calculated by applying the Sauerbrey equation, which is given by Equation S2:

$$\Delta m = -\frac{C \cdot \Delta f}{n} \quad (\text{S2})$$

In the Sauerbrey equation, Δf is the measured frequency shift, C is the Sauerbrey constant ($-17.7 \text{ ng Hz}^{-1} \text{ cm}^{-2}$ for the used 5 MHz crystals), n is the number of the overtone under consideration (n = 1, 3, 5, etc. considered automatically by the software) and Δm is the mass change of the crystal. The reported frequency changes Δf are normalized with respect to the third overtone number.

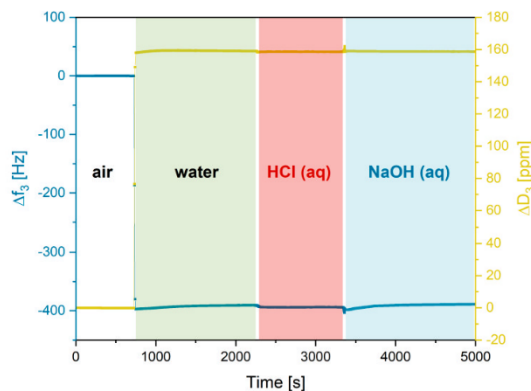


Figure S10: QCM-D measurement of empty crystals in different aqueous media and measurement on air before.

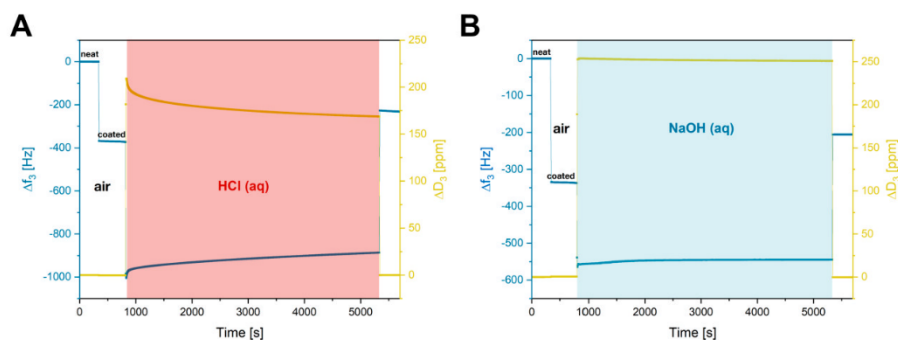


Figure S11: QCM-D measurements of thin films of non-crosslinked P(DEVP-stat-DAIVP-stat-VPA) in different aqueous media and measurements in air before and after exposure to the liquids, checking for potential leaching of samples. (A) Investigation of sample behavior under acidic conditions (pH 1) and (B) investigation of sample behavior under alkaline conditions (pH 13).

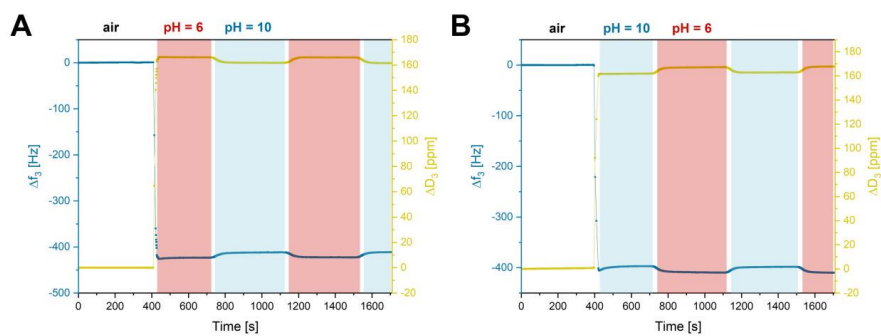


Figure S12: QCM-D measurement of uncoated sensors in air and different aqueous media. (A) Cycling of the pH value between pH 6 (0.1 M citrate buffer) and pH 10 (0.1 M carbonate buffer) over two cycles and (B) Cycling of the pH value between pH 10 (0.1 M carbonate buffer) and pH 6 (0.1 M citrate buffer) over two cycles.

5. REFERENCES

- (1) Halama, K.; Schaffer, A.; Rieger, B. Allyl Group-Containing Polyvinylphosphonates as a Flexible Platform for the Selective Introduction of Functional Groups via Polymer-Analogous Transformations. *RSC Adv*, **2021**, *11* (61), 38555–38564. DOI: 10.1039/d1ra06452e. Published Online: Nov. 30, 2021.
- (2) Salzinger, S.; Soller, B. S.; Plikhta, A.; Seemann, U. B.; Herdtweck, E.; Rieger, B. Mechanistic Studies on Initiation and Propagation of Rare Earth Metal-Mediated Group Transfer Polymerization of Vinylphosphonates. *J. Am. Chem. Soc.* **2013**, *135* (35), 13030–13040. DOI: 10.1021/ja404457f. Published Online: Aug. 21, 2013.
- (3) Schaffer, A.; Kränzlein, M.; Rieger, B. Synthesis and Application of Functional Group-Bearing Pyridyl-Based Initiators in Rare Earth Metal-Mediated Group Transfer Polymerization. *Macromolecules* **2020**, *53* (11), 4345–4354. DOI: 10.1021/acs.macromol.0c00642.
- (4) Mohan, T.; Kargl, R.; Doliška, A.; Vesel, A.; Köstler, S.; Ribitsch, V.; Stana-Kleinschek, K. Wettability and Surface Composition of Partly and Fully Regenerated Cellulose Thin Films From Trimethylsilyl Cellulose. *J. Colloid Interface Sci.* **2011**, *358* (2), 604–610. DOI: 10.1016/j.jcis.2011.03.022. Published Online: Mar. 12, 2011.
- (5) Mohan, T.; Niegelhell, K.; Nagaraj, C.; Reishofer, D.; Spirk, S.; Olschewski, A.; Stana Kleinschek, K.; Kargl, R. Interaction of Tissue Engineering Substrates with Serum Proteins and Its Influence on Human Primary Endothelial Cells. *Biomacromolecules* **2017**, *18* (2), 413–421. DOI: 10.1021/acs.biomac.6b01504. Published Online: Jan. 24, 2017.
- (6) Błażewska, K. M. McKenna Reaction—Which Oxygen Attacks Bromotrimethylsilane? *J. Org. Chem.* **2014**, *79* (1), 408–412. DOI: 10.1021/jo4021612. Published Online: Dec. 20, 2013.

10.2.3 Supporting information for chapter 6

Supporting Information

High-Fidelity Direct Ink Writing of Poly(vinylphosphonate)- Reinforced Polysaccharide Inks With Tunable Properties

*Anton S. Maier^{1,‡}, Florian Lackner^{2,‡}, Julia Fink^{3,4}, Tobias Steindorfer², Elisabeth Hofmann⁴,
Karin Stana Kleinschek², and Bernhard Rieger^{1,*}*

¹Technical University of Munich, Germany; TUM School of Natural Sciences, Department of Chemistry, WACKER-Chair of Macromolecular Chemistry; Lichtenbergstraße 4, 85748 Garching, Germany

²Graz University of Technology, Austria; Institute for Chemistry and Technology of Biobased Systems (IBioSys); Stremayrgasse 9; 8010 Graz, Austria

³COREMED – Centre of Regenerative and Precision Medicine JOANNEUM RESEARCH Forschungsgesellschaft GmbH; Neue Stiftingtalstraße 2; 8010 Graz, Austria

⁴Research Unit for Tissue Regeneration, Repair and Reconstruction, Division of Plastic, Aesthetic and Reconstructive Surgery, Department of Surgery, Medical University of Graz, Auenbruggerplatz 29/4, 8036, Graz, Austria.

[‡]These authors contributed equally.

Corresponding Authors

* rieger@tum.de; karin.stanakleinschek@tugraz.at

TABLE OF CONTENTS

1. Materials and Methods	S3
2. Statistical Copolymerization of Diethylvinylphosphonate (DEVP) and Diallylvinylphosphonate (DAIVP)	S9
3. Direct ink writing	S17
4. Transmitted light microscopy	S20
5. Stress-strain measurements	S21
6. References	S22

S2

1. MATERIALS AND METHODS

General Experimental

All air and moisture-sensitive compounds were prepared using standard Schlenk techniques or in a glovebox with argon (99.996 vol.-%) from Westfalen as inert gas. All glass instruments were oven-dried prior to use. Unless otherwise stated, all chemicals and solvents were purchased from Sigma-Aldrich, ABCR GmbH, or TCI Chemicals and used without further purification. Dry solvents were obtained from an MBraun MB-SPS-800 solvent purification system or by drying over activated alumina and stored over activated 3 Å molecular sieves. Deuterated solvents were purchased from Sigma-Aldrich and dried over activated 3 Å molecular sieves. The monomers diethyl vinylphosphonate (DEVP), diallyl vinylphosphonate (DAIVP), the complex $\text{Cp}_2\text{YCH}_2\text{TMS}(\text{thf})$ and the initiator 4-(4-(((tert-butyl)dimethylsilyloxy)methyl)phenyl)-2,6-dimethylpyridine were synthesized according to literature-known procedures.¹⁻³ The monomers were dried over calcium hydride and distilled prior to polymerization. The nanofibrillated cellulose (NFC) suspension (3 wt.% solid content) was purchased from the University of Maine, USA (R-COO^- ; 0.35 ± 0.05 mmol/g).

Rheology

Rheological characterizations were performed on a modular compact rheometer MCR 502 rheometer from Anton Paar with plate-plate geometry using an upper plate with a 25 mm diameter at a gap size of 0.5 mm. The samples were applied using a spatula or a syringe and tempered to 25 °C by a Peltier system. Measurements were performed every 10 seconds, and the data was monitored via the Rheoplus software. Rotational frequency sweeps were performed applying

logarithmic ramps of the shear rate between 0.1 and 100 1/s. Oscillatory amplitude sweeps were performed at deformations between 0.01 and 100% at an angular frequency of 10 rad/s.

Lyophilization

Lyophilization was performed on a VaCo 5-II-D from Zirbus Technology GmbH with a pressure of 2 mbar and a condenser temperature of -90 °C. Polymers subjected to freeze-drying were dissolved in 1,4-dioxane or distilled water before freezing in liquid nitrogen under constant rotation.

Size-exclusion chromatography multi-angle light scattering (SEC-MALS)

Polydispersities of the polymers were determined via size-exclusion chromatography (SEC) with sample concentrations of 4 mg mL⁻¹ on two PL Polargel-M columns (Agilent) at 40 °C. A mixture of water and THF (1:1), treated with tetrabutylammonium bromide (9 g L⁻¹) and 3,5-di-tert-butyl-4-hydroxytoluene (340 mg L⁻¹) was used as eluent. Samples were analyzed using a Wyatt Dawn Heleos II light scattering unit in combination with a Wyatt Optilab rEX as RI detector unit.

Nuclear magnetic resonance spectroscopy (NMR)

¹H-NMR- and ³¹P-NMR spectra of polymers were recorded on a Bruker AV-400HD, AV-500HD, or AV-II-500 spectrometer at 400 or 500 MHz (¹H) and 203 MHz (³¹P), respectively. All chemical shifts are given in parts per million (ppm) and referenced to the residual proton signal of the respective solvent (Benzene-d₆: δ = 7.16 ppm, Methanol-d₄: δ = 3.31 ppm). Deuterated solvents were purchased from Sigma-Aldrich or Deutero and dried over activated 3 Å molecular sieves. The NMR spectra were analyzed using the MestReNova software. ¹H DOSY NMR experiments were performed to characterize copolymers and functionalized copolymers.

General procedure for the preparation of inks for direct ink writing (DIW)







In a 50 mL Falcon tube, 700 mg of the respective polymer were dissolved in 7 g of a 3 wt.% aqueous suspension nanofibrillated cellulose (NFC) by mixing at 2000 rpm with a RZR 2005 mechanical stirrer (Heidolph, Germany) equipped with a tailored, 3D-printed mixing tool. Once a homogenous solution was obtained, 233 mg of sodium alginate (Alg) were added to the ink and the resulting ink was thoroughly homogenized at 2000 rpm. Finally, the calculated amounts of initiator and crosslinker were added to the mixture. After one final mixing step, the ink was directly used for DIW to avoid covalent crosslinking upon longer storage.

Direct ink writing 3D printing (DIW)

To generate 3D models, the open-source program FreeCAD 0.19 or 3D Builder 18.0.1931.0 (Microsoft Corporation) was used. DIW was performed on a GeSiM Robotics BioScaffolder 3.2 (GeSiM, Germany). The theoretical models were processed in the GeSiM Robotics BioScaffolder 3.2 software as .stl or .3MF files to obtain the G-code. The printed structures were printed in a layer-by-layer fashion with intermediate ultraviolet (UV) irradiation ($\lambda = 365$ nm) for one second between each layer. The final objects were subsequently post-cured for 60 seconds after the last layer. In case of dually crosslinking approach, samples are immersed for 24 hours in 5mM CaCl₂-containing 150 mM NaCl (aq) solution. The inks were extruded from polyethylene-based, brown cartridges (Nordson, UK) to exclude incident light through tapered tips (Nordson, UK Limited) with an inner diameter of 200, 410 and 580 μ m into polystyrene petri dishes. The scaffolds were printed with extrusion pressures between 22 and 250 kPa with a print speed of 25 mm/s. Further details for the specific printed objects are summarized in Table S1. The

Supplementary Movie shows the printing of overhanging objects with a 30° incline through layer-by-layer deposition with intermediate photochemical crosslinking.

Table S1: Overview of different structures printed within the scope of the study with dimensions and print parameters.

Entry	Model	Picture	Length x Width x Height [mm]	Layers	Infill Distance [mm]	Nozzle Diameter [μm]	Angle Change [°]
1	Letters		13 x 4 x 1	8	0.30	200	0
2	Shape fidelity		8 x 8 x 3	10	0.80	200	90
3	Infill tube		10 x 10 x 12	30	1.00	410	90
4	Hollow tube		10 x 10 x 36	89	-	410	0
5	Tensile test		50 x 8.5 x 2	3	0.60	580	0
6	Cell testing		26 x 26 x 2	2	0.90	800	n.a.

Shape fidelity measurements

As described in Table S1, an infill tube was printed using a 0.41 mm nozzle and 1.00 mm infill distance. Prints were performed for 3, 13, 20, and 30 layers and photographed. The dimensions of the prints, infill angles, and infill distances were measured using Image J 1.53p.

Tensile testing

For the evaluation of mechanical properties, dog bone specimens according to DIN53504S3A with dimensions of 50x8.5x2 mm were printed in a layer-by-layer approach, crosslinked with UV light and optionally ionically with 5 mM CaCl₂-containing physiological NaCl solution and subjected to stress-strain measurements on a Shimadzu AGS-X (Japan) universal mechanical testing machine with a speed of 50 mm/min using standard clams. For each ink composition, a minimum of three specimens were tested. Each specimen was printed following the same printing pathway, ensuring the same fiber orientation of NFC in each sample.

Transmitted light microscopy

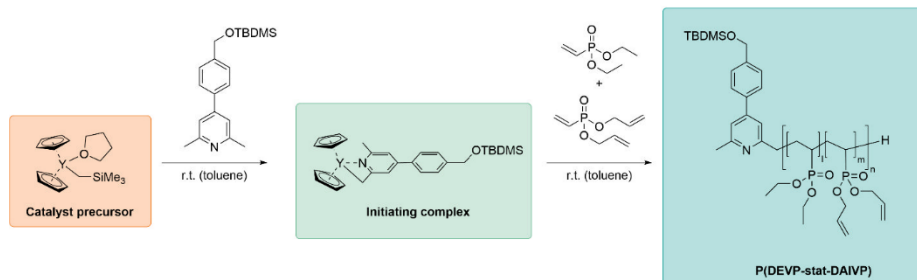
To determine the droplet size emulsions of 1,6-hexanedithiol in NFC/alginate were prepared analogously as for the DIW ink, described previously. A spatula tip of the emulsion was placed microscopic glass slides and the ink was press to thin film with a cover slide an observed with a Panthera Tec Mat (Motic, China) transmitted light microscope with 200x magnification.

Cell viability of primary HUVECs and HEK293 cell line

A pool of primary human umbilical vein endothelial cells (HUVECs) and the human embryonic kidney cell line HEK293 were used. HUVECs were purchased from PromoCell (Heidelberg, Germany) and cultivated in low serum endothelial cell growth medium (PromoCell) with media

supplement and 1% Penicillin/Streptomycin (P/S, Thermo Fisher Scientific). HEK293 were purchased from the Biobank Graz (Graz, Austria) and cultivated in DMEM/F12 medium (Thermo Fisher Scientific) supplemented with 10% FBS (Thermo Fisher Scientific) and 1% P/S. An indirect contact test was performed to test for the interaction of any leachable by-products with the cell monolayer without direct contact with the material. For that, $4 \cdot 10^4$ cells/ml were seeded on a 24-well plate. After 24 hours of incubation, five different specimens were placed into a transwell microplate membrane insert with 8 μm pore size (Greiner bio-one) and submerged with 1 ml cell culture media per well. Cells were incubated for 48 hours with the testing compounds at 37°C and 5% CO₂. The cytotoxicity of the compounds was tested using a PrestoBlue assay. Thus, the cell culture medium was removed and replaced with 500 μl fresh culture media containing 10% PrestoBlue reagent (Invitrogen, MA, USA). The absorbance of the solution was measured after 3h according to the manufacturer's protocol with a SpectraMax iD3 Microplate reader from Molecular Devices, LLC. (San Jose, California). As a control, equally cultured cells without inserts were used and the cell viability was indicated as 100%. Two independent experiments were performed with triplicates for specimens of each sample composition.

2. STATISTICAL COPOLYMERIZATION OF DIETHYLVINYLPHOSPHONATE (DEVP) AND DIALLYLVINYLPHOSPHONATE (DALVP)



All polymerizations were performed according to reported procedures and under an inert atmosphere in a glovebox. In a copolymerization experiment, the calculated amount of Cp₂YCH₂TMS(thf) was dissolved in 2 mL of dry toluene. To this solution, the calculated amount of the initiator 4-(4-((tert-butyl-dimethyl-silyl)oxy)methyl)phenyl)-2,6-dimethylpyridine (1.10 eq.) was added, and the reaction was allowed to continue at room temperature for two hours. After successful formation of the initiating complex was confirmed via ¹H-NMR spectroscopy in C₆D₆ by withdrawing 0.1 mL of the reaction solution, the catalyst solution was diluted with 2 mL of dry toluene. Subsequently, the calculated amounts of the monomers diethyl vinylphosphonate (DEVP) and diallyl vinylphosphonate (DAIVP) were weighed into a syringe, mixed thoroughly, and the mixture was added to the catalyst solution in one motion. The polymerization was proceeded at room temperature for two hours before removing an aliquot from the mixture to confirm quantitative monomer conversion via ³¹P-NMR spectroscopy in MeOD. Then, the polymerization was stopped by adding 0.5 mL of undried methanol and the copolymers were precipitated from pentane. After centrifugation and removal of the supernatant, the residues were taken up in 1,4-dioxane and subjected to lyophilization, yielding the pure P(DEVP-stat-DAIVP) copolymers as white solids.

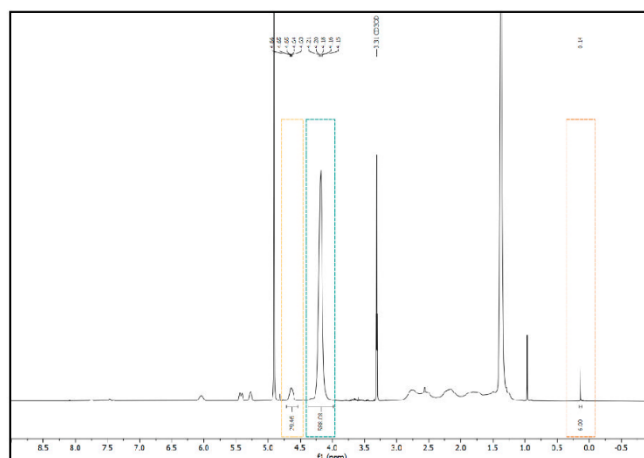


Figure S1: ^1H -NMR spectrum of P(DEVP-stat-DAIVP) (Table 1, Entry 1) in MeOD with signals relevant for molecular weight determination via ^1H -NMR spectroscopy: End-group signals (orange, 0.14 ppm, 6H, -OTBDMS group), DEVP signals (green, 4.18 ppm) and DAIVP signals (yellow, 4.63 ppm).

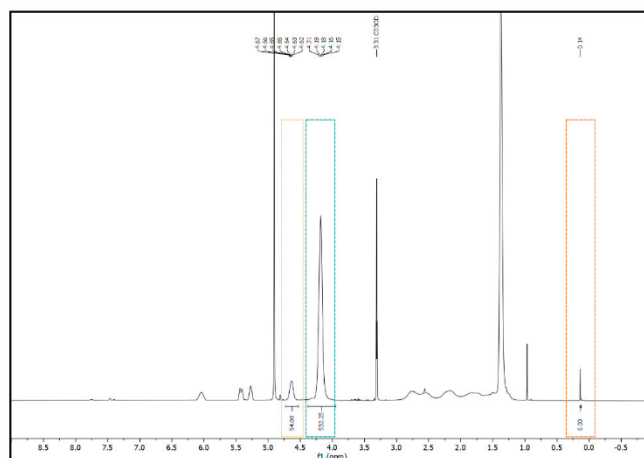


Figure S2: $^1\text{H-NMR}$ spectrum of P(DEVP-stat-DAIVP) (Table 1, Entry 2) in MeOD with signals relevant for molecular weight determination via $^1\text{H-NMR}$ spectroscopy: End-group signals (orange, 0.14 ppm, 6H, -OTBDMS group), DEVP signals (green, 4.18 ppm) and DAIVP signals (yellow, 4.63 ppm).

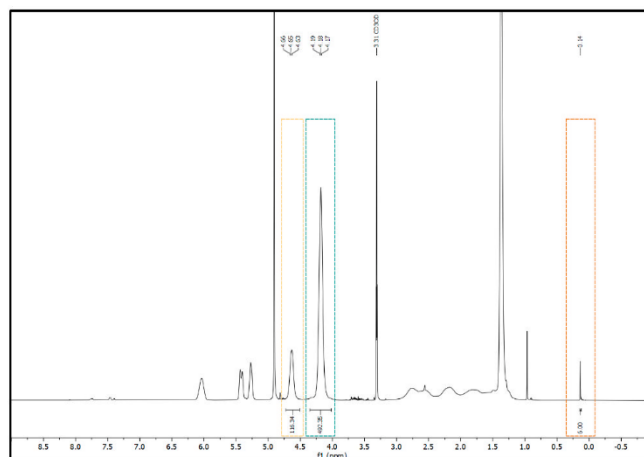


Figure S3: $^1\text{H-NMR}$ spectrum of P(DEVP-stat-DAIVP) (Table 1, Entry 3) in MeOD with signals relevant for molecular weight determination via $^1\text{H-NMR}$ spectroscopy: End-group signals (orange, 0.14 ppm, 6H, -OTBDMS group), DEVP signals (green, 4.18 ppm) and DAIVP signals (yellow, 4.63 ppm).

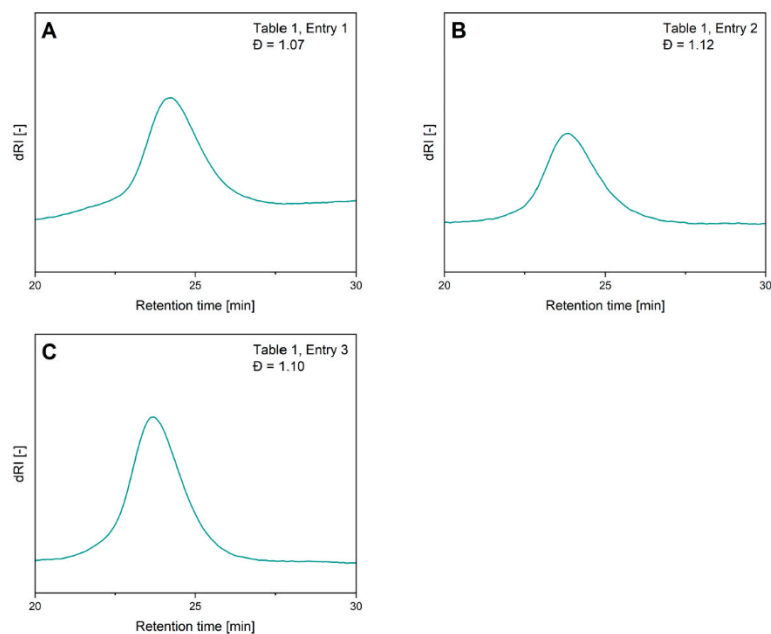


Figure S4: Refractive index detector signals of P(DEVP-stat-DAIVP) (Table 1, Entries 1-3) determined via SEC-MALS in THF/water (1:1) with tetrabutylammonium bromide (9 g L^{-1}) and 3,5-di-tert-butyl-4-hydroxytoluene (340 mg L^{-1}) (order A-C of the spectra corresponds to the order 1-3 in Table 1 of the manuscript).

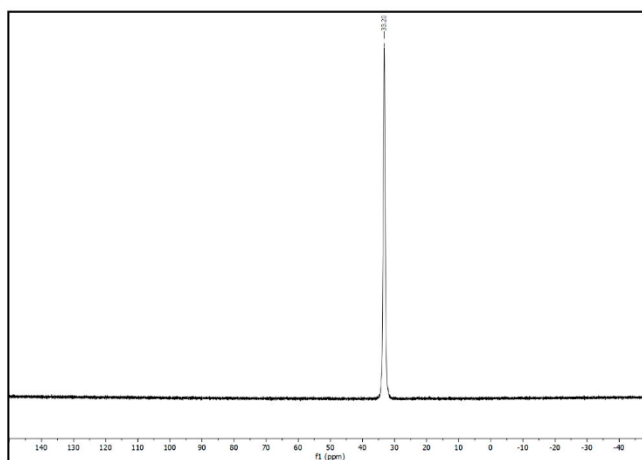


Figure S5: ^{31}P -NMR spectrum of P(DEVP-stat-DAIVP) (Table 1, Entry 1) in MeOD with polymer signal at 33.20 ppm.

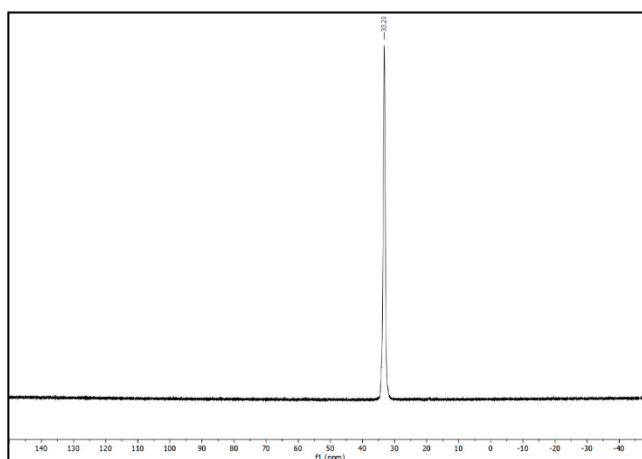


Figure S6: ^{31}P -NMR spectrum of P(DEVP-stat-DAIVP) (Table 1, Entry 2) in MeOD with polymer signal at 33.20 ppm.

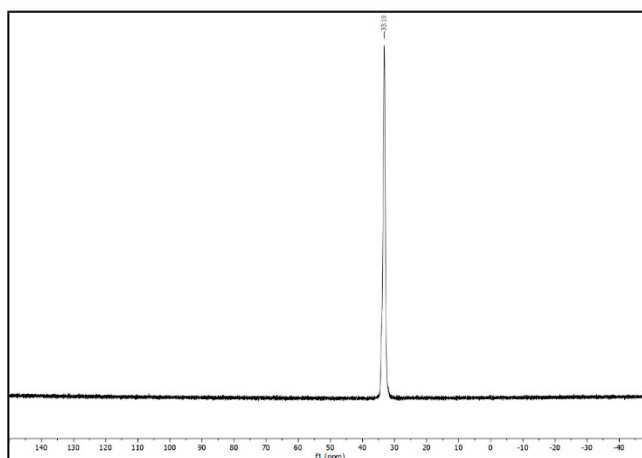


Figure S7: ^{31}P -NMR spectrum of P(DEVP-stat-DAIVP) (Table 1, Entry 3) in MeOD with polymer signal at 33.19 ppm.

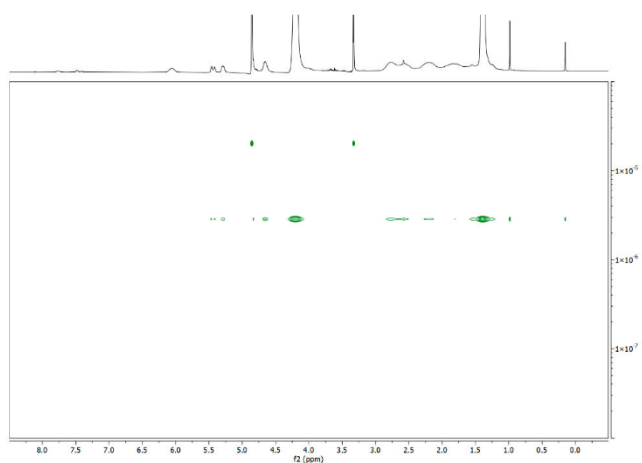


Figure S8: ^1H DOSY NMR spectrum of P(DEVP-stat-DAIVP) (Table 1, Entry 1) in MeOD.

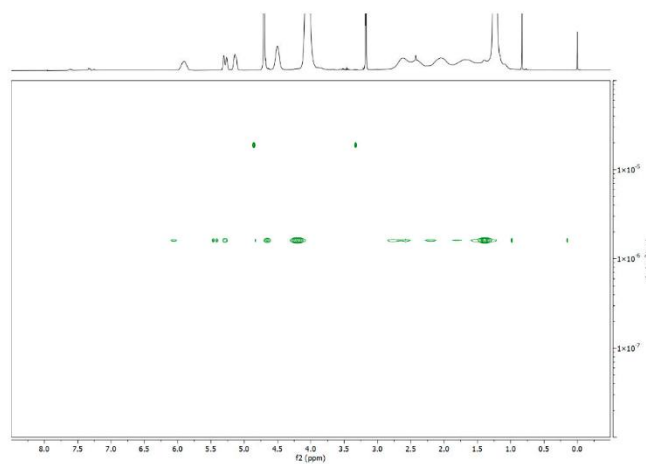


Figure S9: ¹H DOSY NMR spectrum of P(DEVP-stat-DAIVP) (Table 1, Entry 2) in MeOD.

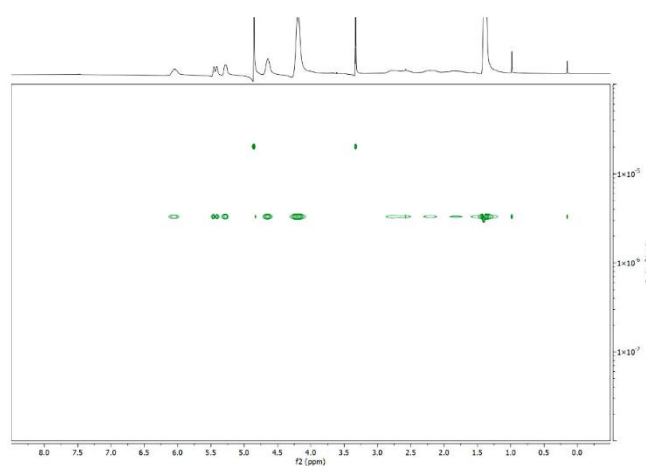


Figure S10: ¹H DOSY NMR spectrum of P(DEVP-stat-DAIVP) (Table 1, Entry 3) in MeOD.

3. DIRECT INK WRITING

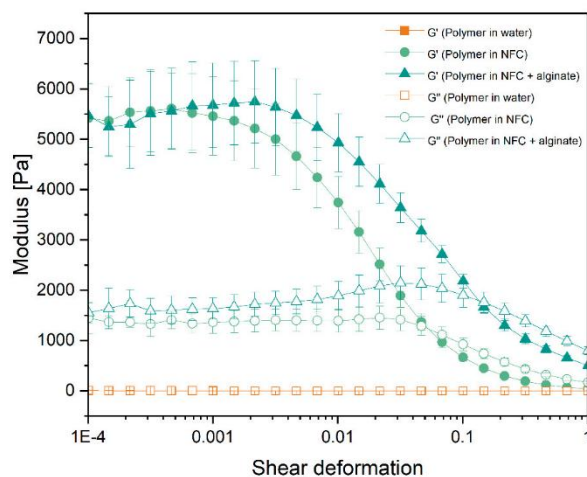


Figure S11: Storage (full symbols) and loss modulus (hollow symbols) of different polymer solutions monitored via oscillatory rheology at an angular frequency of 10 rad/s and deformations between 0.01 and 100%: P(DEVP-stat-DAIVP) (9 wt.%) in water (orange curves), P(DEVP-stat-DAIVP) (9 wt.%) in an aqueous, 3 wt.% NFC suspension (green curves), and P(DEVP-stat-DAIVP) (9 wt.%) in an aqueous, 3 wt.% NFC suspension with alginate as a thickening agent (2.9 wt.%) (blue curves).

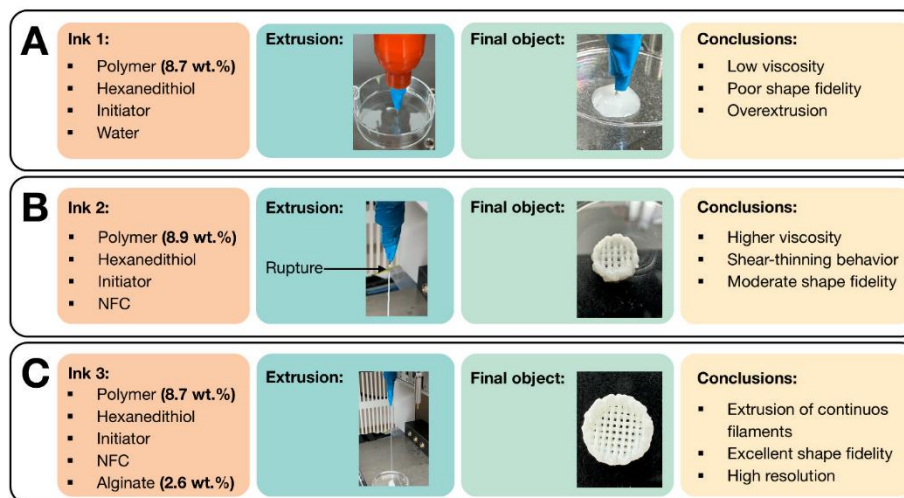


Figure S12: Initial extrusion and printing tests of different inks: P(DEVP-stat-DAIVP) in water with crosslinker and initiator (**A**), P(DEVP-stat-DAIVP) in a 3 wt.% aqueous NFC suspension with crosslinker and initiator (**B**), and P(DEVP-stat-DAIVP) in a 3 wt.% aqueous NFC suspension with crosslinker, initiator, and alginate (**C**).

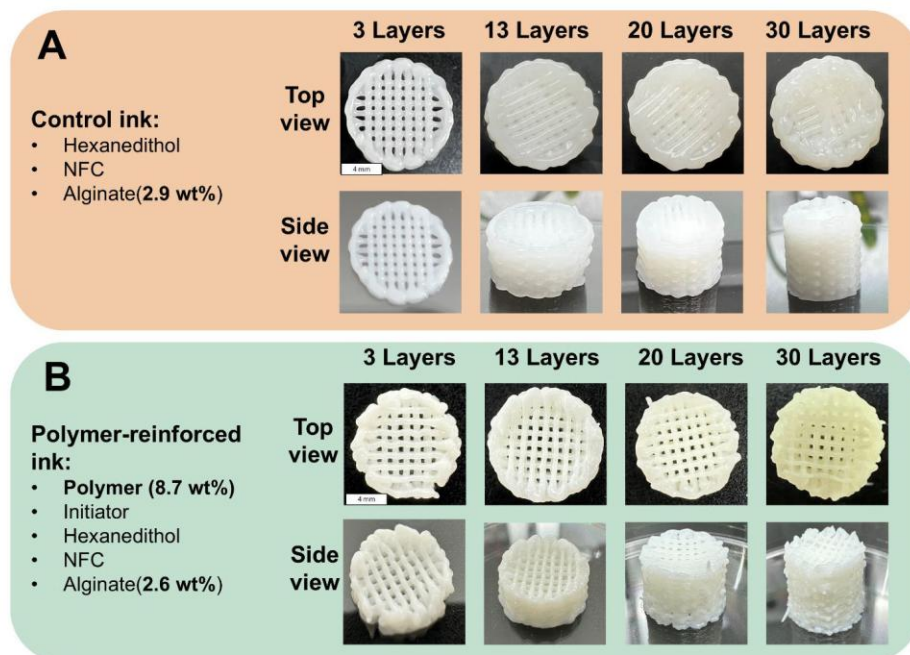


Figure S13: Comparison of the printing resolution and printing stability of a control ink (**A**) and a polymer-reinforced ink (**B**) by printing an infill tube with varying numbers of layers ($n = 3, 13, 20, 30$) using a nozzle with a 0.41 mm diameter and an infill distance of 1.00 mm.

4. TRANSMITTED LIGHT MICROSCOPY

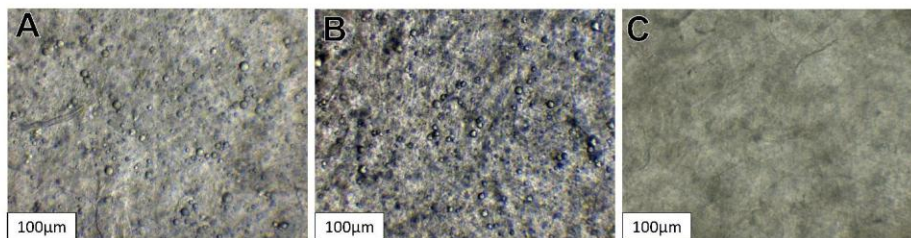


Figure S14: Transmitted light microscopy pictures of the ink directly after mixing (**A**), after 24h storage (**B**), and without the insoluble 1,6 hexanedithiol (**C**). Homogenous droplet distribution is visible with a typical droplet diameter below 20 μm .

5. STRESS-STRAIN MEASUREMENTS

Investigation of the water uptake of specimens with and without ionic crosslinking:

The specimens printed by DIW of NFC/Alg inks subjected to mechanical testing were primarily investigated in terms of water uptake. Therefore, the printed scaffolds were immersed in either a 150 mM NaCl (aq) solution or in a 5 mM CaCl₂-containing 150 mM NaCl (aq) solution and gently shaken for 16 hours on a Unimax 2010 (Heidolf, Germany). Subsequently, the weight of the swollen samples was determined and compared to the initial weight of the specimens after printing. Samples sticking to the petri dish were carefully detached using razor blades.

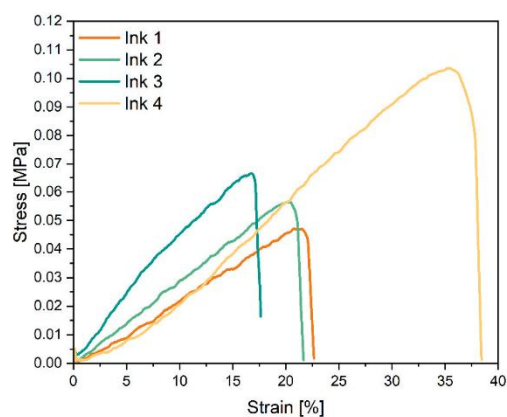


Figure S15: Exemplary stress-strain curves of specimens printed with inks 1-4 and crosslinked in 5 mM CaCl₂-containing physiological NaCl solution.

6. REFERENCES

(1) Halama, K.; Schaffer, A.; Rieger, B. Allyl group-containing polyvinylphosphonates as a flexible platform for the selective introduction of functional groups via polymer-analogous transformations. *RSC Adv.* **2021**, *11* (61), 38555–38564. DOI: 10.1039/d1ra06452e. Published Online: Nov. 30, 2021.

(2) Salzinger, S.; Soller, B. S.; Plikhta, A.; Seemann, U. B.; Herdtweck, E.; Rieger, B. Mechanistic studies on initiation and propagation of rare earth metal-mediated group transfer polymerization of vinylphosphonates. *J. Am. Chem. Soc.* **2013**, *135* (35), 13030–13040. DOI: 10.1021/ja404457f. Published Online: Aug. 21, 2013.

(3) Schaffer, A.; Kränzlein, M.; Rieger, B. Synthesis and Application of Functional Group-Bearing Pyridyl-Based Initiators in Rare Earth Metal-Mediated Group Transfer Polymerization. *Macromolecules* **2020**, *53* (11), 4345–4354. DOI: 10.1021/acs.macromol.0c00642.

10.2.4 Supporting information for chapter 7

Supporting Information

Modifications of Poly(vinylphosphonates) Toward Dynamic Covalent Networks

Jana Knezevic^{1,‡}, Anton S. Maier^{1,‡}, Florian Lackner², Karin Stana Kleinschek², and Bernhard Rieger^{1,}*

¹Technical University of Munich, Germany, TUM School of Natural Sciences, Department of Chemistry, WACKER-Chair of Macromolecular Chemistry, Lichtenbergstraße 4, 85748 Garching, Germany

²Graz University of Technology, Austria; Institute for Chemistry and Technology of Biobased Systems (IBioSys); Stremayrgasse 9; 8010 Graz, Austria

[‡] These authors contributed equally.

Corresponding Author

*rieger@tum.de

TABLE OF CONTENTS

1. Materials and Methods	3
2. Polymer and hydrogel synthesis	7
3. Rheological characterization of dynamic covalent networks	19
4. References	26

1. MATERIALS AND METHODS

General Experimental

All air and moisture-sensitive compounds were prepared using standard Schlenk techniques or in a glovebox with argon (99.996 vol.-%) from Westfalen as inert gas. All glass instruments were oven-dried prior to use. Unless otherwise stated, all chemicals and solvents were purchased from *Sigma-Aldrich* or *BLD Pharm* and used without further purification. Dry solvents were obtained from an *MBraun* MB-SPS-800 solvent purification system or by drying over activated alumina and stored over activated 3 Å molecular sieves. Deuterated solvents were purchased from *Sigma-Aldrich* and dried over activated 3 Å molecular sieves. Synthesis of the monomers diethyl vinylphosphonate (DEVP) and diallyl vinylphosphonate (DAIVP), the initiator 4-(4-(((*tert*-butyldimethyl-silyl)oxy)methyl)phenyl)-2,6-dimethylpyridine and the complex $\text{Cp}_2\text{YCH}_2\text{TMS}(\text{THF})$ followed literature-known procedures.¹⁻³ The monomers were dried over calcium hydride and distilled prior to polymerization.

Nuclear Magnetic Resonance Spectroscopy (NMR)

¹H NMR spectra of small molecules and polymers are recorded either on a *Bruker Ascend* II 300 MHz NMR spectrometer or a *Bruker Ascend* 400 MHz NMR spectrometer, the spectrometer used is indicated in the experimental section. ¹¹B, ¹³C, and ³¹P NMR spectra are measured on a *Bruker Ascend* 400 MHz NMR spectrometer at 128 MHz (¹¹B), 101 MHz (¹³C), or 203 MHz (³¹P), respectively. The NMR spectra were analyzed using the *MestrelNova* software. ¹H DOSY NMR experiments were performed to characterize copolymers and functionalized copolymers on a *Bruker AV-HD400* with 16 scans and were transformed using a Bayesian method of *MestrelNova* software. All chemical shifts are given in parts per million (ppm) and referenced to the residual

proton signal of the respective solvent (Benzene-d₆: $\delta = 7.1$ ppm, Methanol-d₄: $\delta = 3.31$ ppm, DMSO-d₆: $\delta = 2.50$ ppm). Deuterated solvents were purchased from *Sigma-Aldrich* and dried over activated 3 Å molecular sieves. Signal multiplicities are abbreviated as follows: s - singlet, m - multiplet.

Rheology

Rheological characterizations were performed on an MCR 302 controlled-stress rheometer from *Anton Paar* with an upper plate (25 mm diameter) and a lower plate as counterpart (gap size 0.3 mm). The samples were applied in a gel state (0.20 mL) and tempered to 25 °C through an upper and lower Peltier system. Additionally, a protective hood was used. To prevent solvent evaporation during the measurements, a circular, moisturized sponge was placed around the sample under the protective hood while avoiding contact with the sample. Measurements were performed every 10 seconds, and the data was monitored via the *Rheoplus* software. Additional parameters are specified in the description of the corresponding measurement result.

Size-exclusion chromatography multi-angle light scattering (SEC-MALS)

Polydispersities of the polymers were determined via size-exclusion chromatography (SEC) with sample concentrations of 4 mg mL⁻¹ on two PL Polargel-M columns (Agilent) at 40 °C. A mixture of water and THF (1:1), treated with tetrabutylammonium bromide (9 g L⁻¹) and 3,5-di-tert-butyl-4-hydroxytoluene (340 mg L⁻¹) was used as eluent. Samples were analyzed using a Wyatt Dawn Heleos II light scattering unit in combination with a Wyatt Optilab rEX as RI detector unit.

Thermogravimetric analysis (TGA)

The thermogravimetric analyses were carried out with a Q5000 SA from *TA Instruments*. For this purpose, 1-2 mg of the respective sample was placed on a tared platinum crucible and heated under inert gas (Ar) at 10 K/min to 800 °C. The data obtained was analyzed using the *TA Universal Analysis* Software.

Differential scanning calorimetry (DSC)

DSC measurements were recorded on a DSC Q2000 from *TA Instruments* in exo down mode. The temperature program consisted of three consecutive heating and cooling cycles with a continuous heating ramp of 5 K min⁻¹ between -70 °C and 170 °C and for hydrogels at 10 K min⁻¹ between -50 °C and 80 °C. The measurement data was analyzed using the *TA Universal Analysis* software.

Lyophilization

Lyophilization was performed on a VaCo 5-II-D from *Zirbus Technology GmbH* with a pressure of 2 mbar and a condenser temperature of -90 °C. Polymers subjected to freeze-drying were dissolved in 1,4-dioxane or distilled water before freezing in liquid nitrogen under constant rotation.

Dialysis

Product purification via dialysis was rendered with Spectra/Por 7 dialysis membranes (regenerated cellulose) from *Repligen* against deionized water. The applied membranes have a molecular weight cut-off of (MWCO) of 8 kDa and a 5.1 mL/cm volume-length ratio.


Photochemical reactions

To induce a thiol-ene click reaction, the samples were irradiated with LEDs ($\lambda = 365$ nm) at a 20 mm distance, applying a current of 700 mA and a forward voltage of 15.2 V.

Direct ink writing 3D printing (DIW)

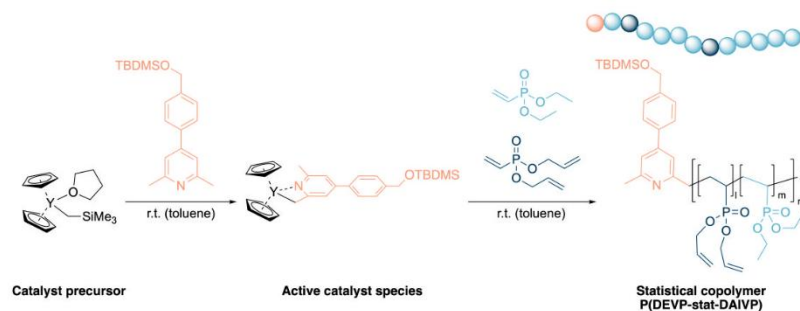
To generate 3D models, the open-source program FreeCAD 0.19 or 3D Builder 18.0.1931.0 (Microsoft Corporation) was used. DIW was performed on a GeSiM Robotics BioScaffolder 3.2 (GeSiM, Germany). The theoretical models were processed in the GeSiM Robotics BioScaffolder 3.2 software as .stl or .3MF files to obtain the G-code. The printed structures were printed in a layer-by-layer fashion. The ink was freshly prepared by combining a polymer-containing and a borax solution and extruded from polyethylene-based cartridges (Nordson, UK) through tapered tips (Nordson, UK Limited) with an inner diameter of 410 μm into polystyrene petri dishes. The scaffold was printed with extrusion pressures between 140 and 160 kPa with a print speed of 10 mm/s. Further details for the printed logo are summarized in Table S1.

Table S1: Overview of printing parameters of the printed logo presented in the manuscript.

Model	Picture	Length \times width \times height [mm]	Infill distance [mm]	Nozzle diameter [μm]	Angle change [$^\circ$]
Logo		17 \times 5 \times 0.4	0.50	410	90

2. POLYMER AND HYDROGEL SYNTHESIS

Polymerization of diethyl vinylphosphonate (DEVP) and diallyl vinylphosphonate (DAIVP) toward statistical copolymers



The $\text{Cp}_2\text{Y}(\text{CH}_2\text{TMS})(\text{thf})$ catalyst (20.4 mg, 54.0 μmol , 1.00 eq.) was dissolved in 2.00 mL toluene, 4-(*tert*-butyldimethylsilyloxy)methylphenyl)-2,6-dimethylpyridine (17.7 mg, 54.0 μmol , 1.00 eq.) then added and the solution stirred for 2 h. After quantitative C–H bond activation was confirmed via ^1H NMR, the reaction mixture was diluted with 2.00 mL toluene, and then a mixture of DAIVP and DEVP was added to the solution. After stirring for additional 2 h, the mixture was quenched with 0.50 mL MeOH, precipitated in 45.0 mL pentane, centrifuged, decanted, and lyophilized from 1,4-dioxane.

^1H NMR (400 MHz, CD_3OD): δ (ppm) = 7.80–7.36 (m, CH_{Ar}), 6.11–5.97 (m, $\text{CH}-\text{CH}_2_{\text{PDAIVP}}$), 5.47–5.37 (m, $\text{CH}-\text{CH}_2_{\text{PDAIVP}}$), 5.32–5.22 (m, $\text{CH}-\text{CH}_2_{\text{PDAIVP}}$), 4.72–4.55 (m, $\text{O}-\text{CH}_2_{\text{PDAIVP}}$), 4.23–4.12 (m, $\text{O}-\text{CH}_2_{\text{PDEVp}}$), 2.56 (s, CH_3), 2.78–1.48 (m, $\text{CH}_2_{\text{polymer backbone}}$), 1.43–1.31 (m, $\text{CH}_3_{\text{PDEVp}}$), 0.97 (s, $\text{C}(\text{CH}_3)_3$), 0.14 (s, $\text{Si}(\text{CH}_3)_2$).

^{31}P NMR (203 MHz, CD_3OD): δ (ppm) = 33.2 (PDEVp/PDAIVP).

Table S2: Amounts of monomers added in the statistical copolymerization experiments of DEVP and DAIVP presented in Table 1 of the manuscript.

[DEVP/DAIVP]	92/11	86/15	81/21
DEVP	819 mg	760 mg	720 mg
DAIVP	107 mg	155 mg	211 mg
Catalyst	20.4 mg	20.4 mg	20.6 mg

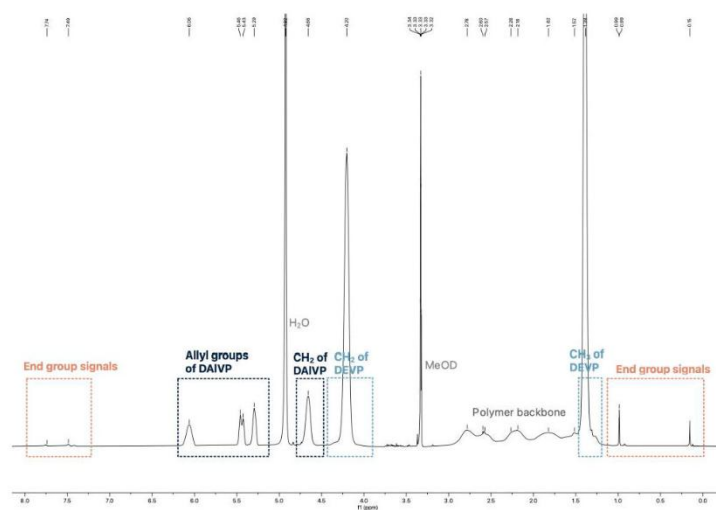


Figure S1: Exemplary copolymer $^1\text{H-NMR}$ spectrum of P(DEVP-stat-DAIVP) (Table 1, Entry 2) in CD_3OD with assignment of the corresponding signals.

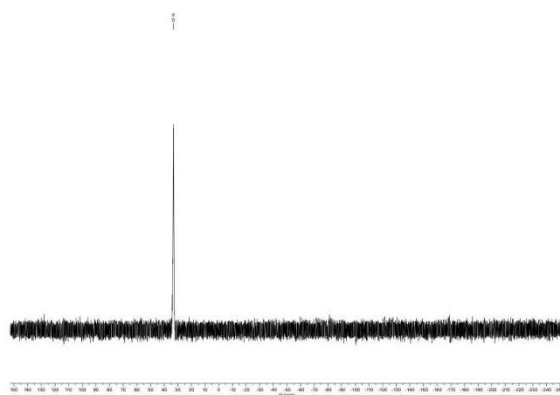


Figure S2: Exemplary ^{31}P -NMR spectrum of P(DEVP-stat-DA1VP) (Table 1, Entry 2) in CD_3OD .

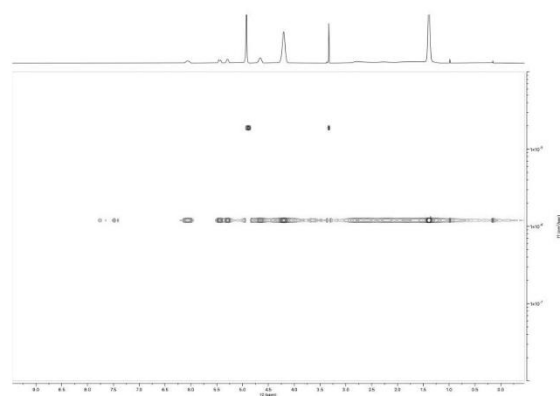


Figure S3: Exemplary ^1H DOSY NMR spectrum of P(DEVP-stat-DA1VP) (Table 1, Entry 2) in CD_3OD .

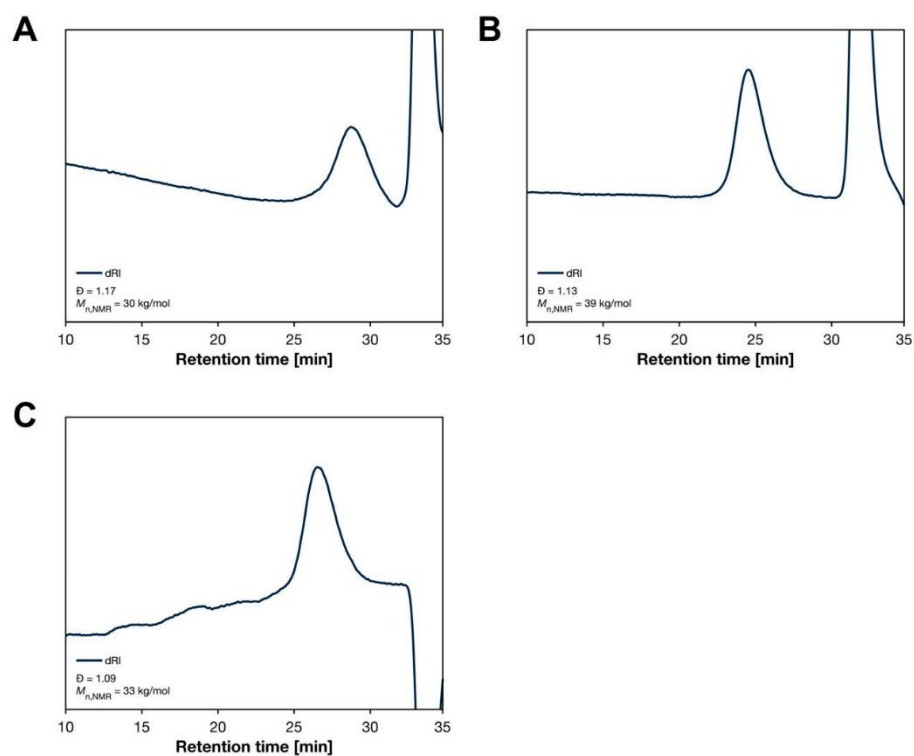


Figure S4: Refractive index detector signal of P(DEVP-stat-DAIVP) copolymers (Table 1 of the manuscript) determined via SEC-MALS in THF/water (1:1) with tetrabutylammonium bromide (9 g L⁻¹) and 3,5-di-tert-butyl-4-hydroxytoluene (340 mg L⁻¹) (order A-C corresponds to the order 1-3 in the manuscript).

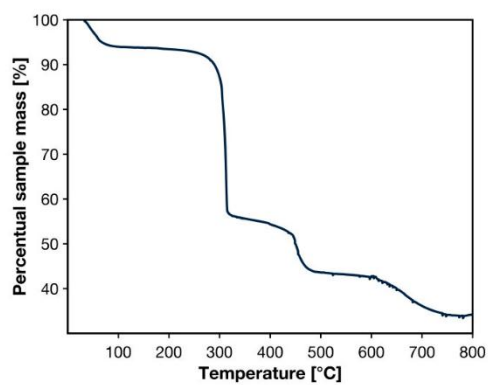


Figure S5: Thermogravimetric analysis of P(DEVP-stat-DAIVP) (Table 1, Entry 3) from room temperature to 800 °C under synthetic air with a heating rate of 10 K min⁻¹.

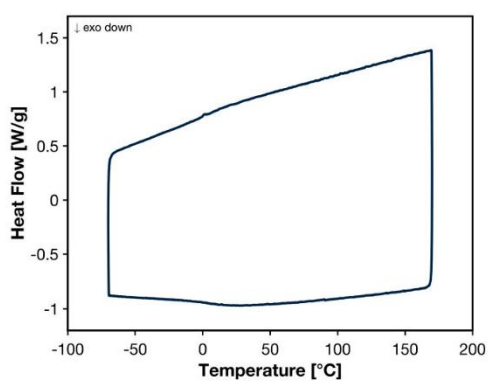
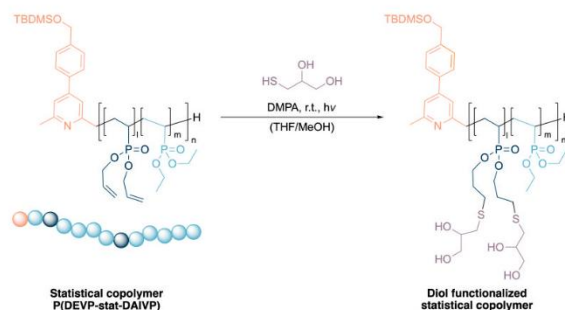


Figure S6: Differential scanning calorimetric measurement of P(DEVP-stat-DAIVP) (Table 1, Entry 3) between -70 °C and 170 °C in exo down mode.

Functionalization of P(DEVP-stat-DAIVP) with 1-thioglycerol

The polymer was dissolved in a mixture of tetrahydrofuran and methanol (THF/MeOH = 5/1) (10 mL solvent per 100 mg polymer) and was treated with 1-thioglycerol (2.50 eq. per allyl group) and catalytic amounts of 2,2-dimethoxy-2-phenylacetophenone (DMPA) (0.10 eq. per allyl group). The mixture was degassed via repeated evacuation and filling with argon (15 iterations) and irradiated ($\lambda = 365$ nm) for 18 h. The volatiles were removed under reduced pressure, and the residue was dissolved in water or a mixture of water and methanol. The solution was then purified by dialysis against water (MWCO = 8kDa) and freeze-dried to yield the functionalized polymers.

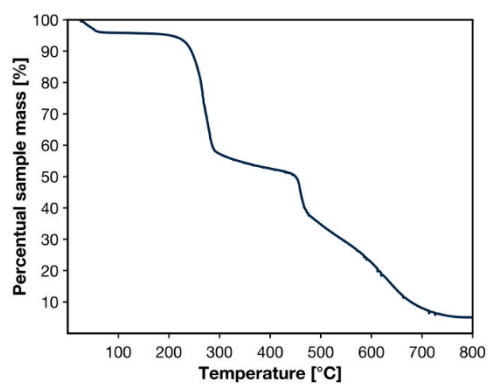


Figure S7: Thermogravimetric analysis of 1-thioglycerol-functionalized P(DEVP-stat-DAIVP) (Table 2, Entry 6) from room temperature to 800 °C under synthetic air with a heating rate of 10 K min⁻¹.

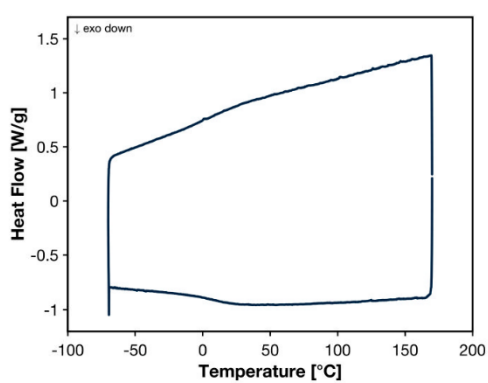
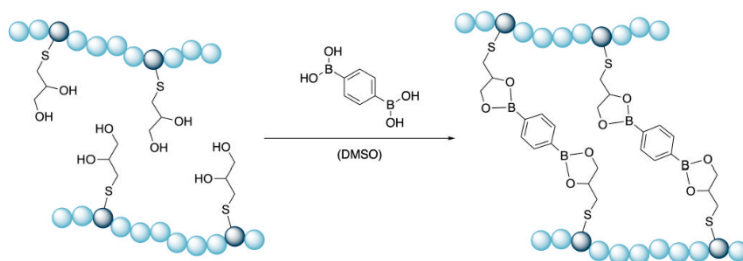


Figure S8: Differential scanning calorimetric measurement of P(DEVP-stat-DAIVP) between -70 °C and 170 °C (Table 2, Entry 6) in exo down mode.

Formation of dynamic covalent networks with benzene-1,4-diboronic acid (DBA)

A 1:1 ratio of diol groups and benzene-1,4-diboronic acid was used for all experiments. To create a dynamic covalent network, diol-functionalized polymer and benzene-1,4-diboronic acid solutions were first prepared by dissolving each component in DMSO. The boronic acid solution is then added to the polymer solution. Polymer solutions with varying degrees of polymer functionalization (13.3%, 17.5%, 24.6%) were prepared at concentrations of 12.5 wt%, 20 wt%, 25 wt%, and 30 wt%.

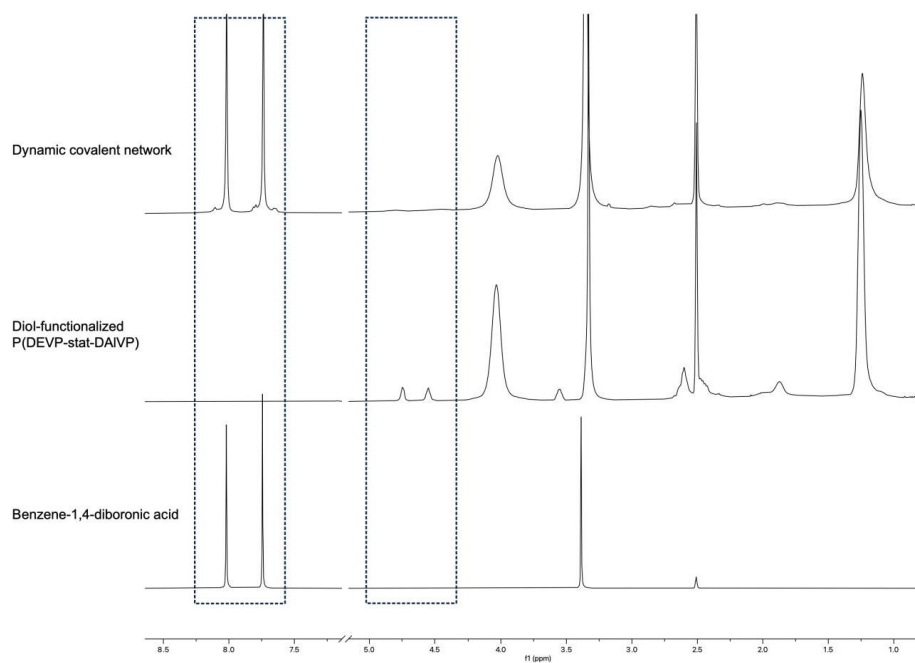
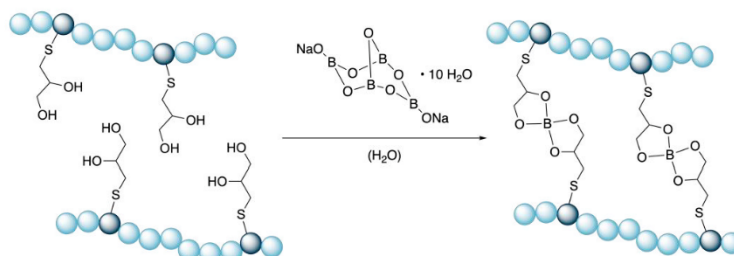


Figure S9: Stacked $^1\text{H-NMR}$ spectra of dynamic covalent network (top), diol-functionalized P(DEVP-stat-DAIVP) (middle) and benzene-1,4-diboronic acid (bottom) in DMSO.

Formation of dynamic covalent networks with sodium tetraborate decahydrate (borax)



A 1:1 ratio of diol groups and borax was used for all experiments. To create a dynamic covalent network, polymer and borax solutions are first prepared by dissolving each component in water, with the borax solution maintained at a constant concentration of 1.20 M. To create the borax stock solution, borax is dissolved by rapidly heating to 80 °C. The corresponding volumes of borax solution necessary to achieve equimolar ratios of diol and borax are then added to the polymer solution. Polymer solutions with varying degrees of functionalization (13.3%, 17.5%, and 24.6%) were prepared at concentrations of 12.5 wt%, 20 wt%, 25 wt%, and 30 wt%.

Table S3: Sol and gel fractions for the DCNs formed with borax in water for different weight percentages and functionalization degrees of the diol-functionalized polymer.

Degree of functionalization	13.3%				17.5%				24.6%			
wt. %	12.5	20	25	30	12.5	20	25	30	12.5	20	25	30
Sol fraction [%]	-	-	73	70	84	77	73	69	83	76	72	69
Gel fraction [%]	-	-	27	30	16	23	27	31	17	24	28	31

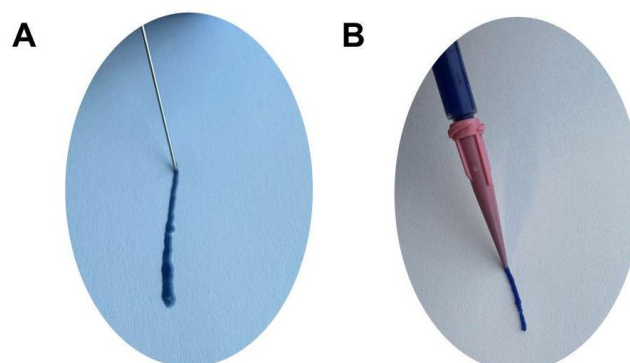


Figure S10: Comparison of the dimensional stability and flow properties of a DCN formed with DBA in DMSO (**A**) and borax in water (**B**).

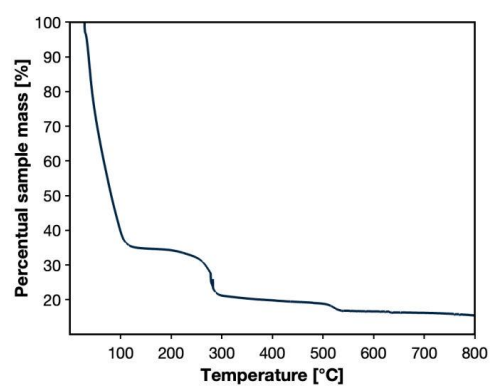


Figure S11: Thermogravimetric analysis of a dynamic covalent network formed from a 1-thioglycerol-functionalized P(DEVP-stat-DAIVP) copolymer and sodium tetraborate decahydrate in water from room temperature to 800 °C under synthetic air with a heating rate of 10 K min⁻¹.

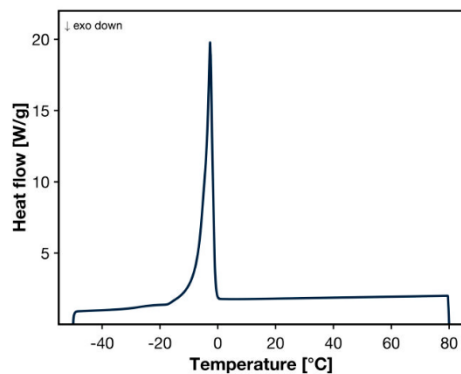


Figure S12: Differential scanning calorimetry of a dynamic covalent network formed from a 1-thioglycerol-functionalized P(DEVP-stat-DAIVP) copolymer and sodium tetraborate decahydrate in water between -50 °C and 80 °C in exo down mode.

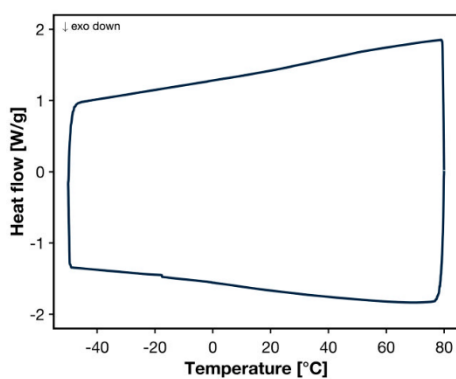


Figure S13: Differential scanning calorimetry of a dynamic covalent network formed from a 1-thioglycerol-functionalized P(DEVP-stat-DAIVP) copolymer and sodium tetraborate decahydrate after removal of water between -50 °C and 80 °C in exo down mode.

3. RHEOLOGICAL CHARACTERIZATION OF DYNAMIC COVALENT NETWORKS

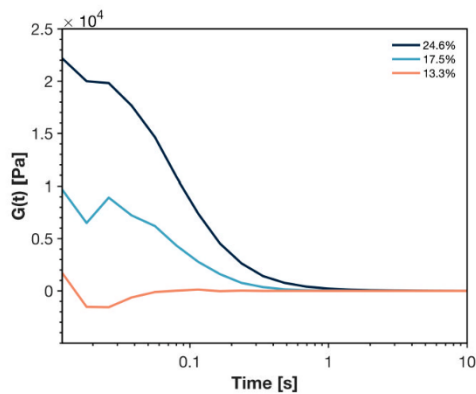


Figure S14: Stress-relaxation data of DCNs formed from diol-functionalized poly(vinylphosphonates) and borax in water for 30 wt.% polymer solutions with increasing functionalization degree. The measurements were performed at room temperature with a deformation of 1%.

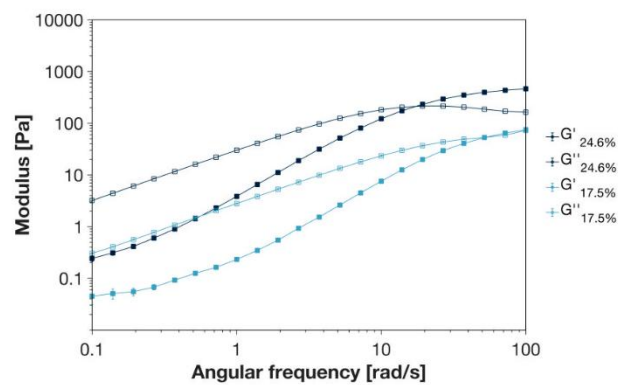


Figure S15: Oscillatory frequency sweeps between 0.1 and 100 rad/s at 1% strain for hydrogels from 1-thioglycerol functionalized P(DEVP-stat-DAIVP) and equimolar amounts of borax with varying polymer functionalization degrees at a polymer concentration of 12.5 wt.%.

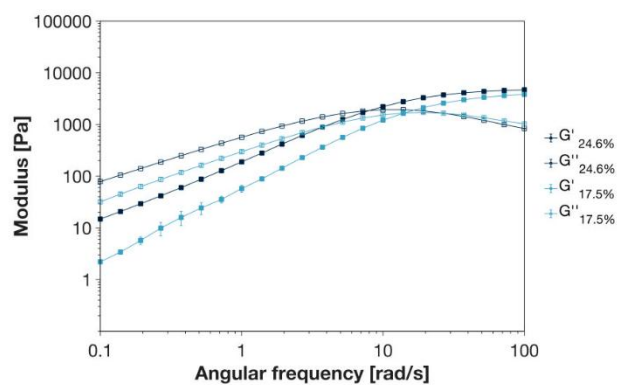


Figure S16: Oscillatory frequency sweeps between 0.1 and 100 rad/s at 1% strain for hydrogels from 1-thioglycerol functionalized P(DEVP-stat-DAIVP) and equimolar amounts of borax with varying polymer functionalization degrees at a polymer concentration of 20 wt.%.

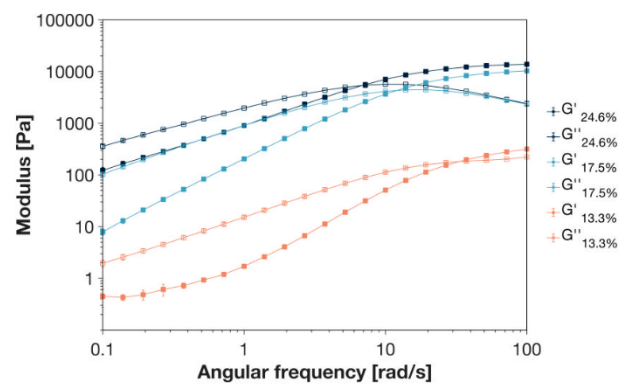


Figure S17: Oscillatory frequency sweeps between 0.1 and 100 rad/s at 1% strain for hydrogels from 1-thioglycerol functionalized P(DEVP-stat-DAIVP) and equimolar amounts of borax with varying polymer functionalization degrees at a polymer concentration of 25 wt.%.

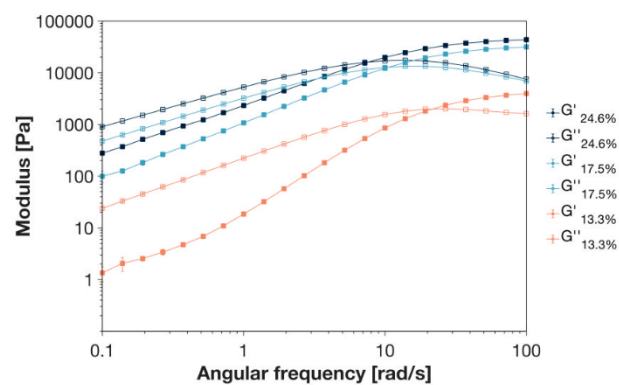


Figure S18: Oscillatory frequency sweeps between 0.1 and 100 rad/s at 1% strain for hydrogels from 1-thioglycerol functionalized P(DEVP-stat-DAIVP) and equimolar amounts of borax with varying polymer functionalization degrees at a polymer concentration of 30 wt.%.

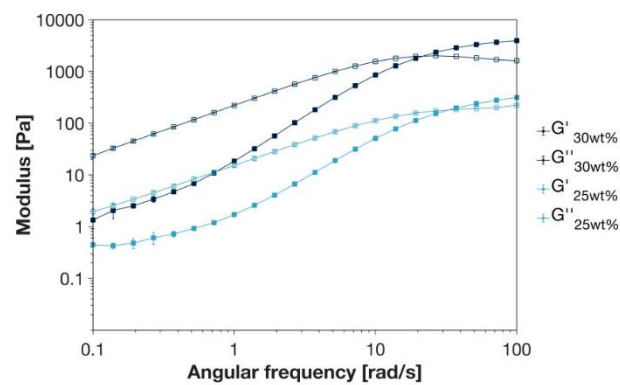


Figure S19: Oscillatory frequency sweeps between 0.1 and 100 rad/s at 1% strain for hydrogels from 1-thioglycerol functionalized P(DEVP-stat-DAIVP) and equimolar amounts of borax with varying polymer concentrations for a 13.3% functionalized copolymer.

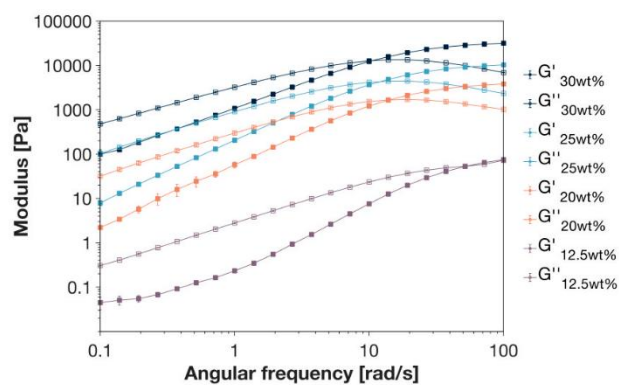


Figure S20: Oscillatory frequency sweeps between 0.1 and 100 rad/s at 1% strain for hydrogels from 1-thioglycerol functionalized P(DEVP-stat-DAIVP) and equimolar amounts of borax with varying polymer concentrations for a 17.5% functionalized copolymer.

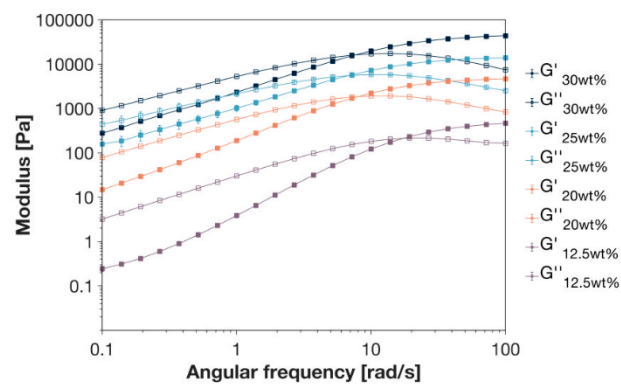


Figure S21: Oscillatory frequency sweeps between 0.1 and 100 rad/s at 1% strain for hydrogels from 1-thioglycerol functionalized P(DEVP-stat-DAIVP) and equimolar amounts of borax with varying polymer concentrations for a 24.6% functionalized copolymer.

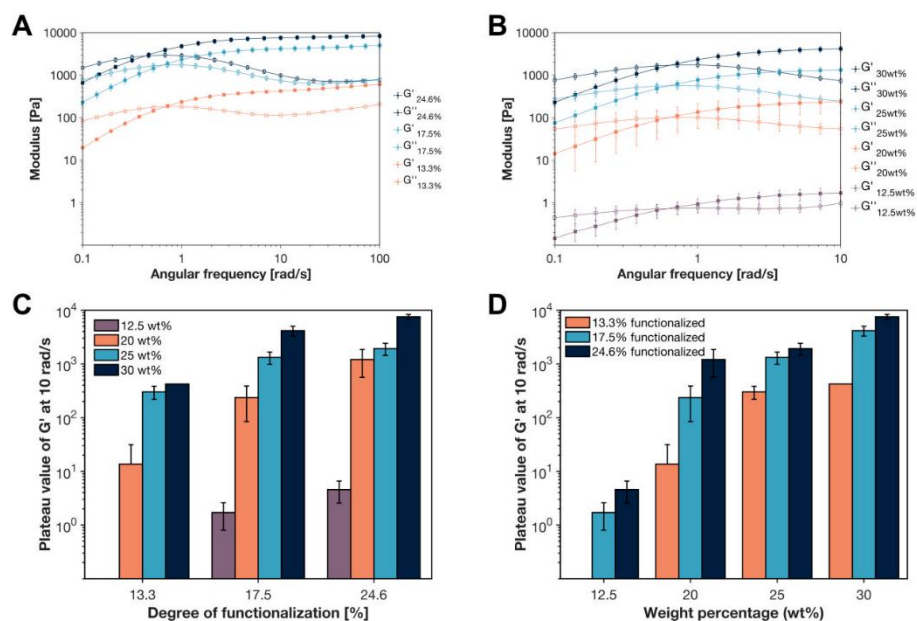


Figure S22: Comparison of the viscoelastic properties of DCNs formed from polymers with different functionalization degrees and concentrations in DMSO. Oscillatory frequency sweeps between 0.1 and 100 rad/s at 1% strain for (A) polymers with different degrees of polymer functionalization with 1-thioglycerol at 30 wt.% polymer concentration and (B) different weight percentages of a polymer with 17.5 % 1-thioglycerol-functionalized units in solution. Comparison of the viscoelastic properties of DCNs formed from diol-functionalized poly(vinylphosphonates) by evaluation of the plateau values of the storage modulus at 10 rad/s for (C) different degrees of diol-functionalization of the polymer and (D) weight percentages of functionalized polymers in solution.

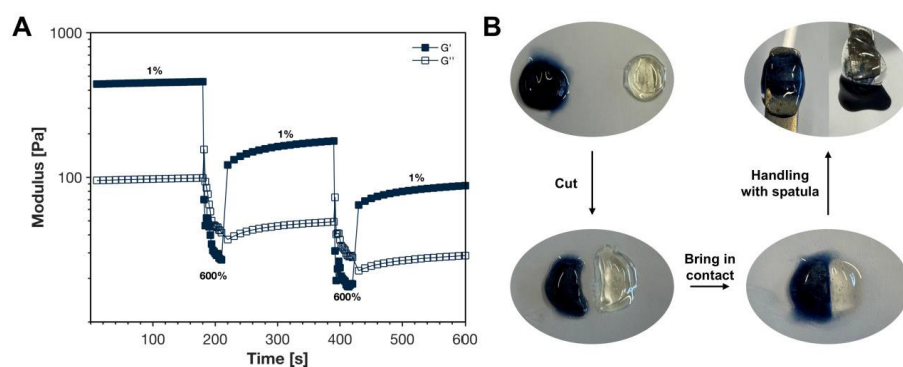


Figure S23: Rheological self-healing experiments of poly(vinylphosphonate)-based DCNs formed in DMSO at an angular frequency of 10 rad/s alternating between low ($\gamma = 1\%$) and high ($\gamma = 600\%$) shear forces (A), and images of the self-healing of two hydrogels (different colors for better visualization of the interface) with subsequent macroscopic sample handling (B).

4. REFERENCES

- (1) Halama, K.; Schaffer, A.; Rieger, B. Allyl group-containing polyvinylphosphonates as a flexible platform for the selective introduction of functional groups via polymer-analogous transformations. *RSC Adv.* 2021, *11* (61), 38555–38564. DOI: 10.1039/d1ra06452e.
- (2) Salzinger, S.; Soller, B. S.; Plikhta, A.; Seemann, U. B.; Herdtweck, E.; Rieger, B. Mechanistic studies on initiation and propagation of rare earth metal-mediated group transfer polymerization of vinylphosphonates. *J. Am. Chem. Soc.* 2013, *135* (35), 13030–13040. DOI: 10.1021/ja404457f.
- (3) Schaffer, A.; Kränzlein, M.; Rieger, B. Synthesis and Application of Functional Group-Bearing Pyridyl-Based Initiators in Rare Earth Metal-Mediated Group Transfer Polymerization. *Macromolecules* 2020, *53* (11), 4345–4354. DOI: 10.1021/acs.macromol.0c00642.

10.3 Reprint Permissions of Copyrighted Material

The contents of Chapter 4 and the corresponding Supporting Information in Chapter 10.2.1 for the manuscript entitled “Cytocompatible Hydrogels with Tunable Mechanical Strength and Adjustable Swelling Properties through Photo-Cross-Linking of Poly(vinylphosphonates)” have been published as Open Access under the terms and conditions of the Creative Commons Attribution CC-BY 4.0.

The contents of Chapter 5 and the corresponding Supporting Information in Chapter 10.2.2 for the manuscript entitled “Water Uptake, Thin-Film Characterization, and Gravimetric pH-Sensing of Poly(vinylphosphonate)-Based Hydrogels” have been published as Open Access under the terms and conditions of the Creative Commons Attribution CC-BY 4.0.

The contents of Chapter 6 and the corresponding Supporting Information in Chapter 10.2.3 for the manuscript entitled “High-Fidelity Direct Ink Writing of Poly(vinylphosphonate)-Reinforced Polysaccharide Inks with Tunable Properties” have been published as Open Access under the terms and conditions of the Creative Commons Attribution CC-BY 4.0.

The contents of Chapter 7 and the corresponding Supporting Information in Chapter 10.2.4 for the manuscript entitled “Modifications of Poly(vinylphosphonates) toward Dynamic Covalent Networks” have been published as Open Access under the terms and conditions of the Creative Commons Attribution CC-BY 4.0.